2022

Synthesis, characterisation, DNA binding interactions, and biological activity of nickel Schiff base complexes

Nawal Masoud O. Assadawi

UNIVERSITY
OF WOLLONGONG
AUSTRALIA

Synthesis, characterisation, DNA binding interactions, and biological activity of nickel Schiff base complexes

Nawal Masoud O Assadawi
Master of philosophy (Chemistry)

Supervisor:
Prof. Stephen Ralph

Associate supervisor:
Assoc. Prof. Christopher Richardson

This thesis is presented as part of the requirement for the conferral of the degree:

Doctor of Philosophy

From

The University of Wollongong

School of Chemistry and Molecular Bioscience

March 2022

Declaration

I, Nawal Masoud O Assadawi, declare that this thesis, submitted in partial fulfilment of the requirements for the award of Doctor of Philosophy, in the School of Chemistry and Molecular Bioscience, University of Wollongong, is wholly my own work unless otherwise referenced or acknowledged. This work has not been submitted for qualification at any other academic institution.

Nawal Masoud O Assadawi

March 2022

Abstract

A series of fourteen new nickel Schiff base complexes was synthesised by a two-step procedure. Initially 2,4,6-trihydroxybenzaldehyde was reacted with 1-(2-chloroethyl)piperidine hydrochloride, 4-(2-chloroethyl)morpholine hydrochloride or 1-(3-chloropropyl)piperidine hydrochloride in the presence of K_2CO_3 to afford three organic precursor compounds featuring different pendant groups. These compounds were then successfully reacted with different diamines in the presence of Ni(II) to form a series of nickel Schiff base complexes featuring four pendant groups. All new organic compounds and nickel complexes were characterised using 1D and 2D nuclear magnetic resonance (NMR) spectroscopic methods, elemental microanalysis and electrospray ionisation mass spectrometry (ESI-MS). The solid-state structures of four nickel complexes were determined by single crystal X-ray crystallography and revealed that the coordination geometry around the nickel ion was square planar in each case.

The ability of the nickel complexes to bind to the double stranded DNA molecule D2, the tetramolecular G-quadruplex Q4, the unimolecular G-quadruplex Q1 in its parallel, anti-parallel and hybrid topologies, the parallel unimolecular G-quadruplex c-KIT1, and the fluorescently labelled unimolecular G-quadruplex F21T, was investigated using ESI-MS and circular dichroism (CD) spectroscopy, Fluorescence Indicator Displacement (FID) assays, Fluorescence Resonance Energy Transfer (FRET) melting assays and molecular docking.

The results of these studies enabled the effect of varying the diamine moiety and the pendant groups on DNA binding properties to be explored. It was found that changing the diamine moiety whilst retaining the same pendant groups often had a

significant effect on binding affinity towards different DNA molecules. For example, changing the diamine moiety from phenylenediamine in (**53**) and (**54**) to the *meso*-1,2-diphenylethylenediamine moiety in (**65**) and (**66**), respectively, resulted in the binding preference changing to favour G-quadruplex DNA over double stranded DNA. In addition, nickel complexes with propylpiperidine pendant groups generally exhibited stronger interactions with a variety of different DNA molecules than analogues containing the same diamine moiety but one of the other two types of pendant groups. For example, complex (**61**), which possessed propylpiperidine pendant groups, exhibited a much greater ability than either (**59**) or (**60**) to form non-covalent adducts with Q4, Q1 and D2 in ESI-MS experiments. This is despite (**61**) having the same diamine moiety and is a result of the latter two nickel complexes having ethylpiperidine and ethylmorpholine pendant groups, respectively. Circular dichroism studies showed that parallel c-KIT1 was the only G-quadruplex whose CD spectrum was significantly affected by (**61**). This result suggests this nickel complex may bind to parallel c-KIT1 with some selectivity over other types of G-quadruplexes.

Complexes (**53**), (**56**) and (**65**) and their analogues with only two pendant groups were evaluated for their cytotoxicity against V79 lung cancer cells using MTT assays. The results obtained suggested introduction of two additional pendant groups does not in general appear to confer additional cytotoxicity onto this class of nickel complexes.

Acknowledgement

First and foremost, I would like to express my deepest gratitude to my supervisor Prof. Stephen Ralph for his continuous support, patience, motivation, and immense knowledge. His guidance helped me throughout my Ph.D project. Thank you Steve for taking time out from your busy schedule to read, correct and revise my thesis, especially in the latter stages. Thank you for your feedback and support while I completed writing my thesis and for your encouragement and belief in me, as I would not have reached this stage without it!

Besides my supervisor, I would like to thank my co-supervisor Assoc. Prof. Christopher Richardson. Thank you for your input and expertise with the synthesis, purification and crystallisation of my complexes, as well as your help with NMR characterisations and crystallography and for your proof reading of this work.

To Assoc. Prof. Carolyn Dillon, thank you for welcoming me to your lab and for guiding me through the challenges of cell work.

I would like to thank my former group members in the Ralph lab and mass sec lab. In particular Dr. Kimberley Davis for teaching me the instrumental techniques and data analysis and for providing thoughtful discussions, best suggestions and insights and support throughout my postgrad years. To Dr. Sean Pham, thank you for training and helping me run the modelling experiments. To Dr Monica Birrento, thank you for your training, guidance and assistance with the FRET studies. To the Richardson and Dillon group members, thank you for your help and assistance in the laboratory whenever needed. To Dr Judith Carrall, thank you for assisting me with learning techniques necessary for my cell work and for your willingness to answer all my queries as I analysed the data.

For technical support, I wish to thank Dr Wilford Lie (School of Chemistry, UOW) for his generosity with his time and advice about NMR spectroscopy and for his wonderful management of the NMR facility. Additionally, I would like to thank Dr. Céline Kelso for her help in the mass spec lab, especially with instrumental issues.

Thank you all for your contribution to the development of my research, I would never have been able to finish writing on time without your guidance and help.

None of this would have been possible without love, support and patience from my family, especially my beloved husband. He was always there encouraging me and cheering me up and stood by me through the good times and bad. I am also grateful to my kids who are the superior and enjoyable part of my life at Australia. I thank my sisters for the laughs, the arguments and the fun chats. You've always had a way of pulling me out of a miserable mood and putting a smile on my face. Last but not least, I would like to thank my parents for their unconditional love, encouragement and support throughout my entire life.

Abbreviations

22AG	human telomeric sequence 5′-AGGG (TTA GGG)$_3$ - 3′
A	adenine
A549	lung cancer cell lines
AD4	AutoDock 4
AV	AutoDock Vina
BRACO19	N-[9-[4-(dimethylamino)anilino]-6-(3-pyrrolidin-1 ylpropanoylamino)acridin-3-yl]-3-pyrrolidin-1-ylpropanamide
B3LYP	Becke, three-parameter, Lee-Yang-Parr
C	cytosine
CD	circular dichroism
$CDCl_3$	chloroform-D
c-KIT	cytokine tyrosine kinase
COSY	correlation spectroscopy
cisplatin	*cis*-diamminedichloridoplatinum(II)
DCM	dichloromethane
DC_{50}	concentration of ligand required to reduce the fluorescence by 50%
DFT	density functional theory
DMSO	dimethylsulfoxide
DNA	deoxyribonucleic acid
ttpy	tolyl-terpyridine (4′-(4-methylphenyl)-2,2′:6′,2″-terpyridine
tMebip	2,2′-(4-*p*-tolylpyridine-2,6-diyl)bis(1-methyl-1*H*-benzo[d]imid-azole))
dsDNA	double stranded DNA
en	1,2-diaminoethane
ESI	electrospray ionisation
Et_2O	diethyl ether
EtOH	ethanol
FAM	6-carboxyfluorescein
FBS	fetal bovine serum
FID	fluorescent intercalator displacement
FRET	fluorescence resonance energy transfer
G	guanine
HLPC	high performance liquid chromatography
HMBC	heteronuclear single-quantum correlation
HSQC	heteronuclear single-quantum correlation
hTERT	human telomerase reverse transcriptase
IC_{50}	inhibitory concentration required to cause death of 50% of the cell population
K562	leukemia cell line
LiCaCo	lithium cacodylate
MCF-7	breast cancer cell lines

MeOH	methanol
MS	mass spectrometry
MTT	3-(4,5-dimethylthiazol-2-yl)-2,5-diphenyltetrazolium bromide
m/z	mass to charge ratio
NH_4OAc	ammonium acetate
NMR	nuclear magnetic resonance
NOESY	nuclear overhauser effect spectroscopy
PBS	phosphate-buffered saline
PCR	polymerase chain reaction
PDB	protein data bank
PDBQT	protein data bank partial charge and atom type
qDNA	quadruplex DNA
salen	N,N′-bis(salicylidene)ethylenediamine
salphen	N,N′-bis(salicylidene)phenylenediamine
SPR	surface plasmon resonance
ssDNA	single stranded DNA
TAMRA	tetramethyl-6-carboxyrhodamine
T	thymine
T_m	melting temperature
TO	thiazole orange
TMPyP	tetra(N-methyl-4-pyridyl-porphine
TRAP	telomerase repeat amplification protocol
TRF	telomeric repeat binding factor
V79	Chinese hamster lung cancer cells
VMD	visual molecular dynamics

Table of contents

Table of figures

Table of tables

Chapter 1 Introduction

1.1 Deoxyribonucleic acid (DNA)

Deoxyribonucleic acid (DNA) is a polymeric biomolecule that is found in most lifeforms. It is a major component of chromosomes and responsible for storing, transmitting and processing cellular genetic information. DNA is composed of many repeating units called nucleotides. Each nucleotide consists of the sugar deoxyribose, a phosphate group, and a nitrogenous base which can be one of the two pyrimidines cytosine (C) and thymine (T), or one of the purines adenine (A) or guanine (G) (Figure 1.1). Within each nucleotide, the nitrogenous base is linked to the deoxyribose sugar unit through an N-glycosidic bond with the 1′-carbon, while the phosphate group is linked to deoxyribose through a phosphoester bond. A single DNA strand is formed when nucleotides are linked together in their 5′ and 3′ positions via phosphodiester bonds.

A double stranded DNA (dsDNA) structure occurs when base pairs in two pieces of single stranded DNA (ssDNA) are held together by hydrogen bonds between complementary pyrimidine and purine bases. The dsDNA structure is further stabilised by base stacking interactions which consist of van der Waals, electrostatic and hydrophobic interactions between the purine and pyrimidine bases.[1]

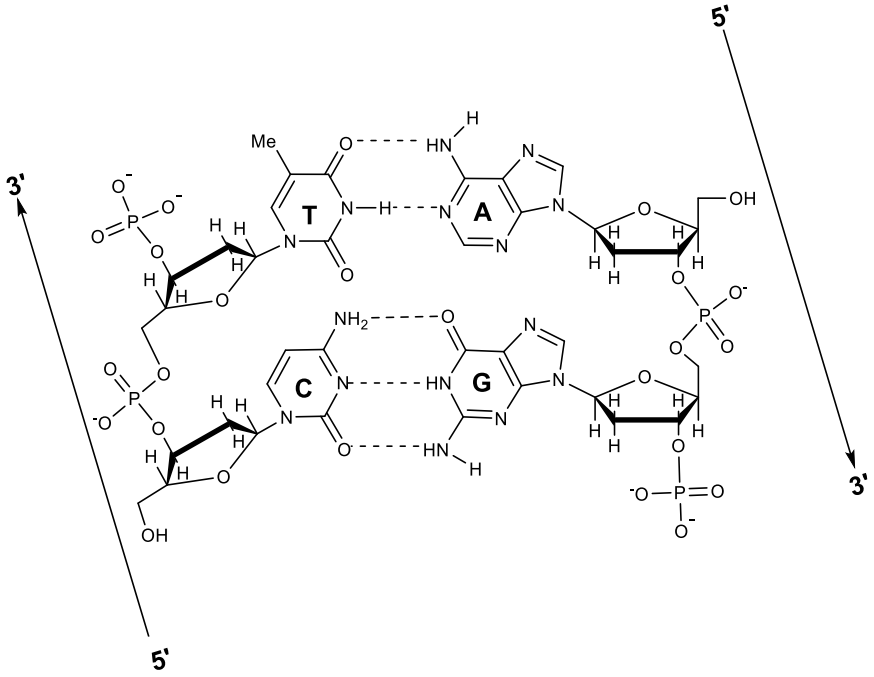

Figure 1.1: A portion of the structure of dsDNA, illustrating Watson-Crick base pairing between complementary bases on the two DNA strands.

The structure of the most common form of DNA (B-DNA) was first determined by Watson and Crick in 1953.[2] The crystal structure of B-DNA revealed that it is composed of two right-handed anti-parallel strands that are held together by specific hydrogen bonding interactions. The base pairs formed are known as Watson-Crick base pairs and are highly specific in that A always pairs with T via two hydrogen bonds while G only ever pairs with C via three hydrogen bonds (Figure 1.1). The preservation of the above base pairs is a fundamental aspect of the DNA replication process as this facilitates synthesis of complementary strands with high fidelity. In B-DNA the nitrogenous bases are stacked perpendicular to the helical axis, with ~10 base pairs per helical turn, resulting in the formation of two grooves known as the major and minor grooves.[3] The width of the major and minor grooves is an important factor involved in determining how drug molecules may interact with DNA.

Most DNA present in cells is found in the classic double-helix B-DNA form. However, there are other less common structures that dsDNA can adopt under certain conditions. For example, in low humidity environments dsDNA can adopt the right-handed A-form structure with ~11 base pairs per helical turn.[3] In A-DNA, the nitrogenous bases are displaced from the helical axis and ejected into the minor groove. In addition, in environments with high salt concentrations dsDNA can adopt the left-handed double helical Z-DNA structure with ~11 base pairs per helical turn. In contrast to the A- and B- forms of DNA the Z-DNA structure is wider, more compact and has a deeper minor groove.[3] The latter results from the displacement of the base pairs from the helical axis of Z-DNA. Another distinctive feature of the structure of Z-DNA is alternating purine–pyrimidine sequences (e.g. GC) with anti and syn conformations of the alternating glycosidic bonds. This conformation gives rise to the wrinkled appearance of the sugar-phosphate backbone in Z-DNA. Alternative hydrogen bonding arrangements between DNA bases also exist which expand the ways in which DNA can fold to form additional secondary structures such as triplexes and guanine quadruplexes (G-quadruplexes).

1.2 G-quadruplex DNA

G-quadruplexes are less common secondary DNA structures that are formed from guanine-rich DNA sequences. These sequences are found in different locations of the genome, including the extended 3′-overhang region consisting of ssDNA that is located at the end of chromosomes in regions known as telomeres. Although the formation of guanine tetrads (G-tetrads) were first reported in 1910, their characterisation was not accomplished until 1962.[4,5] G-tetrads are the basic structural feature of a G-quadruplex. Each G-tetrad is a square planar array of four guanine

bases held together by eight Hoogsteen hydrogen bonds (Figure 1.2 (a)). In a G-quadruplex at least four G-tetrads are stacked on top of each other and held together by π-π base stacking interactions (Figure 1.2 (b)). The central channel of each G-tetrad is stabilised by the presence of monovalent cations (e.g. K^+, Na^+ or NH_4^+).[6,7] The latter coordinate to the electronegative oxygen atoms of the guanine carbonyl groups and minimise the repulsive effects that would otherwise arise from their proximity to each other.[8] The ability of the above cations to stabilise G-quadruplex structures was found to vary according to the following sequence $K^+ > Na^+ > NH_4^+$.[7,9-11] They have been shown to intercalate between adjacent G-quartets joined together by the sugar phosphate backbone of the DNA strands (Figure 1.2 (b)).

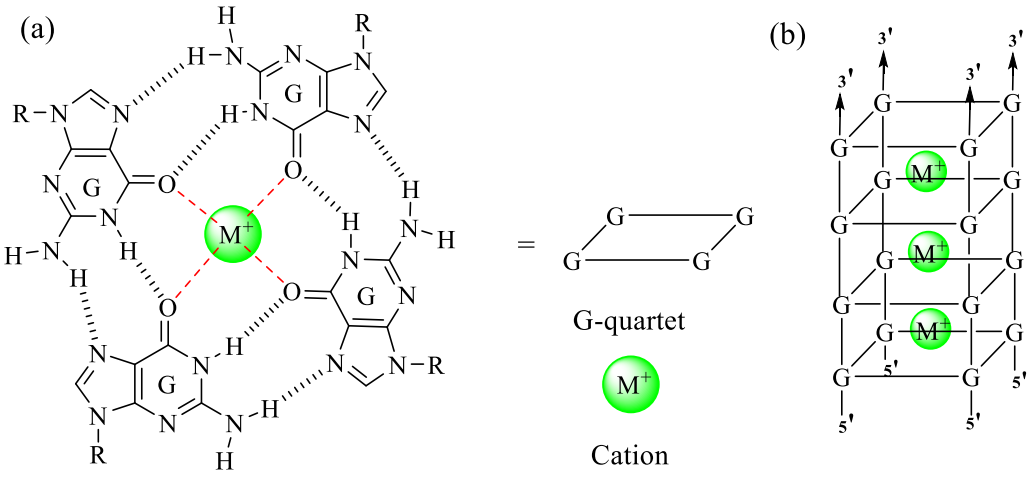

Figure 1.2: Schematic representation of a G-quadruplex structure: (a) four guanines self-associate into a planar G-tetrad with a central cavity occupied by a monovalent cation (green sphere) coordinated to oxygen atoms. (b) G-quadruplex structure formed as a result of π-π stacking of G-tetrads.

G-quadruplex DNA structures can exhibit various topologies depending on a number of factors. These include the nucleobase sequence(s) of the strand(s) they are formed from, whether they are intra- or intermolecular, the number of DNA strands associated with the structure (one, two or four), strand orientation (parallel, anti-parallel or hybrid), and the type of loops connecting the DNA strands (lateral,

diagonal or strand reversal).[8,12] For example, unimolecular G-quadruplexes formed from a single DNA strand can fold into a parallel conformation with external (propeller) loops (Figure 1.3 (a)) or into an anti-parallel conformation with either lateral (edgewise) loops (Figure 1.3 (b)) or a mixture of lateral and diagonal (hybrid) loops (Figure 1.3 (c)). Bimolecular G-quadruplexes are formed from two DNA strands and can fold into a parallel conformation with external loops connecting the adjacent strands or into an anti-parallel conformation with either lateral loops or diagonal loops connecting the adjacent strands (Figure 1.3 (d) and (e)). Tetramolecular G-quadruplexes are formed from four DNA strands which can orient themselves in either parallel (Figure 1.3 (f)) or anti-parallel positions with respect to each other, resulting in different intermolecular structures.

The exact topology exhibited by a G-quadruplex can vary depending on the sequence of nucleotides and the surrounding environment.[13] For example, the human telomeric sequence d[AGGG(TTAGGG)$_3$] forms anti-parallel and parallel G-quadruplex structures in buffers containing Na^+ and K^+ ions, respectively.[14,15] In contrast, the following sequence, which differs slightly from that present in human telomeres, d[GGG(TTAGGG)$_3$T], forms an intramolecular anti-parallel G-quadruplex in buffers containing potassium ions.[16] A number of different DNA sequences containing human telomeric repeats have also been found to form different G-quadruplex structures under different ionic conditions.[17]

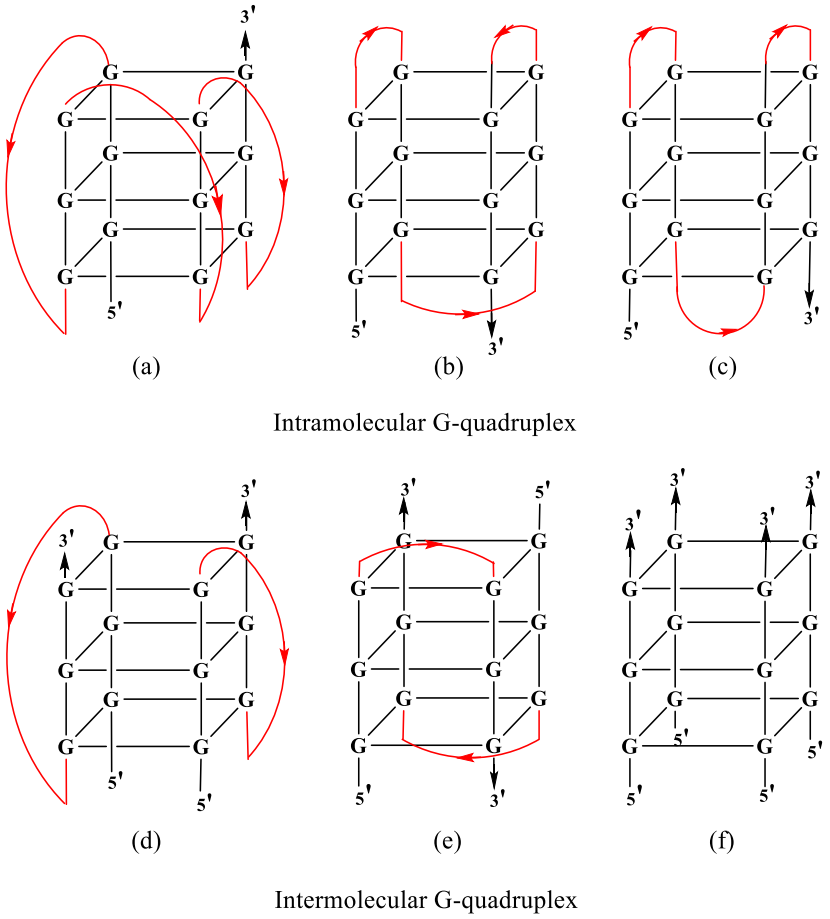

Figure 1.3: Schematic illustration of different G-quadruplex conformations: (a) unimolecular parallel with external loops; (b) unimolecular anti-parallel (chair type) with lateral loops; (c) unimolecular anti-parallel (basket type) with a mix of lateral and diagonal loops; (d) bimolecular anti-parallel with external loops; (e) bimolecular anti-parallel with lateral loops; and (f) tetramolecular parallel. Loops are coloured red. Arrows refer to strand orientation. Adapted from various references.[17-21]

Many of the G-quadruplex DNA topologies discussed above have been found to be stable under physiological conditions, suggesting they may have potential roles in biological activities.[22] Therefore, in recent years, considerable attention has focused on the detection and characterisation of G-quadruplex structures in living cells in order to understand their formation and biological functions.

1.3 Biological aspects of G-quadruplex DNA

The formation of G-quadruplex structures in human cells was clearly demonstrated by the Balasubramanian group through the use of fluorescently labelled structure-specific antibodies (BG4).[23] These revealed the presence of G-quadruplex structures in both telomeric and non-telomeric regions of chromosomes (Figure 1.4). Similar results were subsequently obtained by other research groups using different G-quadruplex specific antibodies (IgG 1H6 and scFv D1).[24,25]

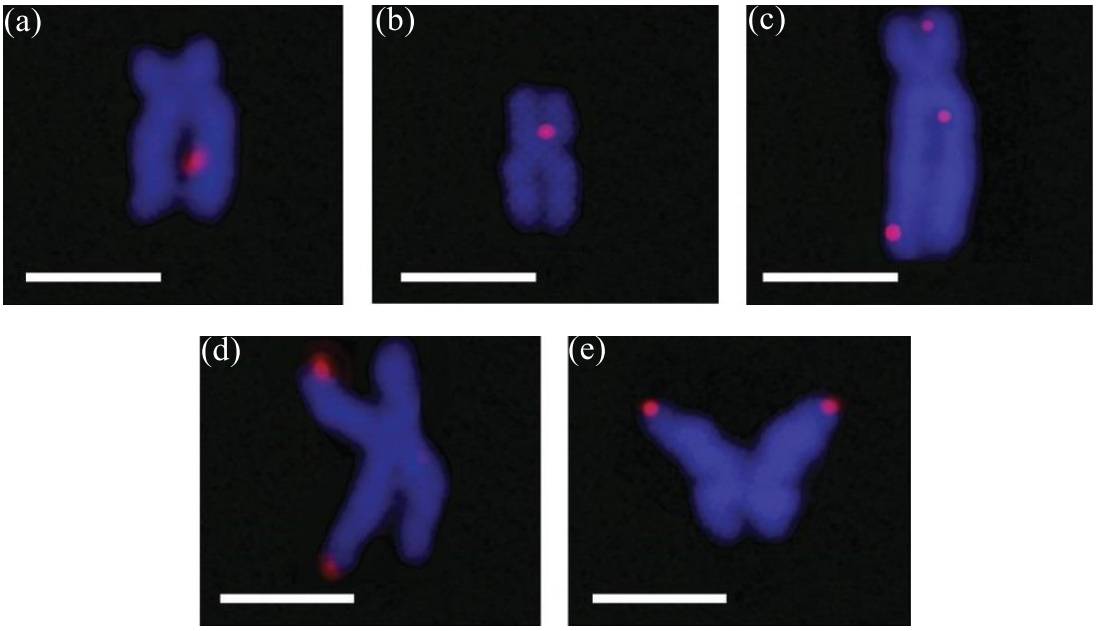

Figure 1.4: Immunofluorescence microscopy analysis of BG4 antibody on chromosomes isolated from HeLa cervical cancer cells. Chromosomes are stained with DAPI DNA dye (blue). (a), (b) and (c) show discrete BG4 foci (red) within the non-telomeric regions, (d) and (e) show discrete BG4 foci (red) at the telomeres. Reprinted by permission from Springer Nature, Giulia Biffi *et al*, *Nature Chemistry*. 2013, Vol 5 (3), p 182-186.[23] Copyright 2013.

According to an in vitro sequencing study, over 700,000 DNA sequences in the human genome are capable of forming G-quadruplexes.[26] Most of these were found in telomeres and promoter regions such as c-MYC, BCL-2, c-KIT, KRAS, and VEGF.[27-38] The predominance of potential G-quadruplex forming sequences in these

regions has led to suggestions they may play a role in several key biological processes including DNA replication, transcription and translation, as well as telomere maintenance and genomic regulatory processes. [9,22,39,40] It has also been speculated that the formation of G-quadruplex DNA structures may be connected to the onset of certain human diseases including different types of cancer.[41-43] Such studies have provided impetus for the development of G-quadruplex binding and stabilising agents as a new class of therapeutic drugs.

1.3.1 The formation of G-quadruplexes from the human telomeric sequence

G-quadruplex formation in many organisms was first observed in telomeric regions.[44] Telomeres are DNA-protein complexes found at the ends of chromosomes that provide protection from genetic instability arising from events which involve merging with neighbouring chromosomes. Human telomeric DNA is composed of a noncoding region of duplex TTAGGG repeats, and a 3′ single-strand overhang region that is also composed of multiple repeats of the same guanine-rich base sequence. This 3′ single-strand overhang is a product of an inherent issue ("end replication problem") that arises during the DNA replication process occurring during cell division. During replication dsDNA is first unwound by the DNA helicase enzyme.[18] This results in leading and lagging ssDNA strands that run in opposite directions (5′ to 3′ and 3′ to 5′ direction, respectively) (Figure 1.5 (a)) and provides an opportunity for G-quadruplex structures to be formed. It has been theorised that the presence of folded G-quadruplex structures may prevent a ssDNA strand from being able to function as a template for replication.[39] A number of helicases which are known to unwind G-quadruplex structures are found in telomeres

in vitro, strongly suggesting that G-quadruplex formation may naturally occur in telomeres in living cells.[22,45-47]

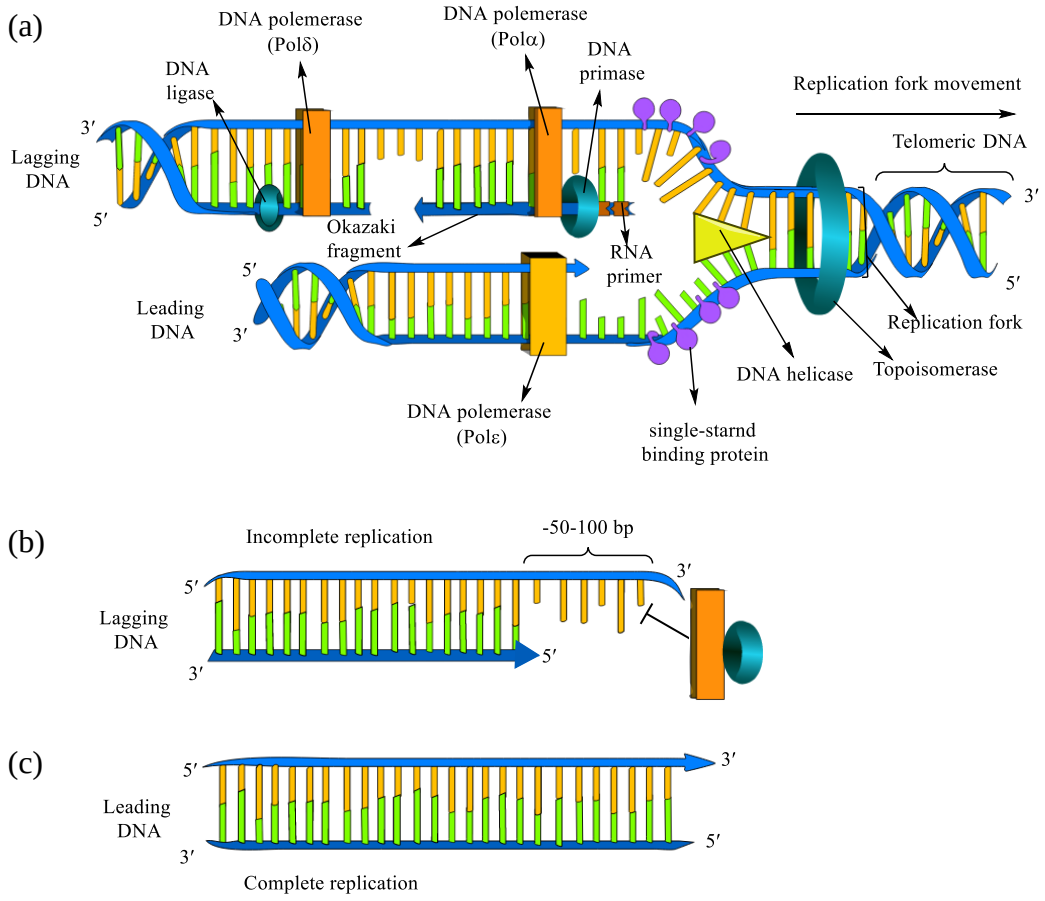

Figure 1.5: (a) Schematic illustration of the DNA replication process highlighting the "end-replication problem". Polymerase ε in eukaryotes replicates the leading strand while polymerase α synthesises discontinuous DNA fragments known as Okazaki fragments along the lagging strand; (b) Incomplete replication of the lagging strand occurs as DNA primase is unable to synthesise the final required primer sequence, and (c) Complete replication of the leading strand. Adapted from various references.[48,49]

DNA replication is performed by a DNA polymerase enzyme (DNA pol α-primase complex) following binding of an RNA primer to the target ssDNA strand. The polymerase works only in the 5′ to 3′ direction along the template DNA strand. Therefore, the leading strand is able to be replicated by the polymerase enzyme in a continuous fashion by closely following the helicase with only one molecule of RNA

primer required to initiate the process. In contrast, the lagging strand is replicated discontinuously in small segments with a series of RNA primers being required to initiate each of the individual DNA synthesis events. This produces a series of discontinuous DNA segments called Okazaki fragments.[50] After synthesis is completed the RNA primers are removed and the gaps in the DNA sequence are filled by a DNA ligase enzyme. A problem arises since the RNA primase in linear chromosomes is unable to synthesise the final primer at the 3′ end of the template DNA strand. This prevents the complete replication of the lagging strand, leaving the DNA with a 3′ single stranded overhang (Figure 1.5 (b)). This failure to completely reproduce a copy of the template strand is called the "end replication problem".[51] As a result, the length of telomeric DNA progressively decreases after each round of DNA replication.[48] Eventually it reaches a critical length, after which a DNA damage response is activated and the cell enters a senescent state, and eventually undergoes apoptosis.[52,53]

To protect the telomere from being recognized as damaged DNA, the 3′ single-strand overhang forms a telomeric loop (T-loop) and generates a local displacement loop (D-loop) by folding back to the double stranded region (Figure 1.6 (a)).[54,55] T-loop formation is mediated by a protein complex called shelterin which consists of six proteins (Figure 1.6 (b)).[55] The shelterin complex caps telomeric DNA through the binding of Telomeric Repeat-binding Factor 1 and 2 (TRF1 and TRF2) to the TTAGGG sequences present in dsDNA[56] and the binding of the Protection of Telomeres 1 protein (POT1) to these sequences in the ssDNA regions.[57] TRF1-Interacting Nuclear factor 2 (TIN2) binds to TIN2-interacting protein 1 (TPP1) and holds TRF1, TRF2 and POT1 together in the complex (Figure 1.6 (b)). Finally, Repressor Activator Protein 1 (RAP1) also binds to TRF2 in order to form the fully

protected telomere. In addition to end capping of the telomere, T-loops also regulate activity of the enzyme telomerase by inhibiting access to the telomere terminus. Therefore, the T-loops have to be unfolded first before telomere extension mediated by telomerase can occur.

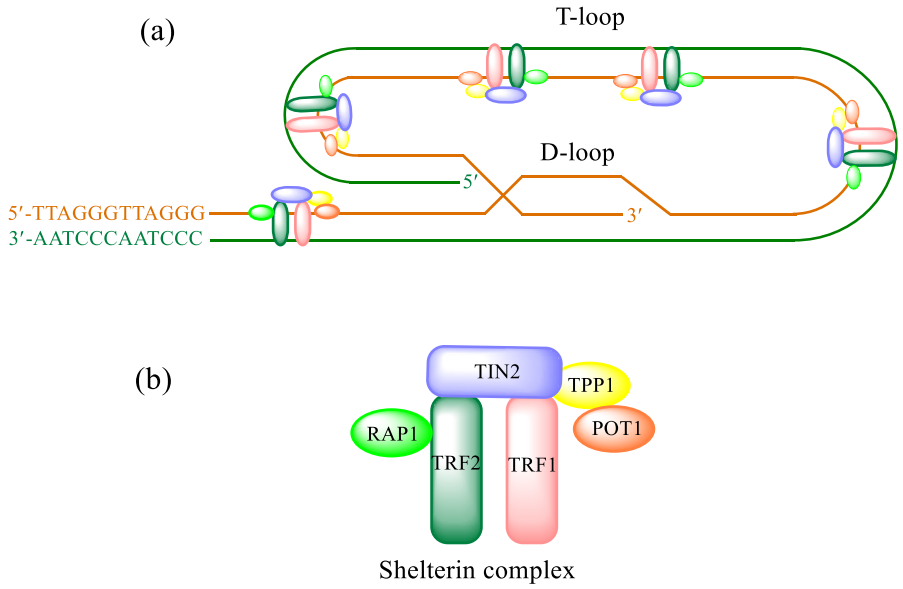

Figure 1.6: (a) Schematic illustration of the structure of a telomere showing the T-loop, D-loop and shelterin; and (b) structure of the shelterin complex involving six different proteins (TRF1, TRF2, TIN2, TPP1, POT1 and RAP1).

1.3.1.1 Telomerase and cancer

Apoptosis is an essential process required to prevent uncontrolled cell division in somatic cells. In contrast, stem cells and germ cells express the enzyme telomerase to maintain telomere length and high proliferation capacities.[58,59] The same occurs with many types of cancer cells which show high levels of telomerase activity.[59] Telomerase is a ribonucleoprotein enzyme that was first discovered in 1984 and normally exhibits minimal activity in somatic cells.[49,52,60] The enzyme is comprised of the catalytic enzyme unit which is called Telomerase Reverse Transcriptase (TERT), and a telomerase RNA component known as TERC. Telomerase serves to

maintain the length of telomeric DNA in human cells by adding the G-rich six-base nucleotide sequence TTAGGG onto the 3′-end of the telomeric single stranded DNA overhang.[52,60] The TERC is produced by RNA polymerase II, and used as the template for the telomeric DNA synthesis process.

Over-expression of telomerase provides a mechanism by which cancer cells can avoid the apoptotic process by which all cells normally eventually die. However, it has been suggested that folding of the G-rich single stranded overhang region present in telomeres into G-quadruplex structures may result in inhibition of telomerase activity, thereby providing a mechanism of targeting cancer progression.[61-65] As a result there has been an increasing amount of research recently directed toward understanding the formation and stabilisation of G-quadruplexes.[64-68] This understanding has made it possible to design small molecules with features that enable them to bind effectively to and stabilise G-quadruplexes, sometimes in a highly selective fashion with respect to the more common B-DNA found throughout cells. Therefore, the development of small-molecule ligands which can bind to G-quadruplexes has become a recent focus of many studies aimed at developing new strategies for cancer therapy.[43,69]

1.4 DNA G-quadruplex binding ligands

The main property sought in novel G-quadruplex ligands is the ability to show a high degree of binding selectivity in favour of these novel secondary DNA structures comparing to dsDNA. It has been reported that the main structural features a ligand must possess in order to exhibit this behaviour are a large planar aromatic system which allows π-stacking interactions with G-tetrads, and positively charged substituents that enable favourable electrostatic binding with the negatively charged

phosphate backbone of a G-quadruplex.[70] Furthermore, the presence of flexible side-chains with specific functional groups that endow the ligand with the ability to participate in selective interactions with the grooves and/or loops of G-quadruplexes has also been shown to be advantageous.[71,72]

The past two decades has seen a remarkable growth in the number of different classes of G-quadruplex binding ligands, with now more than 1000 having been reported in the G-Quadruplex Ligands Database.[73] Most of these have been examined for their ability to bind to and stabilise telomeric G-quadruplex DNA, however only a small number have had their cytotoxicity towards cancer cells explored.[74-77] Some examples of notable G-quadruplex binding ligands will be discussed in the following sections.

1.4.1 Organic G-quadruplex ligands

The compound BRACO-19 (**1**) is one of the most studied organic molecules known to have a high affinity towards G-quadruplexes, and is composed of a central planar aromatic core that enables π–π stacking interactions with G-quartets and three side chains functionalized with tertiary amine moieties (Figure 1.7).[78] The results of a Fluorescence Resonance Energy Transfer (FRET) melting assay revealed that addition of (**1**) resulted in a 25.9 °C increase in melting temperature for the unimolecular G-quadruplex F21T.[79] In contrast only an 11.2 °C increase in melting temperature was observed when the experiment was performed using a control duplex DNA sequence. In addition, (**1**) exhibited selectivity for G-quadruplex DNA over dsDNA in Surface Plasmon Resonance (SPR) experiments, which afforded affinity constants (Ka) of 31.0×10^6 M^{-1} for the human telomeric G-quadruplex (hTel) and 0.5×10^6 M^{-1} for duplex DNA.[80]

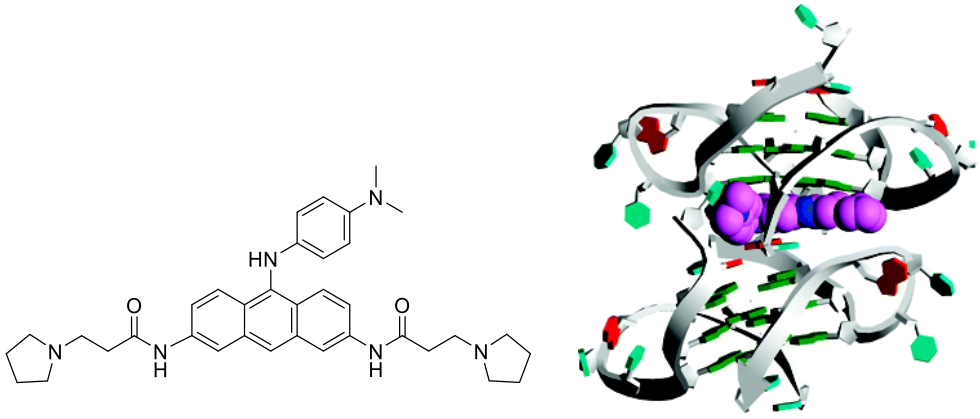

(**1**)

Figure 1.7: Crystal structure of the complex formed between (**1**) and two molecules of bimolecular human telomeric G-quadruplex DNA (PDB ID: 3CE5). Each quadruplex contains three stacked G-tetrads with the BRACO-19 molecule stacking directly onto the 3′ end quartet. Adapted with permission from *Journal of the American Chemical Society*, 2008, Vol.130 (21), p. 6722-6724.[78] Copyright 2008 American Chemical Society.

Results obtained from a sulphorhodamine B (SRB) short-term cytotoxicity assay performed using (**1**) afforded values of IC_{50} of 2.4 and 2.5 μM for MCF7 breast cancer cells and A549 lung cancer cells, respectively. In contrast the IC_{50} obtained with the normal human lung fibroblast cell lines IMR90 and WI-38 were 10.7 and > 25 μM, respectively.[81] These results demonstrate that (**1**) exhibits a degree of cytotoxicity towards some cancer cell lines. BRACO-19 has also been shown to inhibit telomerase activity by decreasing hTERT expression, and to cause telomere shortening by destabilizing the shelterin complex in DU145 prostate cancer cells, UXF1138L human uterus cancer cells and U87 human brain cancer cells.[82-84] Despite these promising initial results, the very poor membrane permeability, low levels of cellular uptake and instability at physiological pH exhibited by (**1**) have to date inhibited its further development for clinical use.[85]

The tetra-cationic porphyrin TMPyP4 (*meso*-tetra(N-methyl-4-pyridyl)porphine) (**2**) is another widely used ligand to study the binding properties of G-quadruplexes due

to its ability to stabilise such structures.[86,87] Compound (**2**) has a structure featuring four cationic functional groups attached to a central porphyrin core. Hurley and co-workers reported for the first time that (**2**) binds to a human telomeric G-quadruplex with high affinity.[61] It has also been demonstrated that (**2**) efficiently inhibits telomerase (IC_{50} = 6.5 ± 1.4 μM) and downregulates the expression of oncogenes like c-MYC, VEGF and KRAS.[61,88] This property may be in part responsible for the inhibition of proliferation of various cancer cell lines treated with (**2**).[89-92] In other studies (**2**) showed a diverse range of binding modes with G-quadruplexes including intercalation between adjacent G-tetrads, stacking onto external G-quartets and interacting directly with TTA sequences that form the loops connecting G-tetrads. An example of the latter binding mode that was revealed by X-ray diffraction studies is shown in Figure 1.8.[93,94]

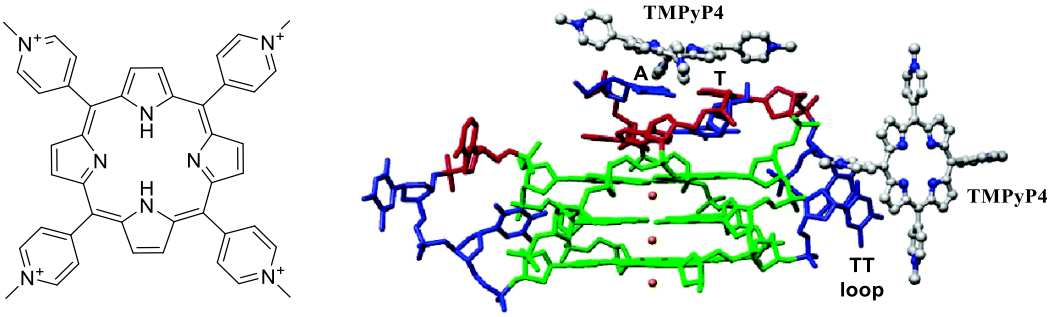

(**2**)

Figure 1.8: Crystal structure of the complex formed between (**2**) and a bimolecular human telomeric G-quadruplex (PDB ID: 2HRI). TMPyP4 binds by stacking onto the TTA nucleotides, as part of the external loop or at the 5′ region of the stacked quadruplex, without direct interaction with the G-tetrads. The crystal structure reprinted with permission from *Biochemistry*, 2007, Vol 46 (9), p. 2390-2397.[94] Copyright 2007 American Chemical Society.

It has been reported that (**2**) loses its ability to inhibit telomerase when also in the presence of high concentrations of dsDNA, and causes cytotoxicity to normal cells under these conditions.[95-97] The ability to bind to dsDNA has been proposed to be a

result of the positive charges present on (**2**).[98] The above results suggest that modifications to the structure of (**2**) are required in order to enhance its binding selectivity in favour of G-quadruplex DNA over dsDNA, and thereby reduce its toxicity to healthy cells. One method for achieving this objective is based on recognition that the central aromatic core of (**2**) is not large enough to engage in strong π–π stacking interactions with G-quartets and prevent interaction with dsDNA. It is therefore not surprising that there have been several aromatic compounds containing larger aromatic systems which have been reported to bind to G-quadruplexes. These include telomestatin (**3**), 5,10,15,20-[tetra-(N-methyl-3-pyridyl)]-26-28-diselenasapphyrin chloride (Se2SAP (**4**)) and MM41 (**5**).

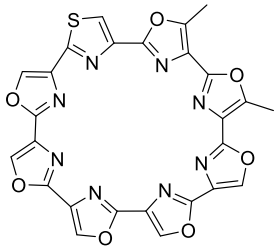

(**3**)

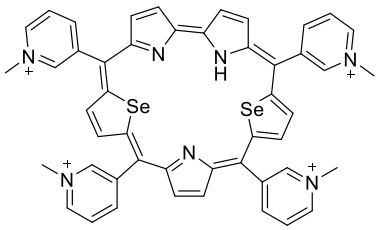

(**4**)

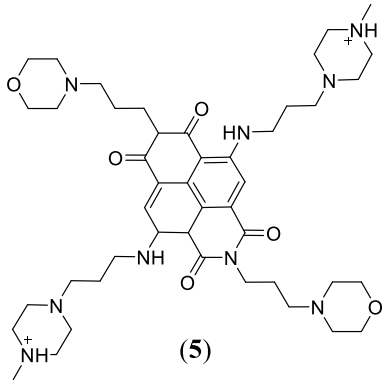

(**5**)

Telomestatin is a neutral molecule originally isolated from *Streptomyces annulatus* and later synthesised in the laboratory.[99] The tremendous propensity for (**3**) to bind to G-quadruplexes is reflected in its ability to induce their formation in the absence of monovalent cations.[100,101] It has also been reported that (**3**) binds selectively to intramolecular anti-parallel telomeric G-quadruplexes over dsDNA due to its cyclic shape and absence of an overall charge.[100,101] Further indirect evidence in support of the ability of (**3**) to bind to G-quadruplexes is provided by the results of a TRAP assay which showed that it was approximately 1000-fold more effective than TPyP4 at inhibiting telomerase (IC_{50} = 5nM).[99,100] Treatment of several cancer cell lines

with (**3**) was shown to cause dissociation of TRF2 and POT1 from telomeres leading to telomere dysfunction and apoptosis.[102-106] Despite the promising results described above, a disadvantage of (**3**) as a drug lead is its poor solubility in water, which may limit its pharmacological effects in *vivo*.[107] In addition, it is difficult to obtain from the natural source or synthesise in the laboratory.

Another example of a multi-heterocyclic compound which exhibits notable G-quadruplex binding ability is (**4**).[108] This compound was synthesised by Hurley and co-workers, who reported that it was able to convert the parallel c-MYC G-quadruplex and the anti-parallel telomeric G-quadruplex into hybrid structures.[101,108] In addition, SPR experiments revealed that (**4**) binds with a high degree of selectivity (50-fold) in favour of a c-MYC G-quadruplex over dsDNA.[108] The ligand was also shown to exhibit greater selectivity for G-quadruplexes over dsDNA than TMPyP4, and to suppress VEGF transcription in different cancer cell lines.[108,109] Unfortunately (**4**) shares one of the same disadvantages as a drug lead as tolemestatin, which is a very low-yielding method of preparation.

The G-quadruplex DNA stabilising compound (**5**) was first prepared by Neidle and co-workers.[110] They also reported the solid-state structure of the complex formed between (**5**) and an intramolecular human telomeric DNA G-quadruplex (Figure 1.9). The chemical structure of (**5**) is similar to that of (**1**) in that it has a central aromatic core with multiple attached pendant groups. It was reported that (**5**) binds strongly to G-quadruplexes present in telomeres and the promoter regions of KRAS and BCL-2. These binding events resulted in down-regulation of expression of these cancer genes and eventually apoptosis.[110,111] In addition, (**5**) has displayed notable cytotoxicity towards several pancreatic cancer cell lines, as well as against the MIA PaCa-2 pancreatic cancer xenograft model (IC_{50} =10 nM), resulting in an ~80% reduction in

tumour volume.[111] Despite these results, (**5**) does not inhibit telomerase activity at concentrations that would be expected to result in inhibition of cancer cell growth.[110] This suggests that the compound may have a complex mode of action. Despite this, it is worth highlighting that the basic structure of (**5**), consisting of a central aromatic core capable of participating in π-stacking interactions with a G-tetrad, and several pendant groups, is one that results in notable levels of G-quadruplex binding.

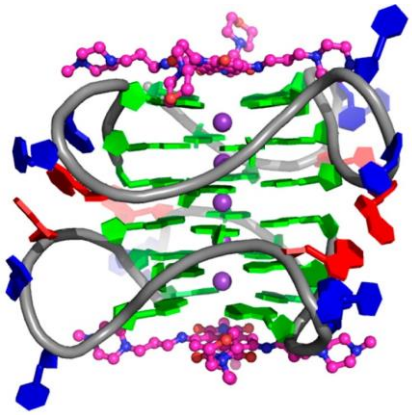

Figure 1.9: Crystal structure of the complex formed between (**5**) and an intramolecular human telomeric DNA G-quadruplex (PDB ID: 3UYH). Two asymmetric units are shown with two stacked intramolecular G-quadruplexes with MM41 (purple) bound to external 3′ G-quartet surfaces. Reprinted with permission from Journal of *Medicinal Chemistry*, 2013, 56 (7), p. 2959-2974.[110] Copyright 2013 American Chemical Society.

1.4.2 Metal complexes as G-quadruplex binding agents

Metal complexes have recently attracted growing interest as G-quadruplex binding agents in part due to their structures, relative ease of synthesis in many cases, and in some instances, demonstrated cytotoxicity towards cancer cells.[112-117] Owing to the strong affinity displayed by many of these complexes, it has been possible to determine some of the most important structural features for efficient binding of metal complexes to G-quadruplexes.[113] These include having an overall positive charge, coordinated ligands which feature an extended aromatic system, and the

metal positioned in such a way that upon binding to a G-quadruplex it becomes located above the ionic central channel of the latter to improve π-stacking interactions between the ligands and the G-quartet.

One of the earliest classes of metal complexes reported to act as G-quadruplex binding agents are metalloporphyrins such as (**6**) – (**8**). This includes complexes produced by inserting metal atoms including Ni(II), Mn(III), Zn(II) and Cu(II) into the centre cavity of (**2**). Each of the resulting complexes showed the ability to bind to and stabilise G-quadruplexes as revealed by binding studies conducted using SPR, and *in vitro* telomerase inhibition assays.[118] In addition, $[Zn(TMPyP_4)]^{2+}$ (**6**) demonstrated the ability to induce the formation of a parallel G-quadruplex DNA topology from a ssDNA molecule, whilst the corresponding manganese complex (**7**) showed an ability similar to the free ligand (**2**) to inhibit telomerase, but also exhibited an ~10-fold binding preference for G-quadruplex DNA over dsDNA.[118] This suggests that inserting the manganese ion into the centre cavity of (**2**) significantly improved DNA binding selectivity.

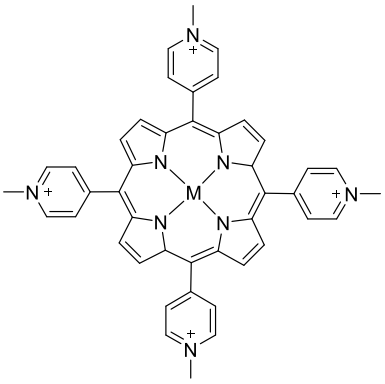

M-TMPyP4
M = Zn (**6**)
M = Mn (**7**)

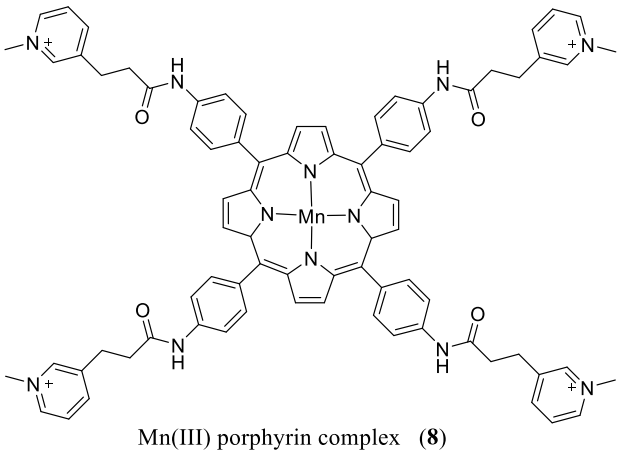

Mn(III) porphyrin complex (**8**)

Meunier and co-workers reported that the Mn(III) porphyrin complex (**8**) binds selectively with, and stabilises, a G-quadruplex formed from the sequence

((GGGTTA)$_4$), by end-stacking on the terminal G-quartets.[119] Complex (**8**) was also shown to inhibit telomerase, and in SPR experiments exhibited a 10000-fold greater degree of binding in favour of G-quadruplex DNA over dsDNA, compared to (**2**).[120] This shows that incorporating the manganese ion into (**2**) and replacing its *meso*-methylpyridinium groups by four flexible, bulkier cationic pendant groups resulted in greater G-quadruplex binding affinity and selectivity.

Teulade-Fichou and co-workers have explored the G-quadruplex binding properties of a range of metal complexes of derivatised terpyridine ligands. For example, the Pt(II) and Cu(II) complexes (**9**) and (**10**) exhibited a high degree of affinity as well as selectivity for G-quadruplex DNA.[121] These complexes were also revealed by FRET melting assays to show a greater ability to stabilise G-quadruplex DNA compared to the corresponding free ligands.[121] The same research group also investigated the DNA binding abilities of another group of metal complexes including (**11**) – (**13**).[122] This study once again confirmed the important effects the metal cation can have on DNA binding, since the corresponding free ligand showed little or no ability to do so in a FRET melting assay. Of the complexes investigated the Pd(II) derivative (**13**) exhibited the greatest ability to stabilise human telomeric G-quadruplex DNA. The results of Electrospray Ionisation Mass Spectrometry (ESI-MS) and UV/Vis spectrophotometric experiments suggested that the greater stabilisation ability of the Pd(II) derivative may attributed to its faster coordination rate (within a minute timescale) to the G-quadruplex DNA molecule compared to the other metal complexes.

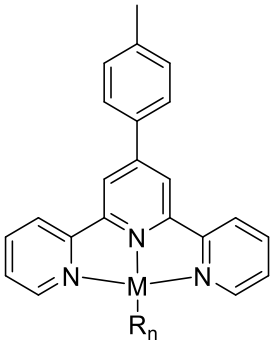

M-ttpy

M = Pt; R =Cl; n =1 (**9**)

M = Cu; R =NO_3; n = 2 (**10**)

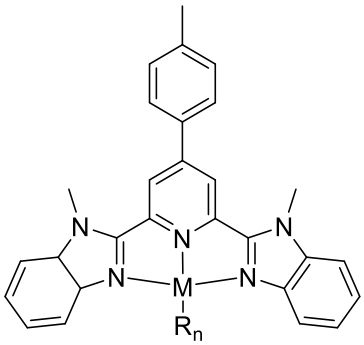

M-tMebip

M = Pt; R =Cl; n = 1 (**11**)

M = Cu; R =NO_3; n = 2 (**12**)

M = Pd; R =Cl; n =1 (**13**)

Takenaka and co-workers reported that the zinc complex (**14**) exhibited enhanced affinity towards the telomeric sequences [TAGGG(TTAGGG)$_3$] and [AGGG(TTAGGG)$_3$] in the presence of K^+ ions in comparison to the corresponding free ligand.[123] Both the free ligand and the metal complex showed notable levels of telomerase inhibition in results obtained by performing TRAP assays.

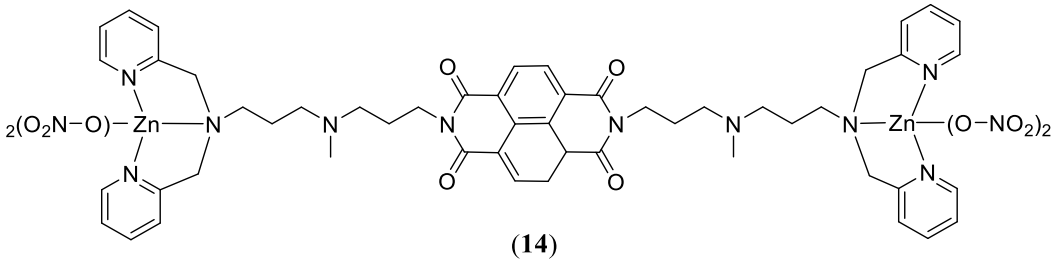

(**14**)

Modified phenanthroline ligands and their metal complexes have also received attention for their ability to bind to G-quadruplexes. For example, Reed and co-workers used FRET assays to investigate the ability of (**15**) – (**17**) to stabilise a G-quadruplex formed by the sequence (5′-FAM-d(GGG[TTAGGG]$_3$)-TAMRA-3′).[112] The platinum(II) complex with the piperidine pendant group (**17**) was found to induce a higher degree of stabilisation of a telomeric G-quadruplex than the corresponding free ligand (**16**). This suggests that the metal plays an important role

in increasing the strength of the interaction with the DNA. In addition, the results of FRET assays indicated that (**17**) exhibits more than a 40-fold selectivity factor in favour of binding to G-quadruplex DNA over dsDNA.

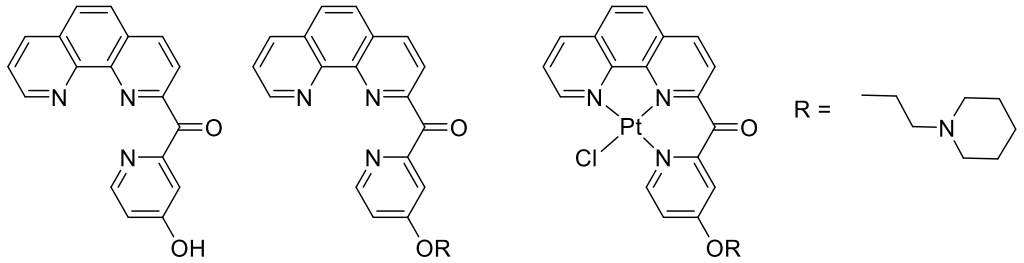

(**15**) (**16**) (**17**)

This study also showed that the free ligand with the piperidine pendant group (**16**) exhibited a greater ability to stabilise a telomeric G-quadruplex than (**15**), which has an identical structure except for the absence of the pendant group. This highlights the role that piperidine substituents, particularly once protonated, can play in enhancing the strength of interactions with G-quadruplexes. The researchers also used TRAP assays to explore the effects of each of the compounds on telomerase activity and found that (**17**) is a more potent enzyme inhibitor than either (**15**) or (**16**). This study, along with a number of those discussed above, highlight the favourable impacts introducing a metal centre and pendant groups can have upon binding affinity and selectivity towards G-quadruplexes.

1.4.3 Metal Schiff base complexes

One of the most widely studied classes of G-quadruplex binding metal complexes are those containing Schiff base ligands.[112,124,125] A pivotal study in this area was that conducted by Reed and co-workers, who reported on the telomerase inhibition and G-quadruplex binding properties of the square planar nickel(II) complexes (**18**) and (**19**).

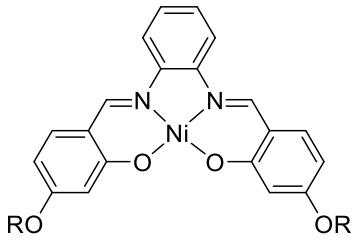

(**18**)

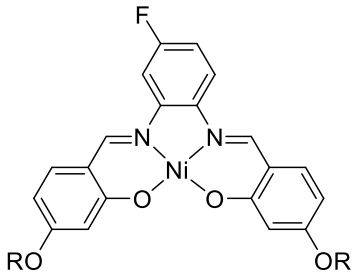

(**19**)

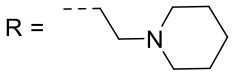

The above complexes were shown to induce telomerase inhibition with $^{tel}EC_{50}$ values of ~ 0.1 μM.[124] The results obtained from qualitative molecular modelling studies suggested the salphen (salicylidene phenylenediamine) ligands in these complexes would be able to interact with the terminal G-quartet of a G-quadruplex via π-π stacking interactions, providing a possible explanation for enzyme inhibition (Figure 1.10). In addition, electrostatic interactions between the positively charged piperidine substituents and functional groups located in the grooves of the DNA were revealed, which may also enhance the overall interaction.[124]

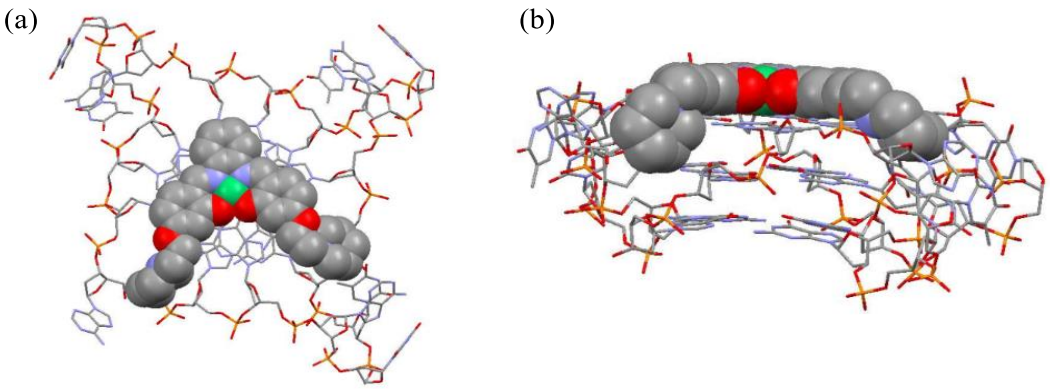

Figure 1.10: (a) top view and (b) side view of the molecular docking of (**18**) with a human parallel intramolecular G-quadruplex formed from four repeats of telomeric DNA (PDB ID: 1KF1).[124]

Later work from the same research group investigated the effects of changing the ligand framework and identity of the metal centre on G-quadruplex DNA binding properties of a number of salen (salicylidene ethylenediamine) and salphen metal

complexes including (**20**) – (**23**).[125] The results of FRET assays revealed the square planar nickel(II) salphen complex (**20**) and copper(II) salphen complex (**21**) showed a significant ability to stabilise human telomeric DNA, and binding selectivity in favour of a G-quadruplex DNA over dsDNA. In contrast, the distorted square pyramidal complexes (**22**) and (**23**) exhibited a much lower ability to raise the melting temperature, T_m, (ΔT_m = 1.4 and 10.5 °C, respectively) compared to (**20**) and (**21**) (ΔT_m = 22.9 and 21.5 °C, respectively).[125] This is consistent with the view that a complex with a square planar geometry is able to participate in stronger π–π stacking interactions with a G-quartet, whereas those with a disordered square pyramidal geometry are inhibited from doing so to different extents owing to sterically undesirable interactions involving axial hydroxido or oxido ligands.

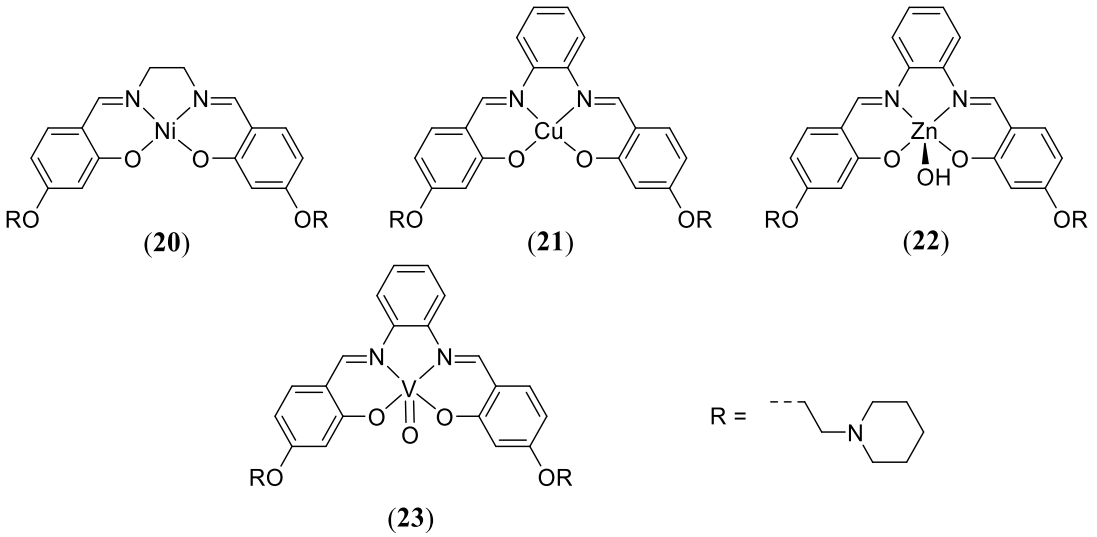

Whilst the G-quadruplex DNA binding properties of a number of different metal Schiff base complexes have now been explored, there have been very few investigations into their cytotoxicity to date. A notable contribution are studies conducted by Ansari and co-workers using complexes such as (**24**) – (**31**).[126,127] In the first of their studies, these researchers used MTT assays to examine the cytotoxicity of a series of manganese complexes of salen and derivatised salen

ligands.[126] This study showed that the Mn(III) complexes were cytotoxic towards, and able to induce apoptosis in malignant MCF7 breast cancer cells, but were non-toxic towards the non-malignant cell line (MCF10). Increasing the number of aromatic rings in the complexes, by replacing the ethylenediamine moiety of (**24**) with either *ortho*-phenylenediamine or 2,3-diaminonaphthalene to give (**25**) and (**26**), respectively resulted in slight increases in anticancer activity (IC_{50} values of 20, 15 and 11 μM for (**24**), (**25**) and (**26**), respectively).[126]

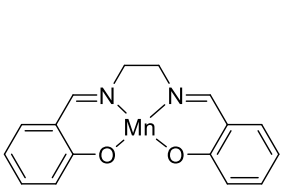

(**24**)

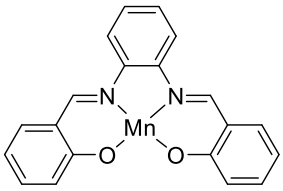

(**25**)

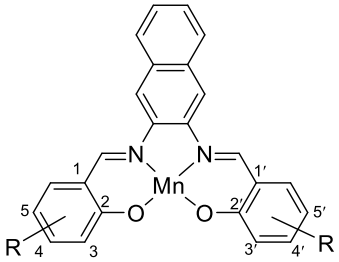

R = H (**26**)
R = 3, 3′ OMe (**27**)
R = 4, 4′ OMe (**28**)
R = 5, 5′ OMe (**29**)

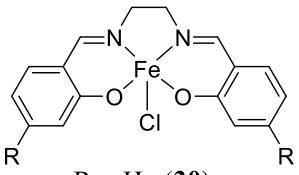

R = H (**30**)
R = OMe (**31**)

The IC_{50} values obtained for (**27**) – (**29**) were also found to vary from ~ 20 – 40 μM, showing that changing the position of substituents on the periphery of the Schiff base ligand can have an effect on cytotoxicity. It is notable that the degree of cytotoxicity and selectivity exhibited by these Mn(III) complexes towards MCF7 cells was very similar to that shown by cisplatin, highlighting the potential of these complexes as anticancer agents. In a subsequent study conducted by the same group it was shown that (**30**) and (**31**) could induce apoptosis in cultured human cancer cells, with a high degree of selectivity toward MCF7 breast cancer cells (IC_{50} = 26 and 12 μM,

respectively) and CCL228 colon cancer cells (IC_{50} = 22 and 12 μM, respectively) compared to non-malignant MCF10 breast cancer cells (IC_{50} = 31 and 38 μM, respectively).[127]

The effects of changing the metal ion or the number of aromatic rings present in a Schiff base ligand on G-quadruplex binding was also examined by Terenzi and co-workers, using complexes (**32**) – (**36**).[128] Each of the complexes featured two positively charged pendant groups located *para* with respect to the phenolic oxygen atoms. This is in contrast to where such substituents are normally located which is *meta* to the phenol. It was reported that each of the three metal complexes (**32**) – (**34**) exhibited selectivity by binding with higher affinity to a telomeric G-quadruplex compared to dsDNA, with (**32**) showing the greatest ability to stabilise the former, as evaluated by UV visible absorption spectrophotometry. The latter complex was also shown by Circular Dichroism (CD) spectroscopy to induce the formation of a G-quadruplex structure from ssDNA molecules containing the human telomeric sequence in the presence and absence of K^+ cations (Figure 1.11). This further exemplified the significant affinity of (**32**) for this type of DNA secondary structure. The results obtained from Polymerase Chain Reaction (PCR) stop assays indicated that (**32**) – (**34**) were cytotoxic towards HeLa and MCF-7 human cancer cell lines. Complex (**32**) was found to be the most cytotoxic, hinting at a relationship with G-quadruplex binding ability.

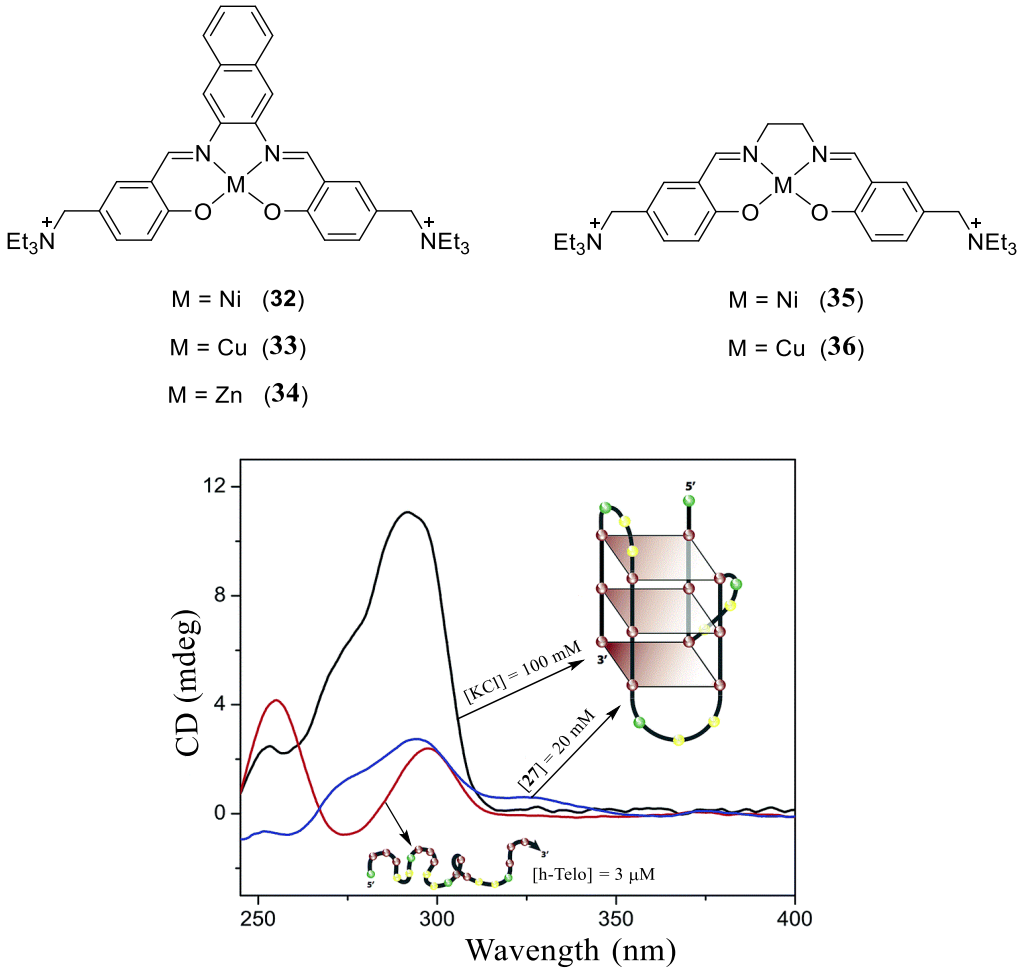

Figure 1.11: CD spectra of unfolded hTel [5′-(AGGGTT)$_3$AGGG-3′] (3 μM) (red line) and the corresponding G-quadruplexes folded in the presence of 100 μM K^+ (black line) and 20 μM (**32**) (blue line). Reprinted with permission from *RSC Advances*, 2014, 4 (63) p. 33245-33256.[128] Copyright 2014 The Royal Society of Chemistry.

In a subsequent study the ability of the salen type complexes (**35**) and (**36**) to stabilise a G-quadruplex was compared to that of (**32**) using UV-Vis spectrophotometry, CD spectroscopic and FRET techniques.[129] It was reported that removing the naphthalene moiety in (**32**) resulted in small decreases in affinity toward G-quadruplex DNA, however selectivity in binding with respect to dsDNA was significantly enhanced. For example, in the case of (**35**) no binding to dsDNA was detected via the FRET assay. It was also noted that (**35**) exhibited selectivity in

its binding to different G-quadruplex topologies, with a preference for interacting with c-KIT1 over both h-TERT and BCL2. Complex (**35**) showed a greater binding affinity towards G-quadruplex DNA than (**36**), again highlighting the effect of varying the metal centre noted previously. This may be result of the near perfect square planar geometry of (**35**) seen in the solid-state structure of the complex, which is in contrast to the distorted coordination environment present around the copper ion in the solid-state structure of (**36**). Complex (**35**) was found to exhibit cytotoxicity towards MCF-7 breast cancer cells in the presence of lipofectamine in an MTT assay (IC_{50} = 29 μM). The cytotoxicity of (**36**) was comparable to but less pronounced than that exhibited by (**35**).

The above results illustrate that, in general nickel complexes of Schiff base ligands are better G-quadruplex binding agents than either their copper or zinc analogues, owing to their typically more rigorous square planar geometries.[125,128-131] As a result it is not surprising that in recent years further research looking to develop salen and salphen complexes that function as anticancer agents as a result of their ability to bind to G-quadruplexes and inhibit telomerase have focussed on this metal.[132-135] Introducing electron withdrawing substituents such as fluorine atoms or a carboxymethyl group, as in complexes (**37**) and (**38**) was found to decrease their ability to stabilise G-quadruplex structures.[132] It was therefore surprising that (**39**), which contains a sulfonic acid group at the same position as the carboxymethyl present in (**38**), decreased binding selectivity but resulted in a greater ability to stabilise the DNA. In addition, in an attempt to enhance the G-quadruplex DNA binding affinity of the metal complex, a third ethylpiperidine substituent was added to a nickel(II) salphen complex, resulting in preparation of (**40**). FRET assays

revealed that (**40**) exhibited a high degree of binding affinity but low selectivity towards a human telomeric G-quadruplex.[132]

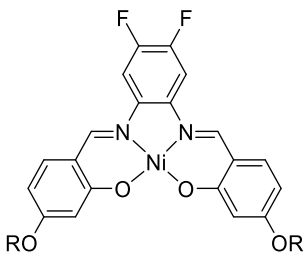

(**37**)

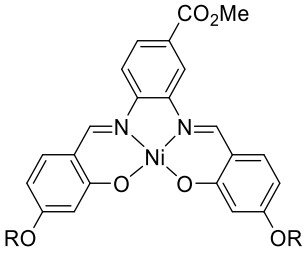

(**38**)

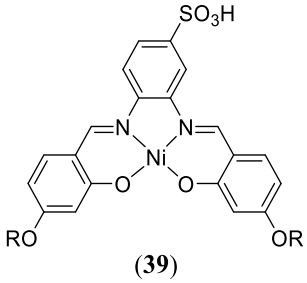

(**39**)

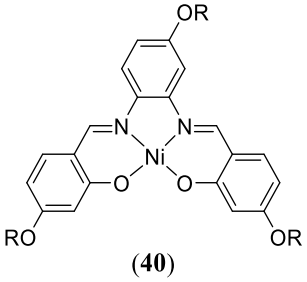

(**40**)

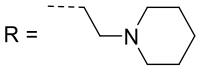

The effect of changing the number and position of dimethyimidazole pendant groups attached to a series of nickel(II) salphen complexes on their G-quadruplex DNA binding properties has also been investigated using complexes **(41**) – **(44**).[134] The results obtained from a TRAP-G_4 assay revealed that all the complexes examined could reduce telomerase activity *in vitro*, with (**44**) proving to be the most potent enzyme inhibitor (IC_{50} = 70 nM). Comparison of these results with those obtained from a standard TRAP assay utilising dsDNA showed (**44**) also exhibits a high degree of binding selectivity towards G-quadruplex DNA over dsDNA.

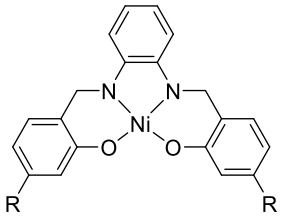

(**41**)

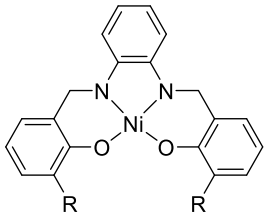

(**42**)

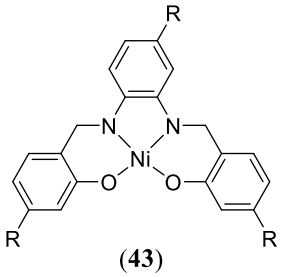

(**43**)

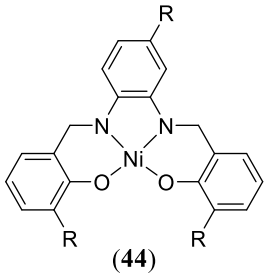

(**44**)

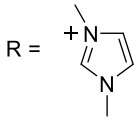

Changing the size and position of aromatic moieties present in nickel Schiff base complexes has also been shown to have a significant effect on their binding interactions with both G-quadruplex and dsDNA.[135,136] For example, results obtained from binding studies performed using ESI-MS or by examining the effect of the complexes on DNA melting temperature suggested (**18**) and (**45**) exhibited the ability to bind to both G-quadruplex and dsDNA. In contrast, (**46**) exhibited a much lower affinity towards the same dsDNA molecule than (**18**) but still showed the ability to significantly interact with a tetramolecular G-quadruplex, as illustrated by its propensity to form non-covalent adducts with the nucleic acid molecule that produced ions detectable by ESI-MS (Figure 1.12 (a)). The lack of ability to bind to dsDNA exhibited by (**46**) was attributed to the orientation of the two aromatic rings derived from the *meso*-1,2-diphenylethylenediamine moiety in a non-coplanar fashion with the rest of the Schiff base ligand. This was proposed to result in significant hindrance to intercalative interactions with the dsDNA base pairs. These results suggest that incorporating the *meso*-1,2-diphenylethylenediamine moiety may be a general approach to engendering metal Schiff base complexes with DNA

binding selectivity in favour of G-quadruplexes. In contrast, (**18**), which features one aromatic ring in the top of the Schiff base ligand coplanar with those in the rest of the molecule, showed significant binding to both G-quadruplex and dsDNA (Figure 1.12 (b)). Affinity towards dsDNA was even more pronounced in the case of (**45**), presumably as a result of a greater ability to participate in intercalative interactions owing to the presence of the three coplanar aromatic groups in the top of the ligand structure. This same structural feature may have, however, limited the ability of **(45)** to bind to G-quadruplex DNA by hindering interactions with the loops of the latter molecules.

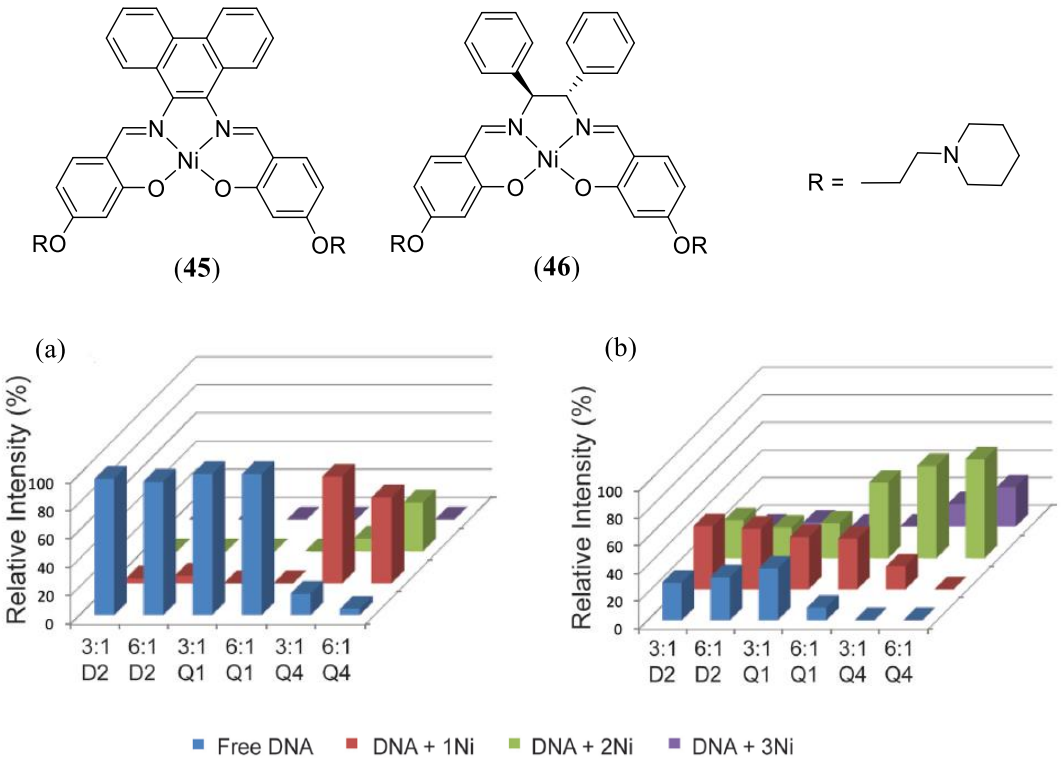

Figure 1.12: Relative abundances of ions in ESI mass spectra of solutions containing either a 3:1 or 6:1 ratio of nickel Schiff base complexes and dsDNA (D2), unimolecular G-quadruplex DNA (Q1) or tetramolecular G-quadruplex DNA (Q4): (a) solutions containing (**46**) and (b) solutions containing (**18**). Reproduced with permission from Royal Society of Chemistry, Kimberley Davis *et al*, Dalton Transactions. 2015, 44, 3136-3150.[135]

More recently, Pham and co-workers showed that the number of pendant groups attached to nickel Schiff base complexes can have a significant effect on their binding interactions with DNA.[137] These workers performed binding studies with several different types of DNA, including multiple topologies of G-quadruplexes, using ESI-MS and several other methods. Each of the nickel complexes studied featured four aromatic rings distributed around the Schiff base ligand and varied only in the number of attached pendant groups. Selected examples of the complexes investigated included (**47**) – (**49**). The results obtained from DNA binding studies indicated that (**47**) and (**48**) which have one and two pendant groups, respectively, exhibit a low degree of affinity towards both G-quadruplexes and dsDNA. Molecular docking studies performed using a G-quadruplex DNA structure and these nickel complexes revealed unfavourable stacking interactions in which the nickel ions were displaced away from above the centre of the G-tetrads, and the upper aromatic ring systems were positioned orthogonal to the G-tetrad. As a result, not all of the aromatic ring systems in these complexes were able to participate in effective π-stacking interactions.

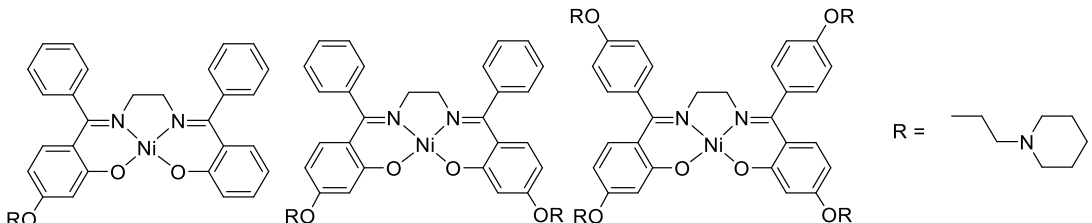

(**47**) (**48**) (**49**)

In contrast (**49**), which features four pendant groups, exhibited a significant ability to bind to both intermolecular and intramolecular parallel G-quadruplexes in spectroscopic binding studies, as well as comparatively low affinity towards dsDNA. For example, results obtained from FRET assays showed that (**47**) and (**48**) slightly increased the melting temperature (T_m) of a unimolecular G-quadruplex by 8.5 and

13 °C respectively, whereas under the same conditions addition of (**49**) resulted in an increase in T_m of 31.4 °C.

The above results were supported by those obtained from molecular docking studies performed using (**48**) and (**49**) (Figure 1.13). This showed that (**49**) was able to bind effectively to the parallel, unimolecular G-quadruplex 22AG (PDB: 1KF1) via π-stacking interactions which resulted in the nickel ion being located directly above the centre of the G-tetrad (Figure 1.13 (a)). In contrast, the nickel ion of (**48**) was not located centrally over the G-quartet (Figure 1.13 (b)).

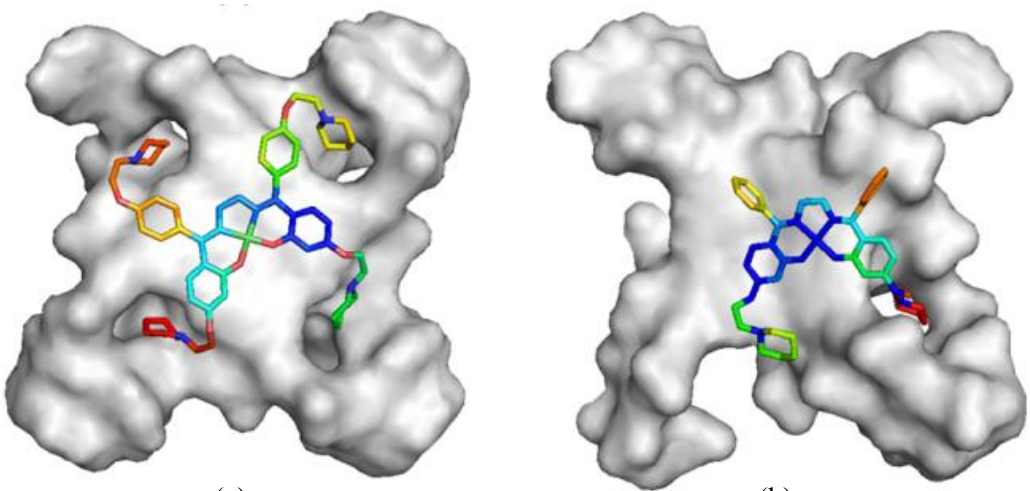

(a) (b)

Figure 1.13: Molecular docking of nickel complexes: (a) (**49**) and (b) (**48**) with a human parallel intramolecular quadruplex formed from four repeats of telomeric DNA (PDB ID: 1KF1). Reproduced with permission from Royal Society of Chemistry, Son Pham *et al*, Dalton Transactions. 2020, 49, 4843-4860.[137]

Furthermore, each of the four aromatic rings of **(49)** were able to position themselves parallel to the surface of the G-tetrad, thereby maximising the effectiveness of π-stacking interactions with the latter. In contrast, two of the aromatic rings of (**48**) were almost orthogonal to the metal ion coordination plane, and not able to participate in π–π interactions with the G-quartet. Furthermore, the pendant groups of

(**49**) were positioned so as to facilitate favourable binding interactions with the loops and grooves of the G-quadruplex.

1.5 Methods of Preparing Metal Schiff Base Complexes

Schiff bases are compounds that have the general formula RHC=N-R′, where R is an alkyl or aryl group and R′ is an aryl group. They are also known as imines, and commonly synthesised by the condensation of a primary amine with a carbonyl compound. Many Schiff bases feature NO or N_2O_2 donor atom sets suitable for binding to metal ions.[138] Coordination of metal ions to Schiff bases is generally readily accomplished simply by heating the ligands with an appropriate metal salt for brief periods, which is one of the reasons why they are attractive candidates as potential drugs.[124,125,132,134,139] For example, (**18**) may be synthesised by following the synthetic procedure outlined in Figure 1.14.[124]

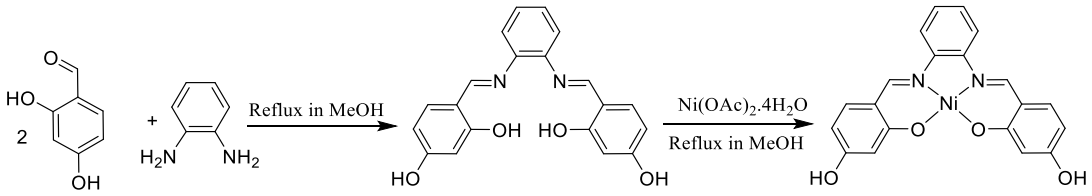

Figure 1.14: Synthetic scheme for the synthesis of (**18**).

Many other synthetic strategies have been reported for the preparation of Schiff bases and their metal complexes. These may be useful when the direct method of preparing the complexes proves surprisingly difficult, and include solid–solid synthesis, ultrasound irradiation, microwave assisted synthesis and mechanochemical synthesis.[140-143] In the following section the latter approach will be described and some recent examples of its application described.

1.5.1 Mechanochemical synthesis by ball milling

Mechanochemical (MC) synthesis involves the chemical activation of solid reactants through mechanical action such as ball milling or grinding.[141,144-147] In some cases a small amount of solvent is included in the reaction mixture to facilitate the stirring process. The latter method is known as liquid assisted grinding (LAG).[148,149] Mechanochemical synthesis methods using grinding equipment have attracted attention due to the advantages they can offer, which include greater yields, as well as the ability to perform reactions at room temperature under solvent free conditions, and with shorter reaction times. In addition, it has been shown that using MC techniques can reduce the amount of undesired by-products obtained in reactions, and thereby minimise the amount of purification that must be performed post synthesis.[150-152]

Ball milling and grinding techniques are the most widespread mechanochemical techniques utilised to apply mechanical forces in order to induce chemical reactions to occur.[143,153-155] Vibratory Ball Mills (VBM) are used for performing reactions on the milligram to gram scale. The starting materials for the reaction to be performed are placed inside the mill, which in the case of the project described in this thesis contained stainless steel jars that are charged with stainless steel balls. (Figure 1.15) The mill is then rapidly swung in a horizontal fashion back and forth with an oscillating frequency of up to 30 Hz. The chemical reagents experience mechanical stresses resulting from the friction and collisions that occur with the milling balls and the inner surface of the jar. The stresses resulting from the action of the ball mill results in the breaking of bonds and creation of new bonds to afford the desired product.

(a) (b) (c)

Figure 1.15: Photographs of equipment used to perform mechanochemical synthesis experiments described in this thesis: (a) Domel mill mix 20 synthesis apparatus; (b) milling jars and (c) milling balls. Pictures reproduced from the Domel website.[156]

Ball milling techniques have been successfully applied to a variety of organic and inorganic synthetic procedures, including amine condensation reactions and formation of metal complexes.[143,154] For example, the synthesis of salen and salphen ligands, and of their corresponding transition metal complexes, by a ball milling approach has been reported.[143,154] James and co-workers reported that salen could be successfully prepared from ethylenediamine and salicylaldehyde, using a liquid assisted ball milling method and conditions outlined in Figure 1.16.[143] The salen formed by this approach was then used in further ball milling experiments to prepare complexes with zinc, nickel and copper. For both the initial ligand preparation and subsequent metal complexation reactions, ball milling was performed for 30 min at 25 Hz and resulted in pure complexes with yields ranging from 96 to 98%.

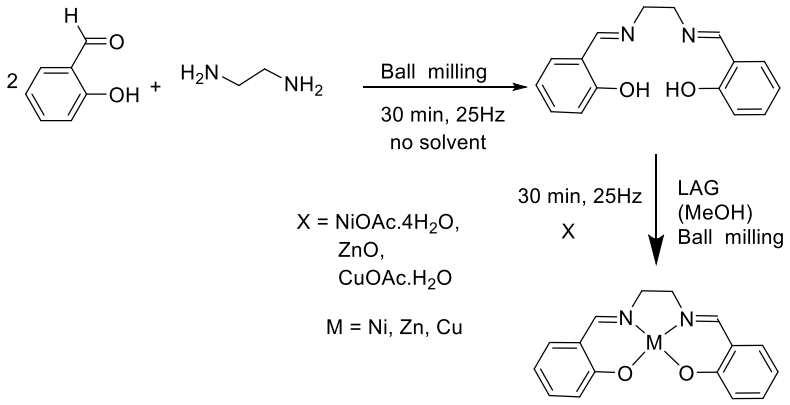

Figure 1.16: Reaction conditions used by James and co-workers in ball milling experiments to synthesise salen and some of its metal complexes.[143]

In addition, Cort and co-workers reported the LAG mechanochemical synthesis of a series of salphen ligands and their zinc, nickel and palladium complexes (Figure 1.17).[154] The yields obtained from these reactions ranged from 60 to 68%.

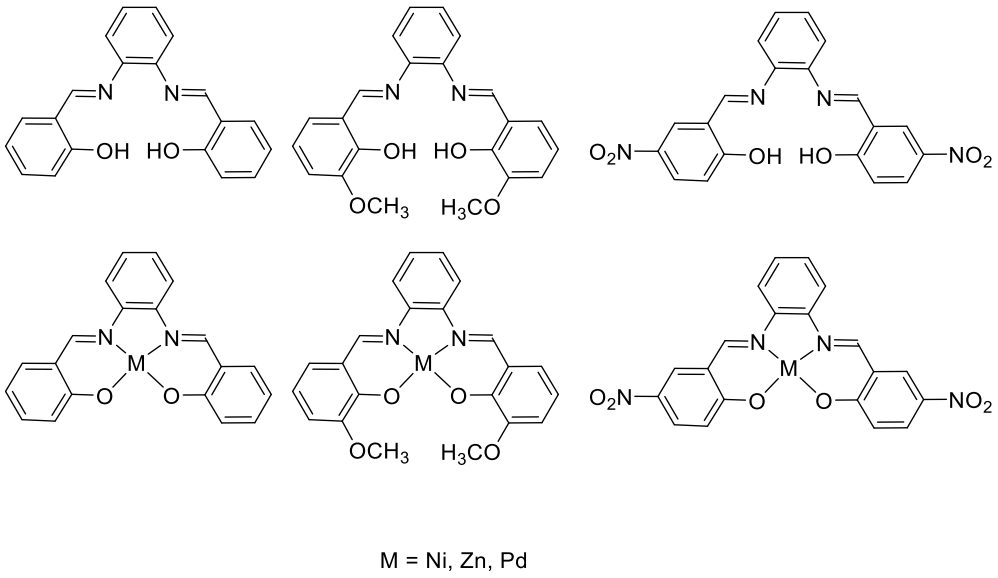

Figure 1.17: Salphen ligands and corresponding metal complexes synthesised by Cort and co-workers using a LAG ball milling approach.[154]

The results obtained from the above studies show that the mechanochemical synthesis approach can be a simple and rapid alternative to solution-based methods for preparing metal Schiff base complexes.

1.6 Aims

A number of metal Schiff base complexes have been used in DNA binding studies owing to their ease of preparation, their stability and because they possess structural features which enhance binding affinity. In the case of nickel Schiff base complexes, it has been shown that the number and position of aromatic groups, and the number and chemical composition of the pendant groups can affect the binding affinity and selectivity towards G-quadruplexes. These observations, including in particular the notable binding affinity and selectivity exhibited by (**49**), together with the significant anti-tumour activity exhibited by the organic compound (**5**), which also features four pendant groups, suggest that it would be worthwhile to prepare and study the DNA binding properties, and cytotoxicity, of a wider range of nickel complexes containing four pendant groups.

Therefore, the main aim of this project was to prepare and characterise a range of new nickel Schiff base complexes (**50** – **67**) featuring four pendant groups and comprehensively explore their DNA binding properties using different spectroscopic methods. Initial attempts to prepare these complexes were adapted from the literature method illustrated in Figure 1.14.[124] In addition, the utility of the ball milling method for preparing the complexes was explored for selected examples.

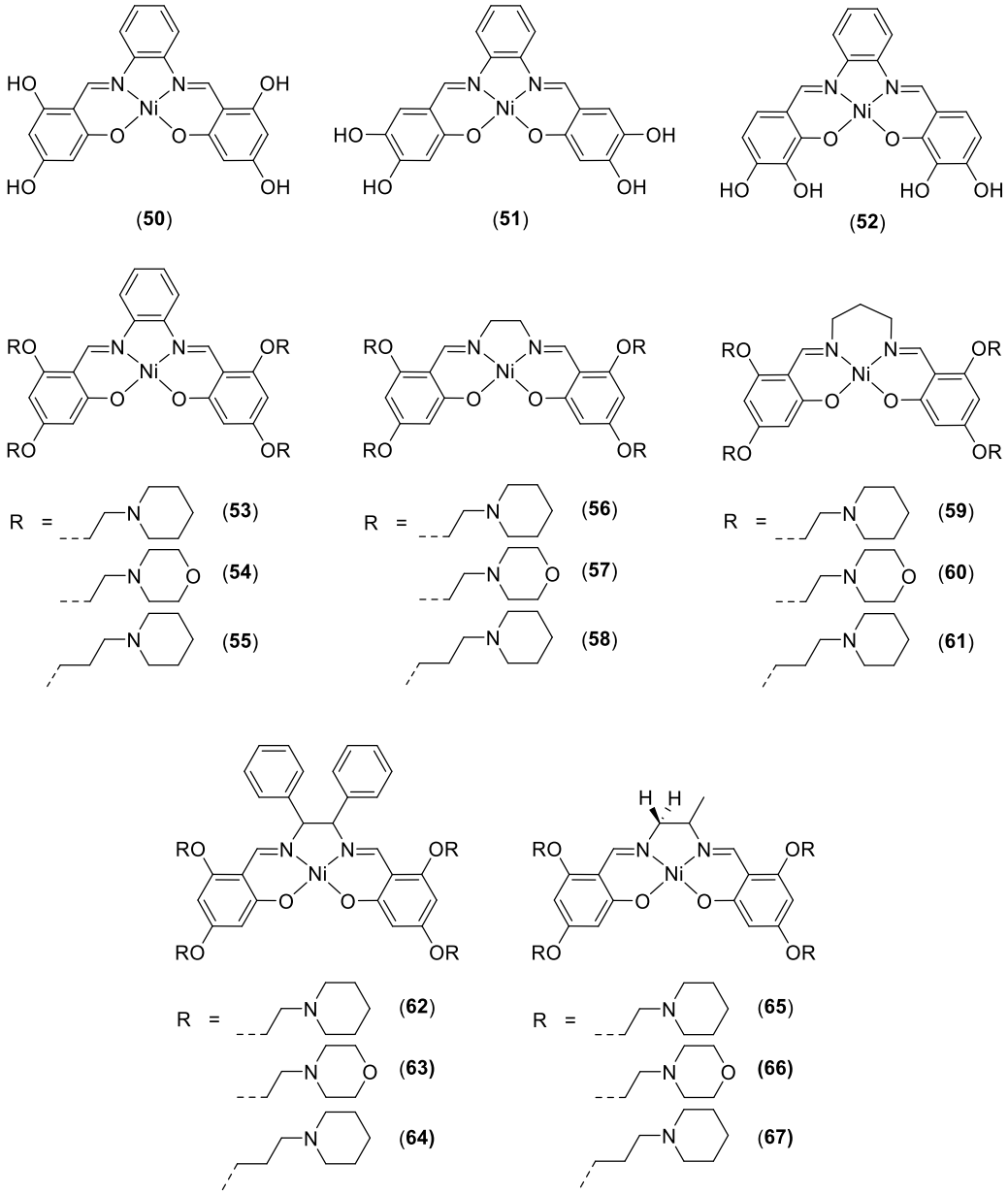

1.7 Outline of the thesis

This thesis is presented as the following chapters:

Chapter 1: This chapter reviews the literature concerning the structure of G-quadruplex DNA and its biological relevance, as well as different classes of both

organic and inorganic G-quadruplex DNA binding agents including metal Schiff base complexes and methods for synthesising the latter.

Chapter 2: This chapter provides detailed information about all the reagents and materials used in experiments, procedures for performing characterisation measurements on all new compounds, and methods for carrying out DNA binding and cytotoxicity studies.

Chapter 3: This chapter provides details of the methods used to synthesise new compounds, and characterisation data. The NMR spectra and ESI mass spectra of selected compounds and complexes are discussed in detail, and the solid-state structures of all compounds characterised using this method are also described.

Chapter 4: This chapter presents the results of binding experiments performed to examine the effect of varying the head group of nickel Schiff base complexes on their binding affinity and selectivity towards different types of DNA, including a dsDNA molecule (D2), a parallel tetramolecular G-quadruplex (Q4) and different topologies of a human telomeric unimolecular G-quadruplex (parallel Q1, anti-parallel Q1 and hybrid Q1) as well as a second parallel unimolecular G-quadruplex (c-KIT1).

Chapter 5: This chapter presents the results of binding experiments performed to examine the effect of changing the pendant groups of nickel Schiff base complexes on their binding affinity and selectivity towards the different types of DNA mentioned above.

Chapter 6: This chapter presents final conclusions based on the work described in the previous chapters as well as suggestions for future research.

Chapter 7: This chapter presents the list of references used throughout this thesis.

Chapter 2 Materials and methods

2.1 Chemicals

All solvents and reagents used in this study were of the highest grade commercially available. Milli-Q^{TM} water (Millipore, Molsheim, France) was used in all experiments. 1-(2-chloroethyl)piperidine hydrochloride, 1-(3-chloropropyl)piperidine hydrochloride, 1-(2-chloroethyl)morpholine hydrochloride, anhydrous magnesium sulfate, 1,2-phenylenediamine, 1,2-ethylenediamine, 1,2-*meso*-diphenylethylenediamine, 1,3-diaminopropane, 1,2-diaminopropane, nickel acetate tetrahydrate, $CDCl_3$, $(CD_3)_2SO$ (DMSO-d_6), high purity DMSO (≥ 99.5%), cesium iodide (Fluka brand), sodium dodecyl sulfate (SDS) and thiazolyl blue tetrazolium bromide (MTT), were all purchased from Sigma-Aldrich (Castle Hill, Australia). All oligonucleotides were also obtained from Sigma-Aldrich.

Potassium carbonate (K_2CO_3), dimethylformamide (DMF), dichloromethane (DCM), dimethylsulfoxide (DMSO), acetic acid, hydrochloric acid, methanol (MeOH), anhydrous diethyl ether (Et_2O), aluminium oxide used for column chromatographic separations, as well as acetonitrile (ACN), ammonia and ammonium acetate (NH_4OAc) were all purchased from Ajax Finechem (Seven Hills, Australia). Thiazole orange (TO) that was used in fluorescence indicator displacement (FID) assays was purchased from Chemscene (New York, USA).

Conical centrifuge tubes (10, 50 mL) and phosphate buffered saline (PBS) tablets (Oxoid brand) were obtained from Thermo Fisher Scientific (Waltham, USA). Fetal bovine serum (FBS, French Bovogen, heat-inactivated), sterile Greiner 10 and 25 mL pipettes, cell culture flasks (250 mL, 75 cm^2 surface area) and 96 well plates for

MTT assays were obtained from Interpath (Heidelberg West VIC, Australia). Penicillin-streptomycin solution, trypsin (2.5%) and Dulbecco's modified Eagle medium (DMEM, low glucose, pyruvate) were obtained from Life Technologies (Scoresby VIC, Australia).

2.2 Characterisation of nickel Schiff base complexes

2.2.1 Physical measurements

Elemental microanalysis determination for the elements carbon, hydrogen**,** nitrogen and nickel were performed at the Campbell Microanalytical Laboratory at the Department of Chemistry, University of Otago, New Zealand. NMR spectra of the nickel complexes dissolved either in DMSO-d_6 or $CDCl_3$ were obtained using Bruker 400 or 500 MHz nuclear magnetic resonance (NMR) spectrometers at 25 °C. The chemical shifts of the resonances observed in ^{1}H and ^{13}C NMR spectra were reported in ppm (δ) relative to either tetramethylsilane (TMS) or the solvent peak as an internal standard. In ^{1}H NMR spectra, the signal from the small amount of $CHCl_3$ present in $CDCl_3$ solvent was reported at 7.26 ppm, while the signal from the small amount of CD_3SOCD_2H present in DMSO-d_6 was reported at 2.50 ppm. For ^{13}C NMR spectra, the resonance from the $CDCl_3$ solvent was set to 77.7 ppm, while that from the DMSO-d_6 solvent was assigned to 39.6 ppm. Hydrogen and carbon resonances were fully assigned through the use of 2D experiments including Correlation Spectroscopy (COSY), Nuclear Overhauser Effect Spectroscopy (NOESY), Heteronuclear Single-Quantum Correlation (HSQC) and Heteronuclear Multiple-Bond Correlation (HMBC) Spectroscopy.

Electrospray ionisation (ESI) mass spectra of alkylated nickel Schiff base complexes were obtained using a Thermo Finnigan linear trap quadrupole (LTQ) mass spectrometer, using solutions prepared in H_2O:MeOH (50:50). Solutions containing metal complexes (20 μM) were injected into the instrument at a flow rate of 20 μL/min. Mass spectra of metal complexes were obtained in positive ion mode. The parameters used to obtain the spectra are listed in Table 2.1.

Table 2.1: Instrument parameters used to obtain positive ion ESI mass spectra of metal complexes

MS parameter	Setting
Capillary (V)	3500
Cone voltage (V)	10-80
RF lens energy (V)	60-80
Source block temperature (°C)	60
Desolvation temperature (°C)	140
Desolvation gas flow (L/hour)	300
Collision energy (V)	2-10
Acquisition mass range (m/z	200-1200
Multiplier	170-200

2.2.2 Crystallography

X-ray structural studies were performed by Dr Christopher Richardson of the School of Chemistry and Molecular Bioscience, University of Wollongong, Australia. X-ray diffraction measurements performed on complexes (**18**), (**20**), (**34**) and (**38**) were carried out at 150 (10) K using a Rigaku XtaLAB Mini II HPC diffractometer with MoKα radiation; λ = 0.71073 Å. Using Olex2,[157] structures were solved with the ShelXT[158] structure solution program using Intrinsic Phasing and refined with the ShelXL[159] refinement package and Least Squares minimisation.

During refinement of crystallographic structures, hydrogen atoms bonded to C were positioned geometrically and the water H atoms were based on peaks from a difference electron density map and potential H-bonded contacts. The H atoms were

initially refined with soft restraints on the bond lengths and angles to regularize their geometry (C-H in the range 0.93 - 0.98 Å, O-H = 0.82 Å) and with the isotropic displacement parameter U_{iso}(H) in the range 1.2 - 1.5 times the equivalent isotropic displacement factor U_{eq} of the parent atom, after which the positions were refined with riding constraints. The only exception to the above was for those H atoms bonded to O which were allowed to refine freely.

2.3 Preparation of Oligonucleotide solutions

2.3.1 Purification of single stranded oligonucleotides

Single stranded oligonucleotides were purchased from Sigma-Aldrich (Castle Hill, Australia), as freeze-dried 'trityl-off' derivatives. The base sequences of DNA molecules which were used in this study are presented in Table 2.2. These oligonucleotides were purified using High Performance Liquid Chromatography (HPLC) by following previously reported procedures.[160-162] Purified DNA solutions were then freeze-dried using a Savant SpeedVac (Selby-Biolab, Australia) prior to storage at -20 °C.

Table 2.2: Properties of DNA molecules used in this study.

Oligonucleotide sequence 5´- 3´	**DNA label**	**Mass (Da)[a]**
GCTGCCAAATACCTCC	D2A	4786.2
GGAGGTATTTGGCAGC	D2B	4977.3
(GCTGCCAAATACCTCC/GGAGGTATTTGGCAGC)	D2	9763.5
$(TTGGGGGT)_4$	Q4	9986.6
$GGG(TTAGGG)_3$	Q1	6653.4
GGG AGG GCG CTG GGAGGA GGG	c-kit1	6698.4

[a] Calculated using the Oligonucleotides Properties Calculator.[164]

When required, freeze-dried samples were dissolved in 1000 µL of Milli-Q™ water. Diluted solutions (300× dilution factor) were prepared by adding 2 µL of one of the

above DNA solutions to 598 μL of Milli-Q^{TM} water. In order to determine the concentration of the final DNA solutions, the absorbance at 260 nm was measured, and the molar absorption coefficients (ε) of the individual nitrogenous bases present in the DNA sequence were used to obtain an overall value of ε for the oligonucleotide itself. Values of ε for the purine and pyrimidine bases were obtained using the Oligonucleotides Properties Calculator.[163]

2.3.2 Preparation of dsDNA (D2)

Solutions containing appropriate quantities of the single stranded DNA (ssDNA) molecules D2A and D2B were mixed together in an Eppendorf tube and dried using a Savant SpeedVac. The resulting pellet was then dissolved in an appropriate volume of NH_4OAc solution (100 mM, pH 7.4) to give a final dsDNA concentration of 1 mM. The DNA was then annealed by heating in a water bath at 61 °C (the melting temperature of the DNA plus 10 °C) for 15 min,[162] after which it was allowed to cool slowly to room temperature overnight. Annealed DNA samples were kept in a freezer at -20 °C prior to further use.

2.3.3 Preparation of parallel qDNA (Q1, c- KIT1 and Q4)

An appropriate quantity of solution containing a specific ssDNA (Q1, c- KIT1 or Q4) was placed in an Eppendorf tube, dried using a Savant SpeedVac and then the resulting pellet dissolved in sufficient NH_4OAc buffer solution (150 mM, pH 7.4) to give a final concentration of 1 mM. Solutions containing the ssDNA molecule Q1 were annealed by heating in a water bath at 95 °C for 15 min, and then slowly cooling to room temperature at a rate of 5 °C/hour in order to obtain a parallel topology.[135,162] Solutions containing the ssDNA c- KIT1 were annealed by heating in

a water bath at 50 °C for 5 min, and then slowly cooling to room temperature in order to obtain the parallel topology. Solutions containing the ssDNA Q4 were annealed by heating in a water bath at 90 °C for 15 min,[137] after which they were allowed to cool slowly to room temperature overnight to form a parallel topology. Annealed DNA samples were kept in a freezer at -20 °C prior to further use.

2.3.4 Preparation of anti-parallel qDNA (Q1)

An appropriate quantity of solution containing the ssDNA Q1 was placed in an Eppendorf tube, dried using a Savant SpeedVac and then the resulting pellet dissolved in a sufficient volume of aqueous solution containing 100 mM NaCl, 15 mM NaH_2PO_4 and 15 mM Na_2HPO_4 (pH 7.4) to give a final concentration of 1 mM. The DNA was then annealed by heating the solution in a water bath at 95 °C for 10 min and then cooling immediately on ice for 30 min, after which it was allowed to come to room temperature.[137,164] Annealed DNA samples were kept in a freezer at -20 °C prior to further use.

2.3.5 Preparation of hybrid-type qDNA (Q1)

An appropriate quantity of solution containing the ssDNA Q1 was placed in an Eppendorf tube, dried using a Savant SpeedVac and the resulting pellet then redissolved in a sufficient volume of aqueous solution containing 100 mM KCl, 15 mM KH_2PO_4 and 15 mM K_2HPO_4 (pH 7.4) to give a final concentration of 1 mM. The DNA was then annealed by heating the solution in a water bath at 95 °C for 10 min and then cooling immediately on ice for 30 min, after which the solution was allowed to come to room temperature.[137,164] Annealed DNA samples were kept in a freezer at -20 °C prior to further use.

2.4 Preparation of metal complex stock solutions

Stock solutions of metal complexes were prepared at 1 mM concentration in the same buffer used for preparation of the oligonucleotide to be used in binding experiments. Since not all metal complexes were completely soluble in the buffer solution alone, some methanol was added to achieve complete dissolution. Most metal stock solutions had an initial concentration of 1 mM and were prepared using a solvent consisting of 80:20 (v/v) buffer:MeOH, however, there were some exceptions. For example, stock solutions of complexes (**20**) and (**36**) were prepared using a solvent consisting of 30:70 (v/v) buffer:MeOH. In addition, in order to ensure complete dissolution of complexes (**7**), (**54**), (**19**) and (**20**) a small amount of 100 mM HCl solution was required, and so a solvent consisting of 79:20:1 (v/v/v) buffer:MeOH:HCl) was used.

2.5 ESI-MS Mass spectrometry experiments

Metal complex stock solutions (1mM), DNA stock solutions (1mM) and the same buffer used for preparation of the DNA stock solution, were used to prepare reaction mixtures containing different ratios of DNA (final concentration = 10 μM) and nickel complex (final concentration = 10, 30, 60 and 90 μM). This gave mixtures with final metal:DNA complex ratios of 1:1, 3:1, 6:1 and 9:1. The volumes of different reagent solutions used to prepare these reaction mixtures are presented in Table 2.3.

Table 2.3: Volumes of stock solutions used to prepare nickel/DNA samples for analysis by ESI-MS.

Metal:DNA complex ratio	Volume of DNA (1 mM stock) (µL)	Volume of metal complex (1 mM stock) (µL)	Volume of buffer (µL)
1:1	1	1	98
3:1	1	3	96
6:1	1	6	93
9:1	1	9	90

ESI-MS was used to investigate the binding of nickel complexes to dsDNA and qDNA. A Waters Q-ToF Ultima^{TM} ESI mass spectrometer (Manchester, UK) was used to acquire mass spectra in negative ion mode. The instrument was calibrated using a cesium iodide (CsI) solution (1 mg/mL), prior to acquiring the spectra of samples containing DNA and nickel complexes. The samples were injected into the mass spectrometer using a Harvard model 22 syringe pump (Natick, USA) at a constant flow rate (10 µL/min). The parameters used to obtain the spectra for all experiments are listed in Table 2.4.

Table 2.4: ESI-MS conditions used for the analysis of DNA/metal complex solutions.

MS parameter	Setting
Capillary (kV)	2.10
Cone (V)	40-50
Source temperature (°C)	25
Desolvation temperature (°C)	80
Desolvation gas flow (L/hour)	100

2.6 Circular dichroism (CD) experiments

A Jasco J-810 spectropolarimeter and 0.1 cm path-length quartz cell was used to obtain CD spectra of solutions different ratios of DNA molecules and nickel complexes between 200 and 400 nm. The instrument parameters used to acquire these spectra are listed in Table 2.5.

Table 2.5: Instrument parameters used to acquire all CD spectra of nickel/ DNA samples.

CD parameter	Setting
Sensitivity	standard
Scanning speed	100 nm/min
Response	4 s
Band width	1 nm
Number of accumulations	6
Temperature	25 °C

In each case the CD spectrum was obtained first for 300 μL of solution containing DNA (20 μM) alone. Aliquots of stock solutions (**Error! Not a valid bookmark self-reference.**) containing both the same type of DNA (20 μM) and the required nickel complex (0.6 mM) were then added to the initial DNA solution in order to produce samples with DNA:metal complex ratios of 1:1, 3:1, 6:1 and 9:1. The reaction mixtures were then mixed and allowed to stand for 3 min prior to measurement of additional CD spectra.

Table 2.6: Volumes of DNA/metal complex stock solutions required for preparation of samples for analysis by CD spectroscopy.

DNA: metal complex ratio	Volume of DNA/nickel complex stock solution added (μL)
1:1	10.4
3:1	23.0
6:1	41.7
9:1	53.6

2.7 Fluorescence intercalator displacement (FID) assays

Initially, 25 μM solutions of parallel Q1 or Q4, or D2, were prepared by diluting 1 mM stock solutions of the required oligonucleotide. A 100 μM stock solution of Thiazole Orange (TO) in DMSO was also prepared. The above stock solutions were then used to prepare a working solution containing DNA (0.25 μM), TO (0.5 μM)

and the appropriate buffer. Fluorescence spectra were first obtained for the working solution containing DNA and TO only. Titration experiments were then performed by addition of a stock solution containing DNA (0.25 μM), TO (0.5 μM) and metal complex (100 μM) to the cuvette containing the initial working solution. During the titration the DNA and TO were kept at a fixed concentration. The samples were mixed and allowed to stand for 3 min prior to measurement of additional fluorescence spectra, which was continued until there was no further significant change in fluorescence intensity.

An Agilent Cary Eclipse fluorescence spectrophotometer and 1 cm path-length quartz cell together with an excitation wavelength of 501 nm was used to obtain fluorescence spectra between 515 and 750 nm.[125,165] The instrument parameters used to acquire these spectra are listed in in Table 2.7.

Table 2.7: Instrument parameters used to acquire FID spectra of nickel/ DNA/TO samples.

FID parameter	**Setting**
Excitation wavelength	501 nm
Emission wavelength	535 nm
Excitation slit width	5 nm
Emission slit width	10 nm
Scan rate	120 nm/min
Detector voltage	600 V
Temperature	25 °C

The fluorescence intensities were measured at the emission wavelength (535 nm) of TO. In order to determine the concentration of nickel complex that caused 50% displacement of TO from the DNA (DC_{50}), Stern–Volmer quenching plots were created using Equation 2.1.[137,165,166]

$$\frac{I_o}{I} = 1 + kc \ldots\ldots\ldots \quad (2.1)$$

In this equation I_o and I are the maximum fluorescence intensity of DNA/TO in the absence and presence of nickel complex, respectively. In addition, c is the concentration of nickel complex and k is the Stern-Volmer constant. When $I_o/I = 2$, c = DC_{50}. Values of DC_{50} were calculated from lines of best fit. Experiments were performed in triplicate in order to obtain an average value of DC_{50} and standard error of the mean.

2.8 Fluorescence resonance energy transfer (FRET) assays.

Metal complex stock solutions (1 mM) were diluted using MilliQ^{TM} water to afford a series of intermediate solutions with concentrations of 5, 10, 20 and 25 μM. The FAM-TAMRA labelled oligonucleotide F21T (HPLC purified) was dissolved in MilliQ^{TM} water to prepare a 100 μM stock solution. This solution was then diluted to a concentration of 0.25 μM using a solution containing 12.5 mM lithium cacodylate (pH 7.4) and 125 mM NaCl.[135,162] The DNA solution was then annealed by heating in a water bath at 95 °C for 5 min after which it was cooled immediately on ice for 30 min.

Fluorescence measurements were recorded using fluorescence capable 96-well plates that were covered with adhesive films after solutions were added. The final volume of the solution in each sample well was 25 μL, which consisted of 20 μL of 0.25 μM stock oligonucleotide, and 5 μL of 5, 10, 20 or 25 μM metal complex stock solution. This gave reaction mixtures in each sample well with a final concentration of 0.2 μM oligonucleotide, and 0, 1, 2, 4, 5 or 10 μM nickel complex. Duplicates of each reaction mixture with a specific nickel:DNA ratio were prepared on each plate. The 96-well plates were then sealed and centrifuged at 1000 rpm for 1 min at 25 °C.

A Bio-Rad CFX96 Polymerase Chain Reaction (PCR) instrument was used to monitor the fluorescence emission as the temperature was gradually increased from 25 to 95 °C at a ramping rate of 1 °C/min. An excitation range of 450 - 490 nm and an emission range of 510 - 530 nm was used. Six filtered LEDs (light emitting diodes) were used as the excitation source. The fluorescence data from at least three separate plates were averaged and normalised between 0 and 1 using GraphPad Prism 8. Values of the melting temperature (T_m) were then obtained by fitting the data with a four-parameter equation.

2.9 DNA melting experiments

A Varian Cary 100 UV-Vis-NIR spectrophotometer with a 1 cm path-length quartz cuvette and a filter size of 101 were used to monitor the absorbance of solutions containing the dsDNA D2 at 260 nm as the temperature was gradually increased from 25 to 90 °C at a ramping rate of 1 °C/min. This resulted in production of a DNA melting curve, which was also obtained for solutions containing nickel complex:D2 ratios of 0:1, 3:1 and 6:1. All solutions contained 1 μM DNA in 100 mM NH_4OAc at pH 7.4. The cuvette containing the solution was covered to minimise solvent evaporation. Solutions containing both DNA and nickel complex were allowed to stand at room temperature for 10 min prior to measurement. The melting temperatures (T_m) were calculated using Varian software that was supplied with the instrument. Experiments were performed in triplicate in order to obtain average values of T_m and standard errors. Melting curves were normalised using GraphPad Prism 8.

2.10 Molecular docking experiments

2.10.1 Preparing receptors (DNA molecules) for docking studies

The crystal structures of unimolecular parallel qDNA and dsDNA used in docking studies were retrieved from the RCSB protein data bank. The base sequences and PDB ID's of the DNA molecules are provided in Table 2.8. In order to validate the DNA structures, it was necessary to use the following Procheck online server: https://swift.cmbi.umcn.nl/servers/html/prepdock.html. These structures were then relaxed by minimizing their energy with the steepest descent algorithm (3000 steps) by using the Accelrys DS visualizer 2.0 software together with the CHARMM22 force field.[167-169] During this step water molecules were deleted from the DNA molecule present in the PDB file. AutoDock Tools v1.5.6 (ADT)[170] software was used to generate PDBQT format files for each DNA molecule by adding partial charges (Q), assigning atom types (T) and protonating the oligonucleotide in the PDB file.

Table 2.8: Structures, base sequences and PDB ID's of oligonucleotides used in molecular docking studies

Structure	PDB ID	Base sequence
Unimolecular parallel G-quadruplex	1KF1[15]	$AGGG(TTA\ GGG)_3$
Duplex DNA	1KBD[171]	(5´- CTG GGG ACT TTC CAGG -3´) /(5´- CCT GGA AAG TCC CCAG -3´)

2.10.2 Preparing the ligands (complexes) docking studies

All initial ligand geometries were designed using ChemDraw Professional v17.1 except for (**53**) and (**65**). For the latter nickel complexes their crystallographically determined geometries were used without further optimisation. Structures derived

using ChemDraw were converted to three-dimensional structures and hydrogen atoms added by using OpenBabel v3.0.0.[172] The resulting structures were then subjected to an initial energy optimization by using Avogadro v1.2.0.[173] These optimisation procedures were performed using the Universal Force Field (UFF) and four steps per update with the Steepest Descent algorithm, after which the Gaussian input file was generated. Subsequently, the structures were fully optimized at the B3LYP/6-31G(d,p) level of theory by using Density Functional Theory (DFT) calculations within the Gaussian09 electronic structure program.[129,174] The calculations were run on the High Performance Cluster (National Computational Infrastructure (NCI)) located at the Australian National University (ANU). The Gaussian output files were generated in a log file format which was then converted to PDB files by using OpenBabel software. In addition, the cif files corresponding to the X-ray crystal structures of (**53**) and (**65**) were also converted to PDB file format by using OpenBabel software. The latter were then converted to PDBQT file format using ADT, which was employed to add partial charges (Q) and assign atom types (T) to each atom in the ligand. ADT was also employed to allow flexibility in the ligand by defining the rotatable bonds.

2.10.3 Molecular docking procedure

Blind molecular docking experiments were performed using AutoDock Vina v1.1.2.[175] The docking procedure used was reported previously.[137] For each docking experiment the DNA receptor was kept rigid while the nickel complex was allowed to be flexible and featured rotatable bonds. The location of the docking site in three dimensions (x, y, z) was determined by using VMD v1.9.3 (Visual Molecular Dynamics software). The grid box which determines the search space was centred at

the receptor, and selected to be 30 × 30 × 70 grid points spaced 0.375 Å apart. This size was chosen as it is sufficiently large to ensure coverage of all active sites on the receptor and to allow the nickel complex to freely rotate in order to get the most stable docking structure.

The last step of the molecular docking procedure was to submit a configuration file to AutoDock Vina v1.1.2.[168,169,175] The configuration file contained all the required docking parameters which includes the location and the size of the docking site in three dimensions, the exhaustiveness, CPUs (central processing units), the required number of binding modes and the names of the receptor and ligand PDBQT files.

Upon completion of a docking experiment two separate output files were generated. The first was obtained in a log file format and contained the docking free binding energies (given in kcal/mol) for all requested binding modes. The second output file was in PDBQT format and contained information about the conformations of the nickel complexes docked with the two different DNA molecules. These configurations were visualized using PyMol v1.3,[176] [176] which was also used to generate the artwork presented in this thesis.

2.11 Cell Culture

Chinese hamster lung cancer (V79) cells were obtained from Prof P. Lay (University of Sydney) as frozen permanents. The cells were stored in liquid nitrogen in 2 mL of solution containing 50% (v/v) DMEM growth medium, 40% FBS and 10% (v/v) DMSO at a density of 4×10^6 cells per mL. When required cells were thawed from a frozen permanent and grown in 25 cm^2 cell culture flasks containing 25 mL complete medium. The latter was comprised of low glucose DMEM growth medium supplemented with 10% fetal bovine serum (FBS) and 1% penicillin/streptomycin.

Culture flasks containing cells were incubated at 37 °C under an atmosphere of 5% CO_2 and 95% air in a Revco Ultima incubator (Twinsburg, USA). The cells were sub-cultured twice a week by using phosphate buffered saline (PBS) (10 ml) for washing the cells and 0.25% (w/v) trypsin in PBS (5 ml) for lifting the cells from the surface of the flasks.

2.12 MTT Assays

2.12.1 Preparation of treatment solutions containing the nickel complexes

Treatment solutions containing nickel complexes were prepared by first dissolving the required amounts in order to obtain the highest concentrations possible in DMSO. The resulting stock solutions were then serially diluted using DMSO to afford a range of intermediate solutions with different concentrations. Each of these was then diluted 50 times with incomplete medium (DMEM) to give the final nickel treatment solutions. The final concentration of DMSO in the latter was 2% (v/v). Nickel treatment solutions were prepared immediately prior to use.

2.12.2 MTT Assays procedure

The cytotoxicity of nickel complexes was assessed using the MTT assay.[177] This assay is used to measure the cellular toxicity of small molecules by quantifying the extent of mitochondrial enzymatic reduction of the yellow compound 3-(4,5-dimethylthiazol-2-yl)-2,5-diphenyltetrazolium bromide (MTT) to form the purple formazan, (*E*,*Z*)-5-(4,5-dimethylthiazol-2-yl)-2,5-diphenylformazan (Figure 2.1).[178] This cellular reduction reaction occurs in viable cells with functioning

mitochondria.[179] The amount of purple formazan produced is directly proportional to the number of viable cells, and an IC_{50} value (concentration of complex which results in only 50% of all treated cells remaining viable) can be determined from this data, with smaller values of IC_{50} indicating the compound(s) is/are more cytotoxic.

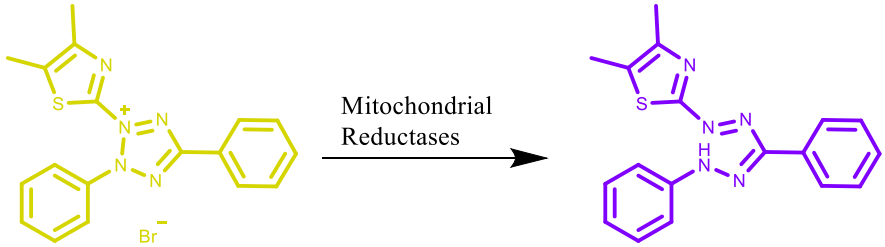

Figure 2.1: Reduction of yellow MTT to form a purple formazan compound.

V79 cells (4 ×10^4 cells in 100 µL/well) were seeded into 96-well plates in complete growth medium and incubated at 37 °C, 5% CO_2 for 24 h prior to treatment to allow the cells to adhere to the bottom of the wells. The cell medium was then removed by aspiration and replaced with freshly prepared treatment solutions (100 µL) with a range of concentrations, while incomplete DMEM medium (100 µL) was added to the control well cells. The plates were then incubated at 37 °C, 5% CO_2 for 24 h after which MTT solution (20 µL, 5 mg/mL in PBS) was added to the wells and the plates incubated at 37 °C, under an atmosphere of 5% CO_2 for 4 h to allow for formazan development. The resulting purple crystals were dissolved by adding a solution of 10% sodium dodecyl sulfate (SDS) in 0.01 M HCl (100 µL) to the wells and then the plates were incubated at 37 °C, 5% CO_2 overnight. The absorbance of the solutions in the wells was then measured at 570 nm (formazan absorbance) and 630 nm (background reading) by using a BMG LabTech Polarstar Omega microplate reader. Concentration-response curves were produced using equation 2.2 to enable

calculation of the percentage MTT conversion for each compound at each concentration of nickel complex.

$$\text{MTT conversion (\%)} = \frac{A_{570}\text{-}A_{630}\ \text{(treated cells)}}{A_{570}\text{-}A_{630}\ \text{(untreated cells)}} \times 100 \qquad (2.2)$$

Experiments were performed in triplicate in order to obtain average values of IC_{50} and standard errors of the mean. Each plate contained 6 control wells and 6 wells for each concentration of nickel complex. The calculated MTT conversion was plotted against the treatment concentrations to enable determination of the IC_{50} value of each compound.

Chapter 3 Synthesis and characterisation of nickel Schiff base complexes

3.1 Introduction

This chapter discusses the results obtained whilst developing methods for synthesising a series of new nickel Schiff base complexes with different amines and substituents attached to the aromatic rings. This includes discussion of NMR spectroscopic characterisation data for representative compounds. Full spectroscopic data and detailed synthetic procedures are also provided in this chapter, along with ESI mass spectrometric and elemental analyses data. The solid-state structures of some of the complexes, which were determined using X-ray crystallography, are also analysed.

3.2 Discussion of synthetic methods

Binding selectivity in favour of G-quadruplex over dsDNA was the main feature sought in the new nickel Schiff base complexes reported in this thesis. It was hoped that the desired selectivity might be obtained through incorporating four pendant groups into the structures of each of the complexes. These would enable additional binding interactions with the loops and the grooves of G-quadruplex DNA structures, whilst simultaneously inhibiting intercalation with dsDNA owing to steric hindrance.

3.2.1 Synthesis of nickel complexes (adapted literature method)

Initial attempts to synthesise nickel Schiff base complexes with four pendant groups were based on an adaptation of a widely used literature method.[124] This adapted procedure involved two steps and is illustrated in Figure 3.1 using the synthesis of complexes (**50**) and (**53**) as an example. In the first step, 1,2-phenylenediamine was reacted with 2,4,6-trihydroxybenzaldehyde in the presence of nickel acetate to afford the precursor complex (**50**). In the second step the isolated precursor complex was reacted with an excess of 1-(2-chloroethyl)piperidine in anhydrous solvent (DMF) in the presence of a weak base (K_2CO_3).

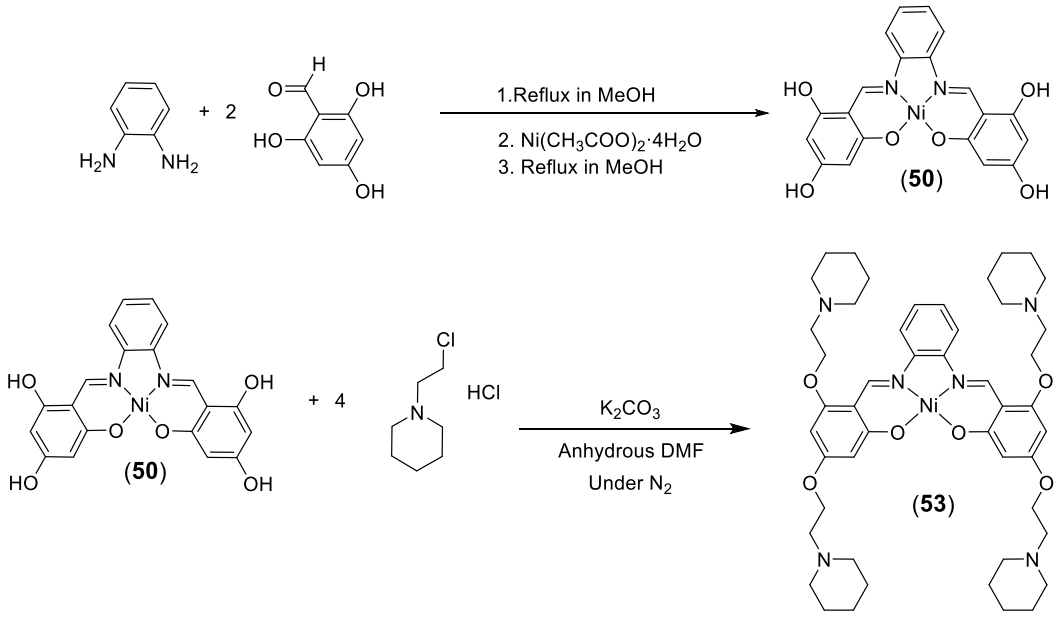

Figure 3.1: Initial reaction scheme used for the solution-based synthesis of nickel Schiff base complexes with four pendant groups.

Precursor complexes (**51**) and (**52**) were synthesized by analogous reactions involving 1,2-phenylenediamine and either 2,3,4- or 2,4,5-trihydroxybenzaldehyde, respectively. During the first synthetic step, prior to the addition of nickel acetate, transparent solutions that were red or orange in colour were formed. Subsequent

addition of nickel acetate resulted in formation of (**50**) and (**51**) as coloured precipitates. In contrast, complex (**52**) did not form a precipitate and a different isolation procedure had to be developed. This involved removal of the solvent by evaporation, and suspension of the resulting solid in water after which (**52**) was isolated via filtration. The three precursor complexes were purified by washing with MeOH, diethyl ether and water, before being dried under vacuum then in an oven (80 ˚C, 24 h).

Complexes (**51**) and (**52**) were obtained as insoluble solids and therefore could not be characterised by NMR spectroscopy and ESI mass spectrometry. Their lack of solubility is attributed to the formation of an extensive network of intermolecular hydrogen bonds in the solid state owing to the presence of multiple hydroxyl groups. In contrast, while (**50**) was insoluble in many common organic solvents such as methanol, ethanol, and chloroform, it was soluble in both DMSO and DMF. The successful formation of (**50**) was therefore able to be confirmed using NMR spectroscopy and ESI mass spectrometry

The alkylation of complexes (**51**) and (**52**) according to the reaction scheme outlined in Figure 3.1 could not conducted due to their insolubility. However, an alkylation reaction was carried out using (**50**) in an attempt to obtain (**53**). This reaction was performed using 8 equivalents of 1-(2-chloroethyl)piperidine over a period of 72 hours at 25 ˚C in DMF under N_2, and afforded (**53**) in ~ 1% yield. Examination of the product mixture using ^{1}H NMR spectroscopy indicated that a significant amount of the starting material had not reacted. In an attempt to improve the yield and purity of (**53**) a range of different reaction conditions were trialled. These included increasing the reaction temperature to 50 ˚C, as well as use of a longer reaction time

(10 days) and larger excess of alkylating agent. However, despite the efforts invested, no improvement in yield and purity were achieved.

The limited success achieved by performing the above reactions may be a result of the presence of traces of water in the reaction mixtures. Complete removal of water was very difficult since (**50**) is obtained as a hydrated complex. In the presence of even traces of water, the K_2CO_3 used in the reaction mixture would have produced significant quantities of hydroxide ions which could have reacted with the alkylating agent before it had a chance to react with (**50**). Another possible explanation for the very low yields of (**53**) in these reactions was that it may have decomposed as a result of heating during the evaporation of the DMF solvent in order to isolate the complex. However, when the procedure was repeated but with the DMF allowed to evaporate slowly at room temperature over a period of 10 days, there was no improvement in the purity or yield of the complex. Therefore, alternative pathways were sought to synthesise the target complexes.

3.2.2 Synthesis of nickel complexes (synthesis by ball milling)

The first alternative approach that was explored was mechanochemical synthesis at room temperature. Complexes (**50**), (**51**) and (**52**) were synthesised by dry milling a mixture of 1 mmol of 1,2-phenylenediamine, 2 mmol of the appropriate aldehyde, and 1.2 mmol of nickel acetate at 20 Hz for 2 h (Figure 3.2). The milling procedure resulted in red clay-like products which probably still contained some water and acetic acid. After being allowed to dry in air overnight, the products were able to be collected by scraping off the walls of the milling jar. They were then washed with cold MeOH and water to afford the final materials in yields ranging from 92 to 98%.

Complexes (**51**) and (**52**) obtained via the mechanochemical route were found to be soluble in DMSO, in contrast to the products obtained via the solution methods. This enabled their characterisation by NMR spectroscopy and ESI mass spectrometry.

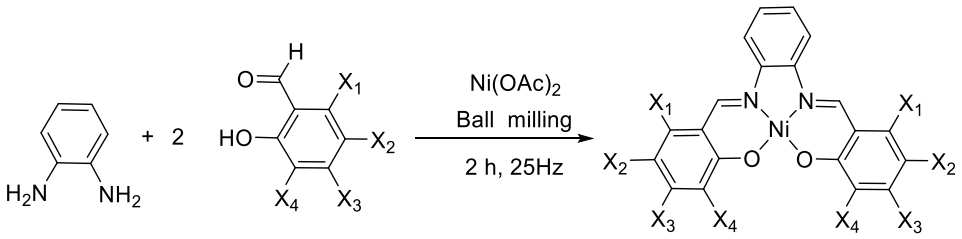

(**50**) X1 = OH , X2 = H, X3 = OH, X4 = H

(**51**) X1 = H , X2 = OH, X3 = OH, X4 = H

(**52**) X1 = OH , X2 = H, X3 = OH, X4 = H

Figure 3.2: Synthetic scheme for production of (**50**), (**51**) and (**52**) by mechanochemical synthesis.

In view of the successful synthesis of the three precursor complexes (**50**), (**51**) and (**52**) it was decided to see if the ball milling approach could be used to successfully react each with 1-(2-chloroethyl)piperidine. An initial attempt to prepare (**53**) used 1 equivalent of (**50**), 4 equivalents of 1-(2-chloroethyl)piperidine hydrochloride and 4.5 equivalents of anhydrous K_2CO_3. After the reaction mixture was subjected to ball milling at a frequency of 25 Hz for 1 h, and subsequent workup, an insoluble dark solid was obtained which could not be characterised by either NMR spectroscopy or ESI mass spectrometry. Altering reaction conditions including milling time, operating frequency, quantities of reagents and introduction of a small amount of DMF did not improve the reaction outcome. Since this method could not be successfully applied to obtain (**53**) it was decided to not use it to attempt to synthesise (**54**) and (**55**) from (**51**) and (**52**), respectively.

3.2.3 Synthesis of nickel complexes (organic precursor method)

In view of the problems described above which were encountered during attempts to prepare the target nickel complexes, a third approach employing a common organic precursor was developed. This new procedure is outlined for one series of complexes in Figure 3.3 and was developed by modifying a previously reported method.[125] The key step in the procedure is the initial selective di-alkylation of 2,4,6-trihydroxybenzaldehyde at only one of the *ortho* as well as the para positions. It was anticipated that only two hydroxyl groups would react, since the second *ortho* hydroxyl group would be protected by a hydrogen bond with the carbonyl oxygen of the aldehyde.

Initial attempts to alkylate 2,4,6-trihydroxybenzaldehyde were made using 1-(2-chloroethyl)piperidine, and were performed in anhydrous acetone in the presence of K_2CO_3. This reaction was performed under a variety of conditions in order to optimise the yield and purity of the desired product, compound (**68**) (Table 3.1).

During initial attempts to synthesise (**68**) an excess of 1-(2-chloroethyl)piperidine was used to minimise the chance of obtaining mono-alkylated compounds as by-products. This led to the formation of a mixture of di- and trialkylated compounds. Therefore, subsequent attempts used either less than or exactly the stoichiometric amount of the alkylating agent. Unfortunately, this again resulted in a formation of a mixture of di- and trialkylated compounds. As each of these initial reaction mixtures used an excess of K_2CO_3, it was decided to then examine the effect of using smaller quantities of the base. This change in reaction conditions enabled the selective di-alkylation reaction to take place successfully. Furthermore, when the reaction

temperature was increased from 25 ˚C to 40 ˚C the reaction time was able to be shortened from 6 to 3 days and the yield increased from 20 to 32%.

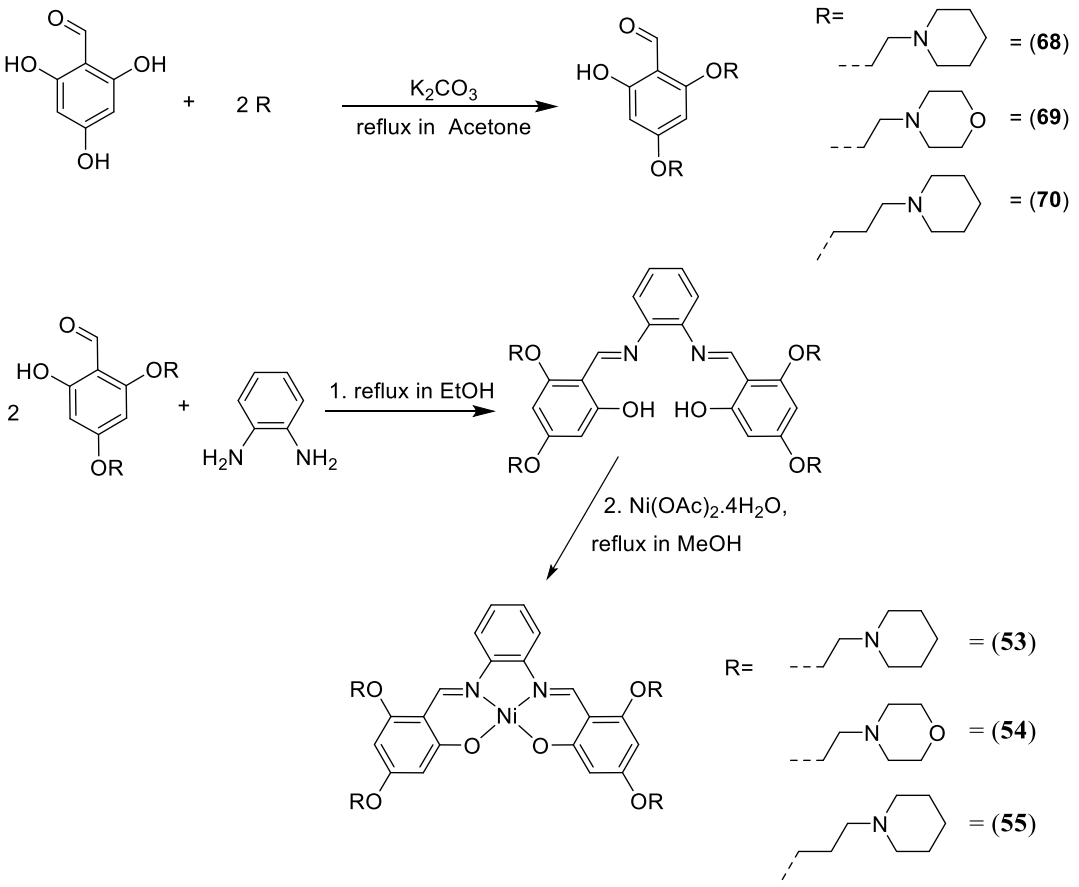

Figure 3.3: Synthetic scheme for the synthesis of nickel Schiff base complexes (**53**), (**54**) and (**55**) using alkylated organic precursor compounds.

Table 3.1: Reaction conditions employed during attempts to prepare (**68**)

Time (days)	**Temperature (°C)**	**Equivalents of benzaldehyde**	**Equivalents of 1-(2-chloroethyl)-piperidine**	**Equivalents of K_2CO_3**	**Yield (%)**	**Product Mixture**
6	25	1	2.5	3	22	di- and tri-alkylated products
6	25	1	2	3	31	di- and tri-alkylated products
6	25	1	1.5	3	26	di- and tri-alkylated products
6	25	1	2	2.5	20	di-alkylated product only
3	40	1	2	2.5	32	di-alkylated product only

Compound (**68**) was soluble in water and a number of organic solvents including DCM, $CHCl_3$ and ethyl acetate. This facilitated its purification, by solvent extraction first of all into $CHCl_3$ and subsequently using ethyl acetate. Confirmation that (**68**) had been successfully prepared was provided by elemental analysis, as well by ESI mass spectrometry and NMR spectroscopy.

After the successful synthesis of (**68**), the same synthetic procedure was used with only minor modifications to enable both (**69**) and (**70**) to be obtained. The changes consisted of replacing 1-(2-chloroethyl)piperidine hydrochloride in the reaction mixture with 4-(2-chloroethyl)morpholine hydrochloride in order to prepare (**69**), and with 1-(3-chloropropyl)piperidine hydrochloride in order to synthesise (**70**). The successful preparation of (**69**) and (**70**) was confirmed by elemental analysis, ESI mass spectrometry and NMR spectroscopy.

Initial attempts to synthesise (**53**), (**54**) and (**55**) used the two-step procedure illustrated in Figure 3.3. In the first step the free Schiff base ligand was synthesised

by bringing to reflux two equivalents of (**68**), (**69**) or (**70**) and one equivalent of 1,2-phenylenediamine in ethanol for 1h. The solvent was then evaporated and replaced with methanol. $Ni(OAc)_2 \cdot 4H_2O$ was then added and the reaction mixture again held at reflux for a further 4 h. This procedure led to very low yields of the desired products as well as recovery of significant amounts of the starting materials (Table 3.2).

Table 3.2: Effect of changing reaction conditions on the yield and purity of (**53**), (**54**) and (**55**) obtained in reactions using organic precursor compounds.

Product	Two-step process		One-step process	
	Reaction time (h)	% Yield	Reaction time (h)	% Yield
(**53**)	1, 4	impure	4	59
	24, 24			
(**54**)	24, 24	impure	4	42
			24	54
(**55**)	24, 24	impure	4	28
			24	50

Increasing the reaction time of one or both of the two steps did not improve the yield or purity of any of the desired products (Table 3.2). Attempts to purify the free Schiff base ligand obtained via the first step were unsuccessful. This included washing the product with water and recrystallisation from different organic solvents including EtOH, acetone and mixtures of DCM/Et_2O and DCM/petroleum spirit. In contrast, when the reaction was performed by bringing to reflux in methanol all of the starting materials in one step the desired products were obtained in low to moderate yield and with high purity (Table 3.2). The formation of the desired tetra-alkylated complexes was confirmed by elemental analysis, mass spectrometry and NMR spectroscopy.

The one step reaction pathway used to synthesise complexes (**53**), (**54**) and (**55**) was used to synthesise all of the remaining targeted tetra-alkylated complexes, except for (**65**) and (**66**), which contain the 1,2-*meso*-diphenylenediamine moiety. The latter

two complexes were, however, able to be successfully synthesised using the two-step reaction approach. In contrast, when attempts were made to prepare these complexes using a one-step procedure, impure products were obtained.

A total of fourteen new nickel Schiff base complexes were synthesised by the reaction of (**68**), (**69**) or (**70**) with one of five different diamines in the presence of nickel acetate, as outlined in Figure 3.4. Each of these synthetic procedures were performed using methanol as the solvent. Upon completions of the reactions, the methanol was removed under reduced pressure, leaving clay like materials, which after washing with acetone or diethyl ether afforded the final products as coloured solids. This purification procedure was sufficient to obtain alkylated complexes with sufficient purity for DNA-binding studies. The purity of the nickel Schiff base complexes was confirmed by elemental analysis, ESI mass spectrometry and NMR spectroscopy.

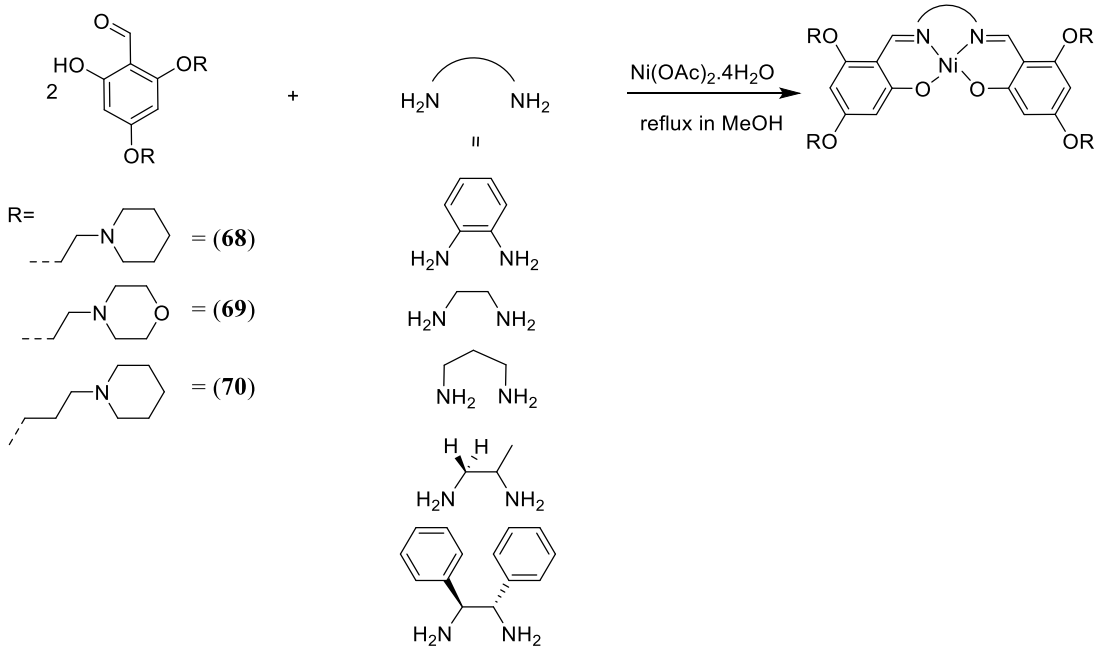

Figure 3.4: General synthetic scheme for the synthesis of nickel Schiff base complexes via organic precursor compounds.

3.3 Experimental section

N,N′-*Bis-4,6-(hydroxysalicylidine)phenylenediaminenickel(II)* (**50**)

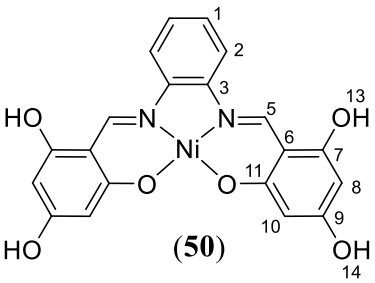

(**50**)

Method A: 2,4,6-Trihydroxybenzaldehyde (302 mg, 1.96 mmol) and 1,2-phenylenediamine (109 mg, 1.00 mmol) were dissolved in MeOH (30 mL), forming a transparent orange solution. This was heated for 1 h under reflux with constant stirring, during which time the solution colour changed to dark orange-brown. $Ni(OAc)_2 \cdot 4H_2O$ (499 mg, 2.00 mmol) was then added to the mixture, and immediately resulted in a deep red-brown precipitate. The solution continued to be heated under reflux for 24 h, after which it was allowed to cool to room temperature. The precipitate that had formed was separated by vacuum filtration and dried. It was subsequently washed with MeOH (50 mL), diethyl ether (25 mL) and water (50 mL), before being dried under vacuum for a further 2 h and then dried in an oven (24 h, 80 °C). Yield: 350 mg (79%). ESI-MS calc: $[M+H]^+ = 437.0$, Found: $[M+H]^+ = 437.0$. ^1H NMR (500 MHz, DMSO-d_6): δ 5.68 (d, 2H, *J* = 2.1 Hz, H10); 5.71 (d, 2H, *J* = 1.9 Hz, H8); 7.17 (m, 2H, H1); 7.77 (m, 2H, H2); 8.54 (s, 2H, H5); 10.04 (br-s, 2H, H14); 10.37 (br-s, 2H, H13).

Method B: 2,4,6-Trihydroxybenzaldehyde (71.6 mg, 0.46 mmol), 1,2-phenylenediamine (25 mg, 0.23 mmol) and $Ni(OAc)_2 \cdot 4H_2O$ (115 mg, 0.461 mmol) were reacted via ball milling (Millmix 20, Domel) for 2 h at 25 Hz. A stainless steel jar of volume 10 mL and stainless steel balls of 10 mm diameter were used. This resulted in formation of a brown solid, which was then washed with methanol (1 x 2 mL), then the filtrate from methanol washing (1 × 2 mL) and finally water (5 × 2

mL) before being oven-dried (24 h, 80 °C). Yield 93 mg (92%). ESI-MS calc: $[M+H]^+$ =437.0, Found: $[M+H]^+$ = 437.0. ^{1}H NMR (500 MHz, DMSO-d_6): δ 5.68 (d, 2H, *J* = 1.97 Hz, H10); 5.72 (d, 2H, *J* = 1.88 Hz, H8); 7.16 (m, 2H, H1); 7.75 (m, 2H, H2); 8.54 (s, 2H, H5); 10.09 (br-s, 1H, H14); 10.44 (br-s, 1H, H13). ^{13}C NMR (125 MHz DMSO-d_6): δ 91.96 (C8); 96.42 (C10); 106.55 (C6); 115.11 (C2); 126.61 (C1); 143.13 (C3); 148.07 (C5); 160.90 (C7); 165.44 (C9); 167.94 (C11).

The proton resonances in the ^{1}H NMR spectrum of (**50**) (Figure 3.5) were assigned on the basis of their chemical shifts, integration, multiplicity and coupling constants. For example, the spectrum exhibited three singlets at 10.44, 10.09 and 8.54 ppm which integrated to two hydrogen atoms each. Since imine groups are electron withdrawing, their protons are typically found at relatively high chemical shifts. Therefore, the singlet at 8.54 ppm was assigned to H5.

In addition, as it was expected that the protons of the OH groups would give rise to even more deshielded singlets, the resonances at 10.44 and 10.09 ppm were assigned to H13 and H14, respectively. The broadness of these two resonances is consistent with their assignment to OH groups, which was confirmed after consideration of the NOESY (Nuclear Overhauser Effect Spectroscopy) spectrum of (**50**) shown in Figure 3.5b. The latter showed the more deshielded singlet (H13) had a cross peak with only one of the two aromatic protons (H8) in the same ring, whereas the singlet at 10.09 ppm exhibited two such cross peaks (to both H8 and H10). The two doublets at 7.16 and 7.75 ppm were assigned to H1 and H2 also with the help of the NOESY spectrum, and in particular the observation of a strong cross peak between the imine protons (H5) and the resonance at 7.75 ppm, which allowed the latter to be identified definitively as H2.

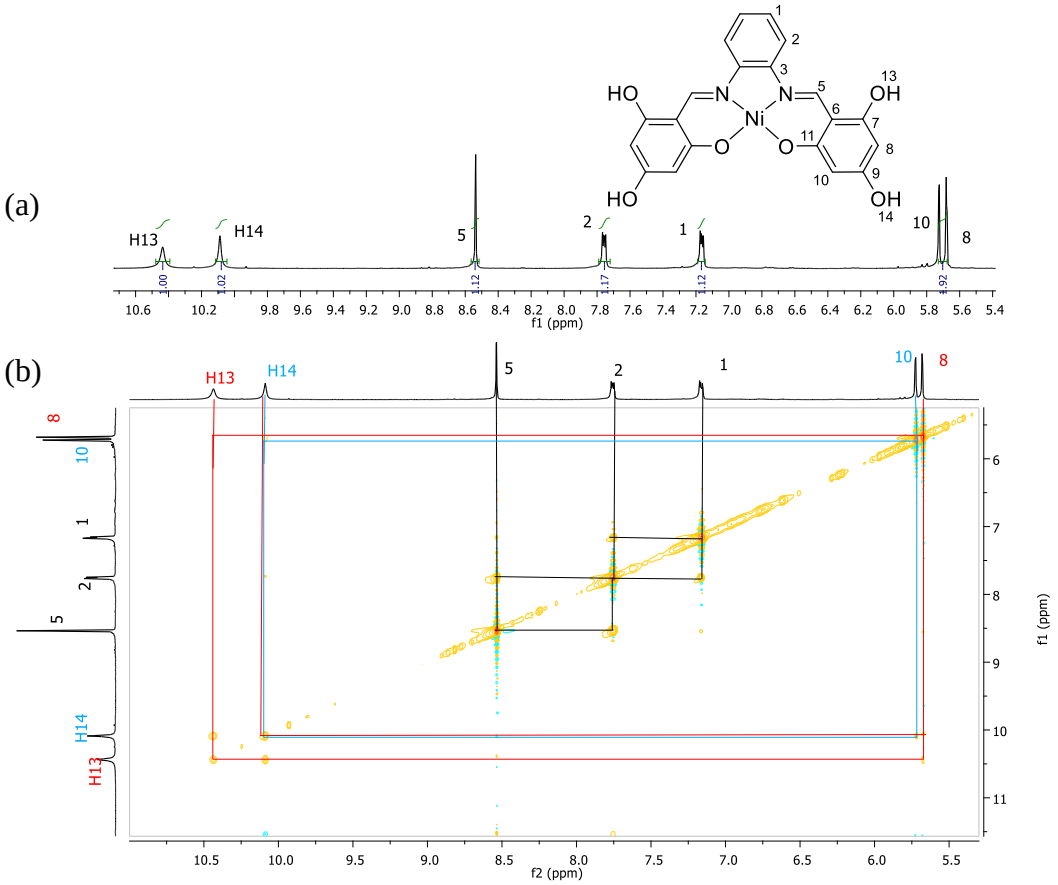

Figure 3.5: (a) ^{1}H NMR spectrum and (b) NOESY spectrum of (**50**) in DMSO-d_6, with highlighted correlations shown.

The ^{13}C NMR spectrum of (**50**) is presented inFigure 3.6(a) and showed the expected number of resonances. An HSQC (Heteronuclear Single-Quantum Correlation Spectroscopy) spectrum (Figure 3.6 (b)) was also obtained to facilitate assignment of resonances from carbon atoms with at least one hydrogen attached. For example, in the HSQC spectrum the carbon resonance at 148.07 ppm showed a cross peak with the proton resonance assigned to H5, thereby allowing assignment of this ^{13}C signal to C5. In addition, the ^{13}C resonances at 91.96, 96.42, 115.11 and 126.61 ppm were able to be assigned to C8, C10, C2 and C1, respectively, via this approach. Since quaternary carbon atoms do not have any C-H bonds they did not exhibit any HSQC

cross peaks. Their assignment therefore required an HMBC (Heteronuclear Multiple-Bond Correlation) spectrum to be obtained.

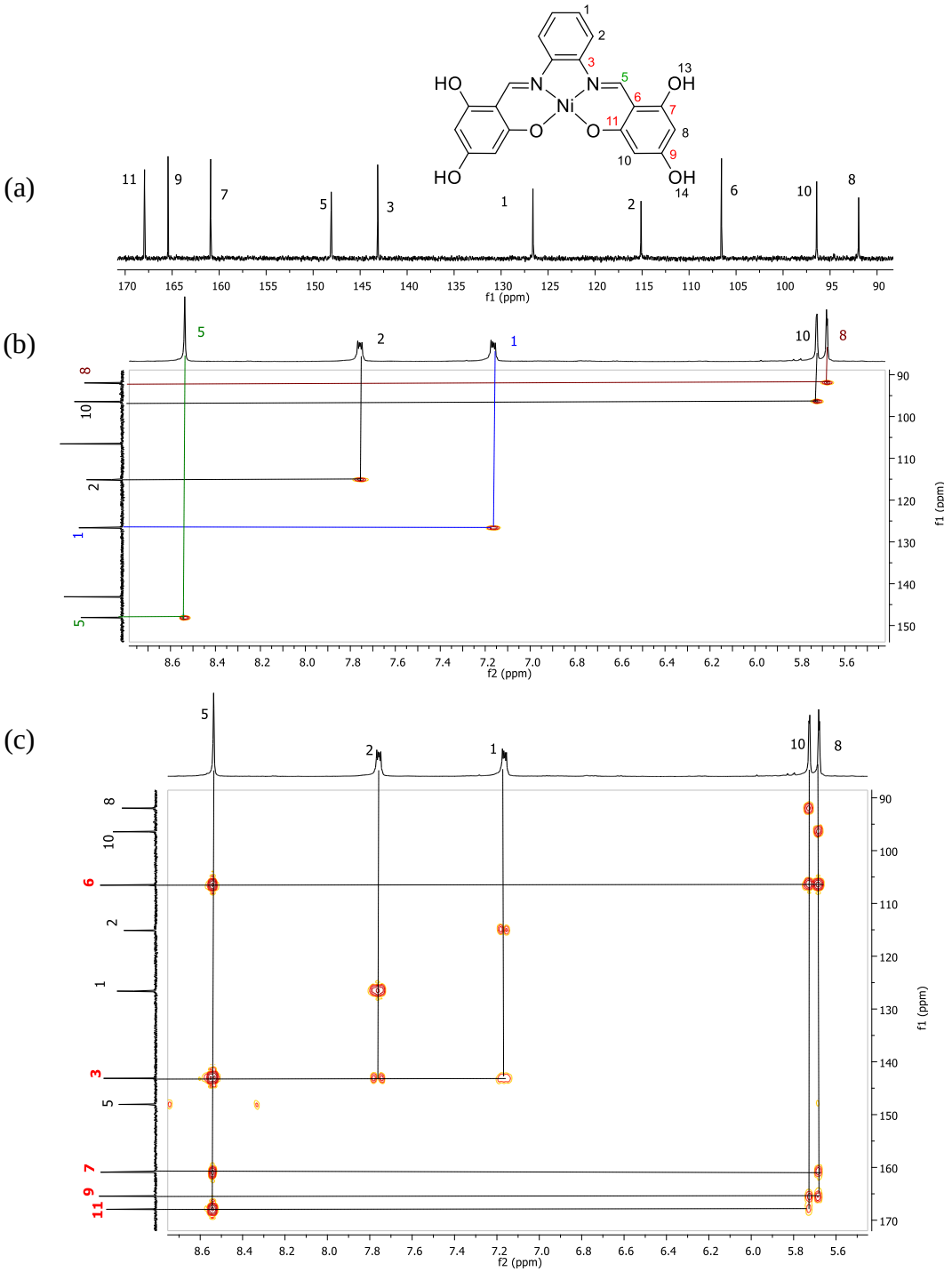

Figure 3.6: (a) ^{13}C NMR, (b) HSQC and (c) HMBC spectra of (**50**), with selected C-H correlations highlighted.

The HMBC spectrum of (**50**) is shown in Figure 3.6(c) and contains two or three cross peaks for each of the five quaternary carbon resonances. Of these, the most shielded was at 106.55 ppm. This resonance was assigned to C6, as it is the only quaternary carbon atom not directly bonded to an O or N atom. Evidence in support of this assignment was provided by the observation of cross peaks in the HMBC spectrum with H5, which is located only two bonds away from C6, and both H8 and H10 which are located three bonds away from C6. The carbon resonance at 143.13 ppm was assigned to C3 as it showed cross peaks in the HMBC spectrum with H5, H2 and H1, which are located two or three bonds away. It was also possible to readily assign the resonance at 165.44 ppm to C9 as it showed cross peaks in the HMBC spectrum with H8 and H10, which are two bonds away, but not H5. This left the two resonances at 160.90 and 167.94 ppm, which showed cross peaks in the HMBC spectrum with H5, to be assigned. The former resonance also showed a cross peak with H8, while the second showed a cross peak with H10. This allowed the assignment of these two resonances to C7 and C11, respectively.

N,N′-*Bis-4,5-(hydroxysalicylidine)phenylenediaminenickel(II)* (**51**)

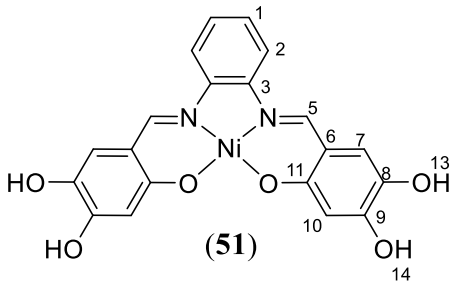

(**51**)

Method A: 2,4,5-Trihydroxybenzaldehyde (154 mg, 1.00 mmol) and 1,2-phenylenediamine (53 mg, 0.49 mmol) were dissolved in MeOH (50 mL), forming a transparent yellow solution. This was heated for 30 min at reflux with constant stirring, during which time the solution colour changed to dark orange. $Ni(OAc)_2 \cdot 4H_2O$ (125 mg, 0.501 mmol) was then added to the mixture, and immediately resulted in a brown precipitate. This solution continued to be heated

under reflux for 3 h, after which it was allowed to cool to room temperature. The precipitate that had formed was separated by vacuum filtration and dried. It was subsequently washed with MeOH (50 mL), diethyl ether (25 mL) and water (50 mL), before being dried under vacuum for a further 2 h and then dried in an oven (24 h, 80 $^{\circ}$C). Yield: 390 mg, 90%. Complex (**2**) was obtained as an insoluble solid and therefore could not be characterised by NMR spectroscopy or ESI mass spectrometry.

Method B: 2,4,5-Trihydroxybenzaldehyde (73 mg, 0.48 mmol), 1,2-phenylenediamine (25 mg, 0.23mmol) and $Ni(OAc)_2 \cdot 4H_2O$ (61 mg, 0.24 mmol) were reacted using ball milling (Millmix 20, Domel) for 2 h at 25 Hz. A stainless steel jar of 10 mL volume and stainless steel balls of 10 mm diameter were used. This resulted in a brown solid, which was washed with methanol (1 × 2 mL), then the filtrate from methanol washing (1 × 2 mL) and finally water (5 × 2 mL) before being oven-dried (24 h, 80 C). Yield 96 mg (95%). ESI-MS calc: $[M+H]^+$ = 437.0, Found: $[M+H]^+$ = 437.0. ^{1}H NMR (500 MHz, DMSO-d_6): δ 6.26 (s, 2H, H10); 6.82 (s, 2H, H7); 7.15 (m, 2H, H1); 7.98 (m, 2H, H2); 8.41 (s, 2H, H5); 8.57 (s, 2H, H14); 10.11 (s, 2H, OH13). ^{13}C NMR (125 MHz DMSO-d_6): δ 104.28 (C10); 113.06 (C6); 115.62 (C2); 115.75 (C7); 126.15 (C1); 138.12 (C8); 142.86 (C3); 152.68 (C5); 156.04 (C9); 163.16 (C11).

N,N′-*Bis-3,4-(hydroxysalicylidine)phenylenediaminenickel(II)* (**52**)

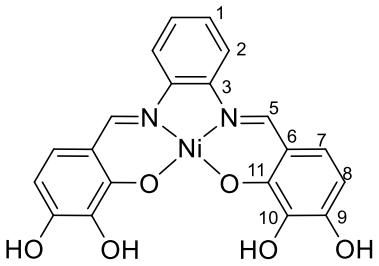

(**52**)

Method A: 2,3,4-Trihydroxybenzaldehyde (157 mg, 1.02 mmmol) and 1,2-phenylenediamine (54 mg, 0.50 mmol) were dissolved in MeOH (50 mL), forming a transparent yellow solution. This was heated for 30 min at reflux with constant stirring, during which time the solution colour changed to dark orange. $Ni(OAc)_2 \cdot 4H_2O$ (127 mg, 0.51 mmol) was then added to the mixture, and immediately resulted in a deep brown color solution. This solution continued to be heated under reflux for 3 h, after which it was allowed to cool to room temperature. The MeOH was removed under reduced pressure, leaving a solid black residue, which was suspended in water and filtered using a vacuum filtration to afford the product as a black solid. It was subsequently washed with MeOH (50 mL), diethyl ether (25 mL) and water (50 mL), before being dried under vacuum for a further 2 h and then dried in an oven (24 h, 80 ˚C). Yield: 143 mg, 65%. (**3**) was obtained as an insoluble solid and therefore could not be characterised by NMR spectroscopy and ESI mass spectrometry.

Method B: 2,3,4-Trihydroxybenzaldehyde (73 mg, 0.47 mmol), 1,2-phenylenediamine (25 mg, 0.23mmol) and $Ni(OAc)_2 \cdot 4H_2O$ (61 mg, 0.24 mmol) were reacted using ball milling (Millmix 20, Domel) for 2 h at 25 Hz. A stainless steel jar and stainless steel balls of 10 mm diameter were used. This resulted in a brown solid, which was washed with methanol (1 × 2 mL), then the filtrate from methanol washing (1 × 2 mL) and finally water (5 × 2 mL) before being oven-dried (24 h, 80 ˚C). Yield 100 mg (98%). ESI-MS calc: $[M+H]^+$ = 437.0, Found: $[M+H]^+$ =

437.0. ^{1}H NMR (500 MHz, DMSO-d_6): δ 6.28 (d, 2H, *J* = 8.76 Hz, H7); 6.95 (d, 2H, *J* = 8.84 Hz, H8); 7.24 (m, 2H, H1); 8.03 (m, 2H, H2); 8.10 (s, 2H, H13); 8.60 (s, 2H, H5); 9.43 (s, 2H, H14). ^{13}C NMR (125 MHz DMSO-d_6): δ 108.74 (C8); 114.41 (C6); 116.07 (C2); 124.63 (C7); 127.02 (C1); 134.14 (C10); 142.93 (C3); 148.78 (C9); 155.27 (C5); 155.41 (C11).

^{1}H NMR spectra of (**50**), (**51**) and (**52**) obtained via the mechanochemical route are shown in Figure 3.7. Comparison of the three spectra reveals that changing the position of the hydroxyl groups significantly affected the chemical shifts of a number of protons. For example, the chemical shifts of one or both of the hydroxyl protons in (**50**) are far less shielded compared to the corresponding resonances in the spectra of (**51**) and (**52**). In addition, notable differences in chemical shift were also observed for some of the protons attached to the same aromatic ring as the hydroxyl groups.

The ^{1}H NMR spectra therefore show that by using the mechanochemical approach it was possible to synthesise (**50**), (**51**) and (**52**). In contrast, using the original solution based method only complex (**50**) could be obtained. A further advantage of the mechanochemical method was that it afforded (**50**) in higher yield in a shorter period of time compared to the solution based approach.

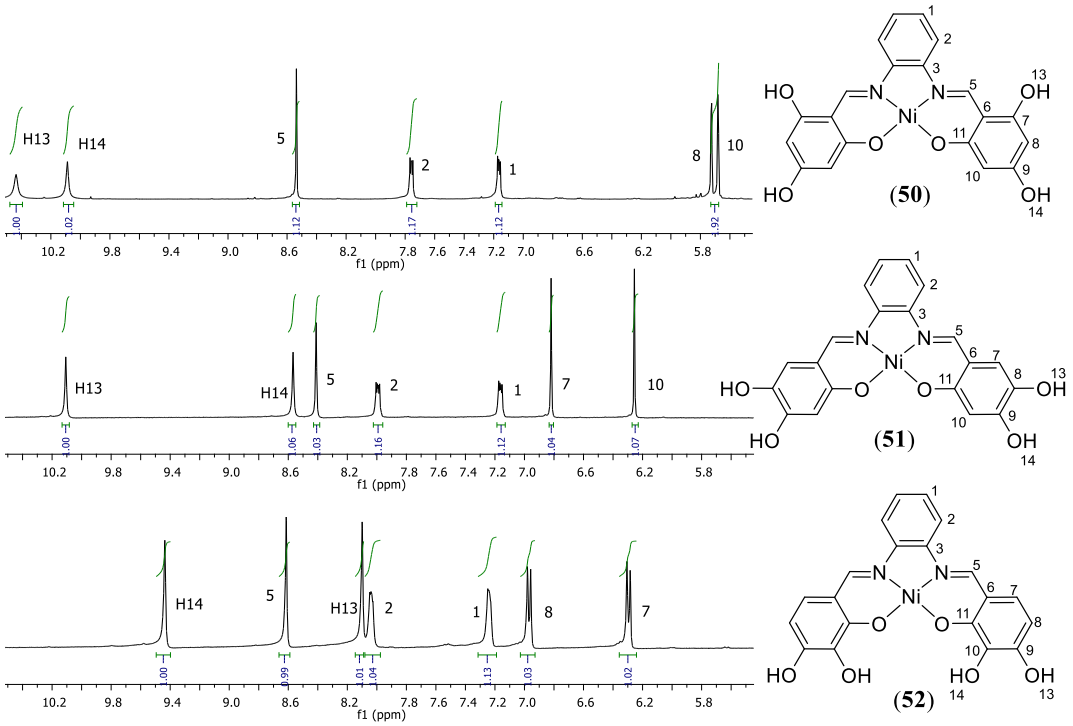

Figure 3.7: ^{1}H NMR spectra of complexes (**50**), (**51**) and (**52**) with atom numbering schemes shown.

2-Hydroxy-4,6-bis(2-(piperidin-1-yl)ethoxy)benzaldehyde (**68**)

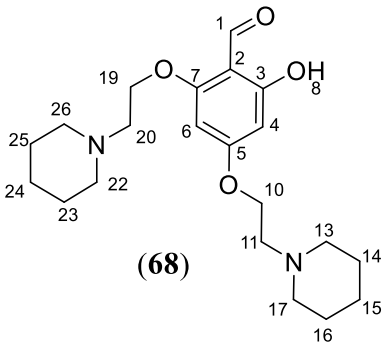

This compound was prepared by modifying a previously reported method.[125] A mixture of 2,4,6-trihydroxybenzaldehyde (100 mg, 0.649 mmol) and anhydrous potassium carbonate (224 mg, 1.62 mmol) in anhydrous acetone (6 mL) was stirred under reflux at 40 °C for 30 min. 1-(2-chloroethyl)piperidine hydrochloride (239 mg, 1.30 mmol) in anhydrous acetone (4 mL) was then added dropwise forming a light pink/orange suspension. The reaction mixture was then heated at 40 °C for a further 72 h. During this time a red precipitate and orange solution developed. The precipitate was removed via gravity filtration, and the acetone filtrate evaporated resulting in an orange oil. The latter was taken up in $CHCl_3$, washed with water seven times, then

dried with $MgSO_4$. The $CHCl_3$ was removed under low pressure to yield an orange oil, which was added to 5 mL ethyl acetate. The undissolved material was removed by gravity filtration before the ethyl acetate solution was left to evaporate in air to afford the product as an orange oil. Yield: 78 mg, 32%. Microanalysis calc. for $C_{21}H_{32}N_2O_4 \cdot 0.1CHCl_3$: C = 65.24; H = 8.33; N = 7.21%. Found: C = 65.22; H = 8.16; N = 7.05%. ESI-MS calc. $[C_{21}H_{32}N_2O_4+H]^+$ = 377.2, Found: $[C_{21}H_{32}N_2O_4+H]^+$ = 377.2. ^{1}H NMR (400 MHz, $CDCl_3$): δ 1.45 (m, 4H, H15 and H24); 1.60 (m, 8H, H14, H16, H23 and H25); 2.48 (m, 8H, H13, H17, H22 and H26); 2.75 (t, 2H, *J* = 5.89 Hz, H11); 2.80 (t, 2H, *J* = 5.79 Hz, H20); 4.11 (t, 2H, *J* = 5.61 Hz, H10); 4.12 (t, 2H, *J* = 5.61 Hz, H19); 5.93 (d, 1H, *J* = 2.1 Hz, H6); 5.99 (d, 1H, *J* = 2.03 Hz, H4); 10.09 (s, 1H, H1); 12.45 (br-s, 1H, H8). ^{13}C NMR (125 MHz $CDCl_3$): δ 24.06 (C15); 24.10 (C24); 25.83 (C14, C16); 25.92 (C23, C25); 54.98 (C13, C17, C22 and C26); 57.47 (C11); 57.48 (C20); 66.39 (C10); 66.94 (C19); 91.68 (C6); 93.67 (C4); 106.09 (C2); 162.75 (C5); 166.18 (C3); 167.33 (C7); 191.88 (C1).

The ^{1}H NMR spectrum of compound **(68)** (Figure 3.8) showed two very deshielded singlets which each integrated to one proton. The first was at 12.45 ppm, which together with its broadened appearance supported assignment to hydroxyl proton H8. The very deshielded chemical shift and broadness of this resonance can be attributed to formation of a hydrogen bond with the neighbouring carbonyl group. The second deshielded singlet at 10.09 ppm was assigned to the aldehyde proton H1. The spectrum also contained two resonances in the aromatic region at 5.93 and 5.99 ppm. These were assigned to H6 and H4, respectively, with the assistance of a NOESY spectrum. It is important to mention that during the assignment of ^{1}H-NMR spectrum, referring to a proton signal is in general referring to all the equivalent

protons on that site. For example, H1 refers to the one proton attached to C1 while H11 refers to the two protons attached to C11.

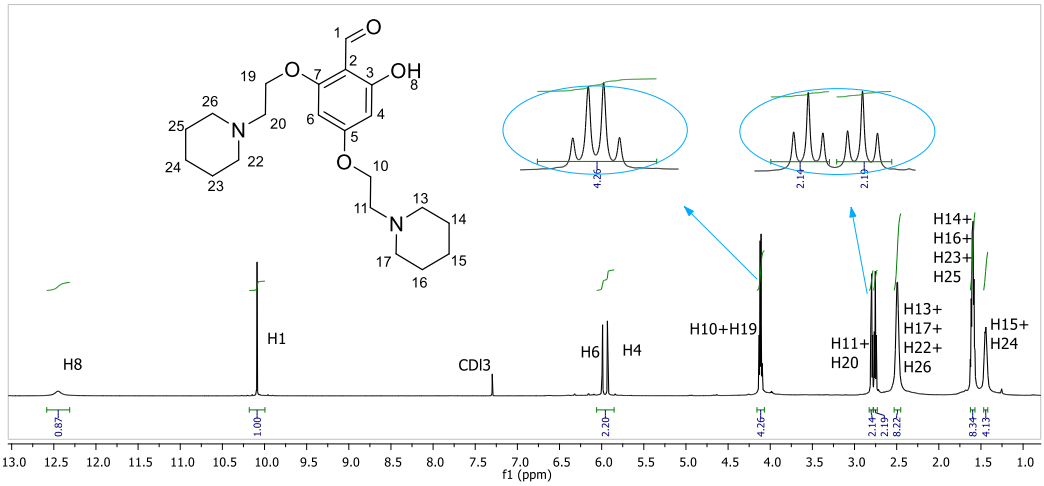

Figure 3.8: ^{1}H NMR spectrum of (**68**) in $CDCl_3$.

The two methylene groups at C11 and C20 were in slightly different chemical environments, resulting in resolvable triplets as a result of coupling to neighbouring CH_2 groups at C10 and C19. In contrast, resonances from the latter two methylene groups were in almost identical chemical environments, resulting in significant overlap of signals that appeared as a quartet. The protons of the piperidine groups gave rise to three multiplets in the most upfield region of the spectrum. These were assigned based on their chemical shifts and relative integrations. For example, the signal at 1.45 ppm integrated to four hydrogens and was assigned to H15 and H24. Assignment of the remaining signals arising from the piperidine protons was facilitated by the observation of cross peaks in the corresponding gCOSY spectrum (Figure 3.9).

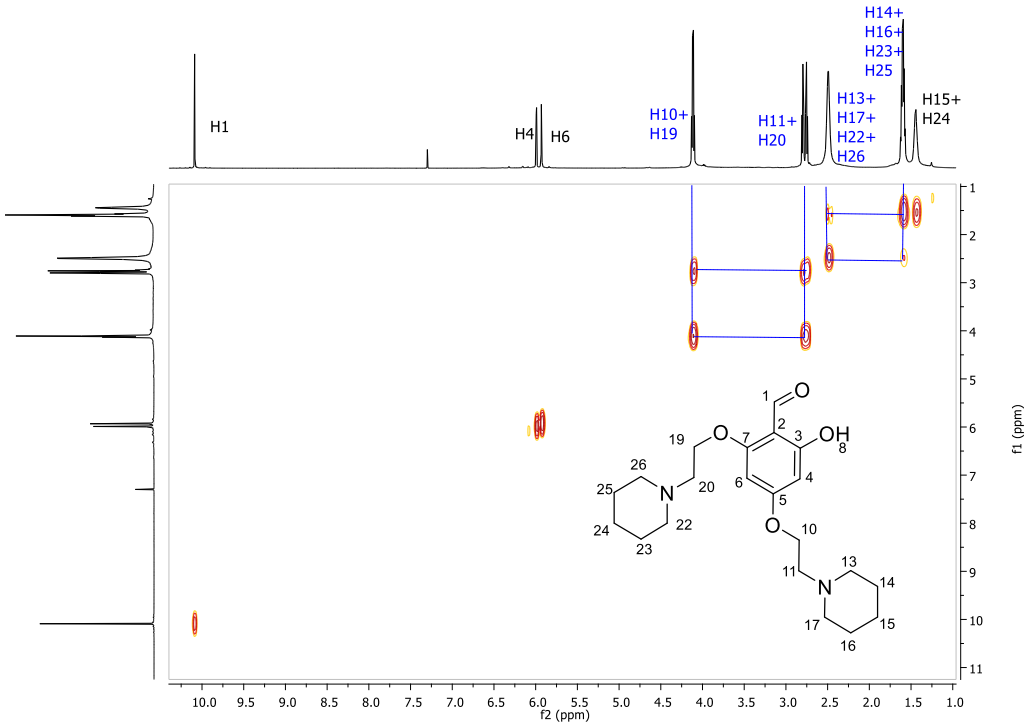

Figure 3.9: gCOSY spectrum of (**68**), with H-H correlations highlighted.

Additional evidence in support of the above assignments was provided by a NOESY spectrum (Figure 3.10). For example, the observation of two strong sets of cross peaks between the quartet at 4.11 ppm and both H4 and H6 provided strong support for the former signal to be assigned to both H10 and H19. A further set of cross peaks was observed for the apparent quartet with the two triplets assigned to H11 and H20. In addition, the latter resonances showed strong cross peaks with the intense multiplet at 2.48 ppm, confirming that the latter should be assigned to the nearest protons on the piperidine ring systems (H13, H17, H22 and H26). Finally, the multiplet at 2.48 ppm showed a set of cross peaks with the resonance at 1.60 ppm, confirming that the latter should be assigned to H14, H16, H23 and H25. The latter resonances showed strong cross peaks with the multiplet at 1.45 ppm, confirming that the latter should be assigned to H15 and H24.

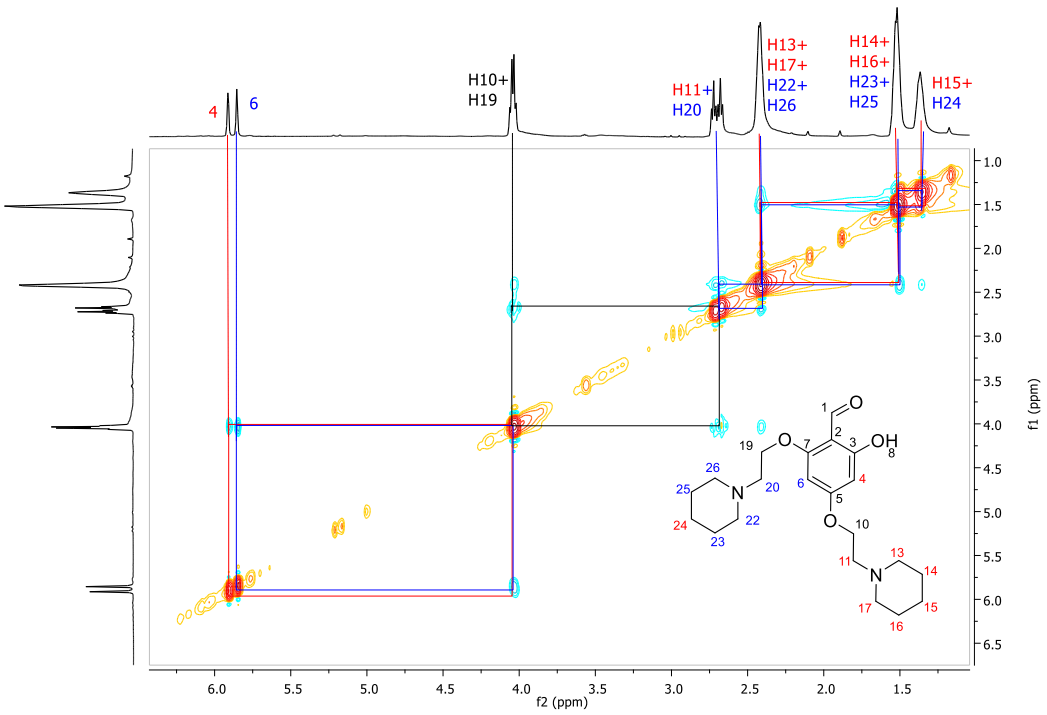

Figure 3.10: NOESY spectrum of (**68**), with H-H correlations highlighted.

The ^{13}C NMR spectrum of (**68**) is shown in Figure 3.11 and exhibited the expected number of resonances. Since the ^{1}H NMR spectrum of (**68**) had been fully assigned, most resonances in the ^{13}C NMR spectrum were able to be attributed to specific carbon atoms on the basis of their C-H correlations in the corresponding HSQC spectrum (also shown in Figure 3.11). For example, the two carbon signals at 91.68 and 93.68 ppm exhibited cross peaks with proton signals at 5.93 and 5.99 ppm, allowing assignment of the former to C6 and C4, respectively. Similarly, the apparent quartet in the ^{1}H spectrum at 2.48 ppm exhibited cross peaks with two carbon resonances at 66.39 and 66.94 ppm, allowing their assignment to C10 or C19. One of the few ^{13}C resonances to not show a cross peak in the HSQC spectrum was that at 191.88 ppm. This was assigned to the carbonyl carbon atom C1 in view of its very deshielded chemical shift.

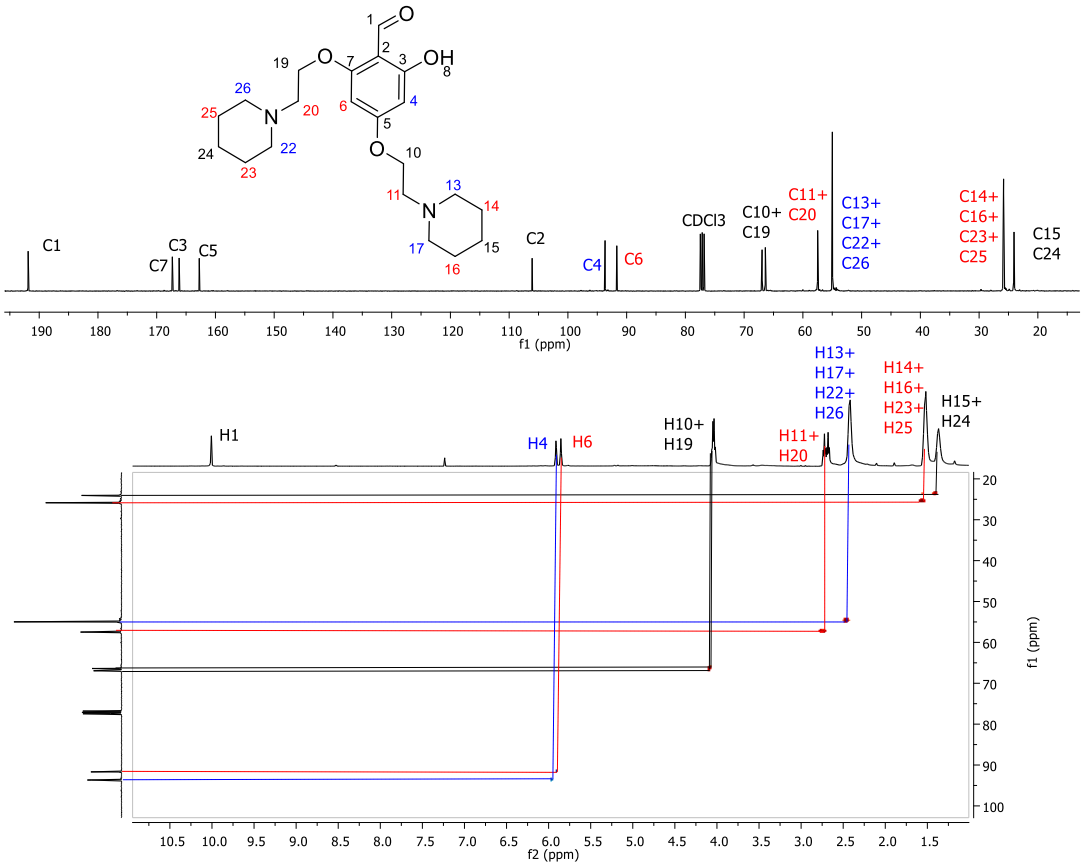

Figure 3.11: ^{13}C and HSQC NMR spectra of (**68**), with selected C-H correlations highlighted.

Assignments for the four quaternary carbon resonances in the aromatic ring was completed after examination of the HMBC spectrum of (**68**) (Figure 3.12). For example, the ^{13}C resonance at 106.09 ppm was the only signal from a quaternary carbon atom to show cross peaks in the HMBC spectrum with H1, H6 and H4. Since each of these resonances is located either two or three bonds away from C2, the former ^{13}C signal was assigned to the latter carbon atom. In contrast, the ^{13}C resonance at 166.18 only showed cross peaks with H1 and H4, strongly suggesting it should be assigned to C3, which is located only two or three bonds away from these two hydrogen atoms. The absence of a cross peak involving the remaining hydrogen

atom, H6, is consistent with this assignment as it is located four bonds away from C3.

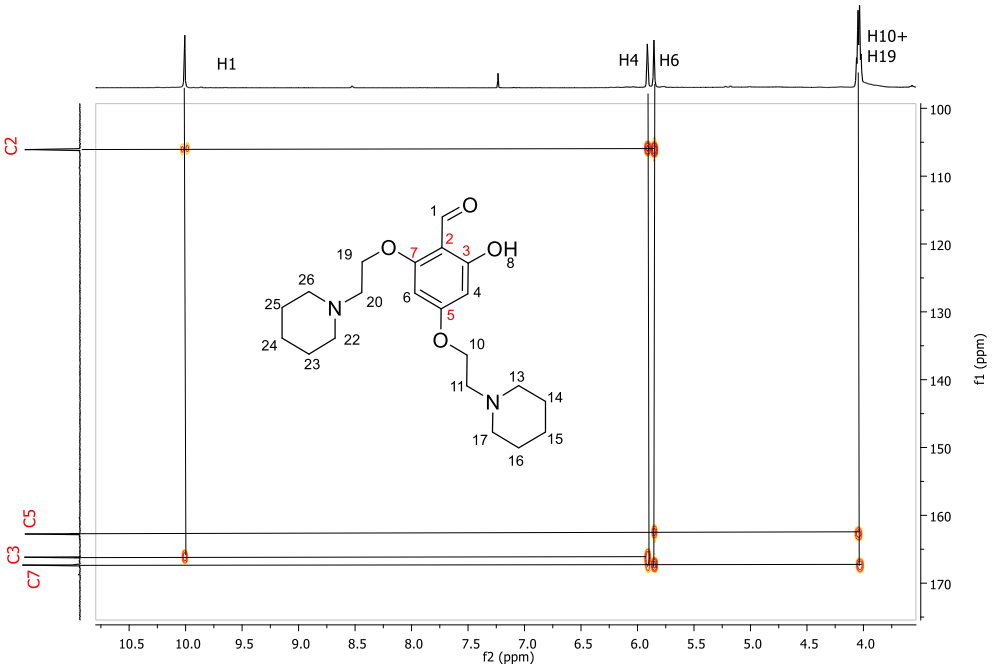

Figure 3.12: HMBC NMR spectrum of (**68**), with selected C-H correlations highlighted.

2-Hydroxy-4,6-bis(2-morpholinoethoxy)benzaldehyde (**69**)

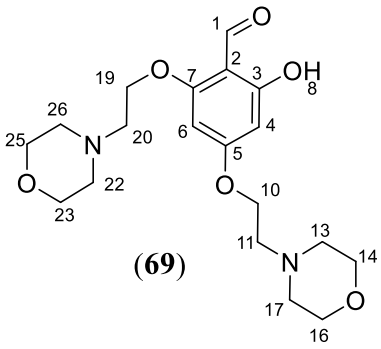

(**69**)

This compound was prepared by modifying a previously reported method.[125] A mixture of 2,4,6-trihydroxybenzaldehyde (100 mg, 0.649 mmol) and anhydrous potassium carbonate (224 mg, 1.62 mmol) in anhydrous acetone (6 ml) were stirred under reflux at 40 °C for 30 min. 1-(2-chloroethyl)morpholine hydrochloride (242 mg, 1.30 mmol) in anhydrous acetone (4 mL) was then added dropwise forming a light pink/orange suspension. The reaction mixture was maintained under reflux for a further 6 days. During this time, a red precipitate and red solution developed. The

precipitate was removed via gravity filtration, and the filtrate evaporated resulting in a red oil, which was taken up in DCM. The DCM solution was washed with water seven times, and then dried with $MgSO_4$. The solvent was then removed under low pressure to yield a red oil, which was added to 5 mL ethyl acetate. A small amount of undissolved material was removed by gravity filtration and the ethyl acetate allowed to evaporate in air to afford the product as a red oil. Yield: 61 mg (25%). Microanalysis calc. for $C_{19}H_{28}N_2O_6 \cdot 0.4H_2O$: C = 58.87; H = 7.49; N = 7.23%. Found: C = 58.89; H = 7.22; N = 7.24%. ESI-MS calc. $[C_{19}H_{28}N_2O_6+H]^+$ =381.2, Found: $[C_{19}H_{28}N_2O_6+H]^+$ = 381.2. ^{1}H NMR (400 MHz, $CDCl_3$): δ 2.48-2.50(m, 8H, H13, H17, H22 and H26); 2.72 (t, 2H, *J* = 5.63 Hz, H11); 2.75 (t, 2H, *J* = 5.60, H20); 3.63-3.67 (m, 8H, H14, H16, H23 and H25); 4.03 (t, 2H, *J* = 5.55 Hz, H10); 4.04 (t, 2H, *J* = 5.55 Hz, H19); 5.85 (d, 1H, *J* = 2.04 Hz, H6); 5.93 (d, 1H, *J* = 1.92 Hz, H4); 10.02 (s, 1H, H1); 12.38 (br-s, 1H, H8). ^{13}C NMR (125 MHz $CDCl_3$): δ 53.00 (C13, C17, C22 and C26); 56.20 (C11 and C20); 65.19 (C10, C19); 65.89 (C14, C16, C23, C25); 90.78 (C6); 92.57 (C4); 105.10 (C2); 161.57 (C5); 165.25 (C3); 166.10 (C7); 190.76 (C1).

2-Hydroxy-4,6-bis(3-(piperidin-1-yl)propoxy)benzaldehyde (**70**)

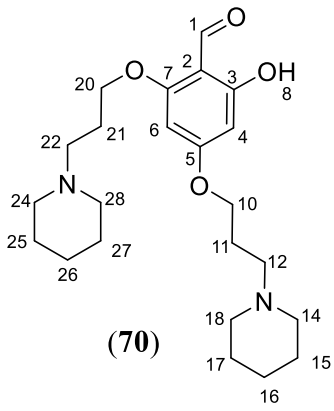

(**70**)

This compound was prepared by modifying a previously reported method.[125] A mixture of 2,4,6-trihydroxybenzaldehyde (100 mg, 0.649 mmol) and anhydrous potassium carbonate (224 mg, 1.62 mmol) in anhydrous acetone (6 mL) were stirred under reflux at 40 °C for 30 min. 1-(3-chloropropyl)piperidine hydrochloride (258 mg, 1.30 mmol) in anhydrous acetone (4 mL) was then added

dropwise forming a light pink/orange suspension. The reaction mixture was maintained under reflux for a further 5 days. During this time, a red precipitate and orange solution developed.

The precipitate was removed via gravity filtration, and the filtrate evaporated affording an orange oil. The latter was taken up in DCM and washed with water seven times, then dried with $MgSO_4$. Subsequently the DCM was removed under low pressure to yield an orange oil, which was added to 5 mL ethyl acetate. A small amount of insoluble material was removed by gravity filtration and then the ethyl acetate solution allowed to evaporate in air to afford the product as an orange oil. Yield: 100 mg (39%). ESI-MS calc. $[C_{23}H_{36}N_2O_4+H]^+$ = 405.3. Found: $[C_{23}H_{36}N_2O_4+H]^+$ =.405.4 Microanalysis calc. for $C_{23}H_{36}N_2O_4 \cdot 0.5DCM$: C = 63.14; H = 8.34; N = 6.27%. Found: C = 63.32; H = 8.42; N = 6.49%.^{1}H NMR (400 MHz, $CDCl_3$): δ 1.36 (m, 4H, H16 and H26); 1.51 (m, 8H, H15, H17, H27 and H25); 1.90 (m, 4H, H11, H21); 2.31 (m, 8H, H14, H18, H24 and H28); 2.38 (m, 4H, H12 and H22); 4.03 (t, 2H, *J* = 6.26 Hz, H10); 4.04 (t, 2H, *J* = 6.26 Hz, H19); 5.83 (d, 1H, *J* = 2.09 Hz, H6); 5.92 (d, 1H, *J* = 1.98 Hz, H4); 10.01 (s, 1H, H1); 12.38 (br-s, 1H, H8). ^{13}C NMR (101 MHz $CDCl_3$): δ 24.43 (C16, C26); 25.99 (C15, C17, C25, C27); 26.58 (C11, C21); 54.66-54.70 (C14, C18, C24, C28); 55.68-55.83 (C12, C22); 67.04-67.12 (C10, C20); 91.53 (C6); 93.37 (C4); 106.00 (C2); 163.00 (C5); 166.23 (C3); 167.67 (C7); 191.74 (C1).

Figure 3.13 shows the ^{1}H NMR spectra of compounds (**68**), (**69**) and (**70**). All assignments for the latter two compounds were made by following the same approach used previously with (**68**).

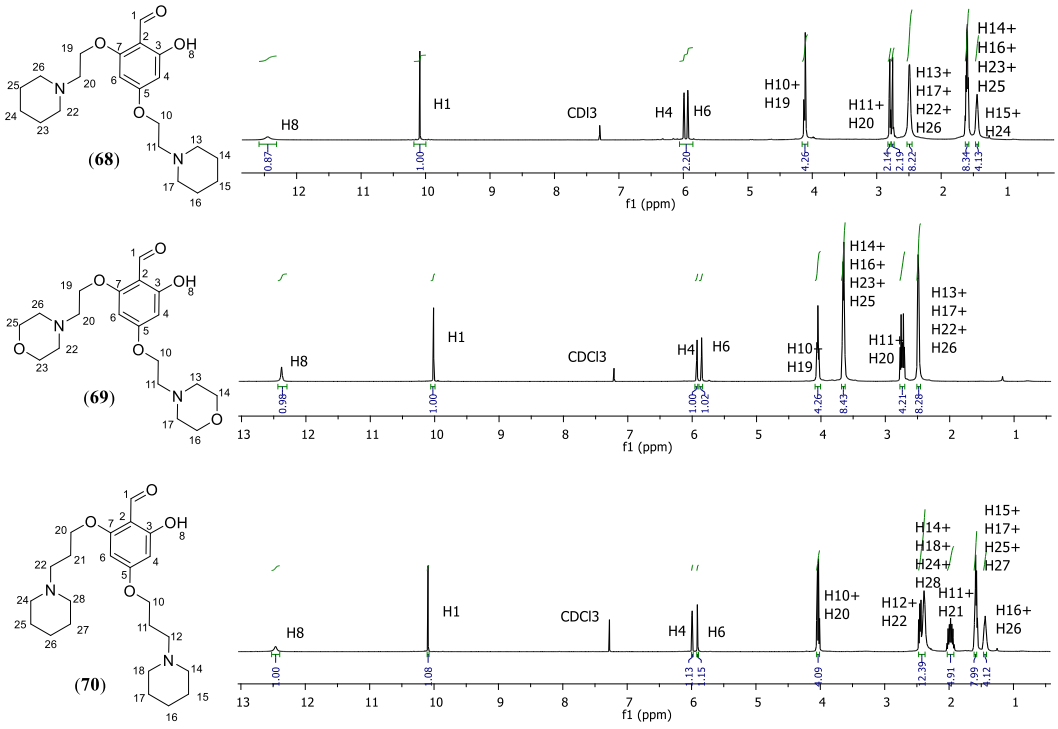

Figure 3.13: ^{1}H NMR spectra of (**68**), (**69**) and (**70**).

Comparison of the three ^{1}H NMR spectra reveals a number of similarities. For example, analogous resonances to those assigned to H1, H6, H4, H10/H19, H13/H17/H22/H26 and H8 in the spectrum (**68**) were found at similar chemical shifts in the spectra of (**69**) and (**70**) and assigned to the corresponding protons in latter complexes. A number of differences were also observed, including observation of an extra signal at 1.98 ppm in the ^{1}H NMR spectrum of (**70**), which was not present in the spectrum of (**68**). This was a consequence of the additional methylene group in the linkers connecting the piperidine moieties to the rest of (**70**). This signal was assigned to H11 and H21. A second difference was that the signal from H15 and H24 in the spectrum of (**68**) was, as expected, no longer present in the spectrum of (**69**). This was a consequence of the replacement of two methylene groups in (**68**) by oxygen atoms in (**69**). This change also resulted in the chemical shifts of the

resonances from protons adjacent to the oxygen atoms in (**69**) being more deshielded than for the corresponding protons in (**68**).

N,N′-*Bis-(4,6-((1-(2-ethyl)piperidine)oxy)salicylidine)phenylenediaminenickel(II)* (**53**)

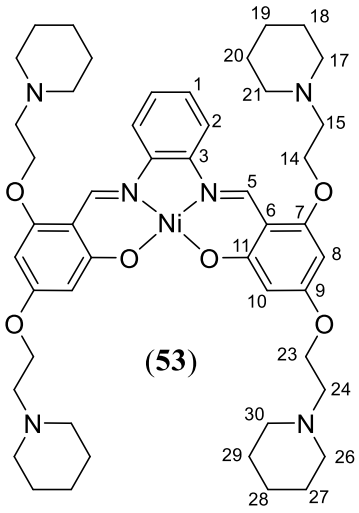

(**53**)

Method A: A suspension of (**50**) (72.9 mg, 0.167 mmol), 1-(2-chloroethyl)piperidine hydrochloride (245 mg, 1.33 mmol) and K_2CO_3 (367 mg, 2.67 mmol) in anhydrous DMF (5 mL) was stirred for 10 d under N_2 at 25 °C. DMF was then evaporated under low pressure to yield a dark brown sludge, which was then dissolved in DCM (15 mL), and washed with water ten times. After the washing step, the DCM solution was dried with $MgSO_4$, and evaporated yielding 39 mg of a dark brown solid. The ^{1}H NMR spectrum of the product showed many signals related to impurities. One of them was assigned to the hydroxyl groups from (**50**), indicating that the starting material did not fully react. Therefore, the obtained product was further purified by using column chromatography on alumina, using DCM/methanol (95/5, v/v) as the eluent, to yield the desired compound (1.9 mg, (1%)). Once again, however, the ^{1}H NMR spectrum of the product showed impurities. In other attempts to synthesise sufficiently pure (**53**), the same procedure as above was followed but higher reaction temperature and/or different concentrations of either (**50**) or 1-(2-chloroethyl) piperidine hydrochloride were used. Again ^{1}H NMR spectra did not show any improvement in the purity of the (**53**) that was obtained. After the limited success of these attempts to synthesise (**53**), it was decided to try a different method to synthesise this complex.

Method B: A solution of (**68**) (68 mg, 0.18 mmol), 1,2-phenylenediamine (9.9 mg, 0.092 mmol) and $Ni(OAc)_2 \cdot 4H_2O$ (23 mg, 0.092 mmol) were dissolved in MeOH (4 mL). The solution was heated with constant stirring under reflux at 65 °C for 4 h. During this time a brown precipitate appeared in the dark brown solution. At the end of the reaction, the MeOH was removed under reduced pressure, leaving a solid brown residue, which was suspended in acetone and then filtered using vacuum filtration to afford the product as a brown powde. Yield: 95 mg (59%). Microanalysis calc. for $C_{48}H_{66}N_6NiO_6 \cdot 2DCM$: C = 57.10; H = 6.71; N = 7.99; Ni = 5.58%. Found: C = 57.26; H = 7.02; N = 8.25; Ni = 5.40%. ESI-MS calc: $[C_{48}H_{66}N_6NiO_6 + 2H]^{2+}$ = 441.5, $[C_{48}H_{66}N_6NiO_6 + 2H]^{2+}$ = 441.2. ^{1}H NMR (500 MHz, $CDCl_3$): δ 1.46 (m, 4H, H19, H28); 1.62 (m, 16H, H18, H20, H27 and H29); 2.48 (m, 8H, H26 and H30); 2.56 (m, 8H, H17 and H21); 2.75 (t, 4H, *J* = 5.80 Hz, H24); 2.85 (t, 4H, *J* = 5.71 Hz, H15); 4.08 (t, 4H, *J* = 5.86 Hz, H23); 4.12 (t, 4H, *J* = 5.70 Hz, H14); 5.72 (d, 2H, *J* = 1.93, H8); 6.23 (d, 2H, *J* = 1.73 Hz, H10); 7.13 (m, 2H, H1), 7.58 (m, 2H, H2), 8.65 (s, 2H, H5). ^{13}C NMR (101 MHz, CDCl3): δ 24.16 (C19); 24.20 (C28); 25.88 (C18, C20); 26.06 (C27, C29) 54.89 (C26, C30); 55.00 (C17, C21); 57.66 (C24), 57.74 (C15), 65.80 (C23); 66.56 (C14); 90.13 (C8); 96.67 (C10); 107.12 (C6); 114.30 (C2); 125.97(C1); 143.58 (C3); 147.98 (C5); 159.97 (C7); 165.11 (C9); 168.44 (C11).

The ^{1}H NMR spectrum of (**53**) is shown in Figure 3.14. Since (**50**) and (**53**) have closely related chemical structures, it is not surprising that there were strong similarities between some aspects of their NMR spectra. For example, the resonances from H1, H2 and H5 were found at 7.16, 7.75, 8.54 ppm, respectively for (**50**), and at 7.13, 7.58, 8.65 ppm, respectively in the spectrum of (**53**). In addition, the resonance corresponding to H8 was found at the same chemical shift (5.72 ppm) in both

spectra. The main difference between the two spectra, aside from the lack of resonances from the dimethylenepiperidine moieties in the case of (**50**), was the location of the resonance from H10. This was found at 5.68 ppm in the spectrum of (**50**) but was located at a significantly more deshielded chemical shift of 6.23 ppm in the case of (**53**).

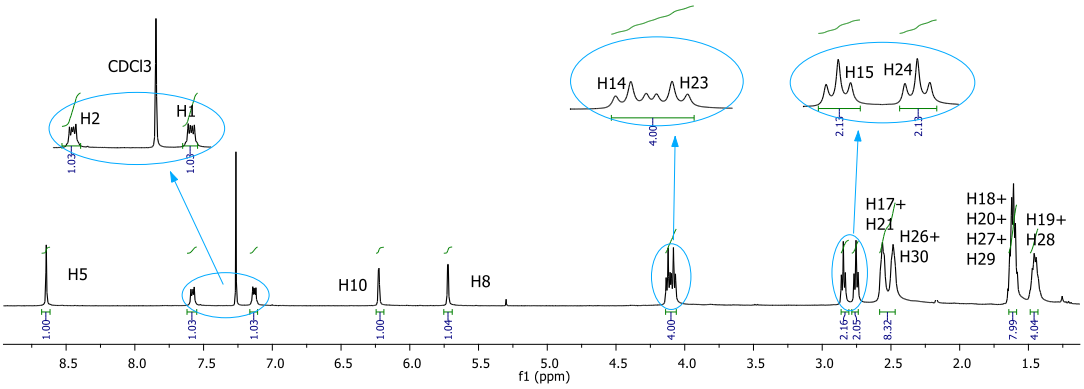

Figure 3.14: ^{1}H NMR spectrum of (**53**), with an expansion of some regions for clarity.

The ^{1}H resonances from the pendant dimethylenepiperidine groups in the top and bottom portions of (**53**) were found at slightly different chemical shifts; however, all appeared in the upfield region of the spectrum at similar chemical shifts to those of the corresponding protons in (**68**). For example, the resonances from H19 and H28 in the spectrum of (**53**) were found at 1.60 and 1.62 ppm, which is near the chemical shifts of the same protons in the spectrum of (**68**) (1.45 and 1.46 ppm). In addition, the resonances from H15 were found at 2.80 ppm and 2.85 ppm in the spectrum of (**50**) and (**53**), respectively, whilst that from H24 was found at the same chemical shift (2.75 ppm) in both spectra. The resonances from H14 and H23 were also found at similar chemical shifts in the spectra of (**68**) and (**53**). This resulted in two close

but resolved triplets at 4.08 and 4.12 ppm, respectively in the spectrum of (**53**). However, overlap of some of the individual signals in these multiplets resulted in an apparent quartet in the spectrum of (**68**).

The above assignments for (**53**) were confirmed using COSY (Figure S3.1) and NOESY (Figure 3.15) spectra of the complex. For example, the single set of cross peaks between the resonance from H5 and that at 7.58 ppm in the NOESY spectrum provided strong support for the latter to be assigned to H2. Additional sets of cross peaks were observed between both H8 and H10, and the nearest methylene groups in the two dimethylene linker moieties in the NOESY spectrum. In addition, the cross peak between H14 and the triplet at 2.85ppm and the cross peak between H23 and the triplet at 2.75 ppm confirmed these two signals should be assigned to the nearest protons on the piperidine ring systems, which are H15 and H24, respectively. The assignments of the remaining protons were confirmed using the same approach.

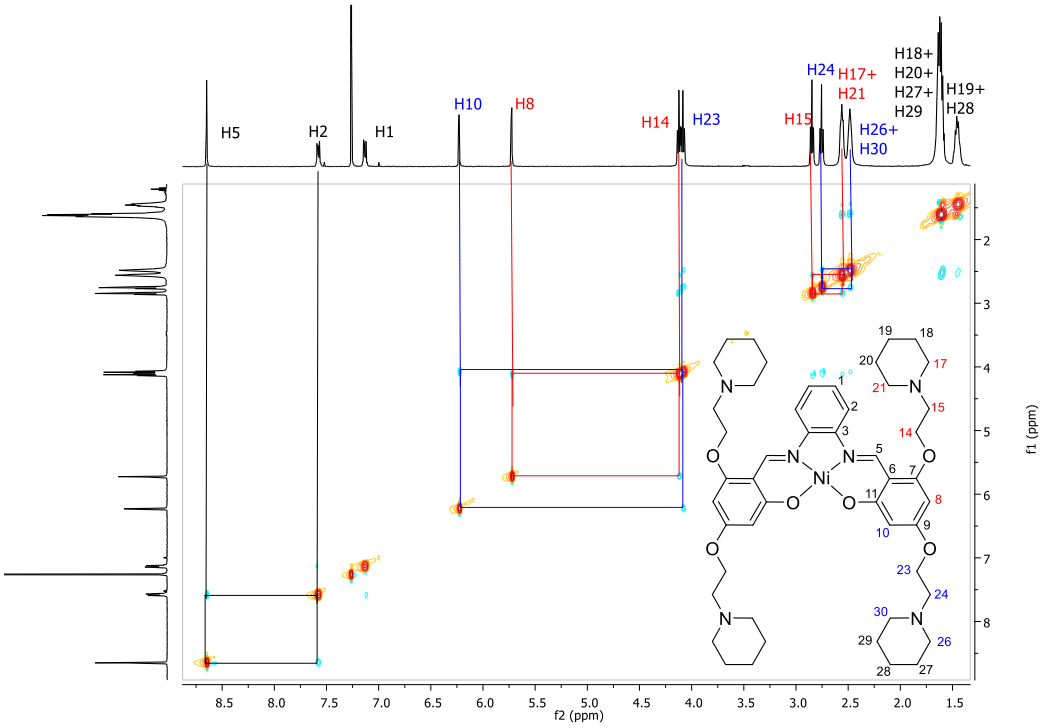

Figure 3.15: NOESY spectrum of (**53**), with selected H-H correlations highlighted.

All of the resonances in the ^{13}C NMR spectrum of (**53**) were readily assigned through a comparison with those in the spectra of (**50**) and (**68**) (Figure 3.16). It was expected, for example, that the ^{13}C resonances from the piperidine ring systems in (**68**) and (**53**) would have similar chemical shifts. This was found to be the case with the resonances from C19 and C28 being found at 24.16 and 24.20 ppm, respectively, in the ^{13}C spectrum of (**53**), whilst the corresponding resonances in the spectrum of (**68**) were observed at 24.06 and 24.10 ppm.

Confirmation of the assignments of the carbon atoms in the spectrum of (**53**) was confirmed after examination of both the HSQC and HMBC spectra of the complex (Figure S3.2 and Figure S3.3, respectively).

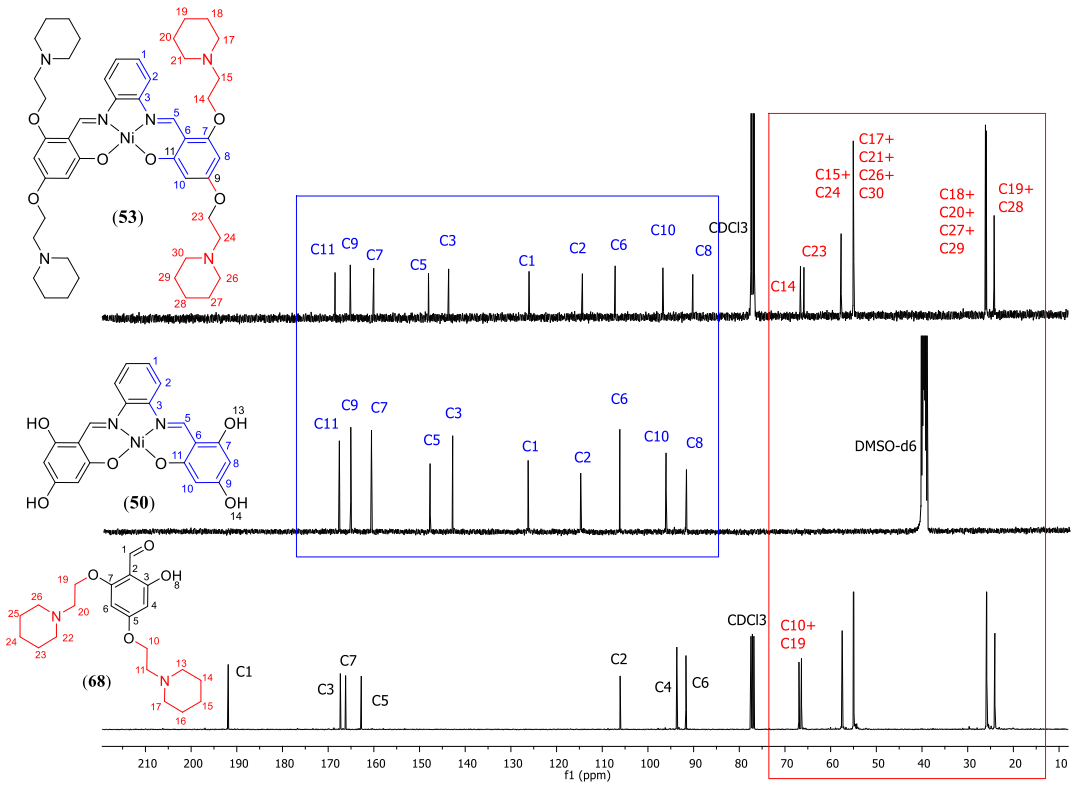

Figure 3.16: Comparison of ^{13}C- NMR spectra of (**53**), (**50**) and (**68**).

N,N′-*Bis-(4,6-((1-(2-ethyl)morpholine)oxy)salicylidine)phenylenediaminenickel(II)*

(**54**)

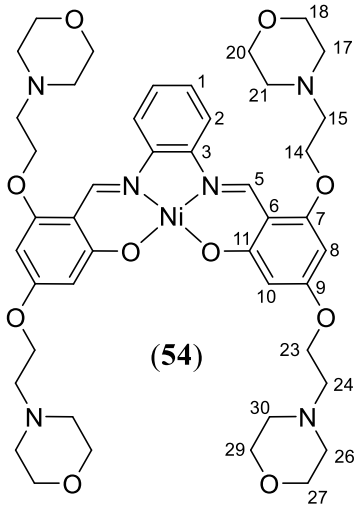

A solution of (**69**) (87 mg, 0.23 mmol), 1,2 - phenylenediamine (14 mg, 0.12 mmol) and $Ni(OAc)_2 \cdot 4H_2O$ (29 mg, 0.12 mmol) was dissolved in MeOH (4 mL). The solution was heated under reflux with constant stirring for 24 h. At the end of the reaction, the MeOH was removed under reduced pressure, leaving a red-brown residue, which was suspended in acetone and then isolated using vacuum filtration to afford the product as a red-brown powder. Yield: 110 mg (54%). Microanalysis calc. for $C_{44}H_{58}N_6NiO_{10}.1.5H_2O$: C = 57.65; H = 6.71; N = 9.17; Ni = 6.40%. Found: C = 57.47; H = 6.53; N = 9.38; Ni = 6.40%. ESI-MS calc: $[[C_{44}H_{58}N_6NiO_{10}]^+ + 2H]^{2+}$ = 445.8. Found: $[[C_{44}H_{58}N_6NiO_{10}]^+ + 2H]^{2+}$ = 445.8. ^{1}H NMR (400 MHz, $CDCl_3$): δ 2.55 (t, 8H, *J* = 4.47 Hz and 4.53 Hz, H26 and H30); 2.62 (t, 8H, *J* = 4.59 Hz and 4.59 Hz, H17 and H21); 2.78 (t, 4H, *J* = 5.60 Hz and 5.52 Hz, H24); 2.87 (t, 4H, *J* = 2.57 Hz and 2.55 Hz, H15); 3.74 (m, 16H, H18, H20, H27 and H29); 4.09 (t, 4H, *J* = 5.55 Hz and 5.57 Hz, H23); 4.14 (t, 4H, *J* = 5.61Hz and 5.56Hz, H14); 5.73 (d, 2H, *J* = 2.06 Hz, H8); 6.23 (d, 2H, *J* = 1.82 Hz, H10); 7.15 (m, 2H, H1), 7.58 (m, 2H, H2), 8.64 (s, 2H, H5). ^{13}C NMR (101 MHz, $CDCl_3$): δ 54.01 (C26, C30); 54.09 (C17, C21); 57.36 (C24); 57.50 (C15); 65.66 (C23), 66.47 (C14), 66.91 (C27, C29); 67.01 (C18, C20); 90.19 (C8); 96.70 (C10); 107.16 (C6); 114.25 (C2); 126.23 (C1); 143.53 (C3); 147.91 (C5); 159.89 (C7); 164.95 (C9); 168.45 (C11).

The ^{1}H NMR spectrum of (**54**) is displayed in Figure 3.17, and shows a number of resonances at very similar chemical shifts to what was observed in the spectrum of (**53**). However, replacing the dimethylenepiperidine moieties with dimethylenemorpholines resulted in two main differences. The first was the absence of the resonances from H19 and H28 in the spectrum of (**54**), owing to the replacement of methylene groups with oxygen atoms. The second difference was that the resonances of all protons (H18, H20, H27 and H29) adjacent to the oxygen atoms in the morpholine groups were found at more deshielded chemical shifts in the spectrum of (**54**).

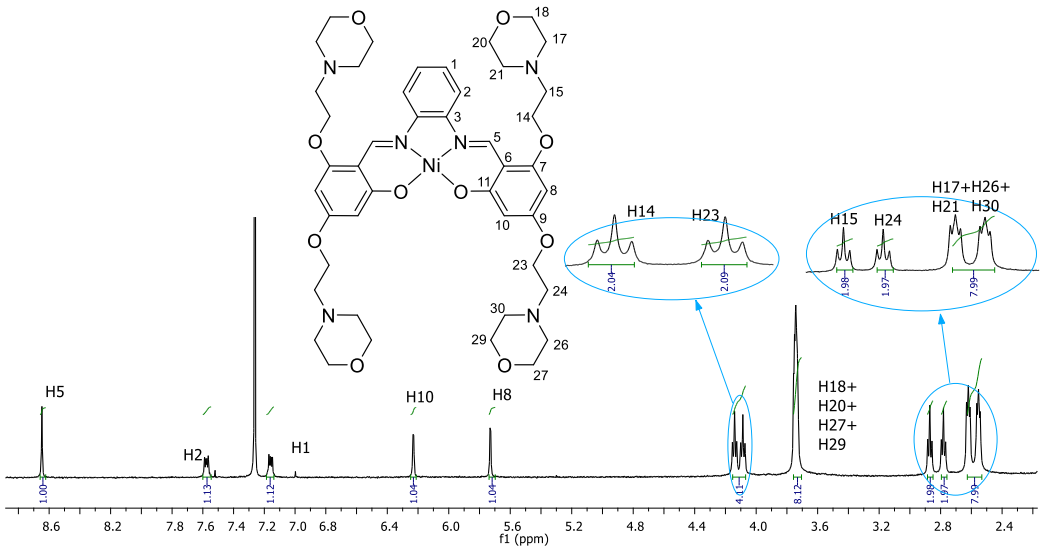

Figure 3.17: ^{1}H NMR spectrum of (**54**), with expansions of some signals, for clarity.

N,N′-*Bis-(4,6-((1-(3-propyl)piperidine)oxy]salicylidine)phenylenediaminenickel(II)*

(**55**)

A solution of (**70**) (98 mg, 0.24 mmol), 1,2-phenylenediamine (14 mg, 0.13 mmol) and $Ni(OAc)_2{\cdot}4H_2O$ (31 mg, 0.13 mmol) was dissolved in MeOH (6 mL). The solution was heated under reflux with constant stirring for 24 h. At the end of the reaction, the MeOH was removed under reduced pressure, leaving a solid residue.

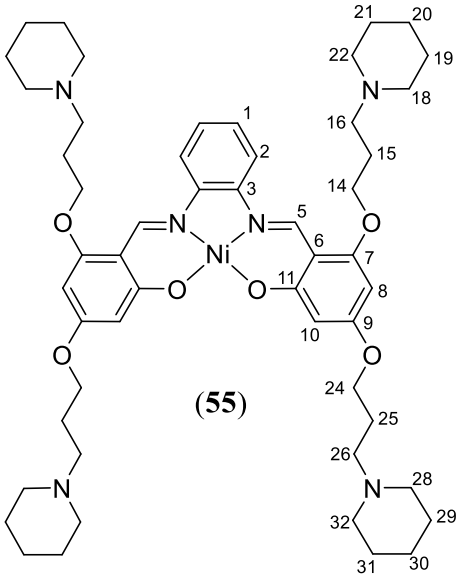

(**55**)

The latter was suspended in acetone and filtered using vacuum filtration to afford the product as a brown powder. Yield: 110 mg (50%). Microanalysis calc. for $C_{52}H_{74}N_6NiO_6.0.25H_2O$: C = 66.27; H = 7.97; N = 8.92; Ni = 6.23%. Found: C = 66.27; H =8.06; N = 9.11; Ni = 6.40%. ESI-MS calc: $[C_{52}H_{74}N_6NiO_6 + 2H]^{2+}$ = 469.9. Found: $[C_{52}H_{74}N_6NiO_6 + 2H]^{2+}$ = 469.9. ^{1}H NMR (500 MHz, $CDCl_3$): δ 1.47 (m, 8H, H20 and H30); 1.66 (m, 16H, H21, H19, H29 and H31); 2.02 (m, 4H, H25); 2.09 (m, 4H, H15); 2.52 (m, 16H, H18, H22, H28 and H32); 2.58 (m, 8H, H16 and H26); 3.96 (t, 4H, *J* = 6.13 and 6.15Hz, H24); 4.03 (t, 4H, *J* = 6.21 Hz, and 6.20 Hz H14); 5.68 (d, 2H, *J* = 1.81, H10); 6.21 (d, 2H, *J* = 1.53 Hz, H8); 7.14 (m, 2H, H1), 7.62 (m, 2H, H2), 8.62 (s, 2H, H5). ^{13}C NMR (101 MHz, CDCl3): δ 24.42 (C20, C30), 25.93 (C19, C21); 25.96 (C29, C31), 26.57 (C15); 26.72 (C25); 54.59 (C18, C22); 54.79 (C28, C32); 55.89 (C16); 56.19(C26); 66.62 (C24); 66.89 (C14); 89.83(C8); 96.50 (C10); 106.97 (C6); 114.30 (C2); 125.94 (C1); 143.54 (C3); 147.67 (C5); 160.12(C7); 165.36 (C9); 168.50 (C11).

The ^{1}H NMR spectrum of (**55**) is shown in Figure 3.18, and is similar to that of (**53**). However, replacing the dimethylenepiperidine groups with trimethylenepiperidine moieties resulted in some changes to the aliphatic region of the spectrum. The two methylene groups nearest the phenolic oxygen atoms in (**55**) were again found to be the most deshielded and gave rise to triplets at 3.96 and 4.03 ppm (H24 and H14, respectively). A complex set of overlapping resonances at 2.52 - 2.58 ppm was

assigned to the two methylenes in the linker nearest the piperidine nitrogen atoms (H16 and H26) as well as to H18, H22, H28 and H32. Finally, the two quintets at 2.02 and 2.09 ppm were assigned to the central methylene groups (H25 and H15, respectively) in the alkyl linker regions. All resonances assigned to the aromatic protons and the imine protons of (**55**) were found at similar chemical shifts to the corresponding protons in the ^{1}H NMR spectrum of (**53**).

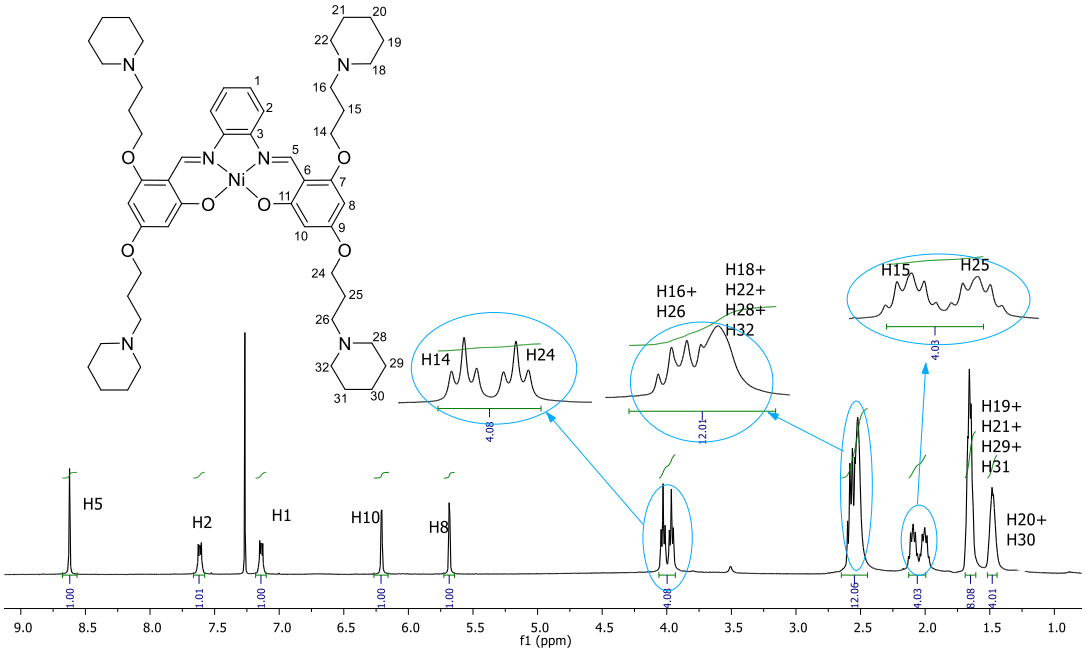

Figure 3.18: ^{1}H NMR spectrum of (**55**), with an expansion of some signals, for clarity.

N,N′-*Bis-(4,6-((1-(2-ethyl)piperidine)oxy)salicylidine)ethylenediaminenickel(II)* (**56**)

A solution of (**68**) (60 mg, 0.16 mmol), ethylenediamine (4.8 mg, 0.080 mmol) and $Ni(OAc)_2 \cdot 4H_2O$ (20 mg, 0.080 mmol) was dissolved in MeOH (4 mL). The solution was heated under reflux with constant stirring for 24 h. During this time a brown precipitate appeared in the dark brown solution. At the end of the reaction, the MeOH was removed under reduced pressure, leaving a solid residue which was suspended in acetone and filtered using vacuum filtration to afford the product as a

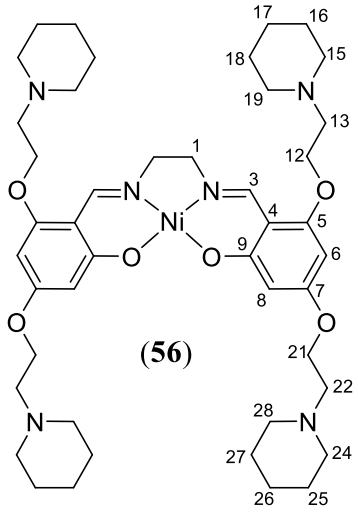

(**56**)

brown powder. Yield: 83 mg (63%). Microanalysis calc. for $C_{44}H_{66}N_6NiO_6 \cdot 1.5H_2O$: C = 61.40; H = 8.08; N = 9.76; Ni = 6.82%. Found: C = 62.07; H = 7.80; N = 9.48; Ni = 6.7%. ESI-MS calc: $[C_{44}H_{66}N_6NiO_6 + 2H]^{2+}$ = 417.5, $[C_{44}H_{66}N_6NiO_6 + 2H]^{2+}$ = 417.2. ^{1}H NMR (400 MHz, $CDCl_3$): δ 1.43 (m, 8H, H17 and H26); 1.59 (m, 16H, H16, H18, H25 and H27); 2.47 (m, 16H, H15, H19, H24 and H28); 2.74 (m, 8H, H13 and H22); 3.31 (s, 4H, H1); 4.03 (m, 8H, H12 and H21); 5.63 (d, 2H, *J* = 2.05, H6); 6.12 (d, 2H, *J* = 1.84 Hz, H8); 7.83 (s, 2H, H3). ^{13}C NMR (101 MHz, $CDCl_3$): δ 24.17-24.22 (C17 and C26); 25.91-25.98 (C16, C18, C25 and C27); 54.89-54.92 (C15, C19, C24 and C28); 57.75-57.76 (C13 and C22); 58.78 (C1); 65.75-66.14 (C12 and C21); 89.19 (C6); 96.90 (C8); 106.04 (C4); 155.97 (C3); 159.29 (C5); 163.73 (C7); 167.26 (C9).

The resonances in the ^{1}H NMR spectrum of (**56**) (Figure 3.19) were readily identified through a comparison with the corresponding spectrum of (**53**), which has a nearly identical, symmetric structure. The only difference between the two structures is that the phenylenediamine moiety in (**68**) is replaced by an ethylenediamine moiety in (**56**). The absence of the aromatic system led to the resonance from the imine protons H3 in (**56**) moving further upfield to 7.83 ppm. In addition, the singlet at 3.31 ppm was assigned to H1 as its integration corresponded to four hydrogen atoms.

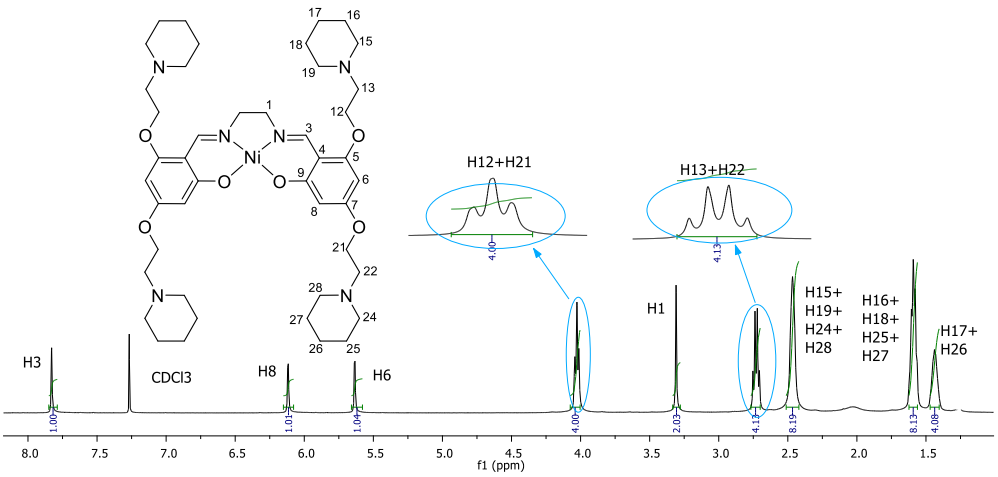

Figure 3.19: ^{1}H NMR spectrum of (**56**), with expansions of some signals, for clarity.

N,N′-*Bis-(4,6-((1-(2-ethyl)morpholine)oxy)salicylidine)ethylenediaminenickel(II)* (**57**)

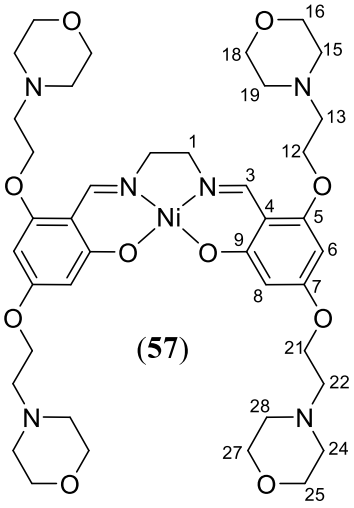

A solution of (**69**) (45 mg, 0.12 mmol), ethylenediamine (3.6 mg, 0.060 mmol) and $Ni(OAc)_2{\cdot}4H_2O$ (15 mg, 0.060 mmol) was prepared in MeOH (3 mL). The solution was heated under reflux with constant stirring for 4 h. At the end of the reaction, the MeOH was removed under reduced pressure, leaving a solid residue. The latter was then suspended in anhydrous diethyl ether and filtered using vacuum filtration to afford the product as a brown powder. Yield: 50 mg (50%). Microanalysis calc. for $C_{40}H_{58}N_6NiO_{10}{\cdot}1.5H_2O$: C = 55.31; H = 7.08; N = 9.68; Ni = 6.76%. Found: C = 55.26; H = 7.11; N = 9.78; Ni = 6.40%. ESI-MS calc: $[C_{40}H_{58}N_6NiO_{10} + 2H]^{2+}$ = 421.8. Found: $[C_{40}H_{58}N_6NiO_{10} + 2H]^{2+}$ = 421.8. ^{1}H NMR (400 MHz, $CDCl_3$): δ 2.54 (m, 16H, H15, H19, H24 and H28); 2.77 (m, 8H, H13 and H22); 3.32 (s, 4H, H1);

3.73 (m, 16H, H16, H18, H25 and H27); 4.04 (m, 8H, H12 and H21); 5.63 (d, 2H, *J* = 2.15 Hz, H6); 6.11 (d, 2H, *J* = 1.97 Hz, H8); 7.82 (s, 2H, H3). ^{13}C NMR (101 MHz, CDCl3): δ 53.98-53.99 (C15, C19, C24 and C28); 57.42-57.47 (C13 and C22); 58.82 (C1); 65.42 (C21); 65.98 (C12), 66.91-66.95 (C16, C18, C25 and C27), 89.21 (C6); 96.89 (C8); 106.06 (C4); 155.88 (C3); 159.18 (C5); 163.57 (C7); 167.28 (C9).

N,N′-*Bis-(4,6-((1-(3-propyl)piperidine)oxy]salicylidine)ethylenediaminenickel(II)* (**58**)

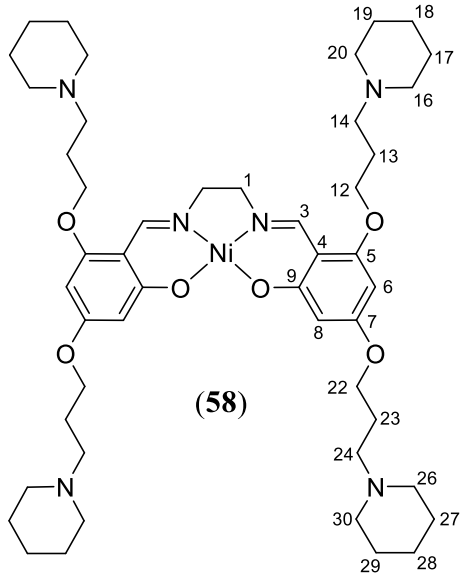

(**58**)

A solution of (**70**) (72 mg, 0.18 mmol), ethylenediamine (5.5 mg, 0.092 mmol) and $Ni(OAc)_2 \cdot 4H_2O$ (22 mg, 0.088 mmol) was prepared in MeOH (4 mL). The solution was heated under reflux with constant stirring for 24 h. At the end of the reaction, the MeOH was removed under reduced pressure, leaving a solid residue. The latter was suspended in anhydrous diethyl ether and filtered using vacuum filtration to afford the product as an orange powder. Yield: 90 mg (57%). Microanalysis calc. for $C_{48}H_{74}N_6NiO_6 \cdot 0.5C_4H_{10}O$: C = 64.79; H = 8.59; N = 9.07; Ni = 6.30%. Found: C = 65.13; H = 8.78; N = 9.14; Ni = 6.30%. ESI-MS calc: $[C_{48}H_{74}N_6NiO_6 + 2H]^{2+}$ = 445.9. Found: $[C_{48}H_{74}N_6NiO_6 + 2H]^{2+}$ = 445.9. ^{1}H NMR (400 MHz, $CDCl_3$): δ 1.44 (m, 8H, H18 and H28); 1.60 (m, 16H, H17, H19, H27 and H29); 1.94 (m, 8H, H13 and H23); 2.42 (m, 12H, H14, H20, H16, H24, H26 and H30); 3.31 (s, 4H, H1); 3.92 (m, 8H, H12 and H22); 5.6 (d, 2H, *J* = 1.96 Hz, H6); 6.11 (d, 2H, *J* = 1.62 Hz, H8); 7.82 (s, 2H, H3).^{13}C NMR (101 MHz, CDCl3): δ 24.34 (C18); 24.37 (C28); 25.90

(C17, C19, C27 and C29); 26.58 (C13); 26.73 (C23), 54.55 (C16, C20); 54.61 (C26, C30); 55.92 (C14); 56.07 (C24); 58.71 (C1); 66.33(C12); 66.54 (C22); 88.73 (C6); 93.62 (C8); 105.74 (C4); 155.66 (C3); 159.35 (C5); 163.86 (C7); 167.22 (C9).

The ^{1}H NMR spectra of (**57**) and (**58**) are shown in Figure S3.4 and Figure S3.5 Both are, not surprisingly, similar to the ^{1}H NMR spectrum of (**56**), as the only difference between the three structures is that the ethylpiperidine moieties in the latter molecule have been replaced with ethylmorpholine and propylpiperidine moieties in (**57**) and (**58**), respectively.

N,N′-*Bis-((4-((1-(3-propyl)piperidine)oxy)salicylidine)-1,3-propylenediamine-nickel(II)* (**59**)

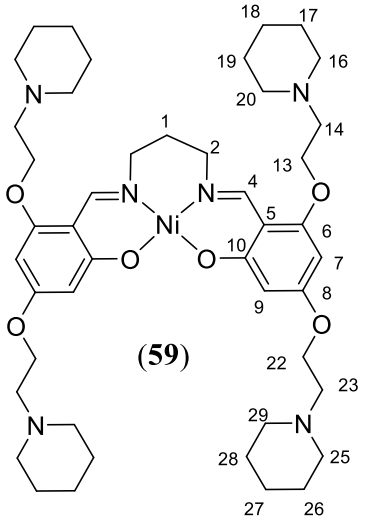

(**59**)

A solution of (**68**) (72 mg, 0.19 mmol), 1,3-diaminopropane (7 mg, 0.09 mmol) and $Ni(OAc)_2 \cdot 4H_2O$ (24 mg, 0.096 mmol) was prepared in MeOH (4 mL). The solution was heated under reflux with constant stirring for 24 h. At the end of the reaction, the MeOH was removed under reduced pressure, leaving a solid residue, which was suspended in anhydrous diethyl ether and filtered using vacuum filtration to afford the product as a deep brown powder. Yield: 44 mg (55%). Microanalysis calc. for $C_{45}H_{68}N_6NiO_6.3MeOH$: C = 61.08; H = 8.54; N = 8.90; Ni = 6.22%. Found: C = 60.75; H = 8.17; N = 8.85; Ni = 5.90%. ESI-MS calc: $[C_{45}H_{68}N_6NiO_6 +3H]^{3+}$ =283.6. Found $[C_{45}H_{68}N_6NiO_6 +3H]^{3+}$ =283.6. ^{1}H NMR (400 MHz, $CDCl_3$): δ 1.43 (m, 8H, H18, and H27); 1.59 (m, 16H, H17, H19, H26 and H28); 1.85 (m, 2H, H1); 2.46 (m, 16H, H16, H20, H25 and H29); 2.71 (m, 8H, H14

and H23); 3.42 (t, 4H, *J* = 6.54 Hz, H2); 4.02 (t, 8H, *J* = 5.90, H13 and H22); 5.60 (d, 2H, *J* = 1.83 Hz, H7); 6.07 (d, 2H, *J* = 1.47 Hz, H9); 7.49 (s, 2H, H4) ^{13}C NMR (101 MHz, $CDCl_3$): δ 24.32-24.37 (C18 and C27); 26.05-26.13 (C17, C19, C26 and C28); 26.71 (C1); 55.01-55.07 (C16, C20, C25 and C29); 55.77 (C2); 57.88-57.90 (C14 and C23); 65.68-66.24 (C13 and C22); 89.03 (C9); 96.03 (C7); 106.40 (C5); 158.46 (C4); 159.53 (C6); 164.03 (C8); 166.65 (C10).

The ^{1}H NMR spectrum of (**59**) is shown in Figure 3.20, and is similar to that of (**56**). This was not surprising as the only difference between the two structures is that the ethylenediamine moiety in (**56**) is replaced by a 1,3-propylenediamine moiety in (**59**). Therefore, the aliphatic region of the ^{1}H NMR spectrum of the latter complex was slightly different. The triplet at 3.42 ppm was assigned to H2 as its integration corresponded to four hydrogen atoms. A gCOSY spectrum (Figure 3.21) was then used to identify that the quintet at 1.85 ppm corresponded to H1.

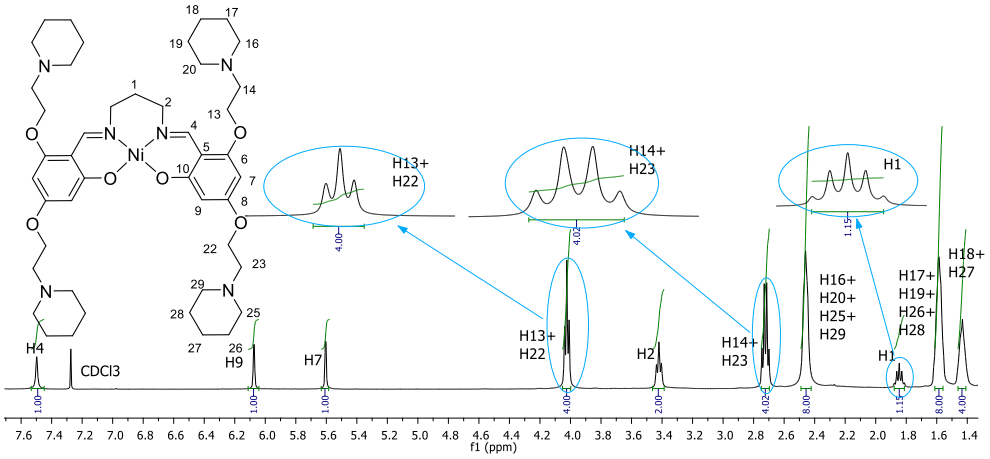

Figure 3.20: ^{1}H NMR spectrum of (**59**), with expansions of some signals, for clarity.

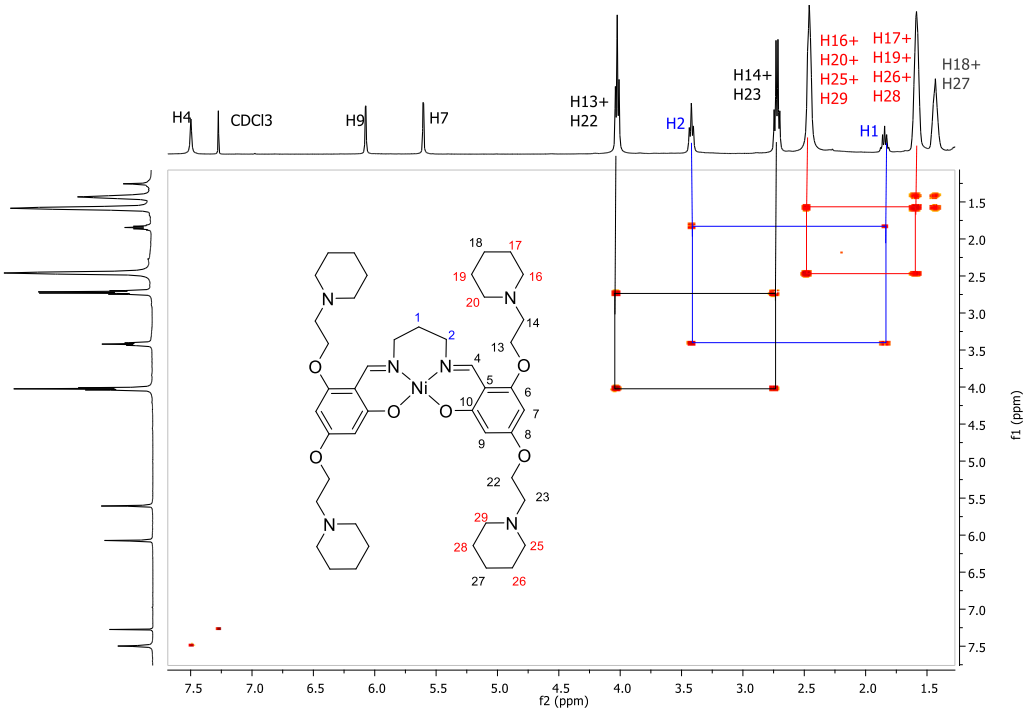

Figure 3.21: gCOSY spectrum of (**59**), with selected H-H correlations highlighted.

N,N′-*Bis-(4,6-((1-(2-ethyl)morpholine)oxy)salicylidine)-1,3-propylenediamine-nickel(II)* (**60**)

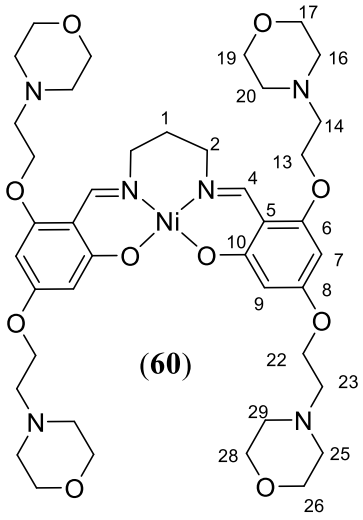

A solution of (**69**) (45 mg, 0.12 mmol), 1,3-diaminopropane (4.4 mg, 0.059 mmol) and $Ni(OAc)_2 \cdot 4H_2O$ (15 mg, 0.060 mmol) was prepared in MeOH (2.5 mL). The solution was heated under reflux with constant stirring for 24 h. At the end of the reaction, the MeOH was removed under reduced pressure, leaving a solid residue, which was suspended in anhydrous diethyl ether and filtered using vacuum filtration to afford the product as a red-brown powder. Yield: 60 mg (59%). Microanalysis calc. for $C_{41}H_{60}N_6NiO_{10} \cdot 0.2C_4H_{10}O$: C = 57.67; H =7.18; N = 9.65; Ni

= 6.74%. Found: C = 57.5; H = 7.46; N = 9.6; Ni = 6.60%. ESI-MS calc: $[[C_{41}H_{60}N_6NiO_{10}]^+ + 2H]^{2+}$ = 428.8. Found: $[[C_{41}H_{60}N_6NiO_{10}]^+ + 2H]^{2+}$ = 428.8. ^{1}H NMR (400 MHz, $CDCl_3$): δ 1.86 (m, 2H, H1); 2.53 (m, 16H, H16, H20, H25 and H29); 2.77 (m, 8H, H14 and H23), 3.43 (t, 4H, *J* = 6.57 Hz and 6.57 Hz, H2); 3.72 (m, 16H, H17, H19, H26 and H28); 4.04 (m , 8H, H13 and H22); 5.60 (d, 2H, *J* = 2.13 Hz, H9); 6.07 (d, 2H, *J* = 2.00 Hz, H7); 7.48 (s, 2H, H4). ^{13}C NMR (101 MHz, $CDCl_3$): δ 26.61 (C1); 53.97 (C16, C20, C25 and C29); 55.80 (C2); 57.43 (C14 and C23); 65.36 (C22), 65.89 (C13), 66.89-66.93 (C17, C19, C26 and C28); 88.93 (C7); 96.05 (C9); 106.32 (C5); 158.28 (C4); 159.32 (C6); 163.78 (C8); 166.49 (C10).

The ^{1}H NMR spectrum of (**60**) (Figure S3.6) was, not surprisingly, found to be similar to that of (**59**), with the only differences being changes to the chemical shifts of some resonances noted previously to occur when the terminal methylenes of the piperidine groups are replaced by oxygen atoms in the morpholines.

N,N′-*Bis-((4,6-((1-(3-propyl)piperidine)oxy)salicylidine)-1,3-propylenediamine-nickel(II)* (**61**)

A solution of (**70**) (100 mg, 0.25 mmol), 1,3-diaminopropane (9.3 mg, 0.13 mmol) and $Ni(OAc)_2{\cdot}4H_2O$ (32 mg, 0.13 mmol) was prepared in MeOH (3.5 mL). The solution was heated under reflux with constant stirring for 24 h. At the end of the reaction, the MeOH was removed under reduced pressure, leaving a solid residue, which was suspended in n-hexane and filtered using vacuum filtration to afford the product as a brown powder. Yield: 140 mg (61%). Microanalysis calc. for $C_{49}H_{76}N_6NiO_6{\cdot}2MeOH$: C = 63.28; H = 8.75; N = 8.68; Ni = 6.06%. Found: C = 63.33; H = 8.67; N = 8.52; Ni = 6.30%. ESI-MS calc: $[C_{49}H_{76}N_6NiO_6 + 2H]^{2+}$ =452.3, Found: $[C_{49}H_{76}N_6NiO_6 + 2H]^{2+}$ = 452.3. ^{1}H NMR (400 MHz, $CDCl_3$): δ 1.44

(m, 8H, H19, and H29); 1.59 (m, 16H, H18, H20, H28 and H30); 1.85 (m, 2H, H1); 1.93 (m, 8H, H14, and H24); 2.40 (m, 12H, H15, H17, H21, H25, H27 and H31); 3.42 (t, 4H, *J* = 5.89 Hz, H2); 3.91 (m, 8H, H13 and H23); 5.57 (d, 2H, *J* = 1.61 Hz, H7); 6.07 (d, 2H, *J* = 1.19 Hz, H9); 7.49 (s, 2H, H4). ^{13}C NMR (101 MHz, $CDCl_3$): δ 24.41 (C19 and C29); 26.10 (C18, C20, C28 and C30); 26.7-26.92 (C1, C14 and C24); 54.76-54.81 (C17, C21, C27 and C31); 55.71 (C2); 56.14-56.28 (C15 and C25); 66.55-66.78 (C13 and C23); 88.69 (C7); 96.01 (C9); 106.22 (C5); 158.23 (C4); 159.70 (C6); 164.30 (C8); 166.65 (C10).

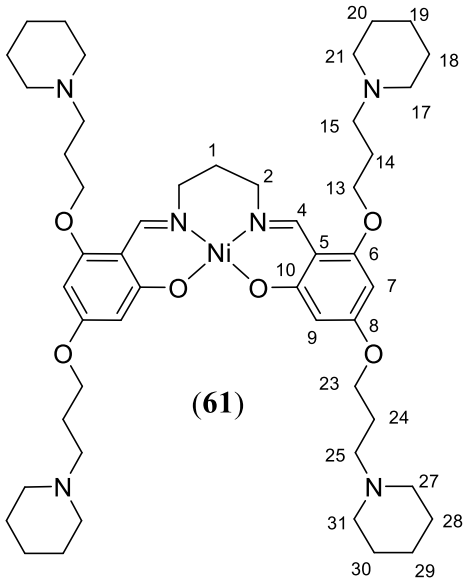

(**61**)

The ^{1}H NMR spectrum of (**61**) is shown in Figure S3.7 and was found to be similar to that of (**59**). A gCOSY spectrum (Figure S3.8) was used to identify that the overlapping resonances at 1.93 and 1.85 ppm corresponded to H14/H24 and H1, respectively.

N,N′-*Bis-(4-((1-(3-propyl)piperidine)oxy]salicylidine)-1,2-propylenediamine-nickel(II)* (**62**)

A solution of (**68**) (74 mg, 0.19 mmol), 1,2-diaminopropane (8.4 mg, 0.11 mmol) and $Ni(OAc)_2{\cdot}4H_2O$ (25 mg, 0.10 mmol) was prepared in MeOH (4.3 mL). The solution was heated under reflux with constant stirring for 24 h. At the end of the reaction, the MeOH was removed under reduced pressure, leaving a solid residue, which was suspended in anhydrous diethyl ether and filtered using vacuum filtration to afford the product as a red-brown powder. Yield: 77 mg (46%). Microanalysis

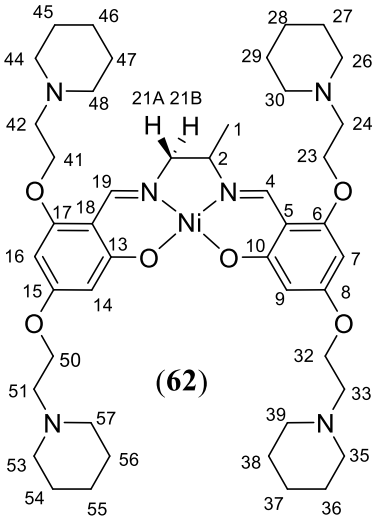

(**62**)

calc: for $C_{45}H_{68}N_6NiO_6 \cdot 0.5H_2O$: C = 63.08; H = 8.12; N = 9.81; Ni = 6.85%. Found: C = 63.23; H = 8.30; N = 9.63; Ni =6.60%. ESI-MS calc: $[C_{45}H_{68}N_6NiO_6 + 2H]^{2+}$ = 424.2, $[C_{45}H_{68}N_6NiO_6 + 2H]^{2+}$ = 424.2. ^{1}H NMR (500 MHz, $CDCl_3$): δ 1.39 (d, 3H, *J* = 6.59 Hz, H1); 1.43 (m, 8H, H28, H37, H46 and H55); 1.59 (m, 16H, H27, H29, H36, H38, H45, H47, H54 and H56); 2.47 (m, 16H, H26, H30, H35, H39, H44, H48, H53 and H57); 2.73 (m, 8H, H24, H33, H42, and H51); 2.83 (dd, 1H, *J* = 2.22 Hz and 12.69 Hz, H21B), 3.34 (m, 1H, H2); 3.58 (dd, 1H, *J* = 5.65 Hz and 12.25 Hz, H21A); 4.03 (m , 8H, H23, H32, H41 and H50); 5.64 (s, 2H, H7 and H16); 6.12 (s, 2H, H9 and H14); 7.79 (s, 2H, H4 and H19). ^{13}C NMR (101 MHz, $CDCl_3$): δ 21.50 (C1); 24.18-24.23 (C28, C37, C46 and C55); 25.92-26.02 (C27, C29, C36, C38, C45, C47, C54 and C56); 54.89-54.94 (C26, C30, C35, C39, C44, C48, C53 and C57); 57.75 (C24, C33, C42 and C51); 63.61 (C2); 65.11 (C21); 65.57-66.20 (C23, C32, C41 and C50); 89.10-89.17 (C7, C16); 96.84-96.93 (C9, C14); 106.09-106.13 (C5 and C18); 154.83 (C19); 156.30 (C4); 159.23-159.26 (C6 and C17); 163.67-163.69 (C8 and C15); 167.13-167.27 (C10 and C13).

Complexes (**62**), (**63**) and (**64**) differ in structure from those described above in having a 1,2-diaminopropane group as the diamine moiety. A consequence of this change was that not only were the atoms in the pendant groups in the top and bottom halves of the molecules in slightly different chemical environments, so too were those on the left- and right-hand sides. This manifested itself in very slight differences in chemical shift for certain clusters of protons. For example, the ^{1}H

NMR spectrum of (**62**) shown in Figure 3.22 shows a broad peak near 1.6 ppm from H27, H29, H36, H38, H45, H47, H54 and H56. In addition, the ^{1}H NMR spectrum of the above three complexes showed a characteristic set of multiplets arising from the protons in the 1,2-diaminopropane groups. This is exemplified by the ^{1}H NMR spectrum of (**62**) shown in Figure 3.22. This shows two doublet of doublets from the diastereotopic protons H21A and H21B, as well as an apparent triplet at 3.34 ppm from H2 and a doublet at 1.39 ppm from the methyl protons. Each of these assignments was confirmed through the use of gCOSY and NOESY spectra.

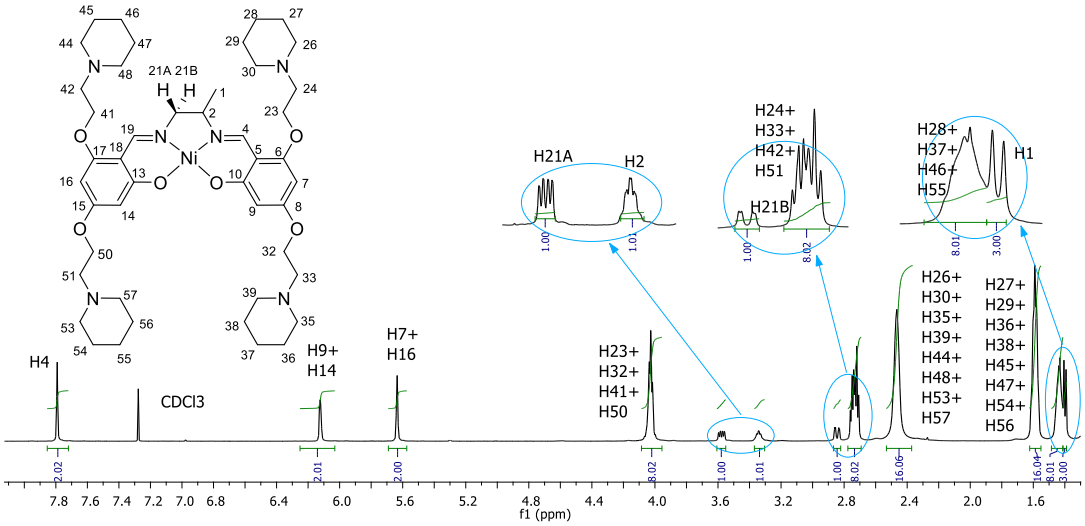

Figure 3.22: ^{1}H NMR spectrum of (**62**), with expansions of some signals, for clarity.

N,N′-*Bis-(4,6-((1-(2-ethyl)morpholine)oxy)salicylidine)-1,2-propylenediamine-nickel(II)* (**63**)

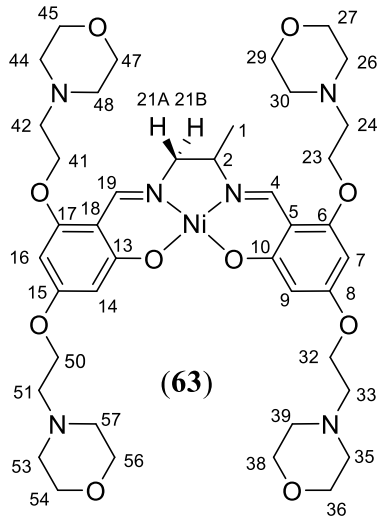

(**63**)

A solution of (**69**) (62 mg, 0.16 mmol), 1,2-diaminopropane (6.1 mg, 0.082 mmol) and $Ni(OAc)_2 \cdot 4H_2O$ (21 mg, 0.084 mmol) was prepared in MeOH (4 mL). The solution was heated under reflux with constant stirring for 24 h. At the end of the reaction, the MeOH was removed under reduced pressure, leaving a solid residue, which was suspended in anhydrous diethyl ether and filtered using vacuum filtration to afford the product as a red-brown powder. Yield: 50 mg (36%). Microanalysis calc: for $C_{41}H_{60}N_6NiO_{10}$: C = 57.55; H = 7.07; N = 9.82; Ni = 6.86%. Found: C = 57.31; H = 7.39; N = 9.79; Ni = 6.60%. ESI-MS calc: $[C_{41}H_{60}N_6NiO_{10} + 2H]^{2+}$ = 428.2. Found: $[[C_{41}H_{60}N_6NiO_{10}]^+ + H]^+$ = 428.2. ^{1}H NMR (400 MHz, $CDCl_3$): δ 1.40 (d, 3H, *J* = 6.52 Hz, H1) 2.54 (m, 16H, H26, H30, H35, H39, H44, H48, H53 and H57); 2.77 (m, 8H, H24, H33, H42 and H51); 2.88 (dd, 1H, *J* = 1.89 Hz and 12.58 Hz, H21B); 3.36 (m, 1H, H2), 3.58 (dd, 1H, *J* = 5.27 Hz and 12.48 Hz H21A); 3.73 (m, 16H, H27, H29, H36, H38, H45, H47, H54 and H56); 4.03 (m, 8H, H23, H32, H41 and H50); 5.64 (s, 2H, H9 and H14); 6.12 (s, 2H, H7 and H16); 7.80 (s, 2H, H4 and H19). ^{13}C NMR (101 MHz, $CDCl_3$): δ 21.45 (C1); 53.98 (C26, C30, C35, C39, C44, C48, C53 and C57); 57.41-57.45 (C24, C33, C42 and C51); 63.63 (C2); 65.16 (C21); 65.38-66.01 (C23, C32, C41 and C50); 66.89-66.94 (C27, C29, C36, C38, C45, C47, C54 and C56); 89.12-89.19 (C9, C14); 96.81-

96.90 (C7, C16); 106.13-106.17 (C5, C18); 154.74 (C4); 156.22 (C19); 159.14-159.17 (C6 and C17); 163.52-163.54 (C8 and C15); 167.12-167.27 (C10 and C13).

N,N′-*Bis-(4,6-((1-(3-propyl)piperidine)oxy]salicylidine)-1,2-propylenediamine-nickel(II)* (**64**)

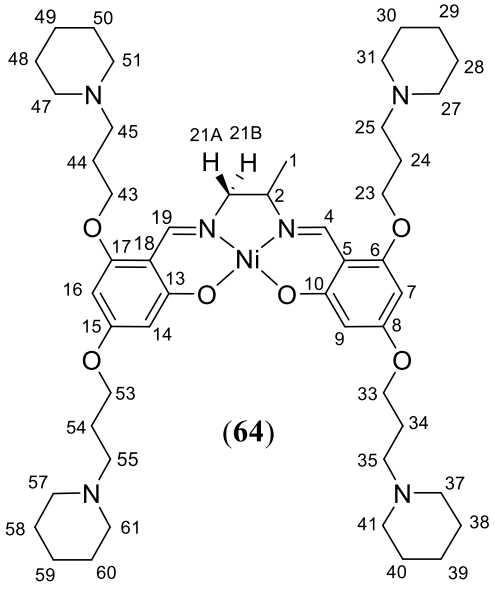

(**64**)

A solution of (**70**) (99 mg, 0.24 mmol), 1,2-diaminopropane (9.1 mg, 0.12 mmol) and $Ni(OAc)_2{\cdot}4H_2O$ (31 mg, 0.12 mmol) was prepared in MeOH (5 mL). The solution was heated under reflux with constant stirring for 24 h. At the end of the reaction, the MeOH was removed under reduced pressure, leaving a solid residue, which was suspended in acetone then filtered using vacuum filtration to afford the product as an orange powder. Yield: 120 mg (54%). Microanalysis calc: for $C_{49}H_{76}N_6NiO_6{\cdot}2H_2O$: C = 62.62; H = 8.58; N =8.94; Ni = 6.25%. Found: C = 62.36; H = 8.51; N = 8.94; Ni = 6.1%. ESI-MS calc: $[C_{49}H_{76}N_6NiO_6 + 2H]^{2+}$ = 452.3, $[[C_{49}H_{76}N_6NiO_6]^{+} + 2H]^{2+}$ = 452.4. ^{1}H NMR (400 MHz, $CDCl_3$): δ 1.40-1.45 (m, 11H, H1, H29, H39, H49 and H59); 1.55-1.62 (m, 16H, H28, H30, H38, H40, H48, H50, H58 and H60); 1.90-1.98 (m, 8H, H24, H34, H44 and H54); 2.39-2.42 (m, 24H, H25, H27, H31, H35, H37, H41, H45, H47, H51, H55, H57 and H61); 2.82 (d, 1H, *J* = 12.42 Hz, H21B); 3.34 (t, 1H, *J* = 6.98 Hz H2), 3.58 (dd, 1H, *J* = 5.48 Hz and 12.11 Hz, H21A); 3.91 (m, 8H, H23, H33, H43 and H53); 5.61 (s, 2H, H9 and H14); 6.12 (s, 2H, H7 and H16); 7.78 (s, 2H, H4 and H19). ^{13}C NMR (101 MHz, $CDCl_3$): δ 21.73 (C1); 24.44-24.47 (C29, C39, C49 and

C59); 26.00-26.01 (C28, C30, C38, C40, C48, C50, C58 and C60); 26.69-26.83 (C24, C34, C44 and C54); 54.63 (C27, C31, C47 and C51); 54.67-54.70 (C25 and C45), 55.98 (C37, C41, C57 and C61); 56.14-56.18 (C35 and C55); 63.64 (C2); 65.07 (C21); 66.43-66.66 (C23, C33, C43 and C53); 88.80 (C9 and C14); 96.67 (C7 and C16); 105.92 (C5 and C18); 154.66 (C4); 156.08 (C19); 159.37 (C6 and C17); 163.92 (C8 and C15) and 167.33 (C10 and C13).

The ^{1}H NMR spectra of (**63**) and (**64**) (Figure S3.9 and Figure S3.10, respectively) were very similar to that of (**62**), with the only significant differences being those described previously for other related series of complexes, which arose from the changes in the structure of the pendant groups.

N,N′-*Bis-(4,6-((1-(2-ethyl)piperidine)oxy)salicylidine)meso-diphenylethylene-diaminenickel(II)* (**65**)

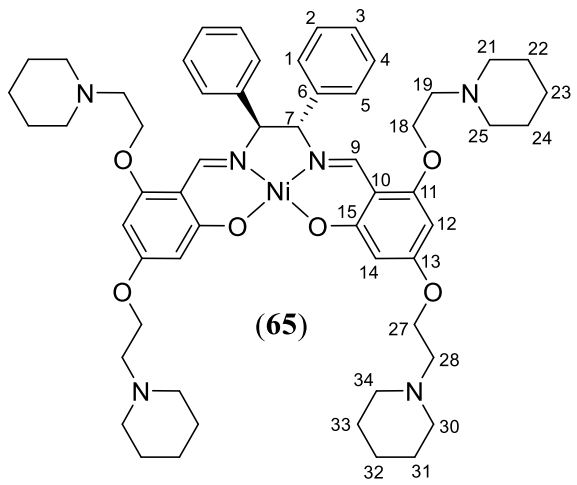

A solution of (**68**) (340 mg, 0.90 mmol) and 1,2-*meso*-diphenylethylene-diamine (96 mg, 0.45 mmol) in EtOH (25 mL) was heated under reflux with constant stirring for 1h. At this time the EtOH was replaced with MeOH (25 mL) and $Ni(OAc)_2 \cdot 4H_2O$ (110 mg, 0.45 mmol) added. The reaction mixture was then brought again to reflux with constant stirring for a further 24 h. At the end of the reaction, the MeOH was removed under reduced pressure, leaving a solid residue, which was suspended in anhydrous diethyl ether and filtered using vacuum filtration to afford the product as a brown powder. Yield: 300 mg (66%). Microanalysis calc: for

$C_{56}H_{74}N_6NiO_6$: C = 68.22; H = 7.57; N = 8.52; Ni = 5.95%. Found: C = 68.13; H = 7.79; N = 8.41; Ni =5.80%. ESI-MS calc: $[C_{56}H_{74}N_6NiO_6 + H]^+$ = 985.5, $[C_{56}H_{74}N_6NiO_6 + 2H]^{2+}$ = 493.3. Found: $[C_{56}H_{74}N_6NiO_6 + H]^+$ = 985.6, $[C_{56}H_{74}N_6NiO_6 + 2H]^{2+}$ = 493.5. ^{1}H NMR (400 MHz, $CDCl_3$): δ 1.33 (m, 4H, H32); 1.44 (m, 12H, H23, H31 and H33); 1.60 (m, 8H, H22 and H24); 2.20 (m, 8H, H30 and H34); 2.47 (m, 8H, H21 and H25); 2.52 (m, 4H, H19); 2.73 (t, 4H, *J* = 5.71 Hz, H28); 3.87 (m, 4H, 18); 4.05 (t, 4H, *J* = 5.72 Hz, H27); 4.69 (s, 2H, H7); 5.56 (s, 2H, H12), 6.17 (s, 2H, H14), 7.19 (m, 4H, H1 and H5), 7.25 (m, 2H, H3), 7.37 (broad-s, 4H, H2 and H4), 7.66 (s, 2H, H9). ^{13}C NMR (101 MHz, $CDCl_3$): δ 23.99 (C32); 24.19 (C23); 25.88 (C22, C24, C31 and C33); 54.51 (C30, C34); 54.86 (C21, C25); 57.56 (C19); 57.70 (C28), 65.55 (C27); 66.11 (C18); 77.74 (C7), 89.07 (C12); 96.74 (C14); 106.22 (C10); 128.17 (C1 and C5); 128.42 (C3); 129.63 (C2 and C4); 135.85 (C6); 156.43 (C9); 159.39 (C11); 164.03 (C13); 167.22 (C15).

The ^{1}H NMR spectra of (**65**), (**66**) and (**67**) showed that the chemical environments of a number of related protons in the top and bottom pendant groups were more dissimilar than for a number of the complexes discussed previously. This is illustrated by Figure 3.23, which compares the ^{1}H NMR spectra of (**65**) and (**56**). For example, resonances from the two sets of methylene groups in the linker regions adjacent to the oxygen atoms in (**65**) (H18 and H27) were found at 3.87 and 4.05 ppm, respectively. This is a greater chemical shift difference than what was found for the analogous methylene ^{1}H resonances (for H12 and H21) in the spectrum of (**56**), which overlapped to give a single multiplet at 4.03 ppm. Similar differences were also found for the resonances arising from the linker methylene groups adjacent to the nitrogen atoms in (**56**) and (**65**). A further difference between the ^{1}H NMR

spectra of (**65**) on the one hand, and those of the complexes discussed above also involves the linker methylene groups. Whilst typically two triplets were observed for both methylene groups in a dimethylene linker moiety, in the case of **(65)** one of the methylene groups (H18) gave rise to two broad and closely spaced multiplets. This was also found to be the case in the spectrum of **(66)** shown in Figure S3.11

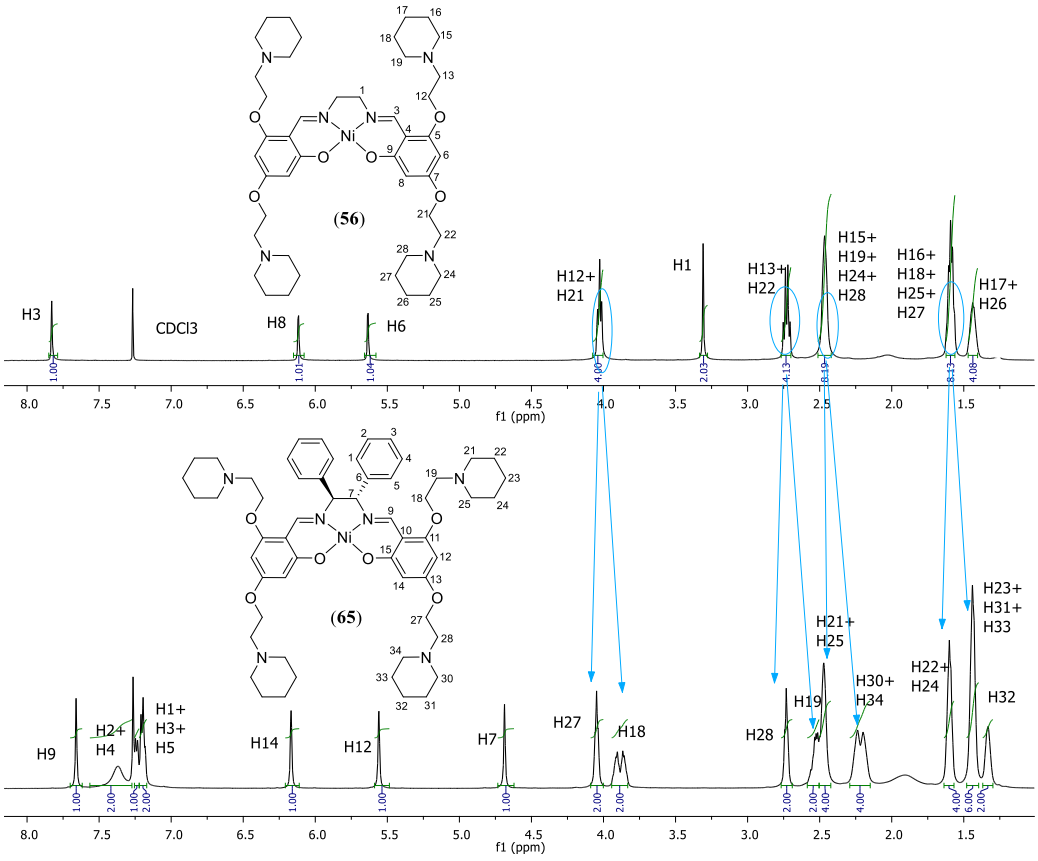

Figure 3.23: Comparison of the ^{1}H NMR spectra of (**56**) and (**65**).

N,N′-*Bis-(4,6-((1-(2-ethyl)morpholine)oxy)salicylidine)-meso-diphenylethylene-diaminenickel(II)* (**66**)

A solution of (**70**) (150 mg, 0.39 mmol), 1,2-*meso*-diphenylethylene-diamine (63 mg, 0.30 mmol) was prepared in EtOH (2.5 mL). The solution was heated under reflux with constant stirring for 1 h. At this time, the EtOH was replaced with MeOH

(2.5 mL) and $Ni(OAc)_2 \cdot 4H_2O$ (49 mg, 0.20 mmol) added to the reaction mixture. The solution was again brought to reflux with constant stirring for a further 24 h. At the end of the reaction, the MeOH was removed under reduced pressure, leaving a solid residue, which was suspended in anhydrous diethyl ether and filtered using vacuum filtration to afford the product as a brown solid. Yield: 150 mg (38%). Microanalysis calc: for $C_{52}H_{66}N_6NiO_{10} \cdot 2H_2O$: C = 60.64; H = 6.85; N = 8.16; Ni = 5.70%. Found: C = 60.69; H = 6.88; N = 8.33; Ni = 5.70%. ESI-MS calc: $[C_{52}H_{66}N_6NiO_{10} + 2\ H]^{2+}$ = 497.9. Found: $[C_{52}H_{66}N_6NiO_{10} + 2H]^{2+}$ = 497.9. ^{1}H NMR (400 MHz, $CDCl_3$): δ 2.26 (m, 8H, H30, and H34); 2.54 (m, 12H, H19, H21 and H25); 2.75 (t, 4H, *J* = 5.53 Hz, H28); 3.54 (t, 8H, *J* = 4.55 Hz, H31, H33); 3.73 (t, 8H, *J* = 4.58 Hz, H22 and H24); 3.88 (m, 4H, H18); 4.05 (t, 4H, *J* = 5.55 Hz, H27); 4.69 (s, 2H, H7); 5.56 (s, 2H, H12); 6.17 (s, 2H, H14); 7.21 (m, 4H, H1 and H5); 7.25 (m, 2H, H3); 7.36 (m, 4H, H2 and H4); 7.66 (s, 2H, H9). ^{13}C NMR (101 MHz, $CDCl_3$): δ 53.89 (C30, C34); 54.17 (C21, C25); 57.49 (C28); 57.58 (C19); 65.60 (C18), 66.40 (C27); 67.03 (C31, C33); 67.09 (C22, C24); 77.95 (C7); 89.31 (C12); 96.90 (C14); 106.45 (C10); 128.44 (C1 and C5); 128.76 (C3); 129.78 (C2 and C4); 135.98 (C6); 156.59 (C9); 159.49 (C11); 164.09 (C13); 167.41 (C15).

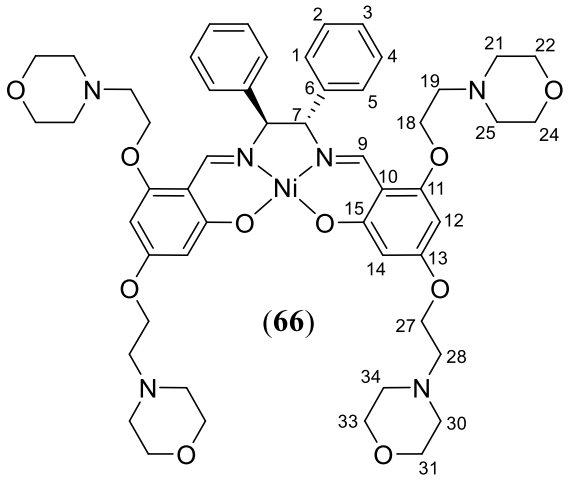

N,N′-*Bis-(4,6-((1-(3-propyl)piperidine)]oxy)salicylidine)meso-diphenylethylene-diaminenickel(II).*(**67**)

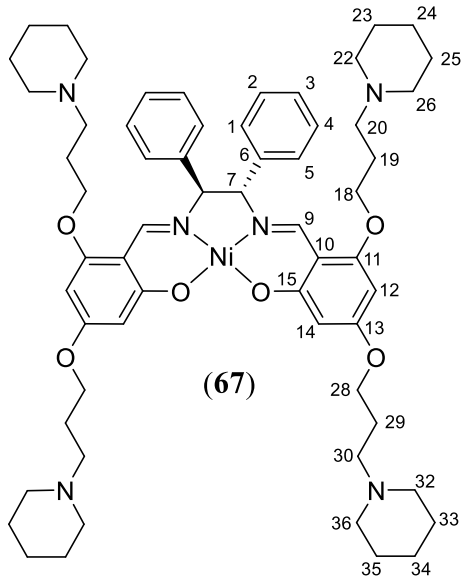

(**67**)

A solution of compound (**70**) (88 mg, 0.22 mmol), and 1,2-*meso*-diphenylenediamine (31 mg, 0.015 mmol) in EtOH (5 mL) was heated under reflux with constant stirring for 1h. At this time the EtOH was replaced with MeOH (5 mL) and $Ni(OAc)_2 \cdot 4H_2O$ (28.3 mg, 0.11 mmol)) added to the reaction mixture. The solution was again brought to reflux with constant stirring for a further 48 h. At the end of the reaction, the MeOH was removed under reduced pressure, leaving a solid residue, which was then dissolved in DCM (15 mL), and washed with water seven times. After the washing step, the DCM solution was dried with $MgSO_4$. The solvent was then removed under low pressure to afford the product as a red- orange solid. Yield: 66.9 mg, 30 %. ESI-MS calc: $[[C_{60}H_{82}N_6NiO_6]^+ + 2H]^{2+}$ = 521.3. Found: $[[C_{60}H_{82}N_6NiO_6]^+ + 2H]^{2+}$ = 521.4. ^{1}H NMR (400 MHz, $CDCl_3$): δ 1.40-1.44 (m, 8H, H24 and H34); 1.50-1.55 (m, 8H, H23 and H25); 1.56-1.61 (m, 8H, H33 and H35); 1.68-1.75 (m, 4H, H19); 1.89-1.96 (m, 4H, H29); 2.15 (t, 4H, *J* = 7.81 Hz and 7.19 Hz, H20); 2.21 (m, 8H, H22, H26), 2.39 (m, 8H, H32, H36). 2.43 (t, 4H, *J* = 7.78 Hz and 7.31 Hz, H30); 3.75-3.83 (m, 4H, H18); 3.93 (t, 4H, *J* = 6.38 Hz and 6.36 Hz, H28); 4.69 (s, 2H, H7); 5.54 (d, 2H, *J* = 2.05 Hz, H12); 6.17 (d, 2H, *J* = 1.82 Hz, H14); 7.17-7.23 (m, 6H, H2, H3 and H4); 7.38-7.40 (m, 4H, H1, H5); 7.66 (s, 2H, H9). ^{13}C NMR (101 MHz, $CDCl_3$): δ 24.41 (C34); 24.47 (C24); 25.93 (C33, C35);

26.01 (C23, C25); 26.50 (C19); 26.67 (C29); 54.49 (C32, C36), 54.63 (C20), 55.92 (C22, C26); 55.96 (C30); 66.46 (C28); 66.51 (C18); 77.81 (C7); 88.86 (C12); 96.58 (C14); 106.13 (C10); 128.36 (C1, C5); 128.15 (C3); 129.57 (C2, C4); 135.94 (C6); 156.27 (C9); 159.59 (C11); 164.32 (C13); 167.30 (C15).

The ^{1}H NMR spectra of (**67**) is shown in Figure S3.12. Owing to the low yield and difficulties of reproducing (**67**), there was not sufficient quantity of this complex to run elemental analysis and DNA binding studies.

3.4 X-ray crystallographic characterisation of nickel complexes

Single-crystal X-ray structure determinations were performed by Dr Christopher Richardson of the School of Chemistry and Molecular Bioscience, University of Wollongong, Australia. Crystals of (**53**) suitable for single crystal X-ray analysis were obtained by slow diffusion of diethyl ether into a solution of the complex in DCM. Crystals of (**54**) and (**63**) were obtained by slow evaporation from DCM/petroleum spirit (1:3) solvent mixtures, and crystals of (**65**) were obtained by slow evaporation from a DCM/pentane (1:3) solvent mixture. The solid-state structures of these complexes are presented as ORTEPs, together with the numbering systems for the non-hydrogen atoms, in Figure 3.24. Details of the collected crystallographic data and structural refinements for the four complexes are summarised in Table 3.3.

Complex (**53**) crystallised in a triclinic crystal system with space group *P*-1, with one molecule of the nickel Schiff base complex and one water molecule in the asymmetric unit. One oxygen atom coordinated to the nickel atom is participating in a hydrogen bond interaction with the oxygen atom of the lattice water molecule. The structure of (**63**) also belongs to a triclinic crystal system with space group *P*-1, but with one molecule of the nickel Schiff base complex and six water molecules in the asymmetric unit. The asymmetric unit of (**54**) belongs to the monoclinic space group *C*2/c and consists of one full metal complex and one water molecule. One oxygen atom coordinated to the nickel atom was found to be participating in hydrogen bonding with a hydrogen atom of the lattice water molecule.

The asymmetric unit of (**65**) belongs to the monoclinic space group $P2_1/c$, and consists of one full metal complex and one water molecule.

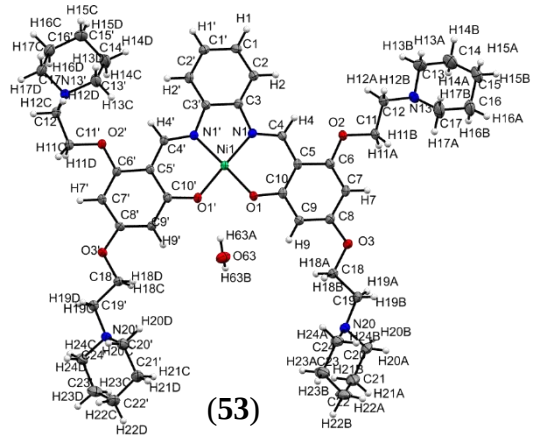

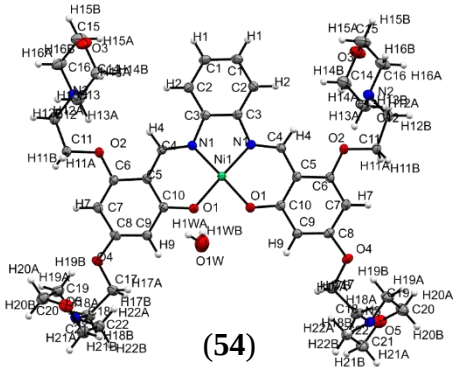

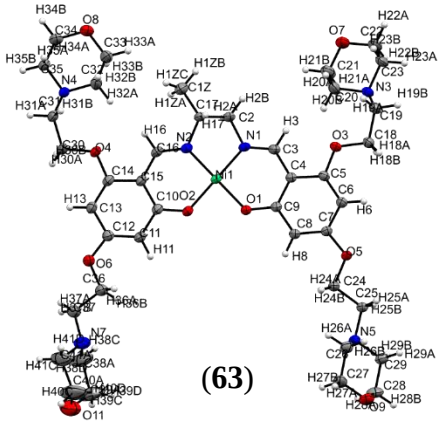

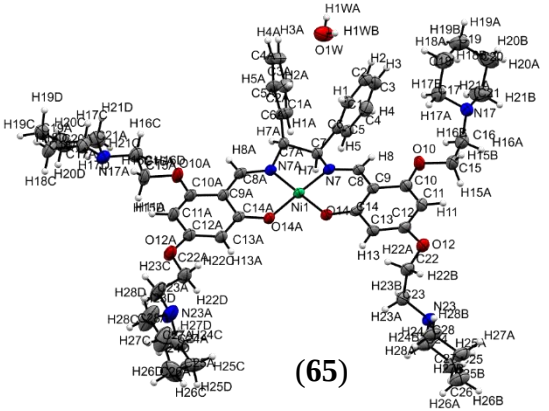

Figure 3.24: Molecular structures of (**53**), (**54**), (**63**) and (**65**)

Table 3.3: Summary of crystallographic data.

Complex label		(**53**)	(**54**)	(**63**)	(**65**)
Formula		$C_{48}H_{66}N_6NiO_6 \cdot H_2O$	$C_{44}H_{58}N_6NiO_{10} \cdot 2H_2O$	$C_{41}H_{60}N_6NiO_{10} \cdot 6H_2O$	$(C_{56}H_{74}N_6NiO_6)_4 \cdot H_2O$
M		899.79	925.70	966.15	990.42
Crystal system		Triclinic	monoclinic	triclinic	monoclinic
Space group		*P*-1	*C*2/c	*P*-1	$P2_1/c$
a (Å)		11.6711(8)	30.6127(5)	9.7651(2)	10.7829(3)
b (Å)		12.5315(9)	15.8401(3)	14.6637(3)	21.9025(5)
c (Å)		16.5737(11)	9.8494(2)	16.8916(3)	22.2389(5)
α (˚)		101.847(6)°	90	78.2060(10)	90
β (˚)		96.035(6)°	96.209(2)	83.1790(10)	99.678(3)
γ(˚)		97.628(6)°	90	89.109(2)	90
V (Å^3)		2329.4(3)	30.6127(5)	2350.83(8)	5177.4(2)
D_{calc} (g m^{-3})		1.283	1.295	1.365	1.271
Z		2	4	2	4
(h,k,l)		-16 ≤ h ≤ 16 -18 ≤ k ≤ 17 -23 ≤ l ≤ 23	-42 ≤ h ≤ 42 -22 ≤ k ≤ 21 -13 ≤ l ≤ 13	-13 ≤ h ≤ 13 -20 ≤ k ≤ 20 -23 ≤ l ≤ 23	-12 ≤ h ≤ 14 -28 ≤ k ≤ 29 -28 ≤ l ≤ 29
Number of unique reflections		13757	6653	12431	12745
Refinement	Final R indexes [I>=2σ (I)]	R1 = 0.0485 wR2 = 0.1131	R1 = 0.0348 wR2 = 0.0989	R1 = 0.0631 wR2 = 0.1432	R1 = 0.0631 wR2 = 0.1432
	Final R indexes [all data]	R1 = 0.0802 wR2 = 0.1232	R1 = 0.0432 wR2 = 0.1028	R1 = 0.1025 wR2 = 0.1609	R1 = 0.1025 wR2 = 0.1609

It was observed that the nickel atom in all four crystal structures adopts a square planar coordination geometry. All bond lengths and angles involving the central nickel ion (Table 3.4) are consistent with standard values.[125,135] The arrangement of the phenylenediamine moieties in (**53**) and (**54**) results in torsion angles N2-C3-C3′-N1 of 2.6(2)˚ and 0.24(2)˚, respectively. In contrast, the arrangement of the *meso*-1,2-diphenylethylenediamine moiety in (**65**) produces a torsion angle of -40.8(3)˚ This results in one phenyl ring being in an equatorial position, whilst the other is found in an axial position (Figure 3.25).

Table 3.4: Selected bond lengths (Å) and angles (˚) for nickel Schiff base complexes.

Bonds	**(53)**	**(54)**	**(63)**	**(65)**
Ni-O1	1.8372(12)	1.8585(17)	1.8406(10)	1.8581(10)
Ni-O2	1.8411(13)	1.8602(17)	1.8407(10)	1.8561(11)
Ni-N1	1.8468(15)	1.859(2)	1.8514(11)	1.8418(13)
Ni-N2	1.8547(14)	1.852(2)	1.8514(11)	1.8398(13)
O1-Ni-O2	84.12(5)	84.97(7)	83.31(6)	85.28(4)
O2-Ni-N2	94.73(6)	93.96(8)	94.99(5)	94.78(5)
O1-Ni-N2	175.52(6)	176.56(9)	178.22(4)	179.64(7)
O2-Ni-N1	176.77(6)	177.41(9)	178.22(5)	179.03(7)
O1-Ni-N1	95.02(6)	94.88(8)	94.99(5)	94.70(5)
N1-Ni-N2	86.37(6)	86.34(9)	86.72(7)	85.24(6)

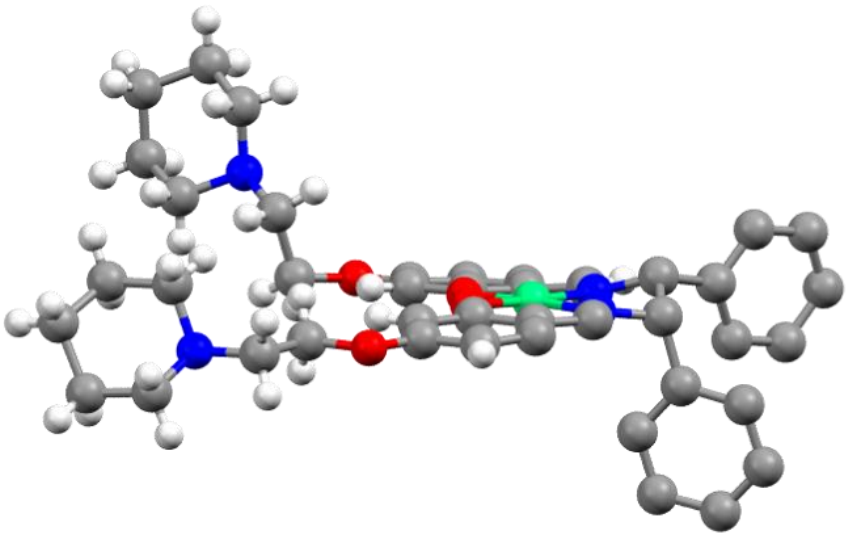

Figure 3.25: Solid state structure of **(65)** highlighting the arrangement of the *meso*-1,2-diphenylethylenediamine group in in the crystal lattice. Some hydrogen atoms and the top ethylpiperidine moieties have been omitted for clarity.

In the crystal lattice of (**53**), the two nickel Schiff base molecules possess a crystallographic inversion centre and are arranged in a slipped co-facial manner (Figure 3.26). The shortest intermolecular distance between the two molecules is 3.168 Å between oxygen atom O1 (coordinated to the nickel atom) and the imine carbon atom C4**.**

In the solid-state structure of (**54**), the molecules of the complex are again arranged in a slipped co-facial manner (Figure 3.27). There are contacts between C3, which is bonded to N1 of one molecule and C10 which is bonded to O1 of the second molecule. The closest contact (2.335 Å) between the two molecules was found between H6B and H22A of the morpholine moieties.

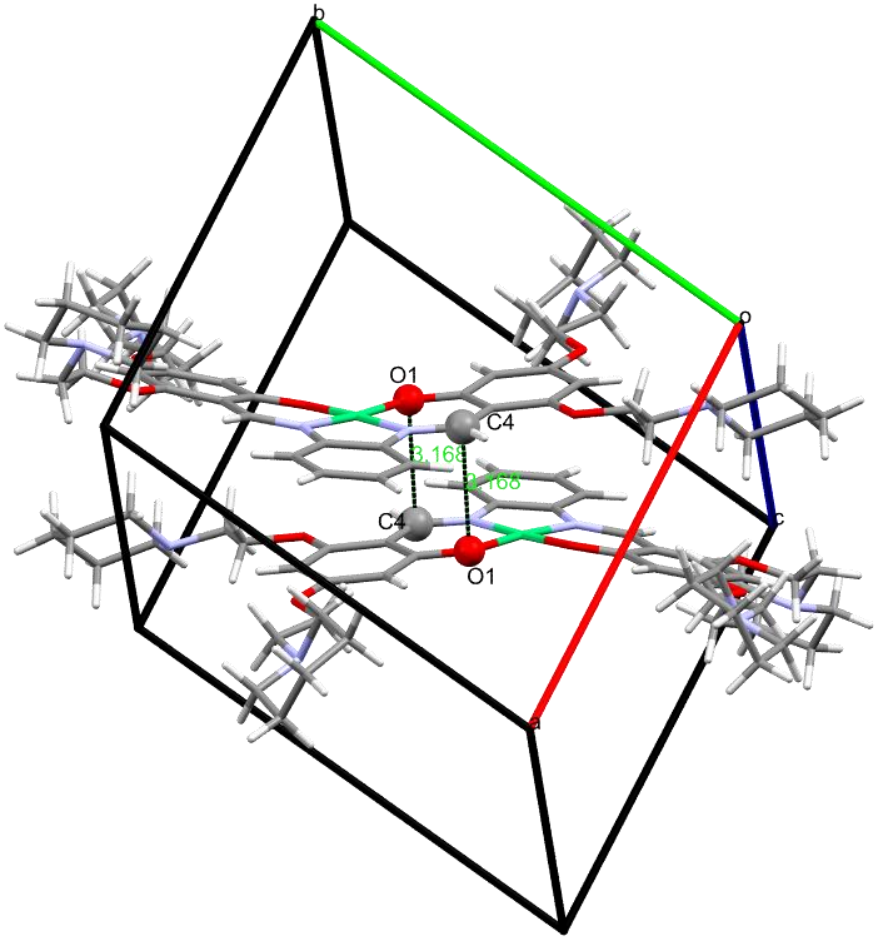

Figure 3.26: Perspective view of the stacking of pairs of complexes in the lattice of (**53**).

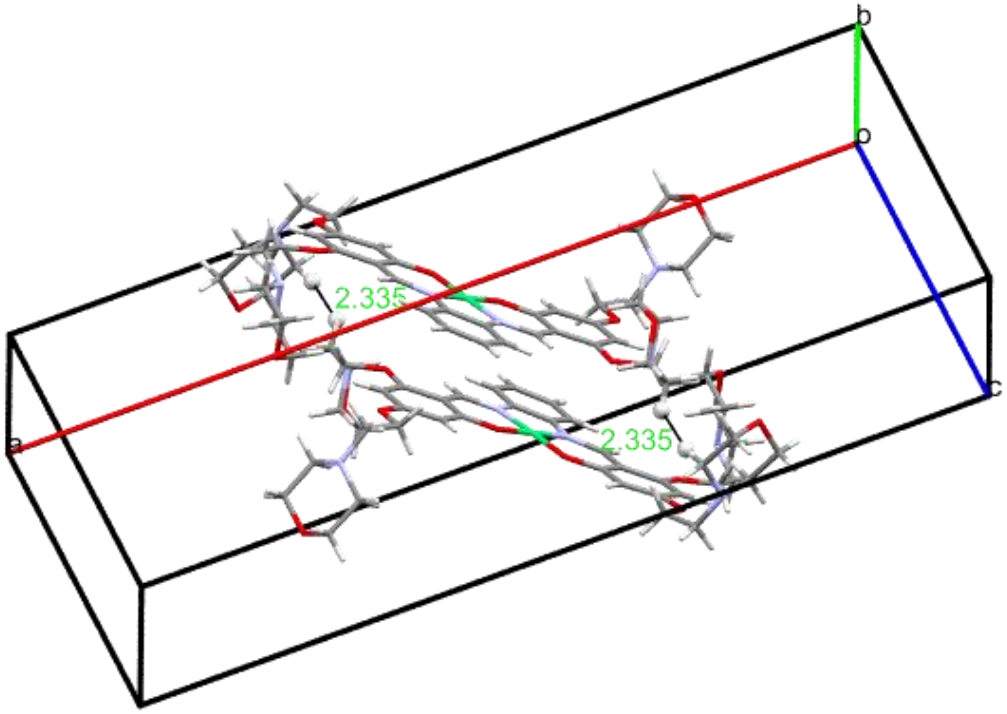

Figure 3.27: Crystal packing of two molecules of (**54**).

Just like the previous two complexes, the two nickel Schiff base molecules in the structure of complex (**65**) are arranged in a slipped co-facial manner. Here the closest separation of 3.287 Å is between the Ni atoms (Figure 3.28).

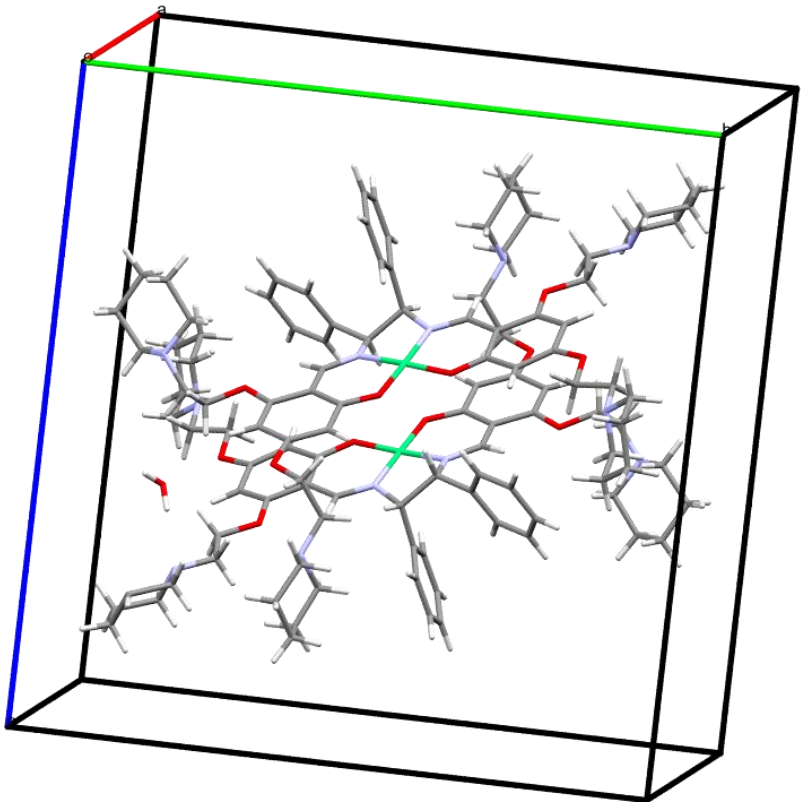

Figure 3.28: Arrangement of nickel molecules in the crystal lattice of (**65**).

The solid state structure of (**63**) possesses a crystallographic inversion centre with the nickel complexes sitting directly on top of one another (Figure 3.29) with a Ni-Ni distance of 3.436 Å. The 1,2-propanediamine moiety is not coplanar with the six membered chelate rings coordinated to the nickel ion. This arrangement results in a torsion angle N1-C2-C17-N2 of -54.7(4)°. A hydrogen bond was observed between the water hydrogen atom H1WB and the nitrogen atom N3 of the morpholine moiety of one of the complexes.

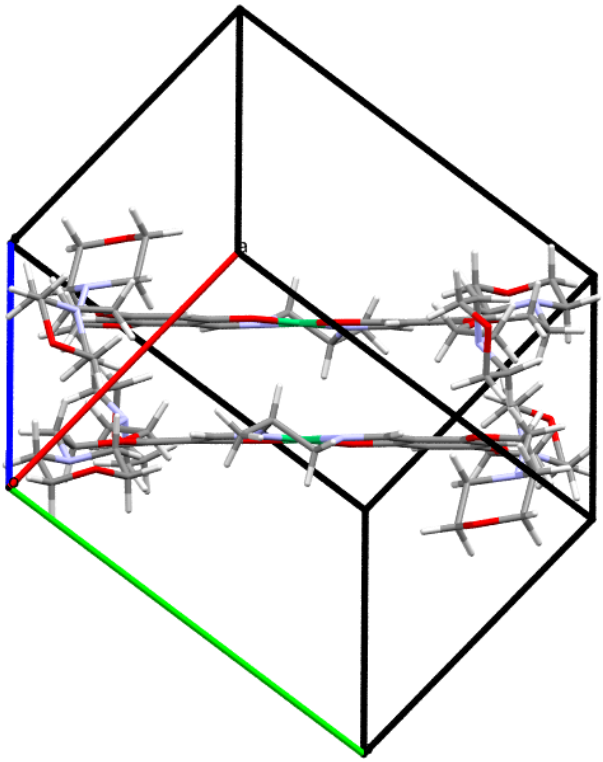

Figure 3.29: Arrangement of nickel molecules in the crystal lattice of (**63**).

Chapter 4 Effect of varying the diamine moiety on DNA binding properties of nickel Schiff base complexes containing four pendant groups

4.1 Introduction and scope

Previous studies have reported that the affinity of organic compounds and metal complexes for G-quadruplex DNA is enhanced by the presence of pendant groups, including those with positive charges which can participate in electrostatic interactions with the phosphate residues of the DNA backbone. For example, the nickel salphen complex (**18**) (Section 1.4.3), which has two pendant ethylpiperidine groups, was found to induce a high degree of stabilisation of telomeric G-quadruplex DNA, and inhibit telomerase activity.[124] In addition, the nickel salphen complex (**44**) (Section 1.4.3) which contains three dimethylimidazole pendant groups exhibited a high degree of binding affinity towards a G-quadruplex, and telomerase inhibition (IC_{50} = 70 nM) in a TRAP-G4 assay.[134] More recently, (**49**) (Section 1.4.3), which features four pendant groups showed notable binding affinity and selectivity towards G-quadruplexes.[137] Furthermore, the tetra-substituted Mn(III) porphyrin complex (**54**) (Section 1.4.2) was found to stabilise the human telomeric quadruplex and to exhibit a 10000-fold degree of binding selectivity in favour of G-quadruplex DNA over dsDNA in SPR experiments.[119] In addition, the tetra-substituted

naphthalenediimide derivative MM41 (**5**) (Section 1.4.1) has been characterised as a potent stabiliser of various G-quadruplex sequences and found to have significant anti-tumour activity against pancreatic cancer cells.[111]

Changing the size and position of aromatic moieties present in nickel Schiff base complexes has also been shown to have a significant effect on their binding interactions with both G-quadruplex and dsDNA.[135,136] For example, the nickel Schiff base complex (**45**) (Section 1.4.3) which contains three coplanar aromatic groups in the top portion of the ligand structure, showed limited ability to bind to G-quadruplex DNA.[136] This was perhaps due to the ability of the large aromatic ring system to hinder interactions with the loops of G-quadruplex DNA structures. In contrast, the large aromatic ring system facilitated participation in intercalative interactions with dsDNA resulting in high binding affinity towards the latter. In contrast, nickel Schiff base complex (**46**) (Section 1.4.3) which contains the non-planar *meso*-1,2- diphenylethylenediamine moiety showed much lower affinity towards the same dsDNA molecule but still showed the ability to significantly interact with a tetramolecular G-quadruplex.[135]

Taking the above results into account, it was decided to systematically explore the effect of altering the structure of the diamine moiety in the "top" of the well-studied nickel Schiff base complex (**18**) as well as increasing the number of ethylpiperidine groups, on affinity towards dsDNA and multiple G-quadruplex topologies. To accomplish this, five new nickel Schiff base complexes (Figure 4.1) were synthesised. Each features four ethylpiperidine pendant groups. These were expected to increase both the affinity and selectivity of the complexes toward G-quadruplex DNA as a result of electrostatic interactions with the grooves and loops of the latter

structures, and also improve the aqueous solubility of the metal complexes themselves. Interactions between the metal complexes and different topologies of G-quadruplex DNA were investigated by ESI-MS, CD and UV-Vis spectroscopy, a FID assay, FRET melting assay and molecular docking. The combination of more than one technique is required for a detailed understanding of DNA-metal complex interactions. Results obtained using these different techniques are presented and discussed in this chapter.

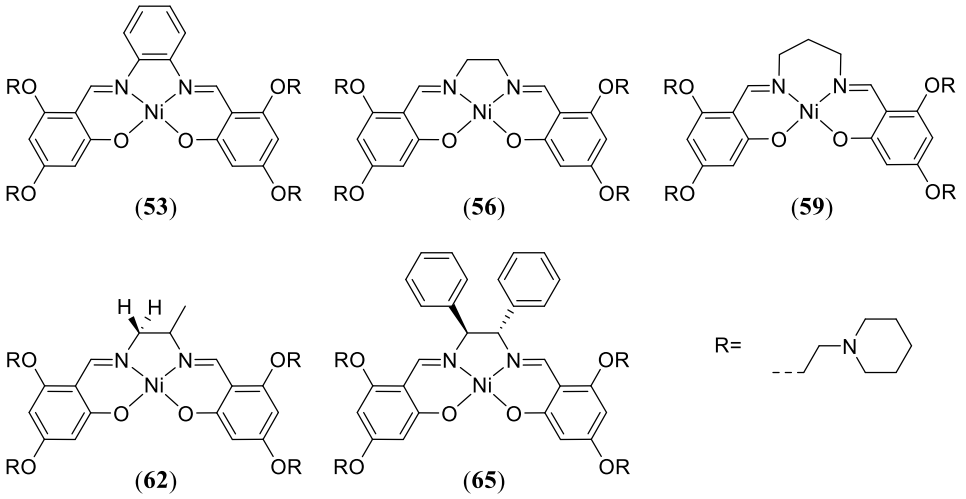

Figure 4.1: Structures of nickel Schiff base complexes containing different diamine moieties used in DNA binding studies. Each contains four ethylpiperidine pendant groups.

4.2 Results and discussion

4.2.1 DNA binding studies performed using ESI mass spectrometry

ESI-MS is a useful screening technique when investigating the interactions between small molecules and DNA.[180-182] During the electrospray process, free DNA molecules and ligand/DNA non-covalent complexes are transferred from solution to the gas phase inside the mass spectrometer with minimal fragmentation, thus preserving the weak interactions present within the latter complexes.[180]

ESI-MS was first used to investigate and compare the binding affinity of the nickel Schiff base complexes shown in Figure 4.1 towards the dsDNA D2, parallel tetramolecular G-quadruplex Q4 and parallel unimolecular G-quadruplex Q1. Initially, a series of negative ion ESI mass spectra were obtained of solutions containing free D2 alone, or a 6:1 ratio of one of the nickel complexes and D2. These spectra are shown in Figure 4.2. Each spectrum shows ions at *m/z* 1626.5 and 1952.0, which are attributed to $[D2 - 6H]^{6-}$ and $[D2 - 5H]^{5-}$, respectively. The abundances of these ions vary from one spectrum to another, suggesting that the nickel complexes bind to different extents to the DNA. For example, ions at *m/z* 1626.5 from D2 are of lowest abundance in Figure 4.2 (b), which is a spectrum of a solution containing a 6:1 ratio of (**53**), which contains the phenylenediamine moiety, and D2. This suggests that (**53**) has the highest affinity towards D2 among the five studied complexes. Evidence in support of this is provided by the observation that the abundances of ions from non-covalent complexes containing one or more nickel complexes bound to D2 appeared to be equal to or slightly greater in the case of the

spectrum shown in Figure 4.2 (b), than for any of the other spectrum. Therefore it appears that (**53**), exhibited the highest affinity of the five nickel complexes for D2.

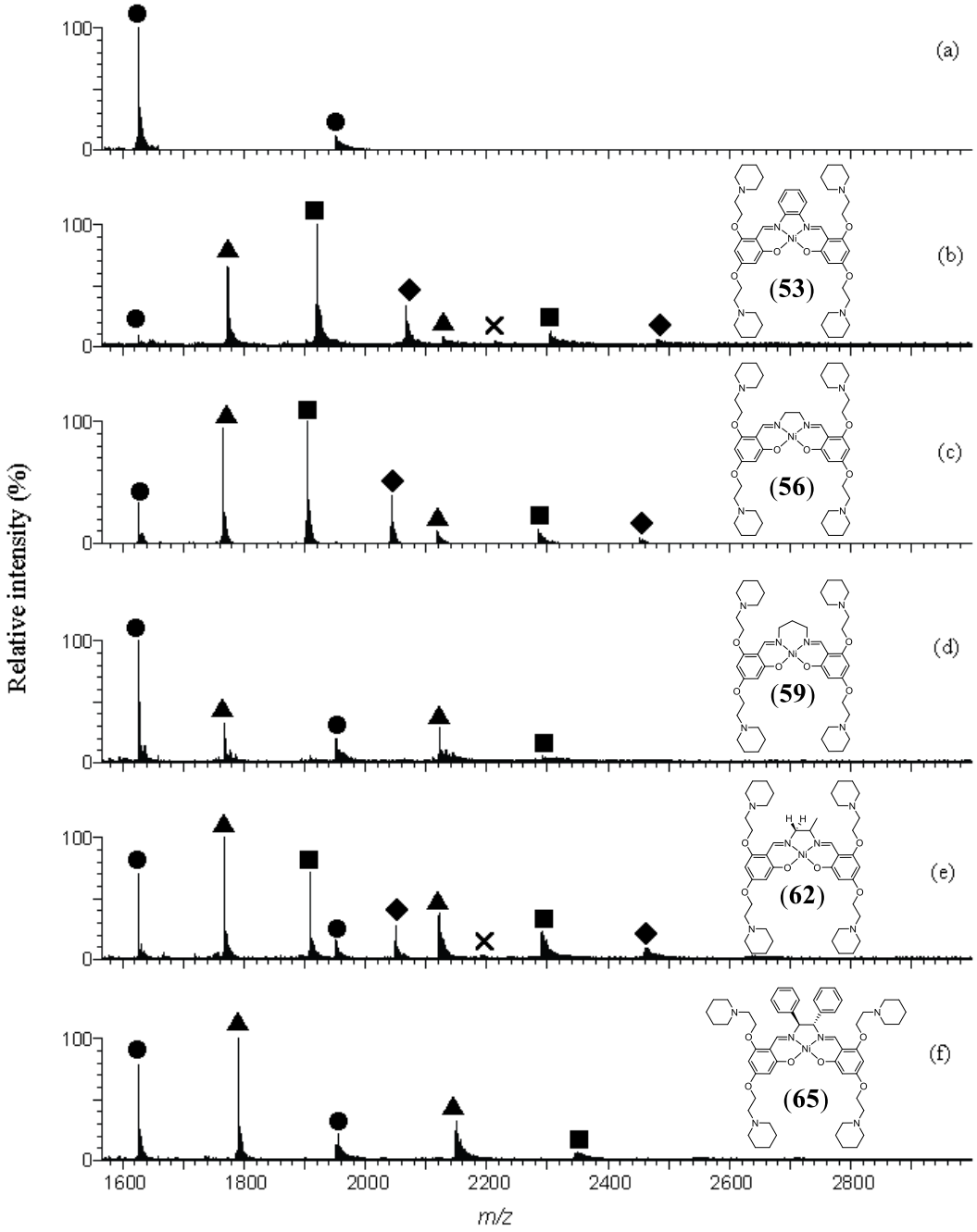

Figure 4.2: Negative ion ESI mass spectra of solutions containing a 6:1 ratio of different nickel Schiff base complexes and D2: (a) Free D2; (b) D2 + (**53**); (c) D2 + (**56**); (d) D2 + (**59**); (e) D2 + (**62**) and (f) D2 + (**65**). ● = free D2; ▲ = [D2 + (Ni)]; ■ = [D2 + 2(Ni)]; ◆ = [D2 + 3(Ni)]; ✕ = [D2 + 4(Ni)].

Inspection of Figure 4.2 also revealed that the relative abundances of ions from non-covalent complexes containing different numbers of nickel molecules bound to DNA is similar in the case of spectra obtained using (**53**) and (**56**). This provided evidence these complexes have similar abilities to form non-covalent complexes with D2 and suggests that changing the diamine moiety of the complex from phenylenediamine to ethylenediamine had little effect on affinity towards dsDNA.

Figure 4.2 (f) provides evidence that ions of high abundance were formed which contained one or two molecules of (**62**) bound to DNA. In contrast to what can be seen in either Figure 4.2 (b) or (c), however, the combined abundances of ions from free DNA were much greater. This suggests that (**62**) has a lower binding affinity towards D2 than either (**53**) or (**56**). Further analysis of Figure 4.2 indicates that the complex with the next highest affinity towards D2 was (**65**), whilst (**59**) showed the lowest ability to interact with the dsDNA. The latter conclusion is supported by the observation of ions of high abundance from free D2, together with ions of only low to medium abundance from non-covalent complexes in Figure 4.2 (d). These results suggest that changing the head-group of the complex from phenylenediamine, to either *meso*-1,2-diphenylethylenediamine or 1,3-diaminopropane significantly reduced binding to the dsDNA. Overall, the results presented in Figure 4.2 suggests that changing the diamine moiety present in a nickel Schiff base complex can have a significant effect on their ability to bind to and form stable non-covalent complexes with D2.

Additional DNA binding experiments were conducted by ESI-MS with each of the five nickel complexes and two parallel G-quadruplex DNA molecules (parallel tetramolecular Q4 and parallel unimolecular Q1). The relative abundances of ions

from free DNA and different types of non-covalent complexes observed in these experiments were calculated by adding the individual abundances of all ions from either free DNA or a specific non-covalent complex in a given spectrum, and dividing the result by the sum of the abundances of all ions present in that spectrum. The resulting values were then converted to percentages and are shown graphically Figure 4.3.

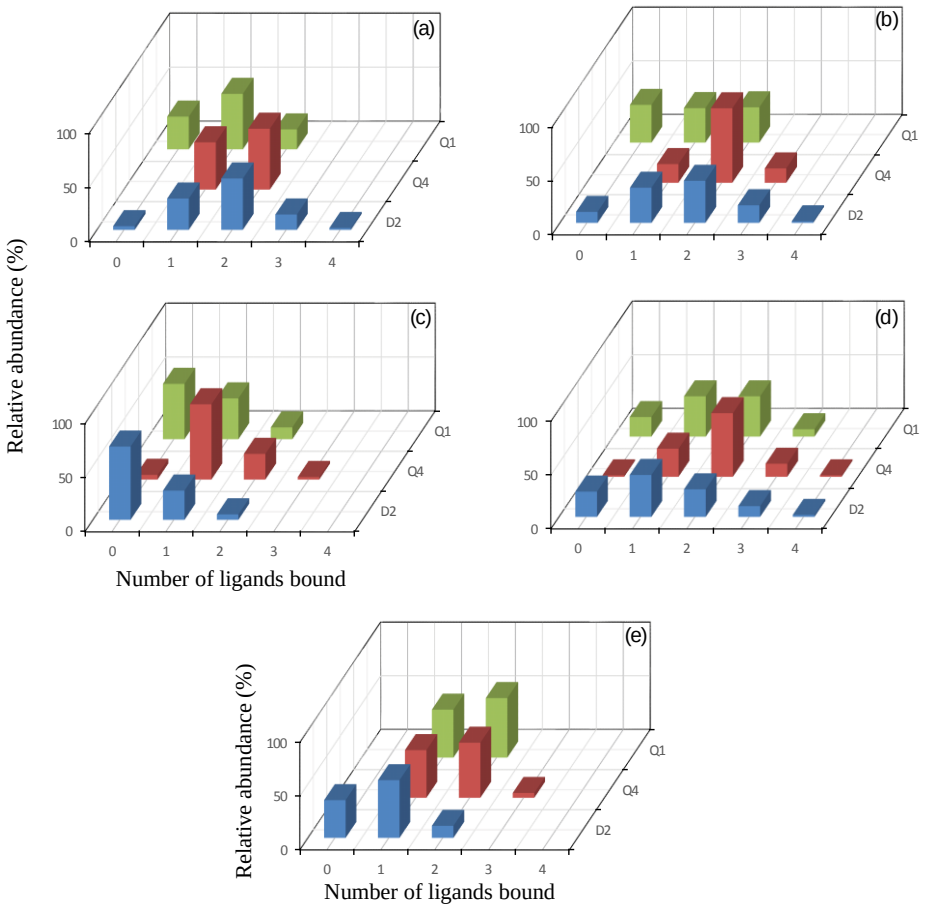

Figure 4.3: Relative abundances of ions in ESI mass spectra of solutions containing a 6:1 ratio of nickel Schiff base complexes and dsDNA (D2), unimolecular G-quadruplex (Q1) or tetramolecular G-quadruplex (Q4): (a) solutions containing (**53**); (b) solutions containing (**56**); (c) solutions containing (**59**); (d) solutions containing (**62**) and (e) solutions containing (**65**).

Presenting the results of mass spectrometry experiments in this fashion facilitates observation of trends in binding affinities amongst complexes for a specific DNA molecule. For example, inspection of Figure 4.3 (e) suggests (**65**) exhibited greater affinity towards both types of G-quadruplexes than D2. This is supported by the observation of ions of high abundance from non-covalent complexes containing one or two bound nickel molecules only in the case of the two G-quadruplexes. In contrast, ions of only low abundance corresponding to [D2 + 2 (**65**)] were observed in the spectrum of the solution containing the dsDNA. Complex (**65**) also appeared to be the only nickel molecule which showed at least comparable affinity towards the unimolecular Q1 and tetramolecular Q4.

Although the structure of (**59**) differs from that of (**56**) in only having an additional methylene group as part of the diamine moiety, comparison of Figure 4.3 (b) and (c) suggests this alteration resulted in the former molecule exhibiting significantly lower affinities towards each of the three DNA molecules. For example, Figure 4.3 (b) shows that the most abundant ions observed in the spectrum of the solution containing (**56**) and Q4 were from non-covalent complexes containing two bound nickel molecules. In contrast, Figure 4.3 (c) shows when (**59**) was present the most abundant ions present in the spectrum of a solution containing the same DNA molecule contained only a single bound nickel molecule. Inspection of Figure 4.3 also suggests that the affinity of the nickel molecules was generally greater towards Q4 than Q1, and that only rarely were non-covalent molecules containing more than two bound nickel molecules formed. This is consistent with binding interactions occurring primarily at the ends of the G-quadruplexes. Overall, the results presented in Figure 4.3 suggest that changing the diamine moiety in this class of nickel

complexes can have a significant effect on their affinity and selectivity towards the three types of DNA molecules studied.

4.2.2 DNA binding studies performed using CD spectroscopy

Circular Dichroism (CD) binding studies were undertaken as described in Chapter 2 to gain further insight into the affinities of the nickel complexes towards the different types of DNA molecules as well as the influence of unimolecular G-quadruplex topology on intermolecular interactions. CD spectroscopy is routinely used to study conformational changes of DNA upon ligand binding, as it is very sensitive to changes in the chirality of nucleic acids,[183,184] with different DNA structures displaying unique CD spectral signatures.[185-187] Furthermore the topology of a unimolecular G-quadruplex is very sensitive to the condition used during the annealing process. Figure 4.4 illustrates the effect of structural variations, including differences in topology, on the CD spectra of nucleic acid molecules. For example, the spectrum of the dsDNA molecule D2 in Figure 4.4 (a) shows positive and negative CD bands with large ellipticities centred at 282 nm and 249 nm, respectively. These are consistent with what has been reported previously for B-form dsDNA.[185]

Figure 4.4 (b) shows the CD spectra of parallel Q4, Q1 and c-KIT1 were essentially identical to each other, and significantly different from that of D2. In each case two positive CD bands with large ellipticities were observed at 210 and 263 nm, whilst a much weaker negative CD band was present at 241 nm. These spectral features are also similar to those observed previously in CD spectra of the same and other parallel G-quadruplexes.[135-137,184,185,188,189]

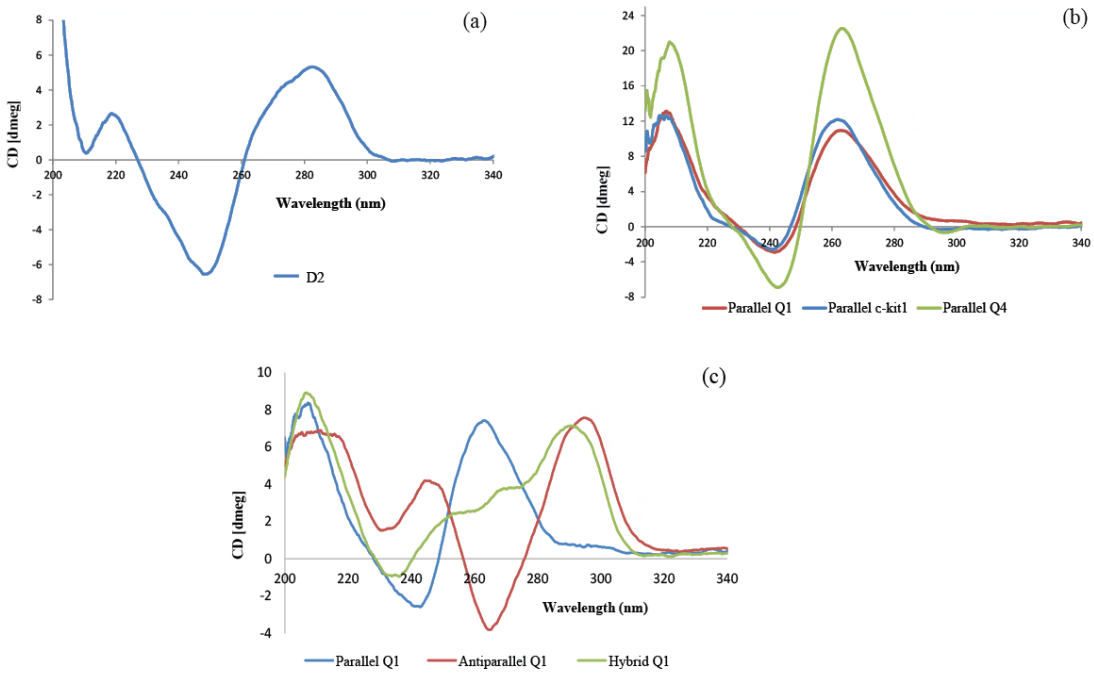

Figure 4.4: CD spectra of different DNA structures. (a) Circular dichroism spectra of D2. B-form D2 was obtained in 150 mM NH_4OAc, pH 7.4. (b) Comparison of the CD spectra of different parallel G-quadruplex DNA molecules (unimolecular Q1, tetramolecular Q4 and unimolecular c-KIT1). The parallel conformations of these molecules were obtained in 150 mM NH_4OAc, pH 7.4. (c) Comparison of the CD spectra of different topologies of the unimolecular G-quadruplex Q1. The anti-parallel conformation was obtained in solutions containing 100 mM NaCl, 15 mM NaH_2PO_4, 15 mM Na_2HPO_4, pH 7.4 while the hybrid conformation was obtained in solutions containing 100 mM KCl, 15 mM KH_2PO_4, 15 mM K_2HPO_4, pH 7.4.

Significant variations were observed between the CD spectra of the different topologies of the unimolecular G quadruplex Q1 (Figure 4.4 (c)). For example, the CD spectrum of anti-parallel Q1 showed two positive CD bands at 245 and 296 nm and a negative CD band at 265 nm. In contrast, the CD spectrum of hybrid Q1 showed a strong positive band at 291 nm with two shoulders at ~ 269 and ~ 255 nm and a negative peak at 233 nm. Similar features were reported previously for CD spectra of the same and other anti-parallel and hybrid unimolecular G-quadruplexes.[137,164,189,190] In addition to variations in DNA class and topology, the CD spectrum of a nucleic acid may be affected by the binding of small molecules. In

some cases, the same general spectral features have been observed although the energy and ellipticity of the CD bands may alter depending on the extent and nature of binding interactions. On other occasions, the CD spectrum may change from that corresponding from one type of topology to another, providing another potential source of information about the nature of the intermolecular interactions occurring. In the following sub-sections, the results of CD spectroscopic investigations performed with the nickel complexes and a variety of DNA molecules is presented and analysed. It was of particular interest to see if some of the trends in binding affinity that were suggested by the results of the ESI-MS studies presented earlier in this chapter were also evident in the data obtained using this additional method.

4.2.2.1 **CD titrations using double stranded DNA D2**

The CD spectra presented in Figure 4.5 show the effect of addition of increasing amounts of the five nickel complexes on the CD spectrum of D2. Changes to the positions and ellipticity of the CD bands were observed that varied significantly with the identity of the nickel complex. These changes are summarised in Table 4.1. Inspection of Figure 4.5 (a) shows addition of (**53**) to D2 caused large decreases in ellipticity for both the positive and negative CD signals of ~ 50%. Whilst there was also a significant shift to higher energy for the negative CD signal, the positive band remained centred close to its initial position. Overall these observations suggest that there was a significant degree of interaction between (**53**) and D2, which is in agreement with the pronounced ability of (**53**) to form non-covalent adducts with D2 in ESI-MS experiments noted earlier.

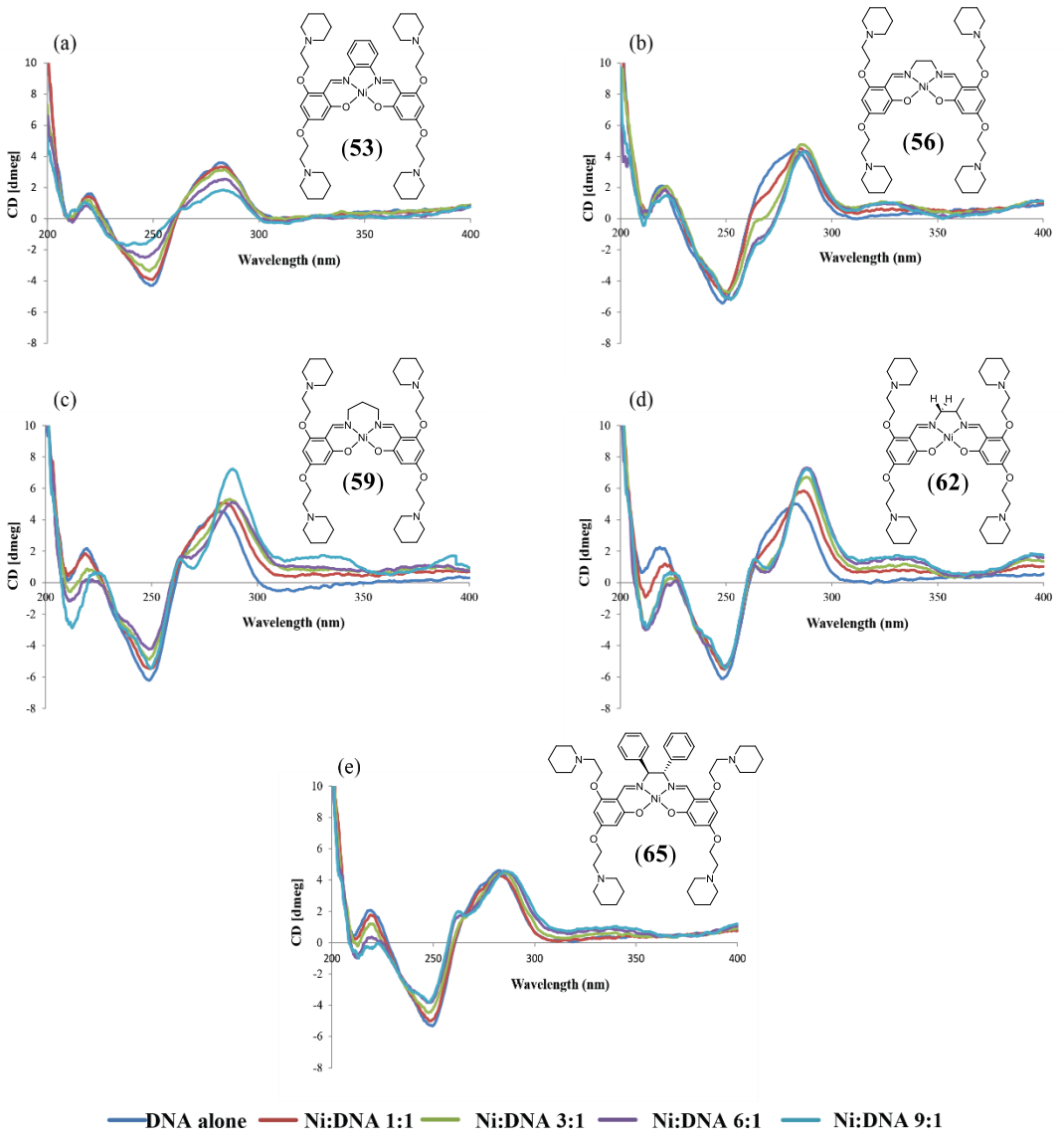

Figure 4.5: Circular dichroism spectra (200-400 nm) of solutions containing different ratios of nickel Schiff base complexes and D2: (a) D2 + (**53**); (b) D2 + (**56**); (c) D2 + (**59**); (d) D2 + (**62**) and (e) D2 + (**65**).

Addition of (**53**) did not result in any change to the general appearance of the CD spectrum of D2, including the number of spectral features. In contrast, addition of the other nickel complexes resulted in the emergence of a shoulder or distinct peak near 265 nm, which is where a CD band would be expected if the dsDNA was now present in the A-form. A similar effect was reported previously when the complex [$(Chro)_2$-Fe(II)] was added to hairpin DNA duplexes containing a GGCC

sequence.[191] This suggests that addition of some of the nickel complexes may be causing distortions to the structure of D2 resulting in it having characteristics of both A- and B-forms.

Table 4.1: Effect of addition of nickel Schiff base complexes on the CD spectrum of D2.*

Nickel complex	Positive CD band at 282 nm		Negative CD band at 249 nm	
	$\Delta\lambda_{max}$ (nm)	$\Delta\varepsilon$ (%)	$\Delta\lambda_{max}$ (nm)	$\Delta\varepsilon$ (%)
(**53**)	1.7	-48.5	-11.6	-59.7
(**56**)	3.3	-2.5	3.7	0.0
(**59**)	5.9	59.7	0.8	-12.0
(**62**)	5.5	44.2	1.8	0.3
(**65**)	3	-1.00	-1.3	-28.5

* All $\Delta\lambda_{max}$ and $\Delta\varepsilon$(%) values are the difference between the values for free DNA and those for a solution containing a nickel:DNA ratio of 9:1. Negative $\Delta\lambda_{max}$ values indicate a blue shift; positive values indicate a red shift.

Despite observation of a number of similar changes to the CD spectrum of D2 when (**56**), (**59**), (**62**) or (**65**) were added, there were also several notable differences involving the major CD bands. Addition of (**56**), for example, did not cause significant changes to the ellipticity of either major CD band. This result was somewhat surprising as (**56**) showed a notable ability to form non-covalent adducts with D2 in ESI-MS experiments. In contrast, addition of either (**59**) or (**62**) resulted in large changes in ellipticity for the positive CD band accompanied by the largest shifts in position of this band, but only relatively small changes to the ellipticity and position of the negative CD band. The large changes to the CD spectrum caused by addition of (**59**) was surprising in view of the limited ability it exhibited to form non-covalent adducts with D2 in ESI-MS experiments. Addition of (**65**) resulted in yet another distinct pattern of changes to the CD spectrum of D2 including the second largest decrease in ellipticity for the negative CD band and an almost negligible influence on the positive CD band. Overall the above changes demonstrate how

sensitive CD spectra are to changes in DNA conformation caused by nickel complexes that in some instances differ only slightly in their structures.

4.2.2.2 CD titrations using parallel tetramolecular Q4

The CD spectra illustrated in Figure 4.6 show the effect of adding increasing amounts of each of the five nickel complexes on the CD spectrum of Q4, while Table 4.2 summarises the changes to the position and ellipticity of the major CD bands.

Inspection of Figure 4.6 shows that none of the nickel complexes caused major changes to the fundamental structure of the CD spectrum of Q4, such as the appearance of new CD bands or shoulders on the side of existing bands. In addition, Table 4.2 shows that addition of the nickel complexes had no significant effect on the position of the major positive and negative CD bands. In contrast, addition of increasing amounts of the nickel complexes resulted in decreases in ellipticity of the positive CD band that varied dramatically. For example, addition of (**65**) to Q4 caused the largest changes to the ellipticity of both the positive and negative CD bands (66 and 71%, respectively). This suggests (**65**) interacts strongly with Q4 which is supported by the results obtained from ESI-MS experiments involving this complex.

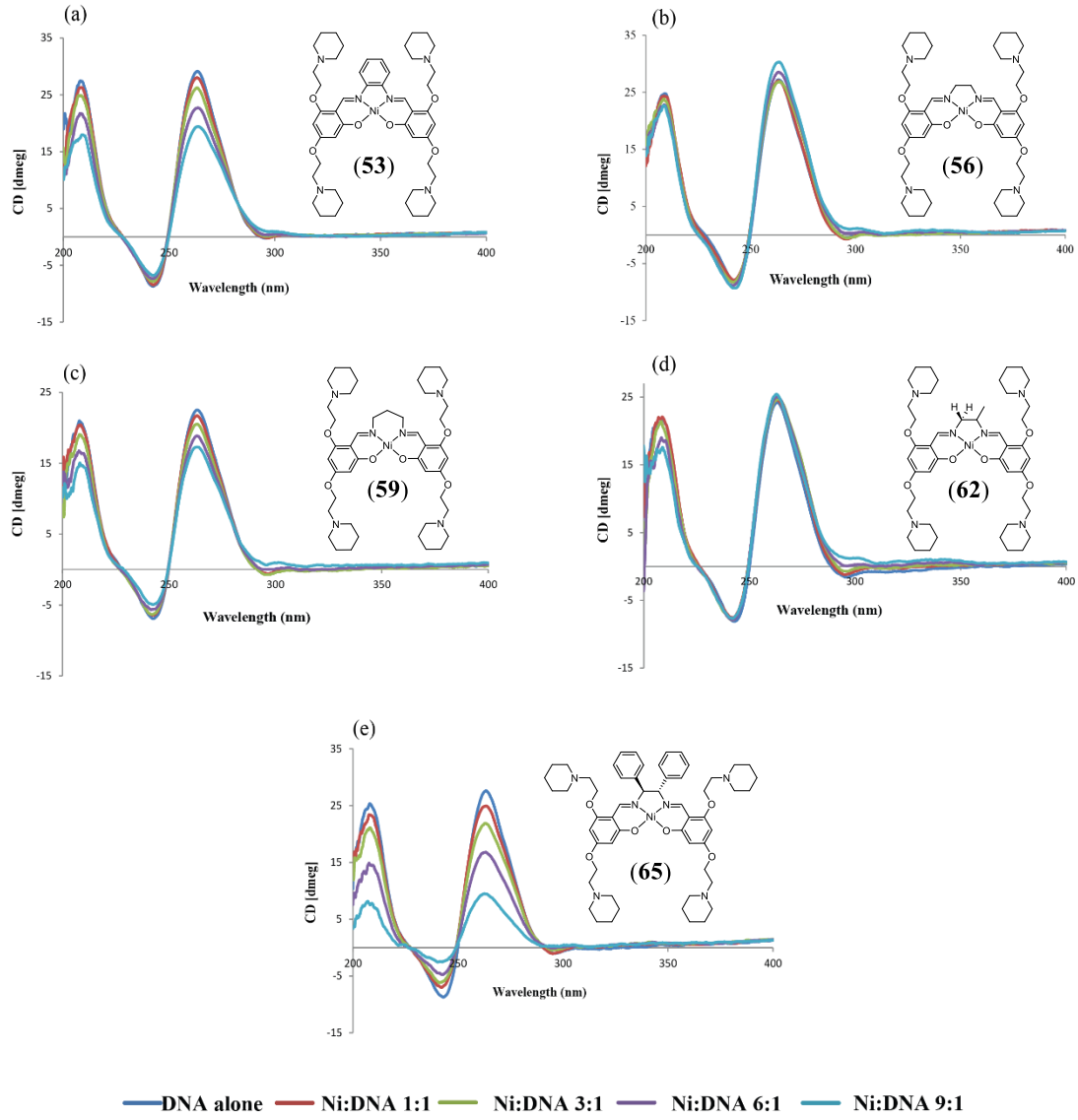

Figure 4.6: Circular dichroism spectra (200-400 nm) of solutions containing different ratios of nickel Schiff base complexes and parallel Q4: (a) Q4 + (**53**); (b) Q4 + (**56**); (c) Q4 + (**59**); (d) Q4 + (**62**) and (e) Q4 + (**65**).

Addition of (**56**) or (**62**) on the other hand failed to induce significant changes to the CD spectrum of Q4. This result suggests these nickel complexes do not interact strongly with Q4, which is in contrast to what was concluded from ESI-MS experiments, which revealed ions of significant abundance from non-covalent complexes consisting of two molecules of these nickel complexes bound to the DNA. Variations between binding affinity series derived using CD spectroscopy and other

methods have been noted previously and attributed to differing sensitivities to alternative aspects of the metal complex/DNA interaction. It may be, for example, that (**56**) and (**62**) are both capable of forming thermally stable non-covalent complexes with Q4, but the mechanism of interaction is different from that used by (**65**) and does not result in significant change to the conformation of the nucleic acid.

Table 4.2: Effect of addition of nickel Schiff base complexes on the CD spectrum of parallel Q4.*

Nickel complex	Positive CD band at 263 nm		Negative CD band at 242 nm	
	$\Delta\lambda_{max}$ (nm)	$\Delta\varepsilon$ (%)	$\Delta\lambda_{max}$ (nm)	$\Delta\varepsilon$ (%)
(**53**)	0.1	-33.4	0.2	-22.1
(**56**)	0.6	2.2	-1	12.3
(**59**)	0	-23.2	0	0.8
(**62**)	-0.1	5.2	-0.4	-5.1
(**65**)	-0.9	-65.7	-2.7	-70.8

* All $\Delta\lambda_{max}$ and $\Delta\varepsilon$(%) values are the difference between the values for free DNA and those for a solution containing a nickel:DNA ratio of 9:1. Negative $\Delta\lambda_{max}$ values indicate a blue shift; positive values indicate a red shift.

4.2.2.3 CD titrations using parallel unimolecular Q1

The potential of nickel Schiff base complexes as therapeutic agents will depend on their cytotoxicity and ability to interact selectively with different G-quadruplex structures. Circular dichroism spectroscopy is perhaps the most convenient technique for exploring the latter property, as the technique can be applied to nucleic acid solutions containing a variety of buffers, designed to confer different specific G-quadruplex topologies. In contrast, ESI-MS can only be applied to studying interactions with the parallel conformation of G-quadruplexes as the buffers required to stabilise the nucleic acid in other topologies result in numerous adducts with univalent cations that result in poor quality spectra.

A series of CD experiments were therefore performed in which the nickel complexes were added to three different conformations of the unimolecular G-quadruplex Q1, as well as the parallel form of a second G-quadruplex, c-KIT1. The results obtained from the experiments performed using parallel Q1 are presented in Figure 4.7 and Table 4.3.

Inspection of Figure 4.7 shows that all nickel complexes caused significant changes to the CD spectrum of Q1, suggesting each interacts with the nucleic acid. This conclusion is in general agreement with the results obtained from ESI-MS experiments which showed each nickel complex was able to form non-covalent adducts with Q1. It should be noted, however, that while the abundance of ions from non-covalent complexes formed between the nickel complexes and parallel Q1 was not generally as great as what was seen with the other two DNA molecules, there were in a number of cases very large changes to the ellipticity of the CD bands in a the spectra shown in Figure 4.7. For example, addition of three of the nickel complexes resulted in decreases in the ellipticity of the large positive CD band at 263 nm of > 50%, while all similarly affected the ellipticity of the much smaller negative CD band at 241 nm. In the case of (**53**) the CD spectrum had almost entirely disappeared at the highest Ni:DNA ratio examined.

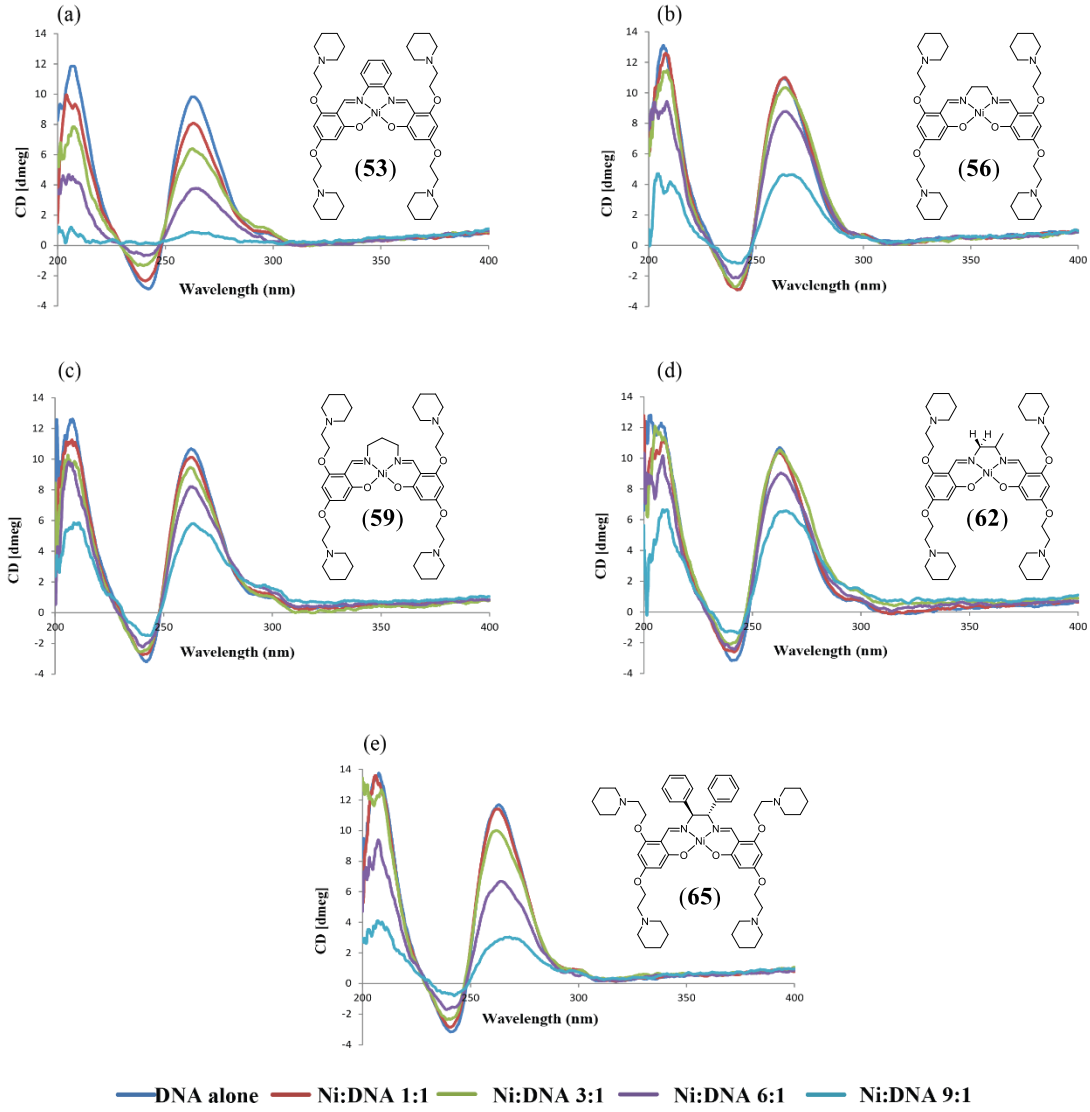

Figure 4.7: Circular dichroism spectra (200-400 nm) of solutions containing different ratios of nickel Schiff base complexes and parallel Q1: (a) Q1 + (**53**); (b) Q1 + (**56**); (c) Q1 + (**59**); (d) Q1 + (**62**) and (e) Q1 + (**65**).

Table 4.3: Effect of addition of nickel Schiff base complexes on the CD spectrum of parallel unimolecular Q1.*

Nickel complex	***Positive CD band at 263 nm***		***Negative CD band at 241 nm***	
	$\Delta\lambda_{max}$ (nm)	**$\Delta\varepsilon$ (%)**	**$\Delta\lambda_{max}$ (nm)**	**$\Delta\varepsilon$ (%)**
(**53**)	-0.5	-90.9	3.2	-100.0
(**56**)	-0.6	-57.4	0.2	-59.5
(**59**)	1.2	-45.6	-0.2	-53.3
(**62**)	3	-38.5	2.9	-56.1
(**65**)	4.9	-73.9	1.7	-74.5

* All $\Delta\lambda_{max}$ and $\Delta\varepsilon$(%) values are the difference between the values for free DNA and those for a solution containing a nickel:DNA ratio of 9:1. Negative $\Delta\lambda_{max}$ values indicate a blue shift; positive values indicate a red shift.

4.2.2.4 CD titrations using anti-parallel unimolecular Q1

CD spectra obtained after adding increasing amounts of the nickel complexes to anti-parallel Q1 are shown in Figure 4.8 while Table 4.4 compiles the changes to both the position and maximum ellipticity of the CD bands observed in these experiments.

Inspection of Table 4.4 shows (**56**) had perhaps the greatest effect on the CD spectrum of anti-parallel Q1, with changes in maximum ellipticity for the CD bands at 265 and 296 nm of -42% and -33%, respectively. This complex also caused significant changes to the CD spectrum of parallel Q1, suggesting it does not discriminate between these two unimolecular G-quadruplex topologies

Figure 4.8 shows that (**53**), (**65**), (**59**) and (**62**) all produced changes to one or more of the bands present in the CD spectrum of anti-parallel Q1, however these were generally not as great as what was observed during the corresponding studies performed with the parallel topology of this G-quadruplex. This suggests many of these complexes exhibit binding selectivity with a preference for parallel unimolecular Q1 over the anti-parallel conformation.

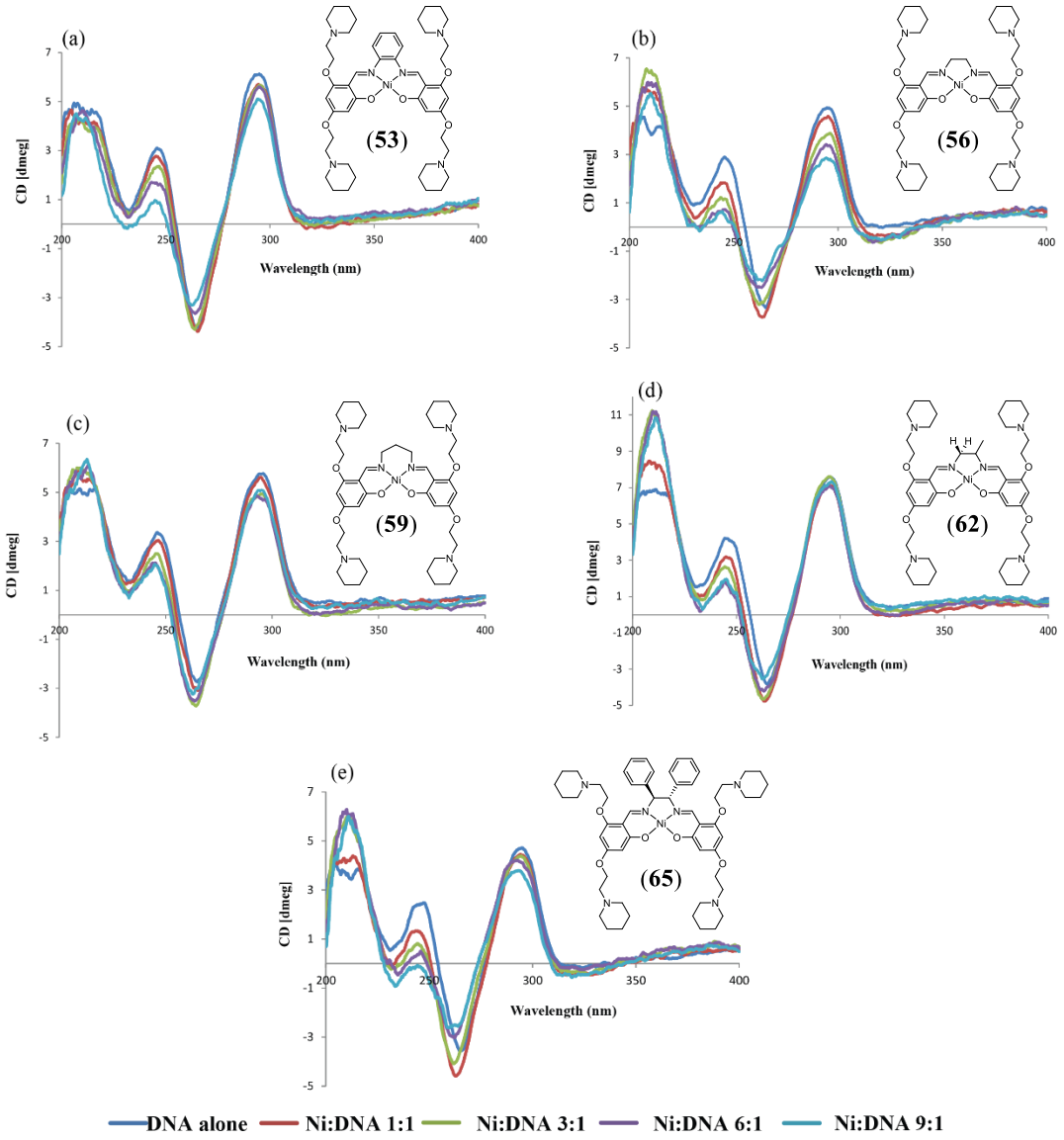

Figure 4.8: Circular dichroism spectra (200-400 nm) of solutions containing different ratios of nickel Schiff base complexes and anti-parallel Q1: (a) Q1 + (**53**); (b) Q1 + (**56**); (c) Q1 + (**59**); (d) Q1 + (**62**) and (e) Q1 + (**65**).

Table 4.4: Effect of addition of nickel Schiff base complexes on the CD spectrum of anti-parallel unimolecular Q1.*

Nickel complex	***Positive CD band at 296 nm***		***Negative CD band at 265 nm***	
	$\Delta\lambda_{max}$ (nm)	**$\Delta\varepsilon$ (%)**	**$\Delta\lambda_{max}$ (nm)**	**$\Delta\varepsilon$ (%)**
(**53**)	-0.8	-16.6	-1.9	-21.9
(**56**)	-0.4	-42.1	-1.6	-33.4
(**59**)	-0.7	-11.7	-2	18.4
(**62**)	1.1	-3.2	-2.7	-7.2
(**65**)	-1.8	-19.6	-5.1	-26.3

* All $\Delta\lambda_{max}$ and $\Delta\varepsilon$(%) values are the difference between the values for free DNA and those for a solution containing a nickel:DNA ratio of 9:1. Negative $\Delta\lambda_{max}$ values indicate a blue shift; positive values indicate a red shift.

4.2.2.5 CD titrations using hybrid unimolecular Q1

The final unimolecular Q1 topology investigated was the hybrid conformation. Its CD spectrum showed a strong positive peak at 291 nm with two shoulders at ~ 269 and ~ 255 nm. In addition, a negative CD band was also present at 233 nm. Complexes (**53**) and (**65**) once again appeared to interact to the greatest extent with this G-quadruplex topology. Upon addition of (**53**) or (**65**) to hybrid Q1, dramatic changed to the CD spectrum were observed. These included the maximum ellipticity of the CD bands at 291 and 233 nm decreasing by 40 % and > 90%, respectively (Table 4.5). In addition, the shoulder at 255 nm disappeared, while a negative CD band and a minor CD positive band appeared at 260 nm and 245 nm, respectively, which are characteristic of an anti-parallel G-quadruplex conformation, (Figure 4.9 (a) and (e)). The same effect has been reported previously after the addition of (**44**) to hybrid Q1.[137] This suggests a population of anti-parallel folded Q1 molecules was now present after the addition of these complexes to hybrid Q1. These observations support the conclusion that both (**53**) and (**65**) exhibited the greatest affinity of all the

nickel complexes examined towards hybrid Q1 and they may cause changes to the conformation of the DNA.

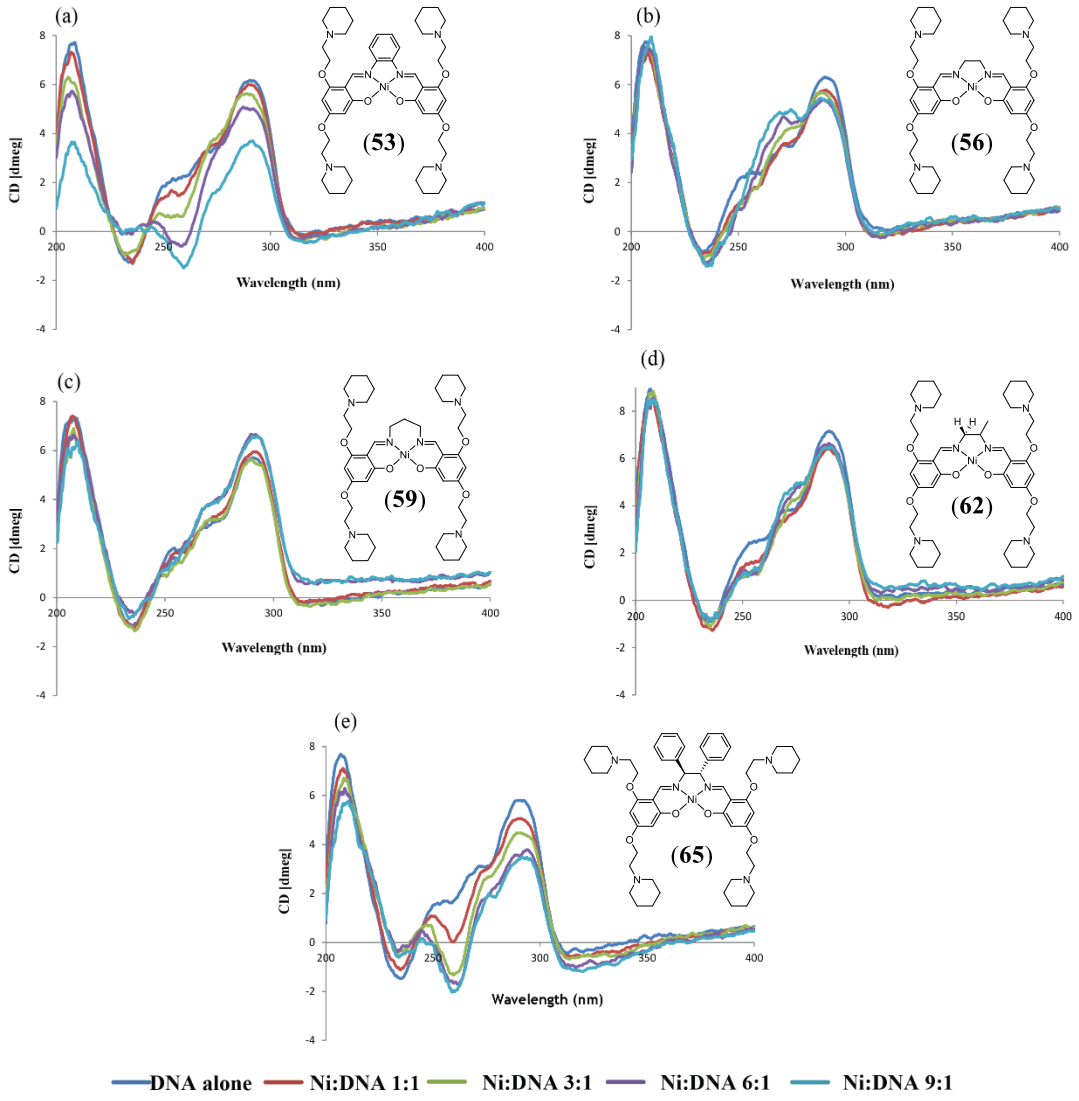

Figure 4.9: Circular dichroism spectra (200-400 nm) of solutions containing different ratios of nickel Schiff base complexes and hybrid Q1: (a) Q1 + (**53**); (b) Q1 + (**56**); (c) Q1 + (**59**); (d) Q1 + (**62**) and (e) Q1 + (**65**).

Inspection of Figure 4.9 (b) shows that in the absence of (**56**), the peak at 290 nm, which arises from the anti-parallel component of the hybrid topology dominates the CD spectrum. In the presence of increasing amounts of the nickel complex, a gradual increase in the parallel contribution to this topology resulted in the appearance of a

shoulder at 269 nm. The maximum ellipticity of this shoulder increased by 27% and it also shifted to higher energies by 3.5 nm as the amount of nickel complex in solution increased. At the same time the second shoulder at 255 nm completely disappeared. This suggests the proportion of parallel component in the hybrid topology of Q1 increased after addition of (**56**).

Of the novel nickel Schiff base complexes, (**59**) and (**62**), had the smallest impact on the CD spectrum of hybrid Q1, suggesting they display the lowest binding affinities. Both nickel complexes exhibited a negligible ability to affect the CD spectrum of anti-parallel Q1, and only had a small effect on the spectrum of parallel Q4. While these complexes had a notable influence on the spectrum of parallel Q1, the changes to the ellipticity of the CD bands they elicited were significantly less than those caused by some of the other nickel complexes. Overall these two complexes therefore do not appear to display any ability to interact selectively with any of the different topologies of G-quadruplex DNA or other DNA molecules.

Table 4.5: Effect of addition of nickel Schiff base complexes on the CD spectrum of hybrid unimolecular Q1.*

Nickel complex	**Positive CD band at 296 nm**		**Negative CD band at 265 nm**	
	$\Delta\lambda_{max}$ (nm)	**$\Delta\varepsilon$ (%)**	**$\Delta\lambda_{max}$ (nm)**	**$\Delta\varepsilon$ (%)**
(**53**)	1.2	-40.1	4.2	-114.6
(**56**)	-1.9	-13.6	2	70.9
(**59**)	-0.5	15.2	-1.7	-24.6
(**62**)	0.7	-9.3	-2.4	0.0
(**65**)	1.3	-40.1	-3.9	-98.6

* All $\Delta\lambda_{max}$ and $\Delta\varepsilon$(%) values are the difference between the values for free DNA and those for a solution containing a nickel:DNA ratio of 9:1. Negative $\Delta\lambda_{max}$ values indicate a blue shift; positive values indicate a red shift.

4.2.2.6 CD titrations using parallel unimolecular c-KIT1

In order to see if the changes to the CD spectrum of parallel Q1 that were observed upon binding of nickel complexes are typical for this type of G-quadruplex, a second set of experiments were performed using the parallel form of the G-quadruplex c-KIT1. The latter is a G-quadruplex-forming sequence containing four guanine tracts found in the promoter region of the c-KIT oncogene.[32,33,192] Over-expression and/or mutations of the c-KIT gene have been implicated in a wide range of human cancers including gastrointestinal stromal tumours (GISTs), small cell lung cancer, leukemia, colorectal cancer and pancreatic cancer.[193-196] It was found that stabilising the G-quadruplex structure of c-KIT1 with small molecules can downregulate the gene expression, and thus suppress cancer cell proliferation.[197,198] This suggests that selective stabilisation of G-quadruplex structures of c-KIT1 may provide a method of treating certain cancers.[199,200] A number of small molecules capable of inducing and stabilising G-quadruplex formation on c-KIT1 DNA have been reported.[201-207]

The CD spectrum of c-KIT1 was found to exhibit a negative peak with low ellipticity at 240 nm and a positive peak with large ellipticity at 262 nm. These features are very similar to those found for parallel Q1 and consistent with what has been reported for G-quadruplexes with a parallel topology.[185] The results obtained from CD studies involving the nickel complexes and parallel c-KIT1 are presented in Table 4.6 and. Figure 4.10.

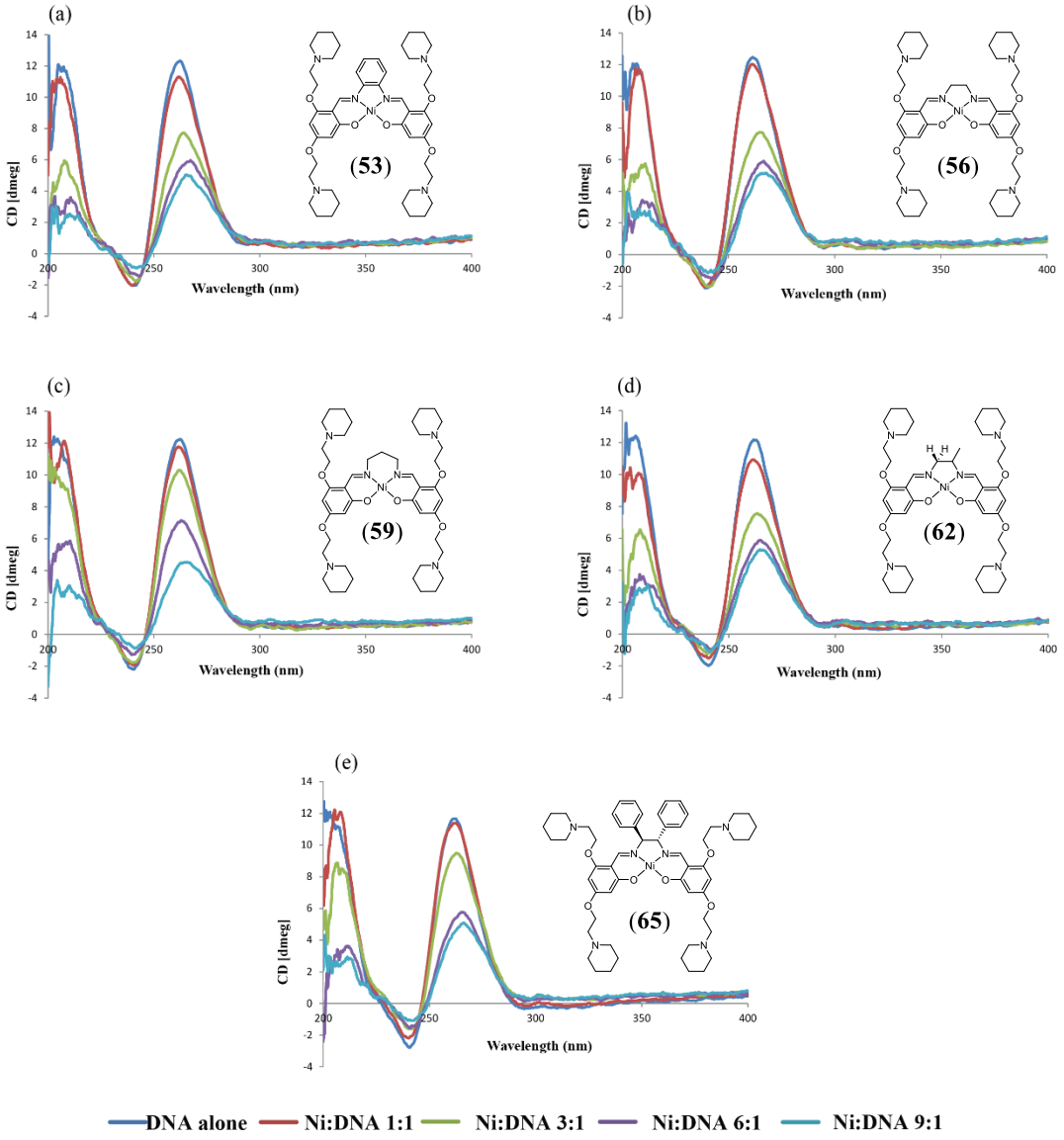

Figure 4.10: Circular dichroism spectra (200-400 nm) of solutions containing parallel unimolecular c-KIT1and different ratios of nickel Schiff base complexes: (a) c-KIT1 + (**53**); (b) c-KIT1 + (**56**); (c) c-KIT1 + (**59**); (d) c-KIT1 + (**62**) and (e) c-KIT1 + (**65**).

Inspection of the spectra shows changes similar to what was observed with parallel Q1, with all five complexes having a significant influence on the CD spectrum of parallel c-KIT1. While (**59**) was found to cause the largest reduction in ellipticity of the positive CD band of the DNA molecule, the changes to this signal caused by all five complexes were overall very similar in magnitude (Table 4.6).

Table 4.6: Effect of addition of nickel Schiff base complexes on the CD spectrum of c-KIT1.*

Nickel complex	Positive CD band at 296 nm		Negative CD band at 265 nm	
	$\Delta\lambda_{max}$ (nm)	$\Delta\varepsilon$ (%)	$\Delta\lambda_{max}$ (nm)	$\Delta\varepsilon$ (%)
(**53**)	2.8	-59.07	1.5	-54.67
(**56**)	6.5	-58.66	1.3	-45.34
(**59**)	2.4	-63.03	0.3	-60.56
(**62**)	2.9	-56.54	0.9	-44.41
(**65**)	4.6	-56.41	1.7	-60.96

* All $\Delta\lambda_{max}$ and $\Delta\varepsilon$(%) values are the difference between the values for free DNA and those for a solution containing a nickel:DNA ratio of 9:1. Negative $\Delta\lambda_{max}$ values indicate a blue shift; positive values indicate a red shift.

4.2.3 DNA binding studies performed using UV-Vis spectrophotometry

UV-Vis absorption spectrophotometry is a very common technique for detecting whether a small molecule stabilises or destabilises dsDNA. This can be accomplished, for example, by running DNA melting experiments in which the melting temperature of free DNA is compared to that of DNA bound to a drug molecule. A series of these experiments were undertaken as described in Chapter 2 to gain insight into the ability of the nickel complexes to stabilise the ds DNA molecule D2.

Melting temperature experiments were performed using solutions containing a 3:1 or 6:1 ratio of one of the nickel complexes and D2. Representative DNA melting profiles for solutions containing D2 alone, and D2 and (**53**), are shown in Figure 4.11. Figure 4.12 illustrates the average effect of adding either 3 or 6 equivalents of different nickel complexes on the T_m of D2.

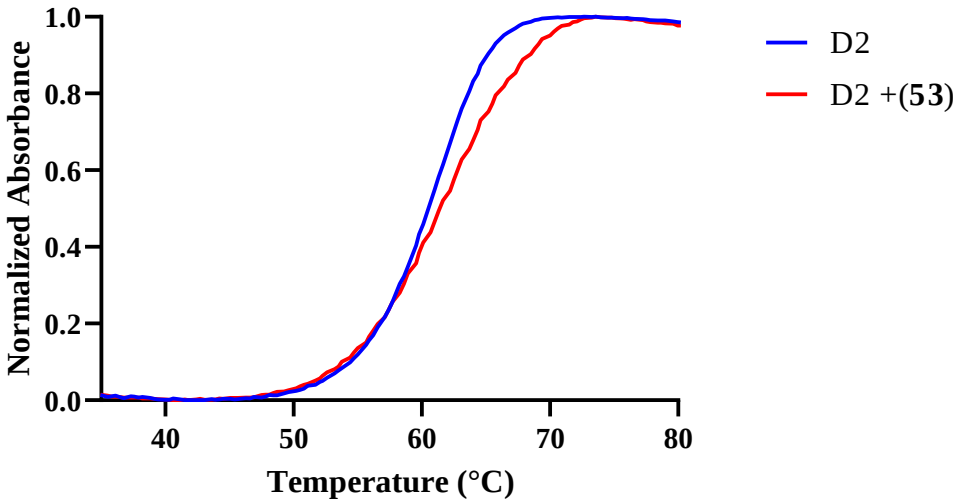

Figure 4.11: Melting curves for solutions containing 1 μM dsDNA D2 alone, and a 6:1 ratio of (**53**) and 1 μM D2.

The melting temperature, T_m, of D2 alone was determined to be 60.4±0.3 °C. Figure 4.12 shows that the T_m of D2 decreased by 1.6 – 2.5 °C in the presence of (**59**), (**62**) or (**65**). This result is similar to that reported for the tetra-alkylated Schiff base complex (**49**),[137] and is in accord with the low abundances of ions from non-covalent complexes in ESI mass spectra of solutions containing either (**59**) or (**65**) and D2. The results obtained from the UV-Vis melting studies therefore provide further evidence that (**59**) and (**65**) have low affinities towards dsDNA. In contrast, ESI-MS showed that (**62**) was capable of forming non-covalent complexes with D2, although not to the same extent as either (**53**) or (**56**). This result therefore does not appear at first glance to be consistent with those obtained from the UV-Vis melting studies, and may reflect the binding interactions of (**62**) with the nucleic acid leading to destabilisation of the secondary structure of the latter molecule.

In contrast to what was observed with the other nickel complexes, both (**53**) and (**56**) caused small increases in the T_m of D2 when added to the nucleic acid. This is

consistent with the results obtained from ESI-MS experiments, which showed more extensive formation of non-covalent complexes with these two nickel complexes than the others. For example, the most abundant ions in ESI mass spectra of solutions containing either (**53**) or (**56**) and D2 consisted of two nickel molecules bound to the nucleic acid. For each of the other nickel complexes the most abundant ions observed in the ESI mass spectrum of a solution containing a 6:1 ratio of Ni:DNA were either attributable to free DNA or a non-covalent complex consisting of just one nickel molecule bound to the nucleic acid.

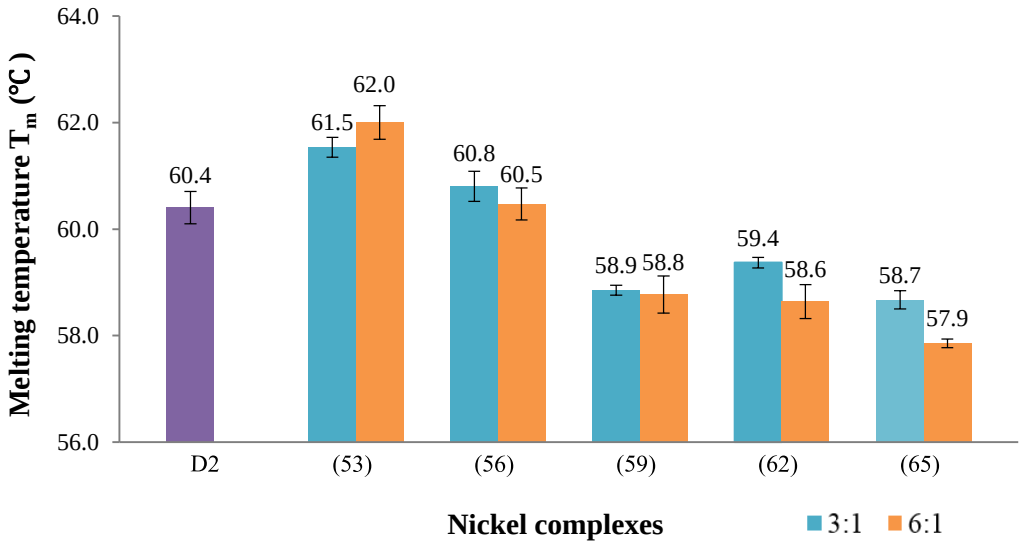

Figure 4.12: Mean melting temperatures (T_m) of solutions containing either a 3:1 or 6:1 ratio of a nickel complex and D2. The experiments were performed in triplicate with error bars showing standard errors.

4.2.4 DNA binding studies performed using FRET melting assays

Fluorescence Resonance Energy Transfer (FRET) is another popular method for studying G-quadruplex-ligand interactions. FRET occurs when an excited donor chromophore transfers energy to an acceptor chromophore through non-radiative

dipole–dipole coupling. The magnitude of the energy transfer is very dependent on the distance between the donor and acceptor chromophores, which makes FRET an extremely sensitive and valuable technique. For example, it can be used to study the conformational changes in a molecule by labelling it at specific sites with donor and acceptor fluorophores. More generally, measurement of the efficiency of FRET can provide an ideal probe of intermolecular or intramolecular distances.

Another application of FRET is in melting assays which are used to measure the degree of stabilisation that small molecules produce in human telomeric DNA labelled with fluorescent donor and acceptor chromophores.[208,209] These assays typically use an oligonucleotide containing at least four repeats of the human telomeric sequence and featuring a fluorophore (F) and quencher (Q) attached to the 5′ and 3′ ends, respectively (Figure 4.13 (a)). When the oligonucleotide is correctly folded to form a G-quadruplex structure FRET occurs as a result of the short average distance between the two chromophores. This involves fluorophore F absorbing excitation energy, and then energy transfer occurring to the nearby acceptor fluorophore Q. The net result is that fluorescence is not observed at room temperature. When the temperature is increased however, the fluorophore and quencher move further apart as a result of DNA denaturation resulting in measurable fluorescence (Figure 4.13 (b)).

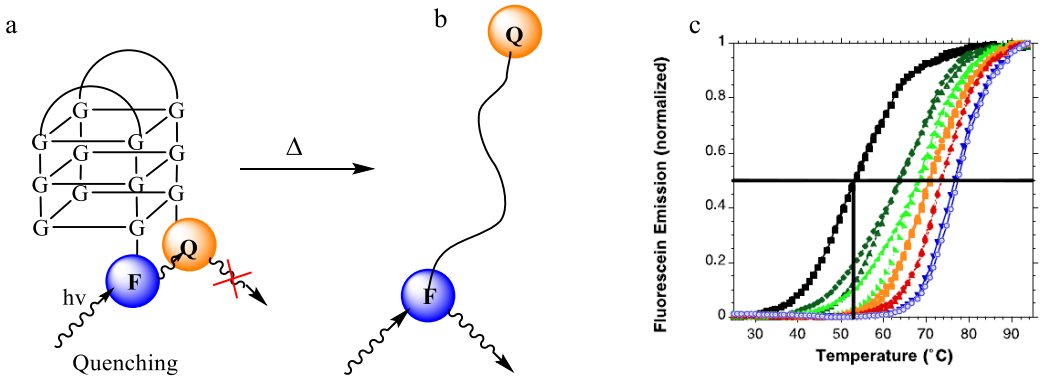

Figure 4.13: Schematic illustration of the melting process of a tagged G-quadruplex: (a) when the DNA is folded, (b) when the DNA is unfolded and (c) melting curves for G-quadruplex DNA in the absence and presence of increased concentrations of G-quadruplex ligand.[208]

Plotting fluorescence emission intensity against temperature yields a sigmoidal melting curve as shown in Figure 4.13 (c), from which the melting temperature T_m, is derived. The latter value is defined as the temperature at which only 50% of DNA is still folded and corresponds to the midpoint between the minimum and maximum emission fluorescence.[208] When a small molecule that is able to bind to and stabilise the DNA in its folded conformation is added, higher temperatures are required to denature the G-quadruplex structure, resulting in shifts in the melting curve and a higher value of T_m. The larger the increase in T_m the more effective the small molecule is at binding to and stabilising the DNA in its quadruplex conformation.

In this project, FRET melting experiments were performed using solutions containing either Na^+ or K^+ ions and the oligonucleotide F21T (FAM-d[GGG(TTAGGG)$_3$]-TAMRA). This has an identical DNA sequence to Q1 but features the fluorophore FAM at the 5´ end and the quencher chromophore TAMRA at the 3´ end.

4.2.4.1 FRET melting studies of F21T in Na^+ solution

The first set of FRET experiments undertaken were performed using F21T annealed in 100 mM Na^+-containing buffer in order to force the unimolecular DNA to adopt an anti-parallel topology.[208] After annealing the G-quadruplex was found to have a T_m of 50.7 °C which is close to the reported value of 50 °C.[208]

Normalised FRET melting curves obtained using F21T in the presence of increasing concentrations of nickel complexes (0-10 μM) are shown in Figure 4.14, while values of ΔT_m derived from the melting curves are presented in Figure 4.15. The latter values are the difference between the T_m for F21T in the presence of a nickel complex and the T_m of F21T alone.

The results presented in Figure 4.14 show that increasing the concentration of all nickel complexes from 1 to 10 μM led to shifts in the melting curves toward higher temperatures. This indicates that interactions with F21T resulted in stabilisation of the nucleic acid secondary structure. Significant increases in T_m were found with complexes (**56**), (**59**) and (**62**) even when the concentration of nickel complex was only 1 μM. Furthermore at higher concentrations (**53**) resulted in ΔT_m values comparable to those elicited by the previous three complexes. In contrast, addition of (**65**) resulted in smaller changes to the melting temperature of F21T at all concentrations examined. This suggests that the *meso*-diphenylethylenediamine group does not enable (**65**) to bind as effectively to and/or stabilise the anti-parallel G-quadruplex topology to the same extent. Addition of complex (**65**) was noted earlier to have an effect on the position and ellipticity of a number of the bands present in the CD spectrum of anti-parallel Q1, although it did not greatly alter the major positive CD band at 296 nm. In contrast, complex (**56**) showed both the

highest degree of stabilisation of F21T (ΔT_m = 34.9 μM at [Ni] = 10 μM) and resulted in by far the largest decrease in ellipticity of the positive CD band.

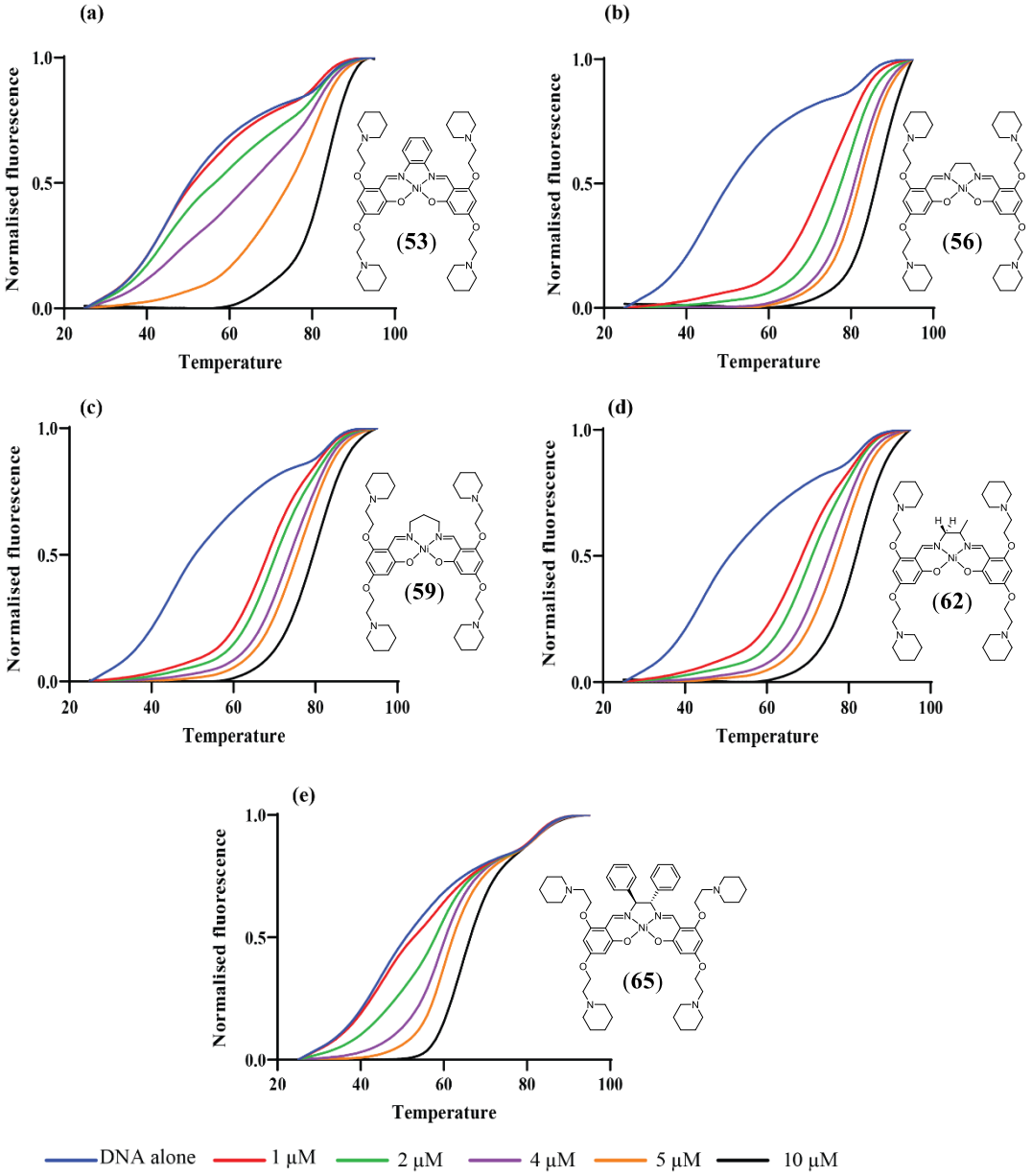

Figure 4.14: Results obtained from FRET melting assays performed using F21T in Na^+ solution with increasing concentrations of nickel Schiff base complexes. (a) (**53**); (b) (**56**); (c) (**59**); (d) (**62**) and (e) (**65**).

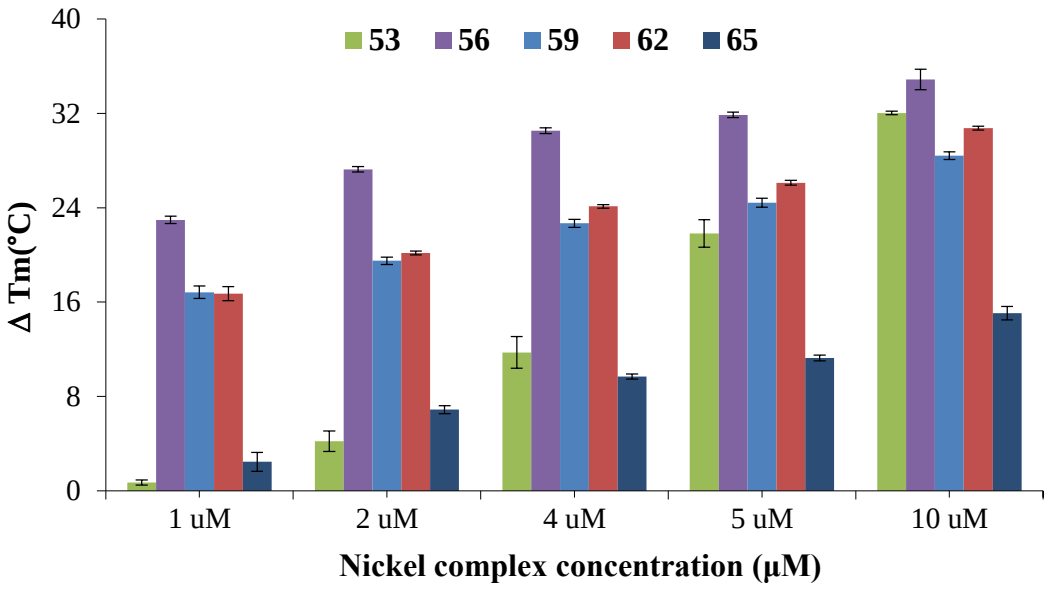

Figure 4.15: Comparison of ΔT_m values for different concentrations of nickel Schiff base complexes added to solutions containing 0.2 μM F21T. The DNA had an anti-parallel topology after annealing in 100 mM NaCl, 10 mM lithium cacodylate pH 7.4. Error bars represent the standard error from six separate experiments.

4.2.4.2 FRET melting studies of F21T in K^+ solution

A second series of experiments was performed using F21T annealed in 100 mM K^+-containing buffer in order to force the DNA to adopt a hybrid topology. The results obtained from these experiments, which are presented in Figure 4.16 and Figure 4.17, show a number of similarities to those observed in experiments performed using the anti-parallel topology of the nucleic acid. Once again complexes (**56**), (**59**) and (**62**) showed marked effects on T_m even at the lowest concentration of added nickel complex (1 μM). Adding higher concentrations of these nickel complexes resulted in only small additional increases in T_m.

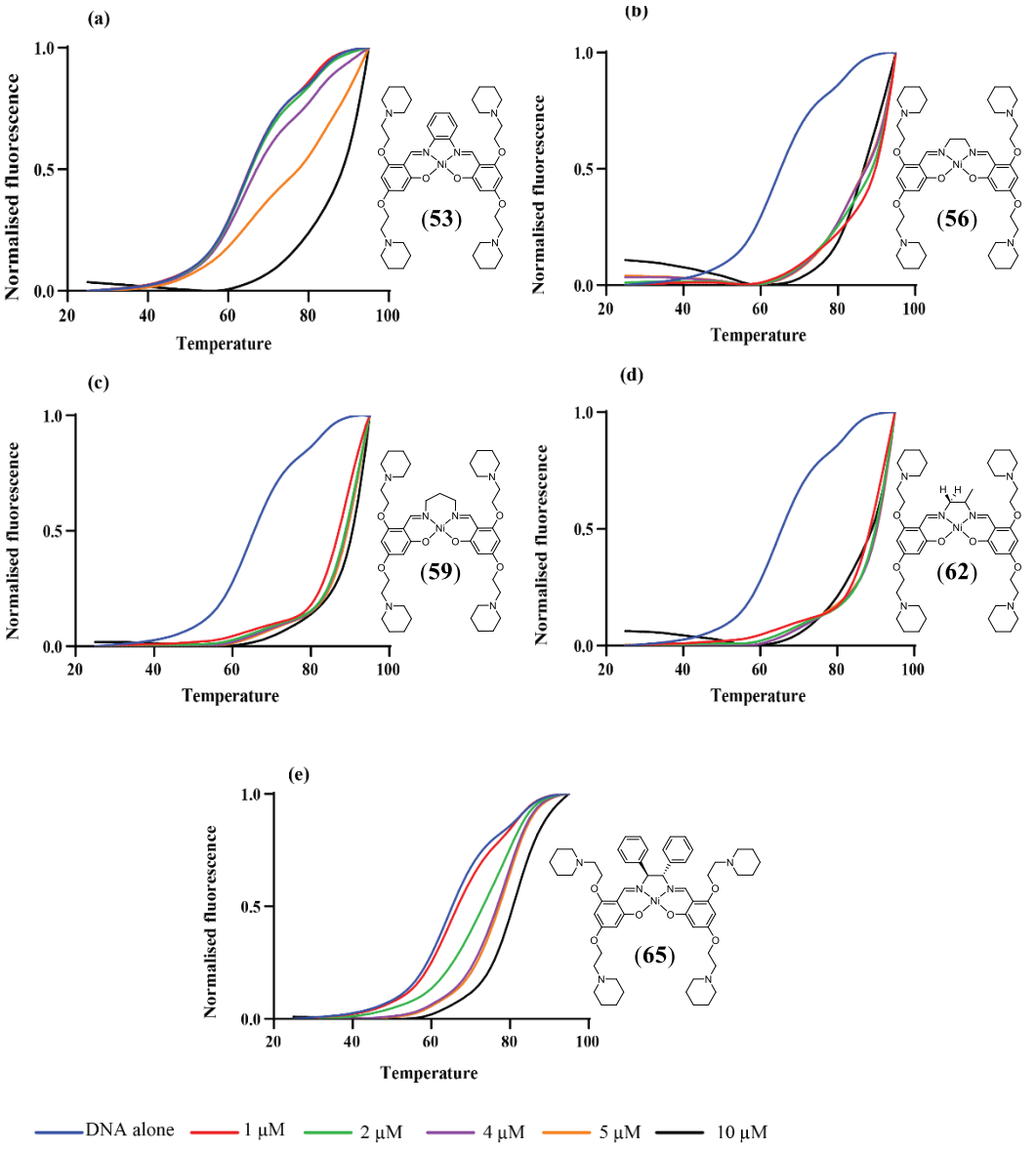

Figure 4.16: Results obtained from FRET melting assays performed using F21T in solutions containing K^+ ions and increasing concentrations of nickel Schiff base complexes. (a) (**53**); (b) (**56**); (c) (**59**); (d) (**62**) and (e) (**65**).

Complex (**53**) again resulted in significant increases in T_m but only at higher concentrations of added nickel complex, while the addition of (**65**) resulted in comparatively small increases in T_m for the hybrid topology at all nickel concentrations, just as it did for the anti-parallel conformation of F21T. These results suggest that (**53**) and (**65**) do not have as marked a stabilising effect on the hybrid

topology of F21T as the other nickel complexes, whereas they were noted earlier to have the largest effects on the CD spectrum of hybrid Q1. This may indicate that the interactions between (**53**) or (**65**) and hybrid unimolecular G-quadruplexes are both different to those which the other nickel complexes participate in, and result in much lower levels of stabilisation of the above topology.

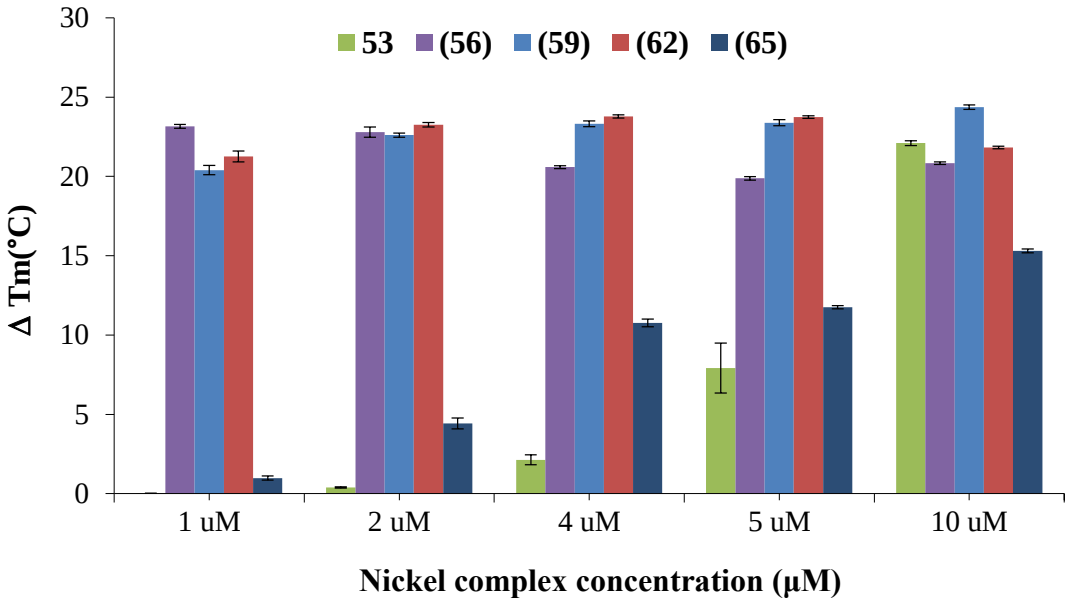

Figure 4.17: Comparison of ΔT_m values for different concentrations of nickel Schiff base complexes added to solutions containing 0.2 µM F21T. The DNA had a hybrid topology after annealing in 100 mM KCl, 10 mM lithium cacodylate pH 7.4. Error bars represent the standard error from six separate experiments.

4.2.5 DNA binding studies performed using FID assays

In order to further explore the DNA binding properties of the nickel complexes, their interactions with different types of DNA were also studied using a Fluorescent Indicator Displacement (FID) assay. This assay examines the ability of molecules of interest to displace a fluorescent DNA-binding ligand such as thiazole orange (TO) (Figure 4.18).[210-213] Thiazole orange normally exhibits very low levels of fluorescence in aqueous solution; however, it increases dramatically upon binding to

nucleic acid molecules.[210] For example, it has been reported that fluorescence emitted by TO increases up to 2000- and 3000-fold upon interaction with dsDNA and qDNA, respectively.[125,210] When another molecule is present that has a higher binding affinity towards the DNA under investigation TO is displaced, and fluorescence decreases. Molecules that result in greater decreases in fluorescence are then assumed to exhibit greater affinity for the DNA. This is expressed quantitatively as a DC_{50} value, which is the concentration of the new molecule required to cause a 50% decrease in fluorescence intensity. Lower values of DC_{50} are therefore expected for molecules with greater binding affinity towards the DNA under investigation.

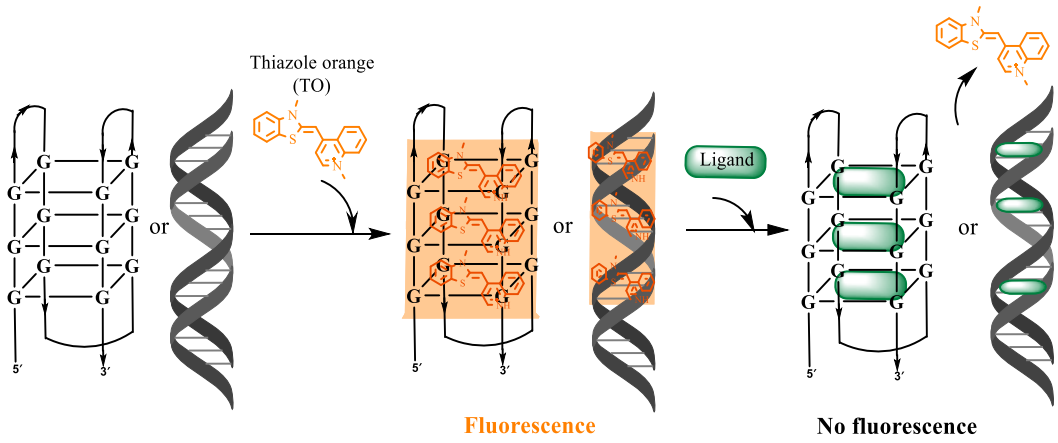

Figure 4.18: a schematic representation of a FID assay performed using TO and a G-quadruplex or dsDNA molecule. Adapted from various references.[214,215]

Thiazole orange has been shown to intercalate between the base pairs of dsDNA and interact with the external G-quartets of a G-quadruplex by an end-stacking mechanism.[212,216,217] Competitor molecules will most effectively displace TO from DNA if they interact via the same mechanism. Therefore, FID assays may provide information about DNA binding modes and sites in addition to overall affinity.

In this project, FID assays were performed by titrating nickel complexes into solutions containing either a G-quadruplex or dsDNA and a pre-determined amount

of TO. The decrease in fluorescence resulting from TO was then monitored resulting in data such as that shown in Figure 4.19, which was derived from an experiment in which increasing amounts of (**56**) were added to a Q4/TO complex. The addition of (**56**) was continued until no further significant decreases in fluorescence were observed, indicating that complete displacement of bound TO had occurred. The resulting data was then plotted as shown in the inset in Figure 4.19 and the DC_{50} value calculated as described in section 2.7 from the gradient and y-intercept of the regression line.

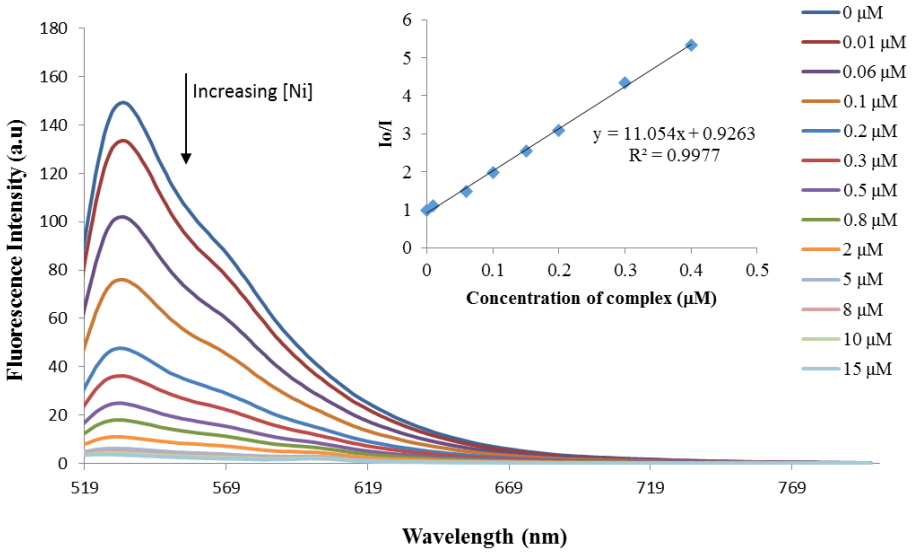

Figure 4.19: Results obtained from an FID assay involving addition of increasing amounts of (**56**) to a TO/Q4 complex. The inset shows a Stern-Volmer plot derived from the data, which was then used to determine the DC_{50} for the nickel complex.

Table 4.7 presents DC_{50} values for the five nickel complexes with three different DNA molecules. The results obtained from FID assays support a number of conclusions that correlate with those derived from analysis of the ESI-MS data presented earlier. For example, the values of DC_{50} obtained for (**59**) in experiments with all three DNA molecules were by far the largest measured, which indicates that

this nickel complex exhibited the lowest binding affinity in each case. This is consistent with the lower abundance of ions from non-covalent complexes containing one or more molecules of this nickel complex in ESI-MS experiments performed with each of the nucleic acid molecules.

Inspection of Table 4.7 also shows that the two lowest values of DC_{50} derived from experiments performed with D2 were obtained with (**53**) and (**56**). These complexes showed the most extensive formation of non-covalent complexes in ESI-MS experiments, with ions from complexes containing two bound nickel molecules more abundant than in experiments performed with the other metal complexes. The values of DC_{50} determined from experiments performed with Q4 were, with the exception of that obtained with (**59**), all very similar, suggesting near identical binding affinities towards the parallel tetramolecular G-quadruplex. This is consistent with the observation that the most abundant ions observed in ESI-MS experiments performed with the other four nickel complexes and Q4 consisted of two nickel molecules bound to the nucleic acid. Table 4.7 also shows that the values of DC_{50} obtained from experiments performed with Q1 were generally similar, aside from that derived from experiments where (**59**) was the complex under investigation. This once again suggests that the four remaining nickel complexes exhibit similar binding affinities towards the nucleic acid. Comparison of the DC_{50} values for the five nickel complexes suggests (**53**) exhibited the greatest binding affinity towards Q1.

Table 4.7: DC_{50} values derived from FID assays performed using nickel complexes and different DNA molecules.

Nickel complex	DC_{50}(μM)		
	dsDNA D2	Parallel Q4	Parallel Q1
(**53**)	0.31 ± 0.03	0.16 ± 0.02	0.15 ± 0.01
(**56**)	0.44 ± 0.04	0.09 ± 0.01	0.49 ± 0.03
(**59**)	2.23 ± 0.13	3.17 ± 0.13	1.18 ± 0.17
(**62**)	1.04 ± 0.09	0.19 ± 0.01	0.45 ± 0.03
(**65**)	0.82 ± 0.03	0.15 ± 0.02	0.31 ± 0.01

4.2.6 DNA binding studies performed using molecular docking

The results presented earlier in this chapter were obtained using techniques suited to providing information about the extent of interaction between the nickel complexes and different DNA molecules and, in some instances, whether those interactions affected the conformation and/or stability of the nucleic acid. In contrast, they did not provide much, if any indication about likely binding modes, with the possible exception of the FID assays. To address this situation a series of computational docking experiments were undertaken using crystal structures of a parallel, unimolecular G-quadruplex (1KF1) and a dsDNA molecule (1KBD). Docking experiments were performed as described in Chapter 2. Figure 4.20 illustrates the top binding mode for each nickel complex with both DNA molecules, based on the results of the computational studies, while the minimum binding energies (ΔG) resulting from these investigations are shown in Table 4.8.

Inspection of Figure 4.20 reveals a number of similarities amongst the binding modes used by the various nickel complexes with both types of DNA, but also some important differences. All nickel complexes except (**65**) preferred to interact via π-stacking interactions with the top G-tetrad of the parallel unimolecular G-quadruplex.

In addition, at least two pendant groups were always positioned to participate in favourable intermolecular interactions with the loops and/or grooves of the nucleic acid. In contrast, the location of nickel ion relative to the G-tetrad was found to vary between complexes. For example, Figure 4.20 (a) shows the nickel ion of (**53**) located directly above the centre of the G-tetrad. This result is similar to what was obtained previously for the nickel Schiff base complex (**18**) which is an analogue of (**53**) but contains only two ethylpiperidine groups in the 4′-positions.[124] Further inspection of Figure 4.20 (a) however, shows the nickel ions of the other molecules were located in different positions above the G-tetrads.

Inspection of Figure 4.20 (a) also suggests that the interactions between (**59**) and 1KF1 were very different to those involving the other nickel complexes. This may be due to this being the only complex featuring a diamine moiety containing a six-membered chelate ring in contrast to the five-membered rings present in all the other complexes. The nickel ion in (**59**) was positioned towards the edge of the guanine residues. The two aromatic rings of the complex were not coplanar with each other, and there was an angle of 47.3 °C between their planes. These rings are co-planar in all the other complexes presented in this chapter with an angle of 2.3 – 19.8 °C between their planes. Two of the pendant groups of (**59**) were found to interact with the second and third TTA loops of 1KF1 while the other two were located on the edge of the G-tetrad and orthogonal to the edge of the guanine residues.

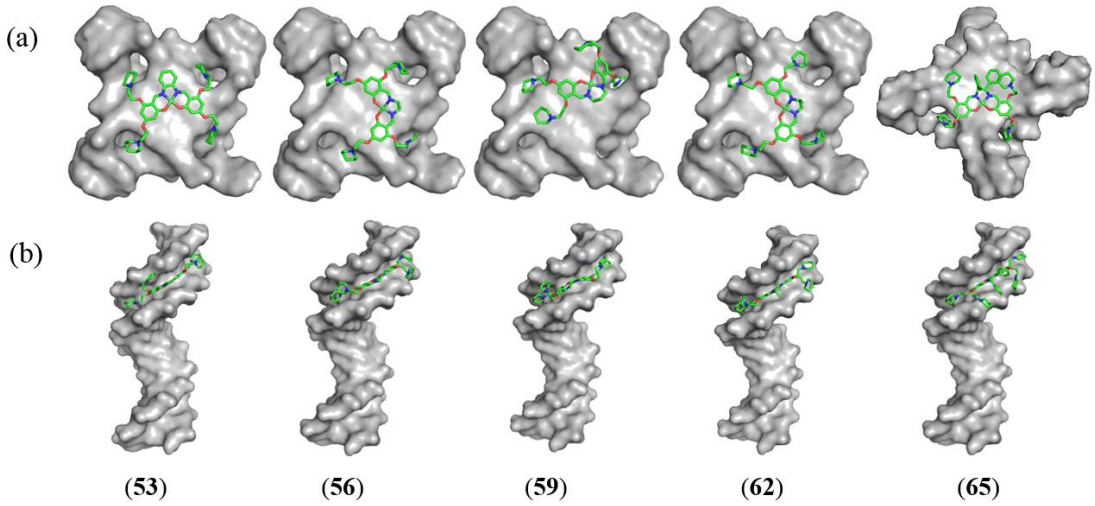

Figure 4.20: Most favourable binding mode resulting from molecular docking studies performed using nickel Schiff based complexes and different DNA molecules: (a) computational studies performed using the G-quadruplex 1KF1 and (b) computational studies performed using the dsDNA 1KBD1.

Figure 4.20 (a) shows one of the aromatic rings of the *meso*-1,2-diphenylethylenediamine moiety of (**65**) was orientated parallel to, and therefore able to π-stack with, the corresponding ring systems of the G-tetrad of 1KF1. In addition, the two bottom pendant groups of (**65**) were bound to the first and second TTA loops of the nucleic acid.

Inspection of Figure 4.20 (b) shows most of the nickel Schiff base complexes participated in very similar binding interactions with the dsDNA 1KBD. In each case the most favourable binding mode involved the minor groove of the nucleic acid. The two pendant groups in the bottom halves of the nickel complexes and the associated aromatic rings were typically positioned in the minor groove in order to optimise favourable intermolecular interactions. Simultaneously, the two pendant groups in the top halves of the nickel complexes and the diamine moieties were positioned so they were orientated away from the minor groove towards the solvent, perhaps in an attempt to avoid unfavourable steric interactions. The docking results

are consistent with those obtained from CD spectroscopic studies, which suggested the binding mode of the nickel complexes with dsDNA was more likely to be groove binding than intercalation in the majority of cases. Inspection of Table 4.8 shows the minimum binding energies of the nickel complexes with 1KBD were distributed over a narrow range from -7.9 to -8.8 kcal/mol. This is consistent with the similar binding mode exhibited by all nickel complexes shown in the docking images (Figure 4.20 (b)).

The largest binding energies were observed with complex (**53**), suggesting it has the strongest overall binding interactions with 1KBD. In contrast, complexes (**59**) and (**65**) exhibited the lowest binding energy with the dsDNA molecule. This is consistent with the results presented in Figure 4.20 (b), which show that the diamine moieties in (**59**) and (**65**) were orientated away from the minor groove more than what was observed in the other complexes. The docking results are consistent with those obtained from ESI-MS and UV-Vis spectroscopic studies, which also showed (**59**) and (**65**) both exhibit low binding affinity towards dsDNA.

The docking results also showed the minimum binding energies of nickel complexes with the G-quadruplex 1KF1 were distributed over a narrow range from -9.6 to -8.6 kcal/mol. This indicates that that the nickel complexes also exhibited very similar binding affinities for 1KF1. The largest binding energy was observed with complex (**53**), suggesting it has the strongest overall binding interactions with 1KF1. In contrast, complex (**59**) exhibited the lowest binding energy with the G-quadruplex. This is consistent with the results presented in Figure 4.20 (a), which show two pendant groups of (**59**) were orientated away from the loops and grooves of the G-quadruplex and therefore unable to participate in favourable binding interactions.

Table 4.8: Binding free energies obtained from docking studies performed using nickel Schiff base complexes and either 1KF1 or 1KBD.

Structure ID	1KF1(qDNA)		1KBD (dsDNA)	
	ΔG (kcal/mol)[a]	Binding mode[b]	ΔG (kcal/mol)[a]	Binding mode[b]
(**53**)	-9.64 ± 0.05	Top, end stacking	-8.8 ± 0.1	Minor groove
(**56**)	-9.02 ± 0.04	Top, end stacking	-8.4 ± 0.1	Minor groove
(**59**)	-8.60 ± 0.10	Top, end stacking	-7.9 ± 0.1	Minor groove
(**62**)	-9.14 ± 0.05	Top, end stacking	-8.7 ± 0.1	Minor groove
(**65**)	-8.64 ± 0.09	Bottom, end stacking	-8.4 ± 0.1	Minor groove

[a] Average values of ΔG with standard errors obtained from the top five docking scores.
[b] "Top" or "Bottom" indicates which terminal G-tetrad was the preferred binding site.

4.2.7 MTT assays

One of the principal objectives of this project was to develop new nickel complexes which are effective anti-cancer agents that elicit biological activity as a result of interacting selectively with G-quadruplex DNA. In order to explore the therapeutic potential of the complexes a series of MTT assays was therefore performed to measure their cytotoxicity.[177] While MTT assays provide a convenient method for achieving this goal, they do not provide specific information about the mechanism of cell death induced by the tested compounds.

The assay is used to measure the cellular toxicity of small molecules by quantifying the extent of mitochondrial enzymatic reduction of the yellow compound MTT to form the purple formazan. The amount of purple formazan produced is directly proportional to the number of viable cells, while non-viable cells exhibit impaired enzymatic activity levels leading to lower production of the formazan. Data obtained from MTT assays is generally presented in the form of a concentration-response curve from which an IC_{50} can be determined. This value corresponds to the

concentration of compound which results in a 50% reduction in formazan production after treatment. The smaller the IC_{50} value, the more cytotoxic the compound.

For this project the in vitro cytotoxicity of complexes (**53**), (**56**) and (**65**) was evaluated by the MTT assay using the V79 lung cancer cell line (Chinese hamster cancer cells). For comparison purposes, the cytotoxicity of complexes (**18**), (**20**) and (**46**) against the same cell line was also evaluated by the MTT assay. The latter three complexes were obtained from Dr Kimberley Davis. Complexes (**18**), (**20**) and (**46**) are analogues of (**53**), (**56**) and (**65**), respectively but contain only two ethylpiperidine groups in the 4′-positions.

The concentration-response curves derived from results obtained from the MTT assay are shown in Figure 4.21, while IC_{50} values derived from those curves are provided in Table 4.9. Each of the curves in Figure 4.21 showed significant drops in cell viability once a threshold concentration of nickel complex was reached. Complex (**65**) exhibited the greatest cytotoxicity (IC_{50} = 6.1 µM) while (**56**) exhibited the lowest (IC_{50} = 48.1 µM), among the tested complexes.

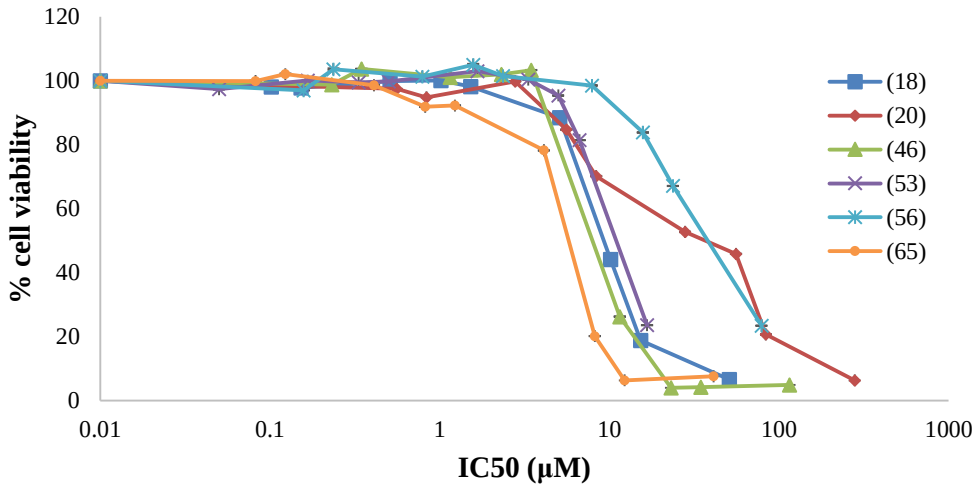

Figure 4.21: Concentration-response curves obtained from 24 h MTT assays using V79 cells treated with different nickel complexes. The error bars represent one standard deviation calculated from triplicate plates.

Table 4.9: IC_{50} values for nickel complexes obtained from 24 h MTT assays performed using V79 Chinese hamster cancer cells.

Nickel complex	IC_{50}(μM)*	**Nickel complex**	IC_{50}(μM)*
(**18**)	9.4 ± 0.4	(**53**)	11.8 ± 0.5
(**20**)	39.9 ± 0.7	(**56**)	48.1 ± 4.0
(**46**)	9.3 ± 0.2	(**65**)	6.1 ±0.3

* IC_{50} value was determined using at least three independent MTT assays.

The IC_{50} values presented in Table 4.9 are greater than those obtained for some other nickel complexes with other cancer cell lines. For example, some of the nickel(II) thiosemicarbazone complexes synthesized by Bal Demirci *et al.* and Haribabu *et al.* showed IC_{50} values < 0.7 μM against a number of cancer cell lines including K562 (leukemia), MCF-7 (breast) and A549 (lung) cell lines.[218,219] The cytotoxicity of the latter complexes was greater than that exhibited by the clinically used anti-cancer drug cisplatin (IC_{50} = 13.2 ± 0.6 μM for K562 cells and IC_{50} = 13.9 ± 0.5 μM for MCF-7 cells).[218,220]

On the other hand the cytotoxicity of the nickel complexes under investigation in this project was more comparable to that of a nickel(II) hydrazone complex synthesized by Li *et al*. This exhibited cytotoxicity towards A549 and HeLa cells with IC_{50} values of 29.2 ± 1.1 and 34.9 ± 2.1 μM, respectively.[221] These values indicate the latter complex was less cytotoxic than cisplatin (IC_{50} = 13.2 ± 0.6 μM for HeLa cells and IC_{50} = 17.2 ± 0.5 μM for A549 cells).[222,223]

The results presented in Table 4.9 suggest (**65**) was slightly more cytotoxic than its analogue with only two pendant groups (**46**) towards V79 cells. In contrast, the reverse trend was observed for the other two pairs of nickel complexes. Therefore, although only a limited data set of complexes was investigated, introduction of two additional pendant groups does not in general appear to confer additional cytotoxicity

onto this class of nickel complexes. It should be remembered, however, that the effects of such structural alterations may vary from one cancer cell line to another.

4.3 Summary

This chapter presents the results of DNA binding studies performed using a number of different analytical techniques and nickel Schiff base complexes bearing different diamine moieties and four ethylpiperidine pendant groups. There were a number of instances where trends in binding affinity determined using one technique matched closely those obtained using other methods. On other occasions, however, there was a lack of correlation between results. This was not unexpected, as the affinities of the complexes towards some DNA molecules were low and/or did not vary greatly, and experimental approaches vary in their sensitivity to different aspects of the drug/DNA interaction.

Changing the structure of the diamine moiety was found to influence both DNA affinity and selectivity. When the phenylenediamine moiety was present, the results of ESI-MS binding studies indicated that the resulting complex (**53**) was able to form non-covalent complexes with dsDNA and both unimolecular and tetramolecular G-quadruplexes. The CD spectrum of D2 changed in a different way in response to addition of (**53**) compared the other four nickel complexes, and (**53**) also produced the greatest increase in T_m for D2 (1.6 ˚C). Both observations may reflect the phenylenediamine group interacting in a unique manner with dsDNA. It should be noted, however, that none of the nickel complexes investigated were very effective at stabilising dsDNA, as larger changes in T_m would have been expected. For example,

the nickel Schiff base complex (**45**) was found previously to increase the T_m of D2 by 6.3 °C.[136]

Complex (**53**) was also found to have a greater ability than most other nickel complexes to affect the CD spectrum of unimolecular G-quadruplexes when the latter were present in either a parallel or hybrid conformation. While the complex containing the phenylenediamine moiety did not prove as effective as most other complexes at displacing TO from D2, Q1 and Q4 molecules, the results obtained from FID assays confirmed the ability of (**53**) to interact with all three nucleic acid molecules noted in ESI-MS experiments.

Changing the diamine moiety from phenylenediamine to ethylenediamine, 1,3-propanediamine or 1,2-propanediamine resulted in a series of complexes that exhibited in some instances very different DNA binding characteristics. In general, the 1,3-propanediamine-containing complex (**59**) exhibited the lowest DNA binding affinity. For example, in ESI-MS experiments it demonstrated less ability to form non-covalent complexes with any of the three DNA molecules investigated than the other four nickel molecules. The low affinity of (**59**) for D2, Q1 and Q4 was confirmed by the results of FID assays, which resulted in larger values of DC_{50} for this nickel complex than for any other discussed in this chapter. Furthermore, whilst addition of (**59**) did elicit changes to the CD spectrum of some DNA molecules these were not as significant as what was seen with other nickel complexes.

Comparison of the data presented in Figure 4.3 shows that changing the diamine moiety from 1,3-propanediamine to either 1,2-ethylenediamine or 1,2-propanediamine resulted in complexes with a greater ability to form non-covalent complexes with D2, Q1 and Q4. This suggests the above structural changes resulted

in increased DNA binding affinity for (**56**) and (**62**), which is supported by the results of FID assays performed with the same three DNA molecules. In contrast, the results of FRET melting assays and CD studies suggested that the latter two complexes and (**59**) all exhibited similar levels of DNA binding affinity towards the anti-parallel and hybrid forms of F21T or Q1.

Complex (**65**), featuring the *meso*-1,2-diphenylethylenediamine moiety, exhibited selectivity in its binding interactions in a number of experiments. For example, the results of ESI-MS studies showed (**65**) exhibited a greater ability to form non-covalent complexes with Q1 and Q4 than with D2. The ability of (**65**) to interact with Q1 in particular was notable as it was the only nickel complex for which no ions attributable to free DNA were observed in ESI mass spectra. Further evidence in support of a binding preference for G-quadruplex DNA over dsDNA was provided by the results of FID assays and CD spectroscopic studies. Analysis of the former afforded a value of DC_{50} for (**65**) with D2 which was in the middle of those exhibited by the remaining nickel complexes. In contrast, complex (**65**) gave the lowest and second lowest values of DC_{50} with Q4 and Q1, respectively, confirming its affinity for these G-quadruplexes.

Complex (**65**) had little impact on the CD spectrum of D2, however it resulted in the largest changes observed amongst all five nickel complexes to the corresponding spectrum of Q4, and also resulted in major changes to the CD spectra of parallel Q1 and c-KIT1. The results of CD and FRET studies performed with anti-parallel and hybrid forms of unimolecular G-quadruplexes indicated it also exhibited the ability to bind to these forms of nucleic acid. More than any other diamine moiety, the *meso*-1,2-diphenylethylenediamine group appears to confer a distinct binding

selectivity trait upon complexes in which it is found. Previous investigations have noted the ability of nickel Schiff base complexes bearing this group to interact more selectively with parallel tetramolecular G-quadruplexes in particular.[135,136]

The results of molecular docking studies indicated that each of the nickel complexes interact with dsDNA via a groove binding mechanism and that intercalation was not a major contributor to the intermolecular interactions. This conclusion is supported by the results obtained from CD studies, as larger changes to the CD spectra of DNA would have been expected if the nickel complexes were interacting via an intercalating binding mode. For example, the magnitude of the changes to the CD spectrum of dsDNA caused by addition of the nickel complexes discussed here is much lower than that reported for octahedral nickel complexes of the general formula $[Ni(phen)_2L]^{2+}$ (L = dpq, dpqC, dppz), which are known to bind to dsDNA via intercalative binding modes.[224]

Molecular docking studies also revealed the nickel complexes interact primarily via an end-stacking mechanism with G-quadruplex DNA. The exact manner with which the complexes interacted varied as a result of differences in their structure, however the binding free energies fell within a relatively narrow range. This suggests that additional changes to the structure of the complexes will be required in order to produce more effective and selective G-quadruplex binding agents.

Chapter 5 DNA-binding properties of nickel Schiff base complexes with different pendant groups

5.1 Introduction and scope

In the previous chapter, results obtained from DNA binding studies performed using nickel Schiff base complexes that differ in the structure of the diamine moiety were presented. Here results are presented from similar studies which were performed to investigate whether DNA binding properties are enhanced by changing the pendant groups on the complexes from ethylpiperidine to either ethylmorpholine or propylpiperidine. The DNA binding properties of some nickel complexes bearing the latter pendant groups has been reported previously.[125,130,135] For example, it was found that replacing the ethylpiperidine with propylpiperidine in the nickel salphen complex (**18**) (Section 1.4.3) resulted in improved G-quadruplex binding and/or selectivity. The synthesis and characterisation of the novel complexes discussed in this chapter were presented in Chapter 3, and their structures are displayed in Figure 5.1 together with those of their analogues discussed in Chapter 4. It was hoped that by replacing the ethylpiperidines with other pendant groups the DNA binding ability and/or selectivity of the resulting complexes would be enhanced. The same biophysical techniques and DNA molecules used in the studies reported on in the previous chapter were again used here to investigate the effects of these structural changes.

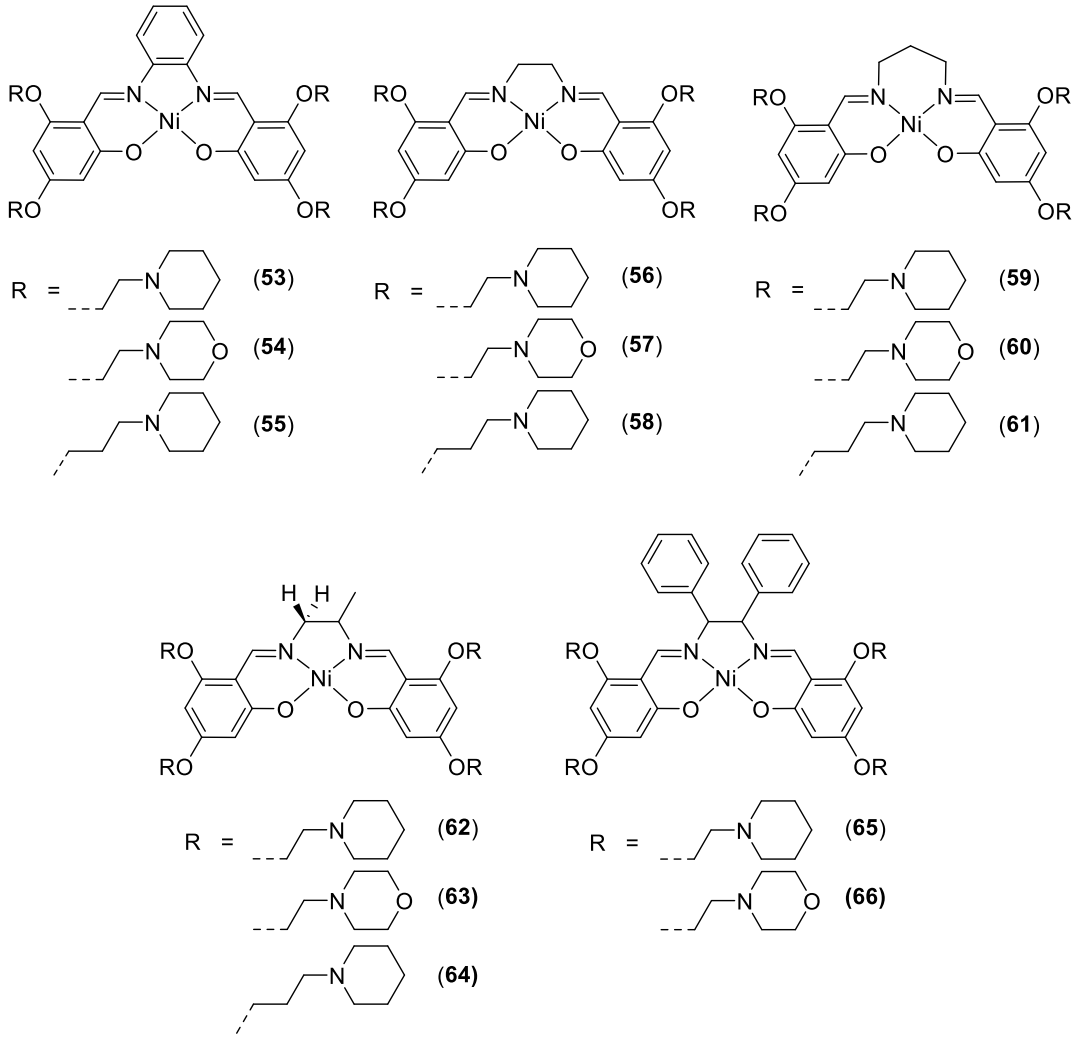

Figure 5.1: Structures of nickel Schiff base complexes containing different pendant groups.

5.2 Results and discussion

5.2.1 DNA binding studies performed using ESI mass spectrometr

ESI-MS experiments were initially performed to compare the affinities of nickel Schiff base complexes containing ethylmorpholine pendant groups and different diamine moieties towards the dsDNA D2. The results of these experiments, which were performed using a 6:1 ratio of Ni:D2, are presented in Figure 5.2.

All of the spectra presented in Figure 5.2 show ions of low to high abundance at *m/z* 1626.5 and 1952.0, which are attributed to $[D2 - 6H]^{6-}$ and $[D2 - 5H]^{5-}$, respectively. The abundances of these ions varied from one spectrum to another, suggesting the nickel complexes bind to D2 to different extents. For example, both ions from free D2 were of lower abundance in Figure 5.2 (b) than for any of the other spectra. This suggests (**54**) has the highest affinity towards D2 of the five complexes containing ethylmorpholine pendant groups. Further evidence in support of this conclusion was obtained after considering the abundances of ions from non-covalent complexes containing two or more nickel molecules bound to DNA in the spectra shown in Figure 5.2. These were much greater in the case of the spectrum in Figure 5.2 (b) than for all other spectra except that shown in Figure 5.2 (c). Close examination of the spectra in Figure 5.2 (b) and (c) showed the abundances of ions from non-covalent complexes containing two or more molecules of (**54**) bound to DNA were slightly greater than for those containing multiple molecules of (**57**). The above results therefore suggests that complex (**54**) containing a phenylenediamine moiety has a slightly higher affinity towards D2 than (**57**), which has an ethylenediamine group, and that the remaining complexes having significantly lower affinities.

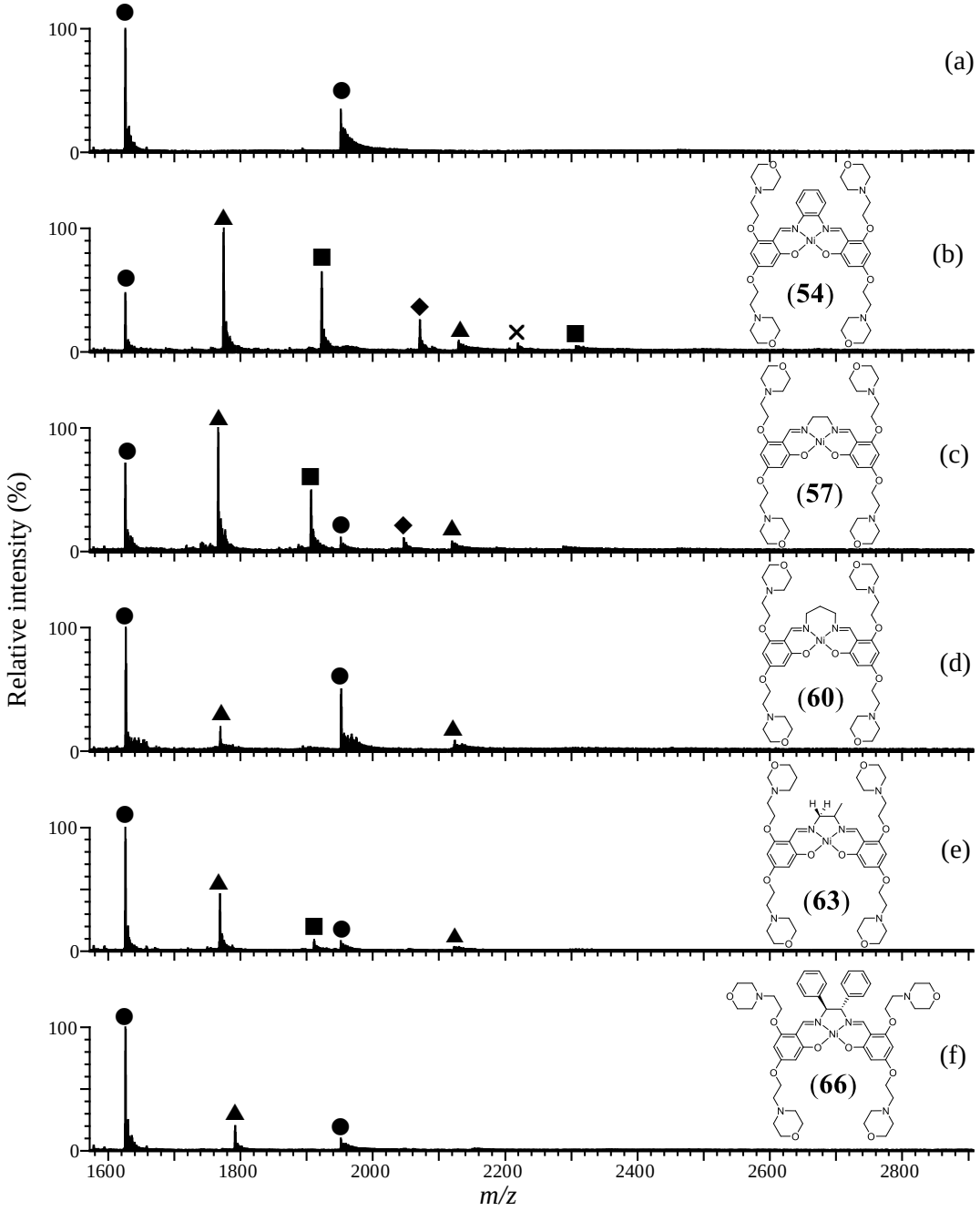

Figure 5.2: Negative ion ESI mass spectra of solutions containing different nickel Schiff base complexes and D2 at a 6:1 ratio: (a) Free D2; (b) D2 + (**54**); (c) D2 + (**57**); (d) D2 + (**60**); (e) D2 + (**63**) and (f) D2 + (**66**). ● = free D2; ▲ = [D2 + (Ni)]; ■ = [D2 + 2(Ni)]; ◆ = [D2 + 3(Ni)]; ✕ = [D2 + 4(Ni)].

A similar conclusion was reached after comparing the spectra of solutions containing D2 and complexes bearing ethylpiperidine pendant groups and different diamine

moieties (Figure 4.2). In the case of the latter spectra, complexes (**53**) and (**56**), which also contain phenylenediamine and ethylenediamine moieties, were found to exhibit greater binding affinities towards D2 than complexes containing other diamine groups.

Inspection of Figure 5.2 shows very low ion abundances corresponding to non-covalent complexes consisting of one or more molecules of (**60**), (**63**) or (**66**) bound to D2. These observations suggest the presence of the 1,3-diaminopropane, 1,2-diaminopropane or *meso*-1,2-diphenylethylenediamine moieties significantly inhibits DNA binding interactions in the case of complexes also containing ethylmorpholine pendant groups.

Additional binding experiments were conducted using nickel complexes containing propylpiperidine pendant groups, as well as either unimolecular or tetramolecular G-quadruplex DNA (Q1 and Q4, respectively). The results of these experiments are presented graphically in the form of relative abundances in Figure 5.3. Also included in Figure 5.3 to facilitate comparison of relative binding affinities are the results of experiments that were performed with analogous complexes containing ethylpiperidine pendant groups. These results were first presented in Chapter 4.

Analysis of Figure 5.3 reveals a number of clear trends in relative abundances. These include the relative abundances of ions from non-covalent complexes containing ethylmorpholine substituents were always lower than that of analogous complexes containing either of the other pendant groups. In many cases this trend was very pronounced. For example, in the case of binding experiments performed using nickel complexes containing ethylmorpholine pendant groups and Q1, the most abundant ions present in the ESI mass spectra were always from free DNA. Furthermore, ions

from non-covalent complexes were always of low abundance. In contrast, for the two other classes of nickel complexes ions from non-covalent complexes consisting of one or more nickel molecules bound to Q1 were often of medium or high abundance.

The above results suggest that the affinities of nickel complexes containing ethylmorpholine pendant groups may generally be less than that of the other two classes of complexes. This conclusion was reported previously for a closely related series of nickel Schiff base complexes also containing these pendant groups.[125,162] One possible explanation for this observation is that the oxygen atoms in the ethylmorpholine pendant groups may result in unfavourable electrostatic interactions with electron rich groups in the DNA molecules.

Examination of Figure 5.3 (b), (e), (h), (k) and (n) show in each case ions of medium abundance corresponding to non-covalent complexes of Q4. In contrast the most abundant ions present in spectra of the same complexes and Q1 were always from free DNA. This suggests a number of the nickel complexes bearing ethylmorpholine substituents exhibited some binding selectivity in favour of Q4 over Q1. In the case of (**60**), (**63**) and (**66**) very low levels of non-covalent complex formation were also observed with D2, suggesting that these complexes exhibited a binding preference for tetramolecular G-quadruplex DNA over both the unimolecular G-quadruplex and dsDNA.

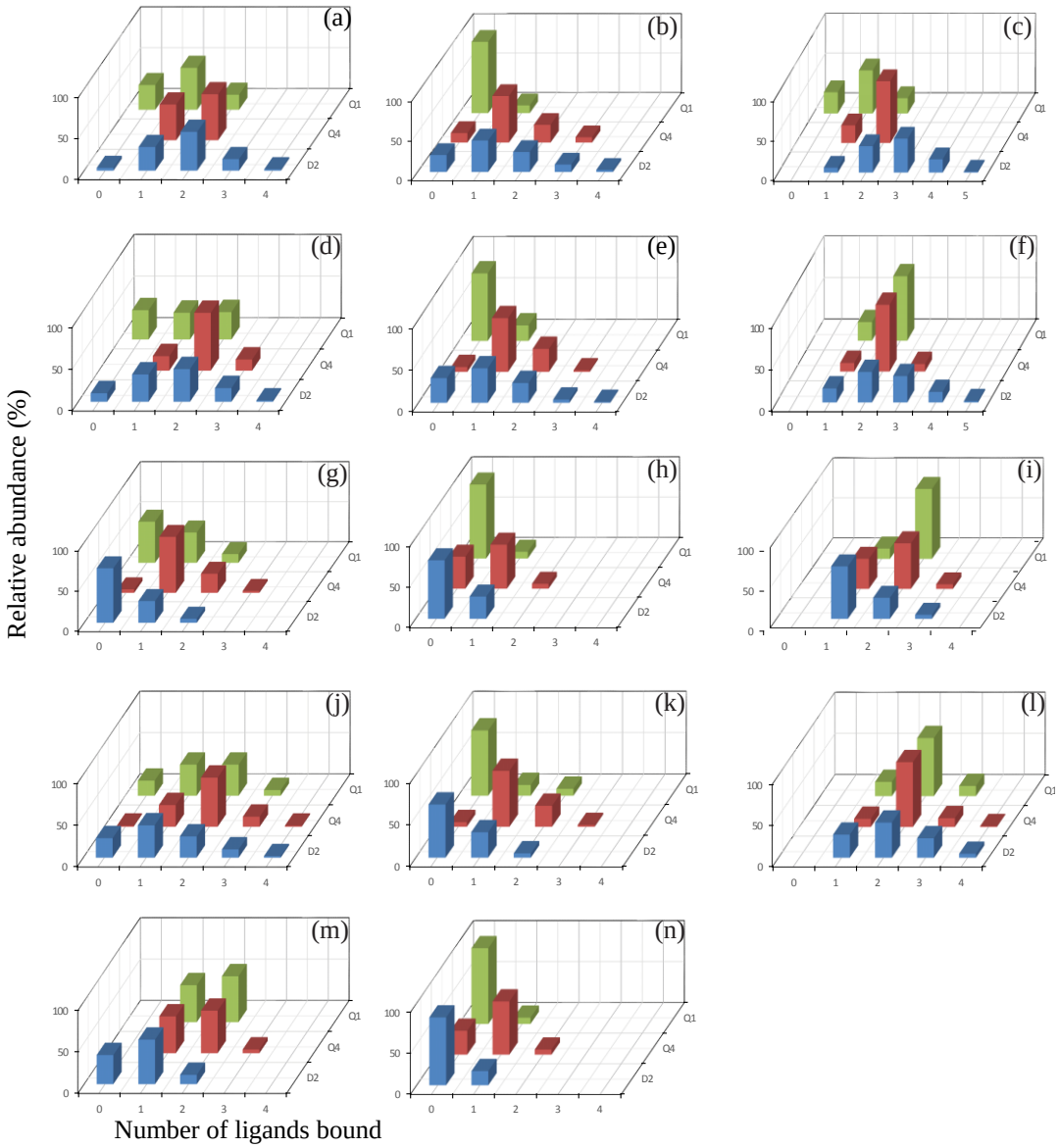

Figure 5.3: Relative abundances of ions in ESI mass spectra of solutions containing a 6:1 ratio of nickel Schiff base complex and dsDNA (D2), tetramolecular qDNA (Q4) or unimolecular qDNA (Q1): (a) solutions containing (**53**); (b) solutions containing (**54**); (c) solutions containing (**55**); (d) solutions containing (**56**); (e) solutions containing (**57**); (f) solutions containing (**58**); (g) solutions containing (**59**); (h) solutions containing (**60**); (i) solutions containing (**61**); (g) solutions containing (**62**); (k) solutions containing (**63**); (l) solutions containing (**64**); (m) solutions containing (**65**) and (n) solutions containing (**66**).

The low binding affinity towards D2 exhibited by (**66**) was expected as other nickel complexes including (**65**), which also contain the *meso*-1,2-diphenylethylenediamine

moiety have been reported to show very low binding affinities towards dsDNA.[135] The explanation put forward previously for this observation was that the presence of the non-planar diamine moiety sterically hinders the approach of the nickel molecule to dsDNA, resulting only in comparatively weak partial intercalation or groove binding interactions.

Another important trend revealed upon examination of Figure 5.3 is the absence of ions from free DNA in spectra of solutions containing a 6:1 ratio of nickel complexes containing propylpiperidine groups and DNA. This was true for each of the three DNA molecules examined, with the exception of solutions containing (**55**) and Q1, which gave a spectrum containing ions of low to medium abundance from free nucleic acid. In contrast, Figure 5.3 shows ions from free DNA were present in spectra of many other solutions containing one of the other two classes of nickel complexes and either D2 or Q4. These observations suggest nickel complexes featuring propylpiperidine pendant groups have higher affinities for each of the three DNA molecules than analogues containing the same diamine moiety, but one of the other classes of pendant groups.

The above conclusion is generally supported by comparison of the relative abundances of ions from non-covalent complexes formed in solutions containing the same DNA molecule and nickel complexes with the same diamine moiety, but different pendant groups. One such group of nickel complexes is (**62**), (**63**) and (**64**), each of which contains the 1,2-propanediamine moiety. The most abundant ions observed in spectra of solutions containing (**64**) (Figure 5.3 (l)) were always from non-covalent complexes containing two nickel molecules bound to the DNA. In contrast, the most abundant ions present in spectra of solutions containing (**63**) and

either Q1 or D2 were from free DNA, while when Q4 was present ions from a non-covalent complex containing only one bound nickel molecule were most prevalent (Figure 5.3 (k)). Figure 5.3 (j) shows that when (**62**) was present the most abundant ions present in solutions containing either Q1 or D2 were from non-covalent complexes containing only one bound nickel molecule.

Further analysis of Figure 5.3 suggests (**55**) and (**58**) may exhibit the highest affinity for D2 amongst all the complexes examined as part of this project. Evidence in support of this is provided by the absence of ions from free DNA, as well as observation of ions of medium abundance from non-covalent complexes containing three bound nickel molecules, as well as ions of low abundance containing up to five nickel complexes bound to D2. It appears that the combination of propylpiperidine pendant groups and either a phenylenediamine or ethylenediamine moiety in the top half of the nickel complexes provided more favourable structures for binding to dsDNA in comparison to the other nickel molecules.

While Figure 5.3 indicates that a number of the nickel complexes were able to form non-covalent complexes with D2 that contained three or more bound molecules, this was rarely the case with either of the G-quadruplexes. This is consistent with the view that the nickel molecules can bind to dsDNA via a combination of electrostatic interactions, groove binding and partial intercalation anywhere along the length of the 16mer dsDNA molecule. In contrast, binding to either of the two G-quadruplexes most likely involves end stacking, resulting in at most two very strong sets of intermolecular interactions. In this context it is noteworthy that solutions containing (**58)**, (**61**) or (**64**) and Q1 resulted in spectra containing very high abundances of ions from non-covalent complexes containing two bound nickel molecules, and very low

abundances of a small number of other ions. This suggests these complexes may be very effective binding agents for unimolecular G-quadruplexes, although not highly selective ones. For similar reasons (**56**), (**58**) and (**64**) appear to be the most effective binding agents of those examined for tetramolecular G-quadruplexes.

Analysis of Figure 5.3 also reveals other similarities and differences in binding behaviour for complexes bearing the same diamine moiety but different pendant groups. One such pair of complexes is (**65**) and (**66**). The former complex was shown previously to form non-covalent ions of medium to high abundance containing one or two nickel molecules bound to either Q1 or Q4. In contrast, complex (**66**) exhibits a binding preference in favour of the tetramolecular G-quadruplex over both of the other types of DNA molecules (Figure 5.3 (n)). Another regular trend in binding behaviour was observed when the 1,3-propanediamine moiety in nickel complexes bearing ethylmorpholine or propylpiperidine pendant groups was replaced with either 1,2-ethylenediamine or 1,2-propanediamine. This was found to generally result in a decrease in binding affinity towards each of the three DNA molecules. A similar trend was noted in chapter 4 for the corresponding complexes featuring pendant ethylpiperidine moieties, highlighting a consistent effect of altering structure on DNA binding behaviour.

5.2.2 DNA binding studies performed using CD spectroscopy

5.2.2.1 CD titrations using double stranded DNA D2

CD spectroscopy was also used to investigate the effect of varying the pendant groups in the nickel complexes on binding to different DNA molecules. The results of experiments in which the effects of adding nickel complexes containing either

ethylmorpholine or propylpiperidine groups on the CD spectrum of dsDNA D2 were investigated are shown in Figure 5.4, and in Table 5.1. These may be compared to results obtained using complexes containing ethylpiperidine groups which were shown in Chapter 4.2.2.1. Inspection of Figure 5.4 shows that addition of (**60**) or (**66**) had little effect on the CD spectrum of D2. This is in accord with the low abundance of ions from non-covalent complexes and high abundance of ions from free D2 observed in ESI mass spectra of these systems (Figure 5.2 (h) and (n)). The concordance between these results obtained using different techniques suggests (**60**) and (**66**) have low affinities towards D2. In contrast, addition of most of the remaining complexes with ethylmorpholine or propylpiperidine pendant groups resulted in notable changes to the CD spectrum of D2. For example, addition of (**54**) resulted in large decreases in ellipticity for both the positive and negative CD bands, as well as a significant blue shift for the latter spectral feature. These changes were very similar to what was reported in Chapter 4 for the same experiment performed with (**53**). In addition, complex (**55**), which also bears the phenylenediamine moiety but contains propylpiperidine pendant groups, also showed similar effects on the CD spectrum with the exception of producing a small increase in ellipticity for the negative CD band. This hints at a slight difference between how (**54**) and (**55**) interact with D2. All three complexes with phenylenediamine groups were also found to result in extensive formation of non-covalent complexes in DNA binding experiments conducted using ESI-MS.

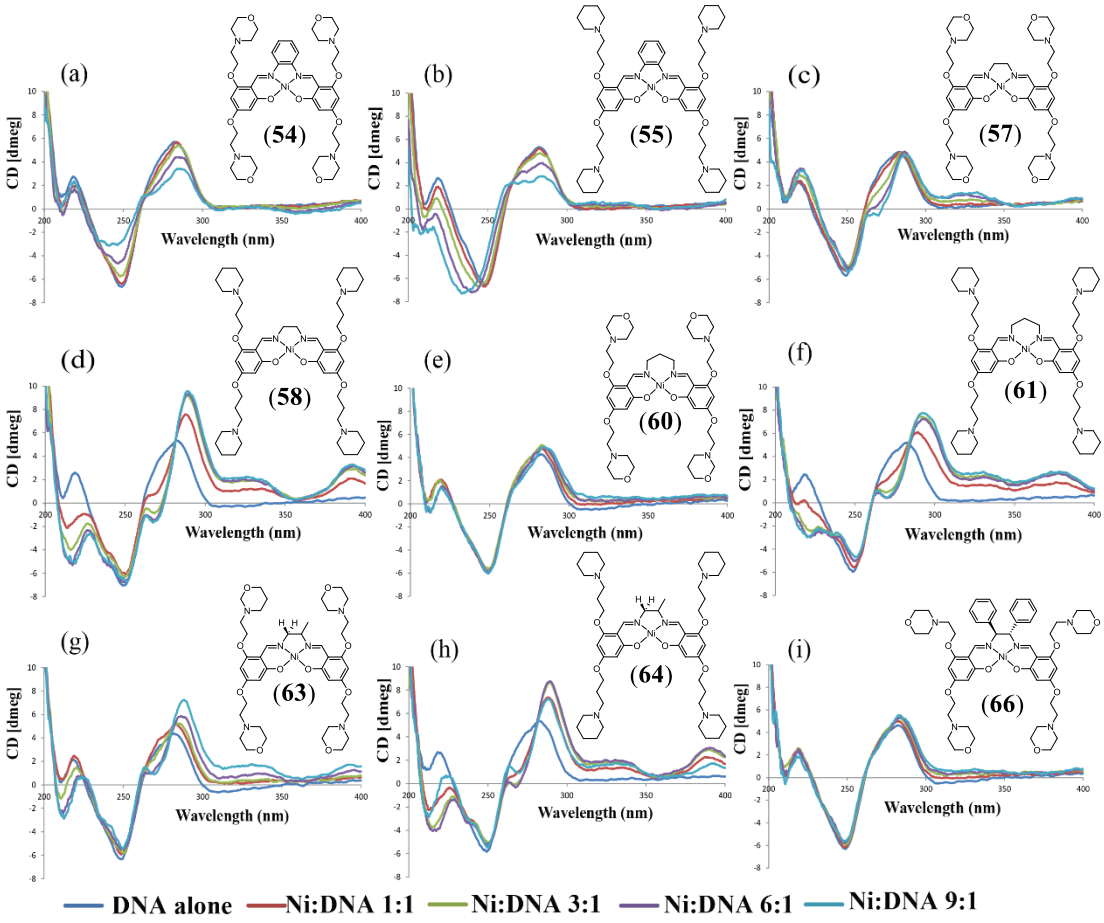

Figure 5.4: Circular dichroism spectra (200-400 nm) of solutions containing D2 and different ratios of nickel Schiff base complexes. (a) D2 + (**54**); (b) D2 + (**55**); (c) D2 + (**57**); (d) D2 + (**58**); (e) D2 + (**60**); (f) D2 + (**61**); (g) D2 + (**63**); (h) D2 + (**64**) and (i) D2 + (**66**).

There were a number of other instances where the changes to the CD spectrum of D2 caused by addition of a complex containing propylpiperidine pendant groups were slightly different to those caused by complexes containing the same diamine moiety and one of the other two types of pendants. This is illustrated by comparison of the effects observed after addition of the complexes containing ethylenediamine moieties. Inspection of Table 4.1 and Table 5.1 show that (**56**) and (**57**) resulted in similar changes to both major CD bands. For example, both caused very small (< 6%) decreases in ellipticity for the positive CD band, whereas the analogous complex

bearing propylpiperidine substituents, (**58**), resulted in very large increase in ellipticity (79.5%). In addition, only addition of (**58**) resulted in the appearance of a new positive CD band at 395 nm. These results suggest that replacing ethylpiperidine in (**56**) or ethylmorpholine in (**57**) with propylpiperidine to give (**58**) increased binding affinity towards D2 and/or altered the nature of the intermolecular interactions. Comparison of the spectra in Figure 5.4 further suggests that (**58**) may interact more strongly than any of the other nickel complexes with D2. This conclusion is consistent with the extensive formation of non-covalent complexes observed in ESI mass spectra of solutions containing this complex and D2.

Table 5.1: Effect of addition of nickel Schiff base complexes on the CD spectrum of D2.*

Nickel complex	**Positive CD band at 282 nm**		**Negative CD band at 249 nm**	
	$\Delta\lambda_{max}$ (nm)	**$\Delta\varepsilon$ (%)**	**$\Delta\lambda_{max}$ (nm)**	**$\Delta\varepsilon$ (%)**
(**54**)	1.6	-40.27	-8.0	-52.67
(**55**)	1.5	-47.19	-14.9	11.74
(**57**)	4.9	-5.74	0.9	-6.35
(**58**)	6.5	79.50	2.4	-4.45
(**60**)	1.5	14.75	-0.4	-0.23
(**61**)	9.8	49.02	1.5	-21.16
(**63**)	6.1	65.99	0.4	-13.77
(**64**)	5	35.85	0.4	0.14
(**66**)	0.8	19.73	-0.6	-10.63

* All $\Delta\lambda_{max}$ and $\Delta\varepsilon$(%) values are the difference between the values for free DNA and those for a solution containing a nickel:DNA ratio of 9:1. Negative $\Delta\lambda_{max}$ values indicate a blue shift; positive values indicate a red shift.

Complex (**63**) had the second largest effect on the ellipticity of the positive CD band of D2 of all complexes examined as part of this project. This result therefore suggests (**63**) interacts more strongly than many of the other nickel complexes with D2, which contrasts what would be expected based on results of the ESI-MS study, which showed addition of (**63**) resulted in little formation of non-covalent complexes. These observations may be rationalised by considering that the two techniques

exhibit varying sensitivities to different aspects of the binding interaction. For instance, the results from ESI-MS reflect the stability of non-covalent complexes in the gas phase, while the results from CD spectroscopy reflect changes to DNA conformation in solution. Therefore, it is possible that either the non-covalent complexes formed between (**63**) and D2 were not stable enough to survive the ESI conditions or that the relatively weak binding interactions of this complex with D2 were still strong enough to change the chirality of D2, and consequently its CD spectrum. It is also noteworthy that addition of complexes (**58**), (**61**), (**63**) and (**64**) all resulted in similar changes to the general appearance of the CD spectrum of D2, suggesting these four complexes might all interact similarly with the dsDNA.

5.2.2.2 CD titrations using parallel tetramolecular Q4

The results obtained from CD spectroscopic experiments in which nickel complexes containing either ethylmorpholine or propylpiperidine groups were added to Q4 are presented in Figure 5.5 and Table 5.2. Inspection of the results reveals that most of the complexes showed much smaller effects on the CD spectrum of the nucleic acid than what was seen in the analogous experiments involving D2. This suggests most of the nickel complexes do not interact strongly with the tetramolecular G-quadruplex. This may be contrast with the overall view of binding interactions between these complexes and Q4 based on the results of ESI-MS experiments, where most systems showed notable levels of formation of non-covalent complexes. A possible explanation for this apparent discrepancy is that the non-covalent complexes detected by ESI-MS do not perturb the chiral structure of the nucleic acid sufficiently to result in notable changes to the CD spectrum of the latter.

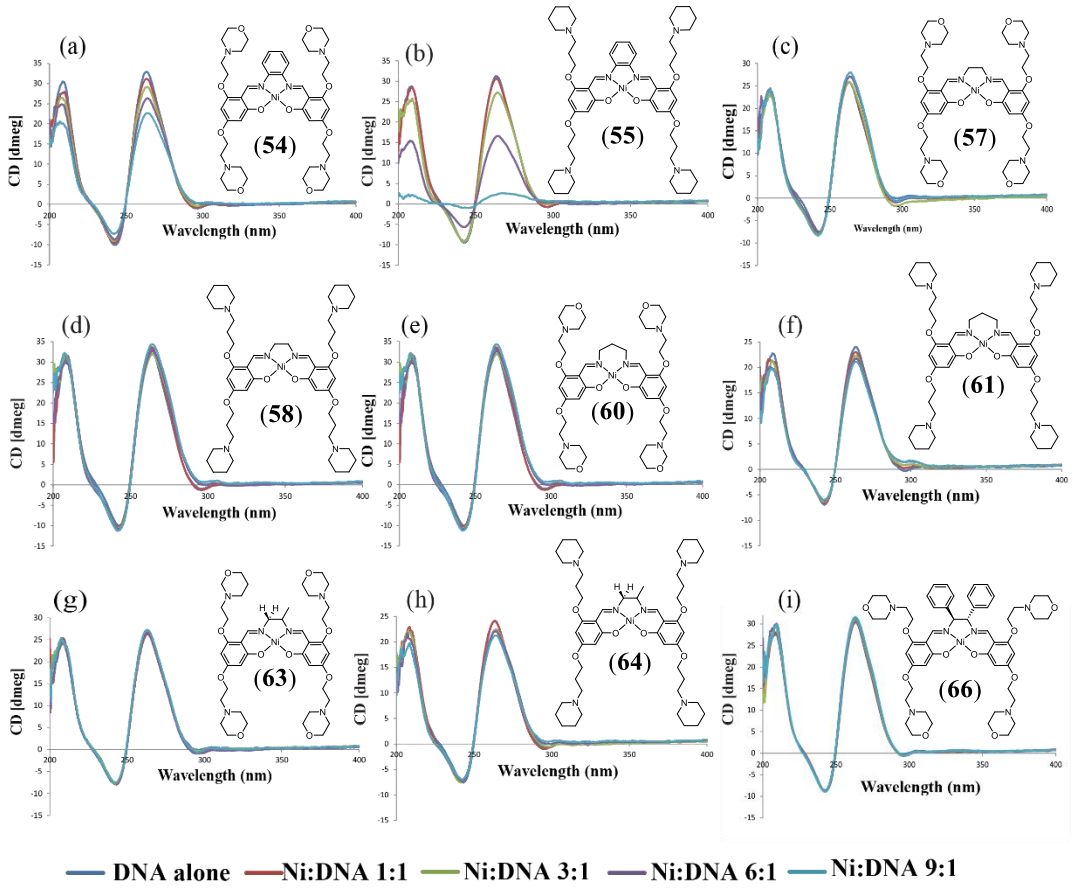

Figure 5.5: Circular dichroism spectra (200-400 nm) of solutions containing parallel Q4 and different ratios of nickel Schiff base complexes. (a) Q4 + (**54**); (b) Q4 + (**55**); (c) Q4 + (**57**); (d) Q4 + (**58**); (e) Q4 + (**60**); (f) Q4 + (**61**); (g) Q4 + (**63**); (h) Q4 + (**64**) and (i) Q4 + (**66**).

The two complexes which most affected the CD spectrum of Q4 were (**54**) and (**55**), both of which contain phenylenediamine moieties. In the case of (**54**), which also contains ethylmorpholine pendant groups, the ellipticities of the major positive and negative CD bands at 263 and 242 nm changed by -31% and -27%, respectively (Table 5.2). These variations are comparable to the changes of -33% and -22% noted earlier for the same experiments performed using the corresponding complex containing ethylpiperidine pendants (**53**) (Table 4.2). When the corresponding complex bearing the longer propylpiperidine pendants (**55**) was added to Q4 even larger decreases in ellipticity of 92% and 89% were observed (Table 5.2). These

results suggest that replacing the ethylmorpholine or ethylpiperidine pendant groups with propylpiperidines enhanced binding affinity towards Q4 by a significant amount.

The nickel complex featuring ethylpiperidine pendant groups which had the largest impact on the CD spectrum of Q4 was (**65**). It is therefore surprising that (**66**), which has the same *meso*-1,2-diphenylethylenediamine moiety but ethylmorpholine pendant groups, had no impact on the CD spectrum of the nucleic acid. Unfortunately, it was not possible to isolate the corresponding complex with propylpiperidine pendant groups, (**67**). Therefore, it was not possible to fully delineate the effects of changes in pendant groups and diamine moieties on binding behaviour towards this nucleic acid molecule.

Table 5.2: Effect of addition of nickel Schiff base complexes on the CD spectrum of Q4.*

Nickel complex	**Positive CD band at 263 nm**		**Negative CD band at 242 nm**	
	$\Delta\lambda_{max}$ (nm)	**$\Delta\varepsilon$ (%)**	**$\Delta\lambda_{max}$ (nm)**	**$\Delta\varepsilon$ (%)**
(**54**)	0.5	-31.2	-0.8	-27.4
(**55**)	4.4	-91.6	2.8	-89.4
(**57**)	1	8.8	-1	7.0
(**58**)	0.8	3.6	-1.5	11.9
(**60**)	0	3.5	-0.1	-0.4
(**61**)	0.2	-12.2	-0.1	-13.1
(**63**)	0	-2.3	-0.4	-7.0
(**64**)	0.5	-11.9	-0.4	-7.6
(**66**)	-0.6	4.0	0	-1.3

* All $\Delta\lambda_{max}$ and $\Delta\varepsilon$(%) values are the difference between the values for free DNA and those for a solution containing a nickel:DNA ratio of 9:1. Negative $\Delta\lambda_{max}$ values indicate a blue shift; positive values indicate a red shift

5.2.2.3 CD titrations using parallel unimolecular Q1

The effect of varying pendant groups on the interactions between metal complexes and G-quadruplexes was investigated further by CD spectroscopy using the parallel

unimolecular G-quadruplex Q1. The results of these experiments are presented in Figure 5.6 and Table 5.3. Comparison of the CD spectra in Figure 5.6 with those shown in Figure 5.5 suggests that some of the nickel complexes may interact more strongly with parallel Q1 than they did with parallel Q4. This is supported by the observation of larger changes in ellipticity upon addition to Q1 in the case of complexes (**58**), (**61**) and (**64**), each of which contain propylpiperidine pendant groups. Large changes in ellipticity were also seen when a fourth complex containing such pendants, (**55**) was added to Q1, although in this case the variations were not as great as when the same complex was added to Q4. Overall the results obtained suggest that complexes containing propylpiperidine pendant groups generally exhibited significant binding interactions with towards Q1. This is consistent with the more extensive formation of non-covalent complexes between these nickel molecules and the unimolecular parallel G-quadruplex observed in ESI-MS experiments, compared to when nickel molecules containing either of the other classes of pendant groups was examined.

Addition of (**54**) to Q1 also caused significantly larger changes to the ellipticity of the CD bands of the nucleic acid than when Q4 was present. This suggests that the presence of the phenylenediamine moiety leads to interactions between the nickel complex and DNA that are sufficiently strong to significantly affect the chirality of the nucleic acid. Therefore, it might be expected that such interactions would result in ions of medium or high abundance from non-covalent adducts formed between the nickel complex and nucleic acid molecules in ESI mass spectra. In contrast, inspection of Figure 5.3 (b) shows the mass spectrum of a solution containing (**54**) and Q1 was dominated by ions from free DNA, whilst the abundances of ions from

non-covalent adducts consisting of a single nickel complex bound to DNA were very low. These results therefore provide further evidence that relatively weak binding interactions between these nickel complexes and DNA may sometimes lead to large changes to the chirality of the latter, and consequently its CD spectrum. Alternatively the contrast between the results obtained using these two techniques may be attributable to thermal instability of non-covalent adducts which makes them undetectable by ESI-MS.

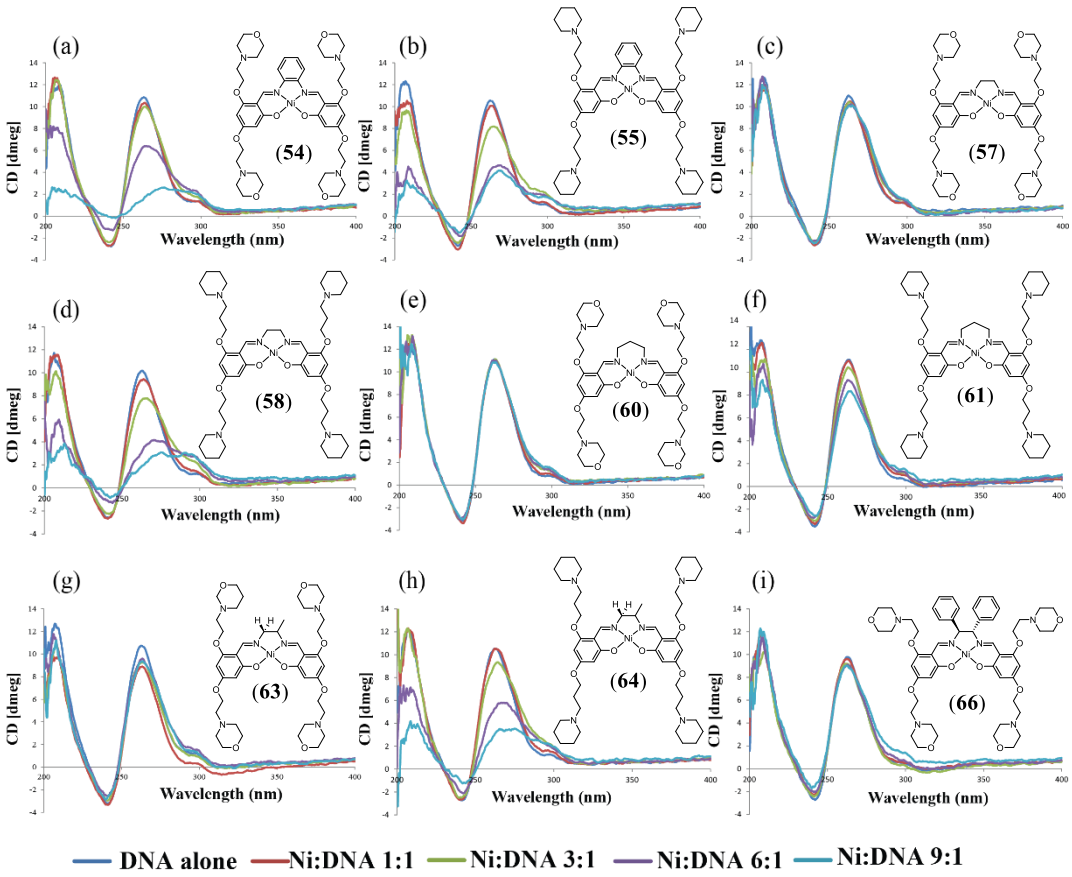

Figure 5.6: Circular dichroism spectra (200-400 nm) of solutions containing parallel Q1 and different ratios of nickel Schiff base complexes. (a) Q1 + (**54**); (b) Q1 + (**55**); (c) Q1 + (**57**); (d) Q1 + (**58**); (e) Q1 + (**60**); (f) Q1 + (**61**); (g) Q1 + (**63**); (h) Q1 + (**64**) and (i) Q1 + (**66**).

Addition of (**57**), (**60**), (**63**) or (**66**) to parallel Q1 only resulted in minor changes to the CD spectrum of the latter, including decreases in ellipticity of the major positive

CD band of < 13% (Table 5.3). These observations are similar to those made during CD studies involving the same complexes and parallel Q4, and provide further evidence of the lesser ability of this class of nickel complexes, each of which contain ethylmorpholine pendant groups, to form non-covalent complexes with parallel G-quadruplexes. A similar conclusion was reached earlier in this chapter after considering the results of ESI-MS experiments performed using all three classes of nickel complexes and different DNA molecules (Figure 5.3).

Table 5.3: Effect of addition of nickel Schiff base complexes on the CD spectrum of parallel unimolecular Q1.*

Nickel complex	**Positive CD band at 263 nm**		**Negative CD band at 241 nm**	
	$\Delta\lambda_{max}$ (nm)	**$\Delta\varepsilon$ (%)**	**$\Delta\lambda_{max}$ (nm)**	**$\Delta\varepsilon$ (%)**
(**54**)	13.4	-76.0	2.9	-93.2
(**55**)	7.1	-60.6	1	-44.2
(**57**)	2.4	-8.1	-2	-2.8
(**58**)	12.2	-69.6	2.2	-66.9
(**60**)	0.8	-2.1	-1	-4.5
(**61**)	1.2	-24.9	1.2	-26.4
(**63**)	0.9	-12.8	-0.7	-11.0
(**64**)	12.2	-66.5	1.1	-54.2
(**66**)	-1.2	-7.9	-2.2	-37.3

* All $\Delta\lambda_{max}$ and $\Delta\varepsilon$(%) values are the difference between the values for free DNA and those for a solution containing a nickel:DNA ratio of 9:1. Negative $\Delta\lambda_{max}$ values indicate a blue shift; positive values indicate a red shift.

5.2.2.4 CD titrations using anti-parallel unimolecular Q1

In the previous section results were presented which demonstrated the ability of nickel complexes with ethylmorpholine or propylpiperidine pendant groups to interact with, and consequently alter the CD spectrum of parallel Q1 to different extents. Since this DNA molecule can also fold into alternative conformations, it was decided to examine whether these nickel complexes might interact in distinctively different ways with these other topologies. The results obtained after adding

increasing amounts of nickel complexes containing either ethylmorpholine or propylpiperidine groups to anti-parallel Q1 are shown in Figure 5.7 and Table 5.4. Comparison of the results shown in Figure 5.7 with those presented in Figure 5.6 reveals a number of trends. Foremost of these is that once again addition of complexes bearing propylpiperidine substituents generally resulted in larger changes to the CD spectra than when analogues containing ethylmorpholine groups were present.

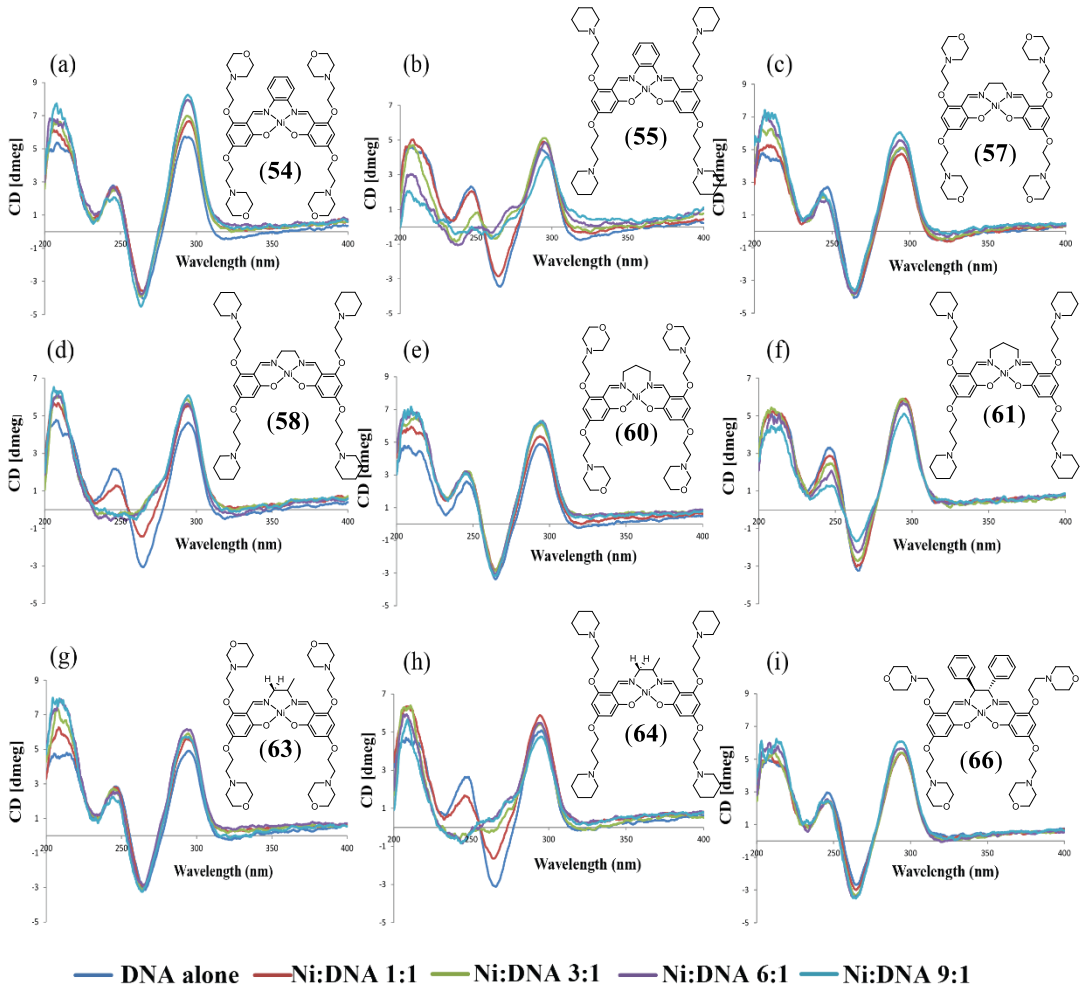

Figure 5.7: Circular dichroism spectra (200-400 nm) of solutions containing anti-parallel Q1 and different ratios of nickel Schiff base complexes. (a) Q1 + (**54**); (b) Q1 + (**55**); (c) Q1 + (**57**); (d) Q1 + (**58**); (e) Q1 + (**60**); (f) Q1 + (**61**); (g) Q1 + (**63**); (h) Q1 + (**64**) and (i) Q1 + (**66**).

The nickel complexes did not, however, uniformly affect the CD spectrum of one type of nucleic acid topology to a greater extent than the other. For example, Figure 5.7 shows addition of (**57**) had a greater effect on the CD spectrum of anti-parallel Q1 than it did with parallel Q1 (Figure 5.6). In contrast, (**54**) had a smaller effect on the CD spectrum of anti-parallel Q1 than what was observed with parallel Q1. In addition, while (**60**) had no effect on the CD spectrum of parallel Q1, it caused an increase of 28% in ellipticity for the major positive CD band of anti-parallel Q1. These results suggest small changes in selectivity in favour of one G-quadruplex topology over another can occur as a result of changes to the structure of the nickel complex.

Table 5.4: Effect of addition of nickel Schiff base complexes on the CD spectrum of anti-parallel unimolecular Q1.*

Nickel complex	**Positive CD band at 296 nm**		**Negative CD band at 265 nm**	
	$\Delta\lambda_{max}$ (nm)	**$\Delta\varepsilon$ (%)**	**$\Delta\lambda_{max}$ (nm)**	**$\Delta\varepsilon$ (%)**
(**54**)	2	44.2	-2.2	11.5
(**55**)	4	-9.8	-5.6	-80.1
(**57**)	-2	18.6	0.4	-10.4
(**58**)	0.1	31.5	-4.4	-82.7
(**60**)	0.9	28.9	-0.9	-6.3
(**61**)	0.6	-12.4	-1.3	-48.5
(**63**)	-2.7	16.6	-1.7	3.4
(**64**)	-0.4	-6.3	-22.2	-73.0
(**66**)	-0.4	12.6	0	30.8

* All $\Delta\lambda_{max}$ and $\Delta\varepsilon$(%) values are the difference between the values for free DNA and those for a solution containing a nickel:DNA ratio of 9:1. Negative $\Delta\lambda_{max}$ values indicate a blue shift; positive values indicate a red shift.

One of the most notable aspects of the results shown in Figure 5.7 was the complete disappearance of the negative CD band at 265 nm and the neighbouring small positive CD band at 245 nm when complexes containing propylpiperidine pendant groups were added. The only exception to this trend was when (**61**) was added,

however it still resulted in larger and different changes to the CD spectrum compared to when the corresponding complex with the same diamine moiety but ethylpiperidine groups was present (**60**). The above spectral changes were accompanied by the appearance of shoulders on the high energy side of the 271 nm CD band in the case of addition of either (**55**) or (**64**). Similar changes to the CD spectrum were not observed when nickel complexes bearing ethylpiperidine pendant groups were added to anti-parallel Q1. These results suggest that the complexes with propylpiperidine pendant groups interact in a distinctly different manner with this G-quadruplex and/or elicit significantly different changes to its conformation which result in the distinctive changes observed in the CD spectra.

5.2.2.5 CD titrations using hybrid unimolecular Q1

Binding experiments were also performed using CD spectroscopy and Q1 present in a hybrid conformation, to see if any of the nickel complexes showed the ability to selectively interact with this topology of the nucleic acid. The results of these experiments are presented in Figure 5.8 and Table 5.5. Inspection of the data shown in Figure 5.6, Figure 5.7 and Figure 5.8 shows that addition of (**54**) resulted in much larger effects on the CD spectrum of the parallel conformation of Q1 than either of its alternative topologies. This suggests that (**54**) may exhibit a degree of binding selectivity in favour of the former G-quadruplex. In contrast, addition of (**55**) resulted in significant changes to the CD spectrum of Q1 present in each of its three conformations, suggesting this nickel complex exhibits little binding selectivity towards unimolecular G-quadruplexes.

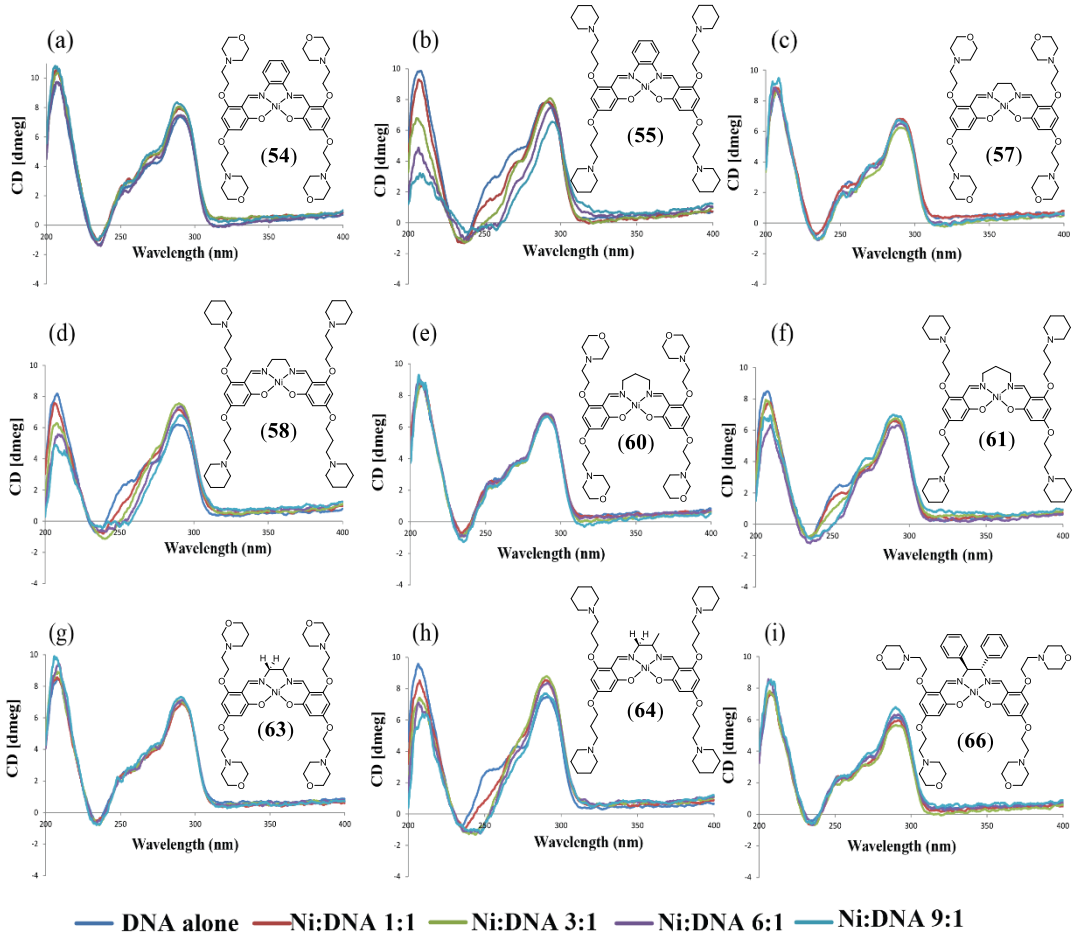

Figure 5.8: Circular dichroism spectra (200-400 nm) of solutions containing hybrid Q1 and different ratios of nickel Schiff base complexes. (a) Q1 + (**54**); (b) Q1 + (**55**); (c) Q1 + (**57**); (d) Q1 + (**58**); (e) Q1 + (**60**); (f) Q1 + (**61**); (g) Q1 + (**63**); (h) Q1 + (**64**) and (i) Q1 + (**66**).

Addition of (**55**) had the greatest effect on the CD spectrum of hybrid Q1. Inspection of Figure 4.9 shows that large changes to the CD spectrum of this nucleic acid topology also occurred when (**53**), which also contains a phenylenediamine moiety was added. This suggests the identity of the diamine can alter the nature of the binding interactions. When (**58**) and (**64**) were added to hybrid Q1 a different pattern of spectral changes was observed compared to when other nickel complexes were present. In the case of (**58**) and (**64**), upon first introducing the nickel complex, so that the ratio of Ni:DNA was 1:1, 3:1 or 6:1, increases in ellipticity of the two

positive CD bands were observed. At higher ratios the ellipticity of these two peaks then decreased. The reasons for this biphasic pattern of changes to the CD spectrum, which was not observed with any of the other nickel complexes, is currently unclear. It is also noteworthy that the four nickel complexes containing propylpiperidine pendant groups had larger effects on the general appearance of the CD spectrum of hybrid Q1 than analogues containing ethylmorpholine groups.

Table 5.5: Effect of addition of nickel Schiff base complexes on the CD spectrum of hybrid unimolecular Q1.*

Nickel complex	**Positive CD band at 291 nm**		**Negative CD band at 235 nm**	
	$\Delta\lambda_{max}$ (nm)	**$\Delta\varepsilon$ (%)**	**$\Delta\lambda_{max}$ (nm)**	**$\Delta\varepsilon$ (%)**
(**54**)	-2.5	12.8	-0.3	-22.5
(**55**)	2.9	-16.5	3.4	-49.4
(**57**)	-1.4	0.3	1.8	26.1
(**58**)	0.9	9.7	4	-41.3
(**60**)	-0.3	-1.5	1.3	47.7
(**61**)	-0.4	5.2	1.6	16.3
(**63**)	-1.5	4.5	0.5	38.4
(**64**)	-0.9	3.1	13.3	50.7
(**66**)	0.2	10.5	1.2	37.2

* All $\Delta\lambda_{max}$ and $\Delta\varepsilon$(%) values are the difference between the values for free DNA and those for a solution containing a nickel:DNA ratio of 9:1. Negative $\Delta\lambda_{max}$ values indicate a blue shift; positive values indicate a red shift.

5.2.2.6 CD titrations using parallel unimolecular c-KIT1

The results presented in Chapter 4 showed that all five nickel complexes bearing ethylpiperidine pendant groups significantly affected the CD spectrum of parallel Q1 as well as that of the parallel conformation of a second unimolecular G-quadruplex, derived from the sequence for the oncogene promoter c-KIT1. This result afforded greater confidence in the binding selectivity patterns revealed by CD spectroscopy. In order to provide further confidence in the conclusions that can be drawn from these DNA binding studies a second set of experiments was conducted by CD spectroscopy using c-KIT1 and nickel complexes bearing either ethylmorpholine or

propylpiperidine pendants. The results of studies described earlier in this chapter showed that addition of nearly all nickel complexes bearing propylpiperidine substituents caused large changes to the CD spectrum of parallel Q1, with the only exception being (**61**). In contrast, nearly all nickel complexes containing ethylmorpholine substituents had virtually no effect on the CD spectrum of parallel Q1, with the only exception being (**54**). The effects of addition of these two classes of nickel complexes on the CD spectrum of parallel c-KIT1 are shown in in Figure 5.9 and Table 5.6.

Inspection of Figure 5.9 shows that once again many of the nickel complexes bearing ethylmorpholine pendants (*e.g.* (**57**), (**60**) and (**63**)) had only a very minor influence on the CD spectrum of parallel c-KIT1, in keeping with what was observed in experiments with parallel Q1. This suggests that these three complexes generally have a low binding affinity towards parallel unimolecular G-quadruplexes. In addition, complex (**54**) once again deviated from the trend seen with the other nickel complexes containing this type of pendant and caused significant changes to all CD bands of parallel c-KIT1. This therefore confirmed that (**54**) consistently affects the CD spectrum of parallel unimolecular G-quadruplexes, unlike all other nickel complexes with this type of pendant group, and suggests that the diamine moiety must play a significant role in the binding interactions.

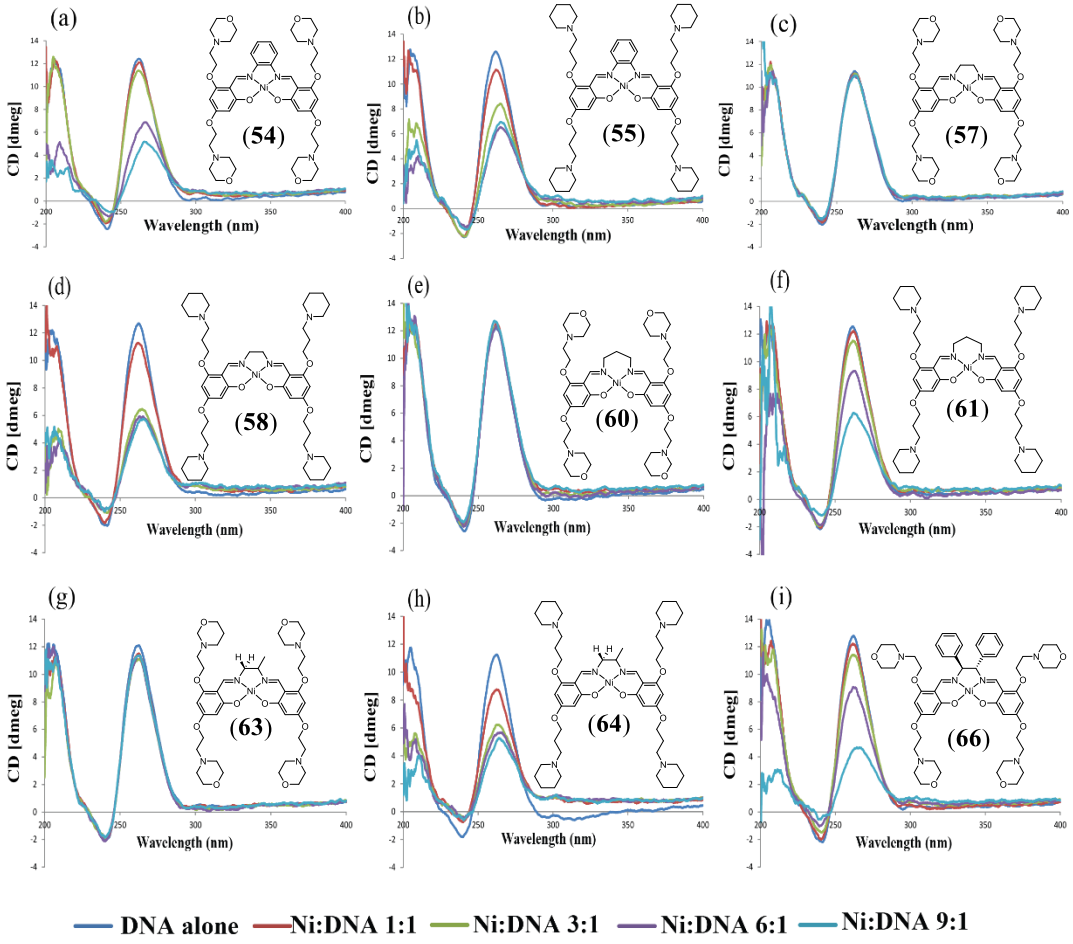

Figure 5.9: Circular dichroism spectra (200-400 nm) of solutions containing parallel c-KIT1 and different ratios of nickel Schiff base complexes. (a) C-KIT1 + (**54**); (b) C-KIT1 + (**55**); (c) C-KIT1 + (**57**); (d) C-KIT1 + (**58**); (e) C-KIT1 + (**60**); (f) C-KIT1 + (**61**); (g) C-KIT1 + (**63**); (h) C-KIT1 + (**64**) and (i) C-KIT1 + (**66**).

The only nickel complex which produced contrasting results in experiments conducted using CD spectroscopy and the two types of parallel unimolecular G-quadruplexes was (**66**). While this nickel complex caused only minor changes to the CD spectrum of parallel Q1, it resulted in the largest changes observed to the ellipticity of the major CD bands of parallel c-KIT1 (Table 5.6). It is worth noting that (**66**) produced either negligible or very minor changes to the CD spectra of each of the other DNA molecules examined using this spectroscopic technique. This

suggests that this nickel complex may exert some very specific binding selectivity in favour of parallel c-KIT1 over each of the other DNA molecules studied.

Table 5.6: Effect of addition of nickel Schiff base complexes on the CD spectrum of c-KIT1.*

Nickel complex	Positive CD band at 262 nm		Negative CD band at 240 nm	
	$\Delta\lambda_{max}$ (nm)	$\Delta\varepsilon$ (%)	$\Delta\lambda_{max}$ (nm)	$\Delta\varepsilon$ (%)
(**54**)	3.7	-58.2	2.1	-60.3
(**55**)	3.4	-44.8	1.3	0.3
(**57**)	0.6	-3.4	-0.6	-22.4
(**58**)	3.4	-54.8	-1.5	-50.7
(**60**)	-1.1	4.4	-0.7	-24.8
(**61**)	0.4	-50.1	1.3	-45.8
(**63**)	0.7	-5.9	-0.8	-11.2
(**64**)	1.5	-53.2	0.6	-66.0
(**66**)	2.1	-63.4	-2.5	-74.8

* All $\Delta\lambda_{max}$ and $\Delta\varepsilon$(%) values are the difference between the values for free DNA and those for a solution containing a nickel:DNA ratio of 9:1. Negative $\Delta\lambda_{max}$ values indicate a blue shift; positive values indicate a red shift.

Comparison of the CD spectra in Figure 5.9 with those shown in Figure 5.6 suggests that most of the nickel complexes with propylpiperidine pendant groups interacted similarly with parallel c-KIT1 to how they did with parallel Q1. For example, addition of (**55**), (**58**) or (**64**) caused dramatic changes to the ellipticity of the positive CD bands of parallel c-KIT1 (Figure 5.9 (b), (d) and (h)), which were comparable to what was observed with parallel Q1.This suggests that the interactions between these three complexes and parallel c-KIT1 are similar to what was observed with parallel Q1 and significantly affect the chirality of both nucleic acids. One small difference between the results obtained with the two types of parallel unimolecular G-quadruplexes centred on complex (**61**). For example, addition of (**61**) resulted in a decrease of 50% in ellipticity for the major positive CD band of c-KIT1 at 262 nm (Table 5.6). This decrease was two times higher than what was observed with the same CD band for parallel Q1 (24%, Table 5.3). Therefore, whilst it appears that (**61**)

does interact in a similar fashion with both parallel unimolecular G-quadruplexes, the magnitude of this interaction was greater in the case of c-KIT1.

5.2.3 DNA binding studies performed using UV-Vis spectrophotometry

To further investigate the interactions between nickel complexes bearing either ethylmorpholine or propylpiperidine pendant groups and dsDNA a series of melting experiments were performed using UV-vis spectrophotometry and D2. The results obtained from these experiments, which were performed by measuring the effect of temperature on the absorbance at 260 nm of solutions containing either 3:1 or 6:1 ratios of nickel complexes and D2, are presented in Figure 5.10. Inspection of Figure 5.10 shows that each of the nickel complexes containing ethylmorpholine groups caused the melting temperature (T_m) of D2 to decrease by between 1 and 2 °C. These results are similar to those obtained in most instances from similar experiments performed using analogous nickel complexes bearing ethylpiperidine pendant groups (Chapter 4.2.3) and suggest that the interactions between these nickel complexes and D2 may be either very weak or destabilise the secondary structure of the nucleic acid. Solutions containing D2 and (**60**), (**63**) or (**66**) gave ESI mass spectra which were dominated by ions from free DNA, supporting the hypothesis that in some of these systems non-covalent adducts were either not present or had low thermal stability. Furthermore, addition of complexes (**60**) and (**66**) had little impact on the CD spectrum of D2, providing further evidence for a general lack of interaction between these nickel complexes and dsDNA.

In contrast to the above, most of the nickel complexes containing propylpiperidine pendant groups resulted in increases in T_m for D2 of between 3 and 12 °C. For example, (**55**) caused the highest increase in T_m of 12 °C when present in a 6-fold excess over the dsDNA. Complexes (**58**) and (**64**) produced smaller increases of 4.6 and 2.6 °C, respectively. These observations suggest that these nickel complexes and in particular (**55**) may interact to a significant extent with D2. This conclusion is consistent with those derived from binding studies performed using ESI-MS and CD spectroscopy. In the case of the former experiments no ions from free DNA were observed when (**55**), (**58**) or (**64**) was added to D2. In contrast, ions from non-covalent adducts containing four and even five nickel complexes bound to D2 were detected. Furthermore, addition of (**55**), (**58**) or (**64**) resulted in very significant changes to the CD spectrum of D2. Of the nickel complexes bearing propylpiperidine pendant groups only (**61**) resulted in small decreases in T_m for D2. It is notable that this complex exhibited a lower ability to form non-covalent adducts with D2 in ESI-MS binding studies, and also resulted in small changes to the CD spectrum of the nucleic acid.

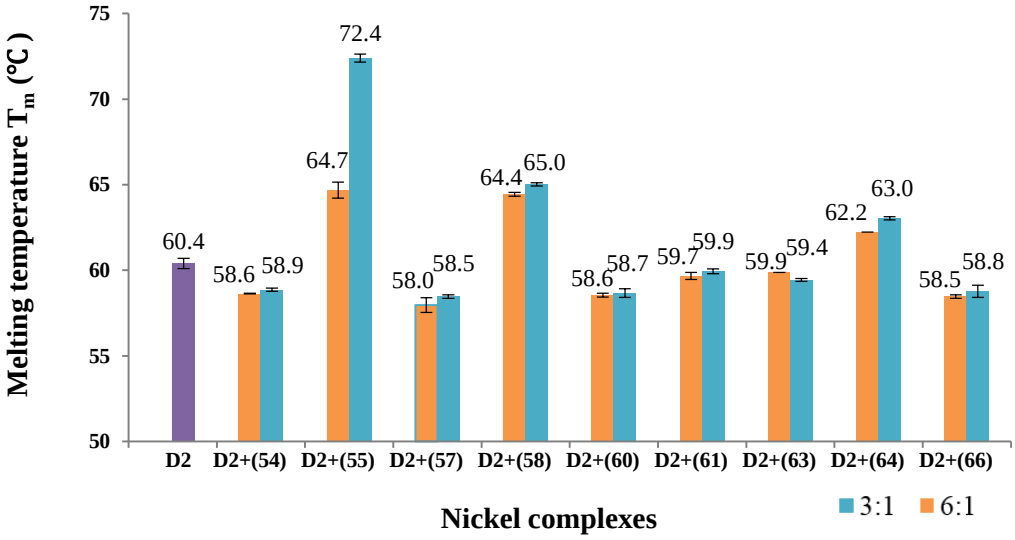

Figure 5.10: Mean melting temperatures (T_m) of solutions containing either a 3:1 or 6:1 ratio of different nickel complexes and D2. The experiments were performed in triplicate with error bars showing standard errors.

5.2.4 DNA binding studies performed using FRET melting assays

In order to provide further support for the conclusions based on binding experiments performed using ESI-MS and CD spectroscopy, it was decided to further investigate the affinity of nickel complexes with either ethylmorpholine or propylpiperidine pendant groups for unimolecular G-quadruplex DNA using FRET melting assays. These were performed using the nickel complexes and two different conformations of a unimolecular G-quadruplex produced from the labelled 21-mer 5′-FAM-$G_3(TTAG3)_3$-TAMRA-3′. Initially F21T was annealed using a buffer containing 100 mM Na^+ which resulted in the molecule adopting an anti-parallel conformation. When an assay was performed using a solution containing anti-parallel F21T alone, the melting temperature, T_m, was determined to be 50.4 ± 0.3 °C. The results obtained from FRET melting assays performed using solutions containing anti-

parallel F21T and increasing concentrations of the nickel complexes are presented in Figure 5.11 andFigure 5.12.

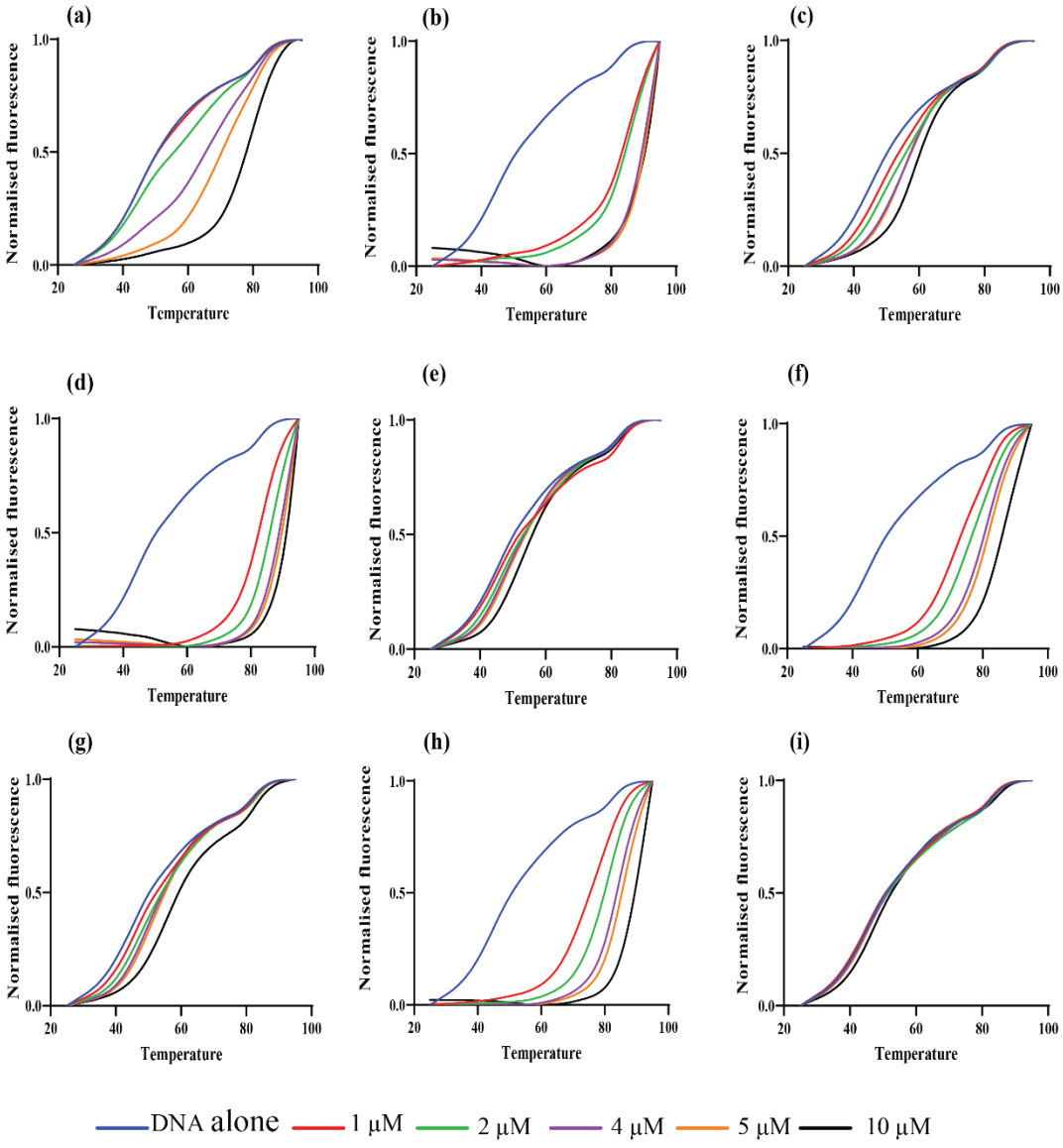

Figure 5.11: Results obtained from FRET melting assays performed using F21T in solutions containing Na^+ and increasing concentrations of nickel Schiff base complexes: (a) (**54**); (b) (**55**); (c) (**57**); (d) (**58**); (e) (**60**); (f) (**61**); (g) (**63**); (h) (**64**) and (i) (**66**).

Figure 5.12 shows that in general nickel complexes containing propylpiperidine groups had a larger effect on the FRET melting curves than the corresponding complexes containing the same diamine moiety but ethylmorpholine pendants. This

result is consistent with the ability of the former complexes to produce more dramatic changes to the CD spectrum of anti-parallel Q1 noted earlier in this chapter. In contrast, nickel complexes containing ethylmorpholine groups had very little effect on the FRET melting curves except in the case of complex (**54**), which contains the phenylenediamine moiety. This result is consistent with that obtained from CD studies performed using anti-parallel Q1 which showed (**54**) had the largest effect on the ellipticity of the positive CD band among the nickel complexes containing ethylmorpholine groups.

The results presented in Figure 5.12 also show that (**66**) had a negligible effect on the FRET melting curve of anti-parallelF21T even at highest concentration of added nickel complex (10 μM). This is consistent with the inability of this complex to alter the CD spectrum anti-parallel Q1, and further demonstrates that the *meso*-diphenyl ethylenediamine group inhibits binding interactions with this quadruplex structure. Comparison of the FRET data shown in Figure 5.12 with that presented earlier in Figure 4.15Figure 4.14, also suggests replacing ethylpiperidine groups with ethylmorpholine resulted in a decrease in T_m values, reflecting weaker binding interactions with anti-parallelQ1. For example, solutions containing 10 μM (**57**), which contains ethylmorpholine pendant groups, resulted in an increase in the T_m for F21T of 10.1 °C, which was much less than the change caused by (**56**) (34.9 °C), which contains the same diamine moiety but ethylpiperidine pendants. In contrast, replacing ethylpiperidine groups with propylpiperidines had the opposite effect on the strength of binding interactions. This is illustrated by the observation that solutions containing 10 μM (**58**), which has propylpiperidine pendant groups increased the T_m of anti-parallel F21T by an even larger amount (39.6 °C). These

findings are also consistent with trends seen in CD studies presented earlier in this chapter.

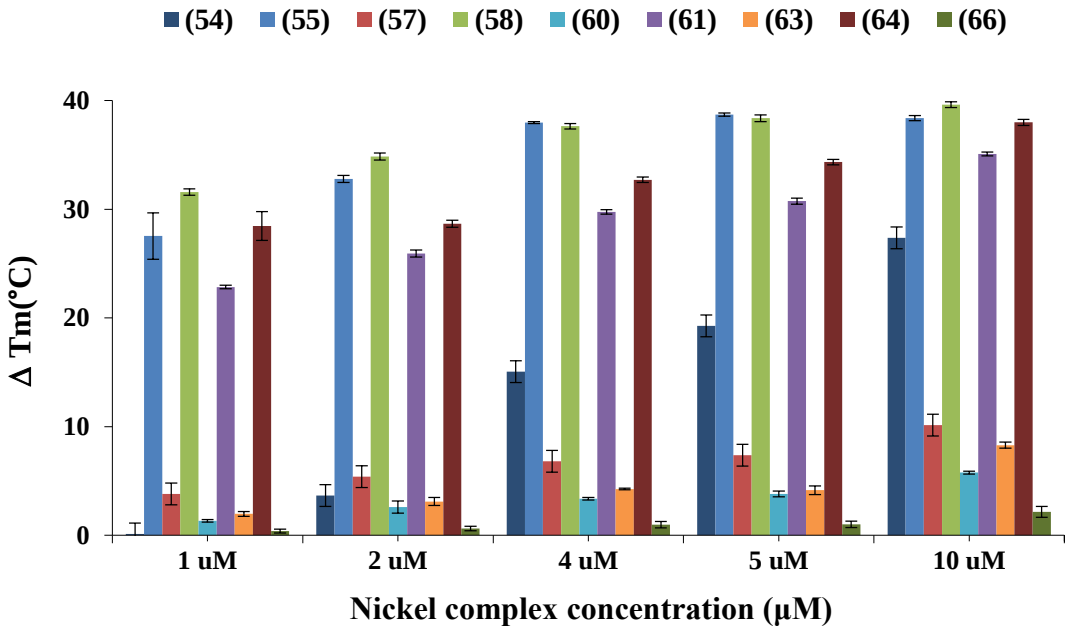

Figure 5.12: Comparison of ΔT_m values for different concentrations of nickel Schiff base complexes added to solutions containing 0.2 µM F21T. The DNA had an anti-parallel topology after annealing in 100 mM NaCl, 10 mM lithium cacodylate pH 7.4 buffer. Error bars represent the standard errors from six separate experiments.

FRET experiments were also carried out with F21T in its hybrid conformation. To achieve this, F21T was annealed in a buffer containing 100 mM K^+ ions. The results of these experiments are present in Figure 5.13 andFigure 5.14. Comparison of these results with those shown in Figure 5.11 andFigure 5.12 show that in general, nickel complexes containing propylpiperidine pendant groups had less effect on the FRET melting curve of hybrid F21T than the anti-parallel conformation. For example, solutions containing 10 µM (**58**) were shown to increase the T_m of hybrid F21T and anti-parallel F21T by 23.7 °C and 39.6 °C, respectively. This is consistent with what was observed in CD studies performed using Q1 present in its anti-parallel and

hybrid conformations as the nickel complexes generally showed a greater ability to alter the CD spectrum of Q1 when present in the former topology.

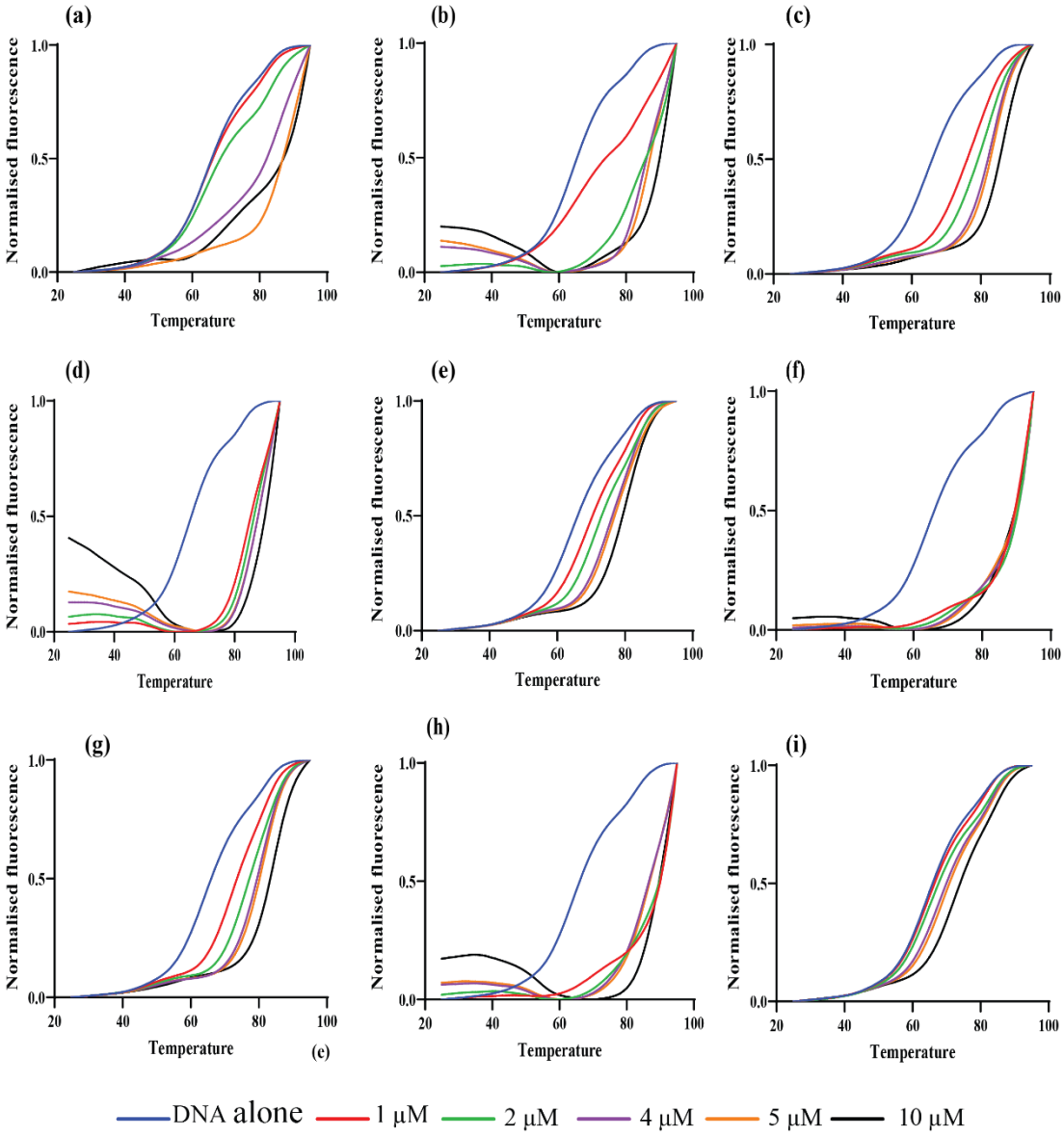

Figure 5.13: Results obtained from FRET melting assays performed using F21T in solutions containing K^+ and increasing concentrations of nickel Schiff base complexes. (a) (**54**); (b) (**55**); (c) (**57**); (d) (**58**); (e) (**60**); (f) (**61**); (g) (**63**); (h) (**64**) and (i) (**66**).

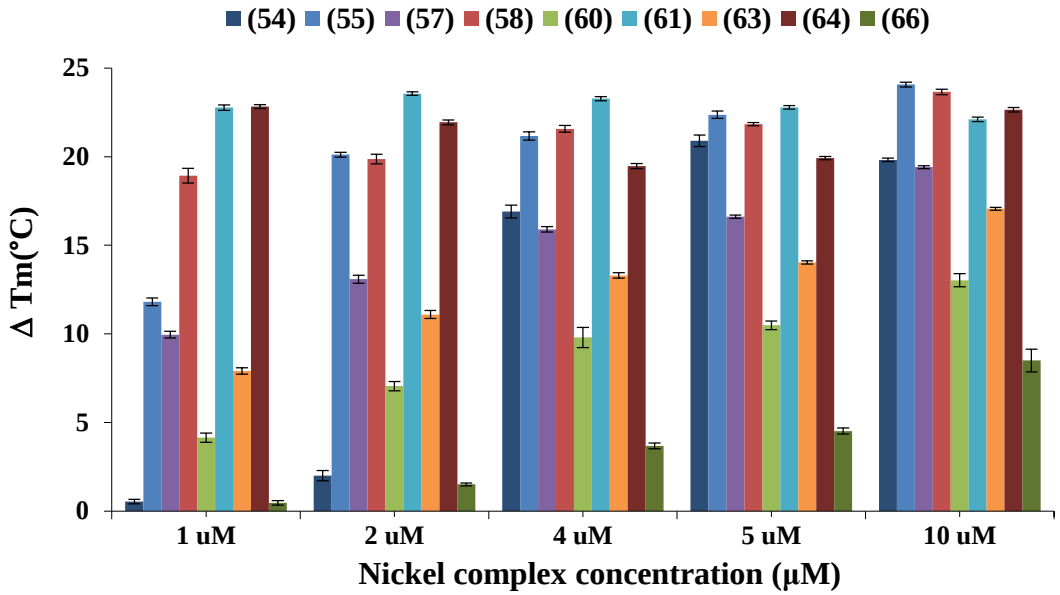

Figure 5.14: ΔT_m induced by different concentrations of nickel Schiff base complexes in the presence of 0.2 µM F21T. Samples were annealed and measured in 100 mM KCl, 10 mM lithium cacodylate pH 7.4 buffer to ensure the G-quadruplex was present in a hybrid topology. Error bars represent the standard error from six separate experiments.

In addition, comparison of the results obtained from both sets of FRET experiments shows that all nickel complexes containing ethylmorpholine pendants except (**54**) had a slightly greater effect on the FRET melting curve of hybrid F21T than on the anti-parallel conformation. For example, solutions containing 10 µM (**57**) increased the T_m of hybrid and anti-parallel F21T by 19.4 °C and 10.1 °C, respectively. These findings are consistent with trends seen in CD spectroscopic studies involving Q1 in its anti-parallel and hybrid conformations.

Whilst nickel complexes containing propylpiperidine groups did not affect the T_m of hybrid F21T as much as for the anti-parallel topology of this nucleic acid, they still produced larger increases than analogues containing ethylmorpholine groups. In addition, (**66**) again had the smallest effect on the FRET melting curve. This suggests

that this complex has limited ability to interact with either the anti-parallel or hybrid topology of this G-quadruplex. Although complex (**66**) did result in small changes to the CD spectrum of Q1 in its hybrid conformation, the effects were obtained only at the highest Ni:DNA ratio (9:1) studied, and therefore are consistent with the result from the FRET experiments.

5.2.5 DNA binding studies performed using FID assays

The results obtained from DNA binding studies conducted using ESI-MS and CD spectroscopy revealed some consistent trends in binding affinities for nickel complexes containing ethylmorpholine or propylpiperidine pendant groups. In order to find further evidence in support of some of these trends and to further investigate the selectivity of nickel complexes for both dsDNA (D2) and G-quadruplex DNA (Q1 and Q4) sequences, a series of FID assays was performed. A representative set of results obtained using complex (**58**) and parallel Q1 is shown in Figure 5.15, and values of DC_{50} derived from experiments performed with all nickel complexes and DNA sequences is presented in Table 5.7.

Inspection of the results reveals that the largest DC_{50} values for each of the three types of DNA were obtained with complexes (**63**), (**66**) and, to a lesser extent (**57**). These observations suggest that these complexes, each of which contain ethylmorpholine pendant groups, exhibit the lowest affinity towards all three types of DNA This conclusion is consistent with the results obtained from ESI MS and CD experiments. For example, the abundances of ions from free DNA was greater in the case of experiments performed with (**63**) and (**66**) and both Q1 and Q4 than for any of the other nickel complexes examined as part of this project (Figure 5.3).

Comparison of the values reported here with those presented earlier for nickel complexes with ethylpiperidine pendant groups (Table 4.7) shows that (**59**) was the only member of the latter class of complexes to also exhibit low binding affinity towards each of the DNA molecules examined.

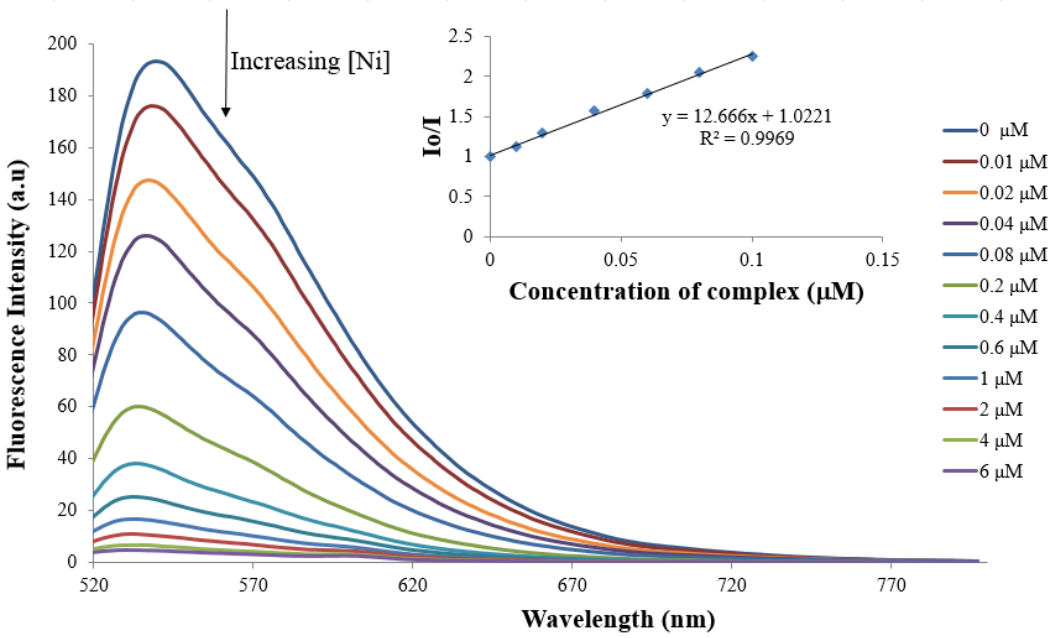

Figure 5.15: Results obtained from an FID assay involving addition of increasing amounts of (**58**) to a solution containing thiazole orange and parallel Q1. The inset shows a Stern-Volmer plot derived from the data, which was then used to determine the value of DC_{50} for (**58**) with this DNA sequence.

Values of DC_{50} for (**60**) were not obtained with any of the three DNA molecules as this complex did not produce a 50% decrease in fluorescence intensity even at the highest Ni:DNA ratios used (100:1) (Figure S5.1,Figure S5.2 andFigure S5.3). These results suggests (**60**), which also contains ethylmorpholine pendant groups, does not interact strongly with any of the DNA molecules. This is consistent with the poor ability of this complex to form non-covalent adducts in ESI-MS experiments (Figure 5.3) as well as its inability to produce changes to the spectra of the same DNA molecules in experiments performed using CD spectroscopy.

Table 5.7: DC_{50} values derived from FID assays performed using nickel complexes with either ethylmorpholine or propylpiperidine pendant groups and different DNA molecules.

Nickel complex	DC_{50}(μM)		
	dsDNA D2	**Parallel Q4**	**Parallel Q1**
(**54**)	0.39 ± 0.05	0.41 ± 0.06	0.23 ± 0.02
(**55**)	0.20 ± 0.03	0.04 ± 0.01	0.03 ± 0.003
(**57**)	0.80 ± 0.02	1.24 ± 0.04	15.53 ± 0.19
(**58**)	0.18 ± 0.02	0.04 ± 0.00	0.08 ± 0.00
(**60**)	-	-	-
(**61**)	0.35 ± 0.04	0.19 ± 0.02	0.27 ± 0.04
(**63**)	3.68 ± 0.04	2.24 ± 0.12	>25
(**64**)	0.09 ± 0.00	0.06 ± 0.00	0.09 ± 0.00
(**66**)	1.21 ± 0.07	2.53 ± 0.23	22.55 ± 0.11

Further analysis of the DC_{50} values in Table 5.7 reveals that the lowest DC_{50} values for the three types of DNA were obtained in experiments performed with (**55**), (**58**) and (**64**), each of which contain propylpiperidine pendant groups. These observations suggest these three nickel complexes exhibit the greatest affinity towards all three types of DNA of the two classes of complexes examined here. This conclusion is consistent with the results presented earlier in this chapter obtained using other methods. Furthermore, comparison of the results presented in Table 5.7 with those shown in Table 4.7 suggests that the binding affinities of the above three complexes were in all cases greater than that for any of the nickel complexes bearing ethylpiperidine substituents.

5.2.6 DNA binding studies performed using molecular docking

Comparison of the DNA binding results presented in this chapter for nickel complexes containing either ethylmorpholine or propylpiperidine pendant groups, with those shown in Chapter 4 for analogues with ethylpiperidine pendants revealed

a number of trends. One of the most notable of these was that nickel complexes with propylpiperidine pendants generally exhibited the greatest binding affinity towards most types of DNA examined, whereas those with ethylmorpholine substituents showed the lowest. In addition, complexes featuring the 1,3-propanediamine moiety often showed lower binding affinities towards specific DNA molecules than analogues with the same pendant groups but featuring different diamines. The data presented, however, does not directly shed light on any of the binding mechanisms present in these systems. Molecular docking simulations were therefore performed using the nickel complexes containing either ethylmorpholine or propylpiperidine groups, and both a G-quadruplex DNA (PDB ID: 1KF1) and a dsDNA (PDB ID: 1KBD). The binding mode corresponding to the top docking score for each combination of binding partners is illustrated in Figure 5.16 while Table 5.8 summarises the minimum binding energies (ΔG) for each system.

Most of the nickel complexes preferred to interact via π-stacking interactions with the top G-tetrad of the parallel unimolecular G-quadruplex. This was observed with the complexes examined in chapter 4 as well and indicates that most of the nickel complexes interact with 1KF1 in a similar binding mode. The two exception to this trend were (**58**) and (**61**), which instead preferred to bind to the bottom G-tetrad.

Inspection of Figure 5.16 (a) reveals the nickel ions in (**54**), (**55**) and (**60**) were located near the centre of the G-tetrads. This allowed all aromatic rings of these complexes to bind effectively to the guanine bases within the G-tetrad of 1KF1 via π-stacking interactions. In addition, the four positively charged pendant groups in these three complexes were positioned favourably to participate in intermolecular interactions with the loops and/or grooves of the G-quadruplex. In the case of

complex (**61**), three of its pendant groups were involve in binding interactions with different grooves of 1KF1 while the forth pendant group is positioned flat towards the edge of the guanine residues.

Figure 5.16 reveals a slightly different preferred binding mode for complexes (**57**) and (**58**), which feature ethylenediamine moieties, with 1KF1. While both aromatic rings in these nickel complexes were positioned so that they are lying flat on the G-tetrads, the resulting interactions are not as optimal as for (**54**) and (**55**) as the nickel ions were not located centrally above the G-tetrads. This resulted in the two lower pendant groups of (**57**) and (**58**) being positioned on top of the guanine residues instead of located so they could interact with the loops and grooves of the DNA. In addition, one of the two remaining morpholine rings of (**57**) was positioned on the surface of the groove and therefore also not able to participate in optimised intermolecular interactions with the G-quadruplex. In contrast, both piperidine rings in the top pendant groups of (**58**) were positioned so that they can participate in favourable intermolecular interactions with the loops and/or grooves of the G-quadruplex. This supports the conclusions drawn from ESI MS studies which showed (**58**) was able to form non-covalent complexes with parallel Q1 while (**57**) did not.

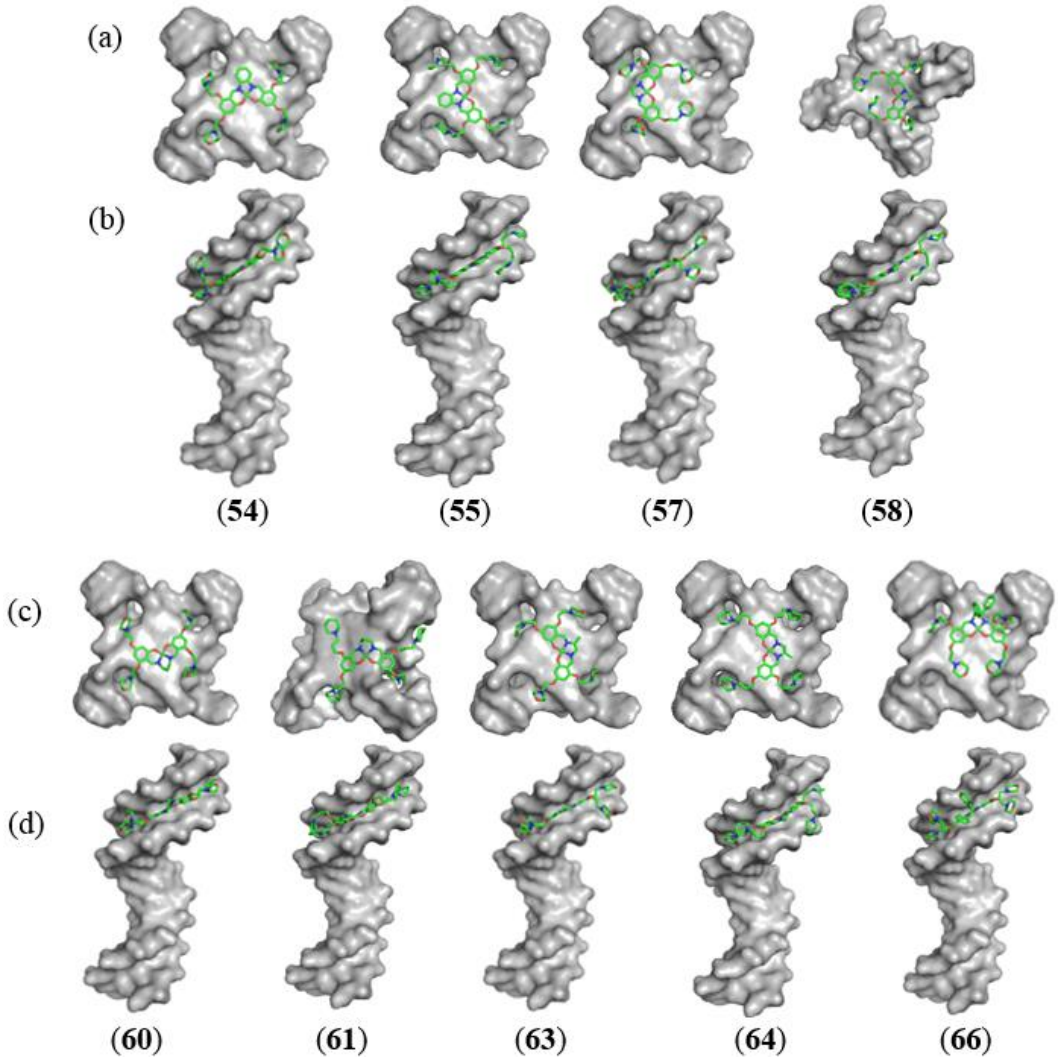

Figure 5.16: Most favourable binding modes resulting from molecular docking studies performed using nickel Schiff base complexes containing ethylmorpholine or propylpiperidine pendant groups and either: (a) and (c) the parallel unimolecular G-quadruplex 1KF1 or (b) and (d) the dsDNA 1KBD.

The nickel ions in (**63**) and (**64**), which contain 1,2-diaminopropane moieties, were not positioned directly above the centre of the G-quartet of 1KF1. However, the four positively charged pendant groups were positioned favourably to participate in intermolecular interactions with the loops and/or grooves of the G-quadruplex. In addition, similar to what was found with (**62**), the diamine moieties in (**63**) and (**64**)

were not coplanar with the six membered chelate rings coordinated to the nickel ion. Furthermore, the latter were not found to be coplanar with each other.

Figure 5.16 (a) shows that the two top pendant groups of (**66**) were bound to the second and third TTA loops of 1KF1. In contrast, the two bottom pendant groups of (**66**) were positioned on top of the guanine residues instead of located so they could interact with the loops and grooves of the DNA. The two aromatic rings of the diamine moiety were also not positioned to participate in favourable π-stacking interactions with the G-tetrad. This supports the conclusions drawn from ESI MS studies which showed (**66**) was an unable to form non-covalent complexes with parallel Q1.

The docking results presented in Figure 5.16 (b) for the 1KBD showed that all nickel complexes preferred to bind to the minor groove of the dsDNA. The two bottom pendant groups of the nickel complexes and the two associated benzene rings were typically positioned in the minor groove in order to optimise favourable intermolecular interactions. The two top pendant groups and the diamine moieties were positioned so that they were orientated away from the minor groove, perhaps in an attempt to avoid unfavourable steric interactions. Inspection of Table 5.8 shows that the minimum binding energies of the nickel complexes with 1KBD were distributed over a narrow range from -8.04 to -8.78 kcal/mol, which is similar to that for the complexes presented in chapter 4. This indicates that that the nickel complexes had very similar affinities for 1KBD. The largest binding energy was observed with complex (**63**), suggesting it has the strongest overall binding interactions with 1KBD. In contrast, complex (**58**) exhibited the lowest binding energy with the dsDNA molecule.

The docking results also showed that the minimum binding energies of nickel complexes with the G-quadruplex 1KF1 were distributed over a narrow range from -8.30 to -9.86 kcal/mol. The largest binding energy was observed with complex (**54**), suggesting it has the strongest overall binding interactions with 1KF1. In contrast, complex (**58**) exhibited the lowest binding energy with the G-quadruplex. This is consistent with the results presented in Figure 5.16 (a), which show that two pendant groups of (**58**) were positioned on top of the guanine residues and therefore not able to interact with the loops and grooves of the G-quadruplex. In contrast, four pendant groups of (**54**) were positioned favourably to participate in such intermolecular interactions.

Table 5.8: Binding free energies obtained from docking studies performed using nickel Schiff base complexes containing either ethylmorpholine or propylpiperidine pendant groups and 1KF1 or 1KBD.

Structure ID	**1KF1(qDNA)**		**1KBD (dsDNA)**	
	ΔG (kcal/mol)[a]	**Binding mode[b]**	**ΔG (kcal/mol)[a]**	**Binding mode[b]**
(**54**)	-9.86 ± 0.05	Top, end stacking	-8.78 ± 0.08	Minor groove
(**55**)	-9.42 ± 0.04	Top, end stacking	-8.3 ± 0.2	Minor groove
(**57**)	-8.74 ± 0.09	Top, end stacking	-8.56 ± 0.05	Minor groove
(**58**)	-8.3 ± 0.1	Bottom, end stacking	-8.04 ± 0.05	Minor groove
(**60**)	-9.0 ± 0.1	Top, end stacking	-8.4 ± 0.1	Minor groove
(**61**)	-8.56 ± 0.05	Bottom, end stacking	-8.05 ± 0.04	Minor groove
(**63**)	-9.2 ± 0.0	Top, groove	-8.9 ± 0.1	Minor groove
(**64**)	-8.94 ± 0.05	Top, groove	-8.3 ± 0.1	Minor groove
(**66**)	-8.84 ± 0.09	Top, groove	-8.5 ± 0.1	Minor groove

[a] Average values of ΔG with standard errors obtained from the top five docking scores.

[b] "Top" or "Bottom" indicates which terminal G-tetrad was the preferred binding site.

5.3 Summary

The results presented in this chapter can be analysed to examine the effects on DNA binding affinity of changing both the pendant groups and diamine moieties of the nickel complexes. The largest effects were caused by varying the pendant groups. It was found, for example, that nickel complexes with ethymorpholine pendant groups did not interact strongly with any of the DNA molecules investigated. For example, (**66**) only interacted in a relatively weak fashion with the DNA molecules examined. This conclusion is supported by the absence of ions of high abundance from non-covalent adducts in ESI mass spectra, the lack of significant changes to the CD spectra of DNA in most cases after addition of this nickel complex, the relatively small change in T_m for F21T observed when (**66**) was added, and the large values of DC_{50} obtained from FID assays performed with this complex. In the case of the dsDNA D2, the reduction in T_m observed when (**66**) was added provides further evidence that binding interactions are weak and/or have a destabilising effect.

Further evidence of the poor binding characteristics of complexes bearing ethylmorpholine substituents was provided by the results of FID assays performed using complex (**60**). The latter failed to displace TO sufficiently to enable values of DC_{50} to be obtained with any of the three DNA molecules investigated. This highlighted (**60**) as the only nickel complex whose binding interactions were not strong enough with any DNA molecule to displace the indicator molecule.

In contrast to the above, the results obtained from ESI-MS and CD spectroscopic studies, as well as FRET and FID assays, showed that nickel complexes with propylpiperidine pendant groups generally interacted more strongly with different DNA molecules than analogues containing the same diamine moiety but one of the

other two types of pendants. For example, the relative abundances of ions in ESI mass spectra from non-covalent complexes containing one or more (**55**) bound to D2, Q1 or Q4 was greater than for non-covalent complexes containing either (**53**) or (**54**). This was also found to be the case for all other groups of three nickel complexes featuring the same diamine moiety but different pendants. Comparison of DC_{50} values amongst triads of nickel complexes with the same diamine moiety revealed they were always lower for the complexes bearing propylpiperidine pendant groups, and the latter consistently resulted in the largest values of ΔT_m in FRET experiments, particularly with anti-parallel F21T.

Finally, it should also be noted that only complexes containing propylpiperidine pendant groups significantly increased the T_m of D2 in melting experiments, with the largest increases observed for (**55**), (**58**) and (**64**).

Whilst it was hoped that analysis of the results presented in this chapter might also reveal additional information about the effects of changing the diamine moiety on DNA binding, in practice it was hard to distinguish these from the larger influence of altering the pendant groups. For example, it was noted in the previous chapter that (**53**) resulted in ions of significant abundance in ESI-MS experiments with all three types of DNA. This was also found to be the case with complex (**55**), but not (**54**), despite both also featuring the phenylenediamine moiety. It is also worth noting that complex (**55**) significantly changed the CD spectrum of Q4. This result suggests (**55**) has an appropriate combination of structural features to endow it with high affinity for this G-quadruplex. This conclusion is supported by the results of FID assays involving Q4, which resulted in the lowest DC_{50} value being obtained for (**55**).

The results presented in Chapter 4 also highlighted (**59**), which possess the 1,3-propanediamine group, as generally exhibiting very low binding affinity towards most DNA molecules. This was also found to be the case for complex (**60**) featuring the same diamine moiety. For example, it was not possible to determine values of DC_{50} from experiments performed with this complex and any DNA molecule owing to its very poor DNA binding ability. Complex (**61**) on the other hand exhibited a greater ability than either (**59**) or (**60**) to form non-covalent adducts in ESI-MS experiments, despite having the same diamine moiety. This is attributed to the over-riding influence of the propylpiperidine pendant groups in the former nickel complex.

Another unique observation was that parallel c-KIT1 was the only G-quadruplex whose CD spectrum was significantly affected by (**61**). This result suggests this nickel complex may bind to parallel c-KIT1 with some selectivity over other types of G-quadruplexes, however additional spectroscopic studies are required to corroborate this result.

Chapter 6 Conclusions and future directions

6.1 Conclusions

The main goal of this project was to prepare a range of new nickel Schiff base complexes that could act as selective G-quadruplex DNA binding and stabilising agents. The design of the new nickel Schiff base complexes was based on structural features previously identified as favourable for these purposes. This included an aromatic core as well as multiple positively charged pendant groups. It was proposed that the above goal might be best achieved through incorporating four pendant groups into the structures of each of the complexes. These would enable additional binding interactions that would vary with the loops and the grooves of different G-quadruplex DNA structures, whilst simultaneously inhibiting intercalation with dsDNA owing to steric hindrance.

Initial attempts to synthesise nickel Schiff base complexes with four pendant groups were based on an adaptation of a widely used two-step literature method.[124] It was possible to synthesise the precursor hydroxylated nickel Schiff base complexes using the first step of this method but not the final target complexes with the pendant groups. For example, alkylation of the precursor complex (**50**) to form (**53**) using the literature method was unsuccessful. One possible explanation for the failure of this reaction centres on the presence of traces of water in reaction mixtures coming from the hydrated starting material, complex (**50**). This is because in the presence of even just traces of water, the K_2CO_3 used in the reaction mixture would have produced

significant quantities of hydroxide ions which could have reacted with the alkylating agent before it had a chance to react with (**50**).

In view of the above problem, an alternative mechanochemical synthetic procedure was investigated for synthesising the desired complexes. Unfortunately, this method also proved to be ultimately unsuccessful. The mechanochemical synthetic approach was successfully applied to the synthesis of hydroxylated nickel Schiff base complexes, with yields of up to 98 % being obtained with reaction times as short as 2 h. Despite this success, the subsequent attachment of pendant groups could not be achieved under any set of reaction conditions.

In view of these problems, a third approach to obtaining the target complexes was developed which employed a common organic precursor, and centred on a modification of a previously reported method.[125] This new synthetic approach was based on selective dialkylation of 2,4,6-trihydroxybenzaldehyde to obtain a set of organic precursor compounds featuring different pendant groups, which were then used in condensation reactions with different diamines and nickel(II) acetate to produce a suite of fourteen new tetra-alkylated nickel Schiff base complexes in moderate to good yields. The complexes were fully characterised by NMR spectroscopy, ESI-MS and microanalysis. In addition, the solid state structures of four of the nickel complexes were determined using X-ray crystallography.

The solid state structures of (**53**), (**54**), (**63**) and (**65**) revealed that the nickel ion in each case adopted a square planar coordination geometry. In addition, all bond lengths and angles involving the central nickel ion were consistent with standard values.[125,135] The presence of the *meso*-1,2-diphenylethylenediamine moiety in (**65**) produced a torsion angle of -40.8(3)˚ which resulted in one phenyl ring being in an

equatorial position, whilst the other was located in an axial position. It is possible that this structural feature may have inhibited the ability of (**65**) to interact extensively with dsDNA. This proposal was supported by the results of a molecular docking study performed using (**65**) and 1KBD, which showed that the diamine moieties in the nickel complex was orientated further away from the minor groove than what was observed with the other nickel complexes. This resulted in (**65**) exhibiting the lowest free binding energy with 1KBD. In addition, the poor affinity of (**65**) for dsDNA revealed by the docking study was consistent with results obtained from ESI-MS and UV-Vis spectroscopic studies, which also highlighted that (**65**) exhibits a low binding affinity towards dsDNA.

The synthetic strategy developed to obtain the new nickel complexes resulted in a diverse range of chemical structures featuring different diamine moieties and pendant groups. The results of DNA binding studies performed using various spectroscopic methods showed that these different structural features resulted in a variety of G-quadruplex binding behaviours. For example, when examining a range of complexes featuring the same pendant groups, such as (**53**), (**56**), (**59**), (**62**) and (**65**), the identity of the diamine moiety was found to influence the DNA binding behaviour of the complexes. In addition, when the DNA binding behaviour of a series of complexes featuring the same diamine moiety and aromatic core was investigated, such as (**53**), (**54**) and (**55**), the structure of the pendant groups was found to have a major effect on DNA affinity.

There was generally good agreement between the results of DNA binding investigations undertaken using different spectroscopic methods and molecular docking simulations. For example, the results of ESI-MS binding studies indicated

that (**53**) was able to form non-covalent complexes with dsDNA and both unimolecular and tetramolecular G-quadruplexes. This suggested that (**53**) was able to interact to a significant extent with each of these different types of DNA molecules, which was consistent with the results obtained from FID assays. Furthermore, (**53**) was also found to have a greater ability than most other nickel complexes with ethylmorpholine pendant groups to affect the CD spectrum of unimolecular G-quadruplexes when the latter were present in either a parallel or hybrid conformation.

Changing the diamine moiety from phenylenediamine to ethylenediamine, 1,3-propanediamine or 1,2-propanediamine, whilst retaining the same pendant groups, often resulted in very different DNA binding characteristics for a series of related nickel complexes. For example, complex (**59**), which contains the 1,3-propanediamine moiety, gave larger values of DC_{50} for D2, Q1 and Q4 in FID assays than any other complex bearing ethylmorpholine pendant groups. This suggests (**59**) exhibited the lowest affinity of this group of nickel complexes towards each of these DNA molecules. The results of ESI-MS binding studies supported this conclusion, and also showed that changing the diamine moiety in (**59**) from 1,3-propanediamine to either ethylenediamine or 1,2-propanediamine resulted in complexes with a greater ability to form non-covalent complexes with D2, Q1 and Q4. This suggests the above structural changes resulted in increased DNA binding affinity in the case of complexes (**56**) and (**62**), which was also supported by the results of FID assays performed with these nickel complexes and the same DNA molecules.

The presence of the *meso*-1,2-diphenylethylenediamine moiety in (**65**) resulted in a complex which exhibited selectivity in its binding interactions in a number of

experiments. For example, the results of ESI-MS studies showed (**65**) exhibited a greater ability to form non-covalent complexes with Q1 and Q4 than with D2. Further evidence in support of a binding preference for G-quadruplex DNA over dsDNA was provided by the results of FID assays and CD spectroscopic studies. In addition, the results of CD and FRET studies performed with anti-parallel and hybrid forms of unimolecular G-quadruplexes indicated (**65**) also exhibited the ability to bind to these nucleic acid structures. These results are consistent with previous investigations which noted the ability of nickel Schiff base complexes bearing the *meso*-1,2-diphenylethylenediamine moiety to interact selectively with parallel tetramolecular G-quadruplexes.[135,136]

Some of the most profound effects on DNA binding behaviour were found to result from varying the identity of the pendant groups present in the nickel complexes. For example, the results obtained from ESI-MS and CD spectroscopic studies, as well as FRET and FID assays, showed that nickel complexes with propylpiperidine pendant groups generally interacted more strongly with different DNA molecules than analogues containing the same diamine moiety but one of the other two types of pendants. For example, (**59**), which possess the 1,3-propanediamine group and ethylpiperidine pendant groups, generally exhibited very low affinity towards most DNA molecules in binding experiments. This was also found to be the case for complex (**60**) featuring the same diamine moiety but ethylmorpholine pendants. Complex (**61**) on the other hand exhibited a much greater ability than either (**59**) or (**60**) to form non-covalent adducts in ESI-MS experiments, despite having the same diamine moiety. This was attributed to the over-riding influence of the propylpiperidine pendant groups in (**61**). Similar trends in binding affinity were

found for all other groups of three nickel complexes featuring the same diamine moiety but different pendants. It should also be noted that only nickel complexes containing propylpiperidine pendant groups significantly increased the T_m of D2 in melting experiments. Another unique observation was that parallel c-KIT1 was the only G-quadruplex whose CD spectrum was significantly affected by (**61**). This result suggests this nickel complex may bind to parallel c-KIT1 with some selectivity over other types of G-quadruplexes, however additional spectroscopic studies are required to corroborate this result.

The results of molecular docking studies indicated that each of the nickel complexes interacted with dsDNA via a groove binding mechanism and that intercalation was not a major contributor to the intermolecular interactions. This conclusion was supported by the results obtained from CD studies, as larger changes to the CD spectra of dsDNA would have been expected if the nickel complexes were interacting via an intercalating binding mode. Molecular docking studies also revealed that each of the nickel complexes interacted primarily via an end-stacking mechanism with a unimolecular G-quadruplex. The exact manner with which the complexes interacted varied as a result of differences in their structure, however the binding free energies fell within a relatively narrow range. This suggests that additional changes to the structure of the complexes will be required in order to produce more effective and selective G-quadruplex binding agents.

Complexes (**53**), (**56**) and (**65**) and their analogues with only two pendant groups (**18**), (**20**) and (**46**) were evaluated for their cytotoxicity against V79 lung cancer cells using MTT assays. The results obtained suggested (**65**) was slightly more cytotoxic than its analogue (**46**). In contrast, the reverse trend was observed for the

other two pairs of nickel complexes. Therefore, although only a limited data set of complexes was investigated, introduction of two additional pendant groups does not in general appear to confer additional cytotoxicity onto this class of nickel complexes. It should be remembered, however, that the effects of such structural alterations may vary from one cancer cell line to another.

6.2 Future directions

There is a range of approaches which can be taken to improve upon the DNA affinity and selectivity of the novel nickel complexes reported in this thesis. First of all it would be worthwhile to investigate the effects of changing the pendant groups from those present in the current complexes to alternatives with different functional groups such as amino acids or short peptides, alkyl pyrrolidines, quaternary amines, or alkyl pyridinium moieties. In addition, it would be informative to investigate the effects of changing the position of the pendant groups in the current complexes. A suitable group of complexes for investigation could be obtained, for example, by preparing the initial organic precursor starting with either 2,3,4- or 2,4,5-trihydroxybenzaldehyde, instead of the 2,4,6- isomer. Condensation of the resulting compounds with diamines in the presence of nickel ions would then yield a range of new complexes whose DNA-binding abilities could significantly differ from those reported in this thesis, by virtue of being able to more favourably position their pendant groups in the grooves of some G-quadruplexes. It would also be worth investigating the effects of replacing the nickel ion in the complexes studied in this thesis by other metal ions with a preference for a square planar coordination geometry such as palladium(II) or platinum(II), on DNA-binding interactions.

During the synthesis of the nickel complexes (**65**) and (**66**), the free ligands corresponding to both complexes were successfully isolated, however their DNA binding properties were not explored. It would be interesting to examine the effect of the absence of the metal ion on the DNA binding interactions of these ligands, as their more flexible structures may facilitate a different set of interactions with some DNA molecules.

While the molecular docking experiments presented here predicted the expected binding modes for the nickel complexes the results of these experiments should be confirmed using molecular dynamics simulations (MDs). This is because a limitation of molecular docking experiments is that they consider DNA molecules to be rigid and therefore do not allow them to adjust conformation during the docking process as would be expected in solution. Molecular dynamics simulations, on the other hand, can incorporate conformational changes that occur as a result of DNA-ligand interactions in solution. Furthermore the latter technique is more likely to generate accurate results by also incorporating interactions with solvent molecules.

While MTT assays provided a convenient method for exploring the therapeutic potential of the nickel complexes, they do not provide specific information about the mechanism of cell death induced by the tested compounds. Therefore, other biological assays such as fluorescence microscopy and flow cytometry assays are required. For example, Annexin V staining in conjunction with flow cytometry could be used to determine whether the mechanism of cell death caused by the nickel complexes is apoptotic or necrotic in nature. This, along with the effect of the nickel complexes on other human cancer cell lines and normal cell lines is important

information that could be used to direct further investigations into the therapeutic potential of this classes of metal complexes.

Supplementary Figures

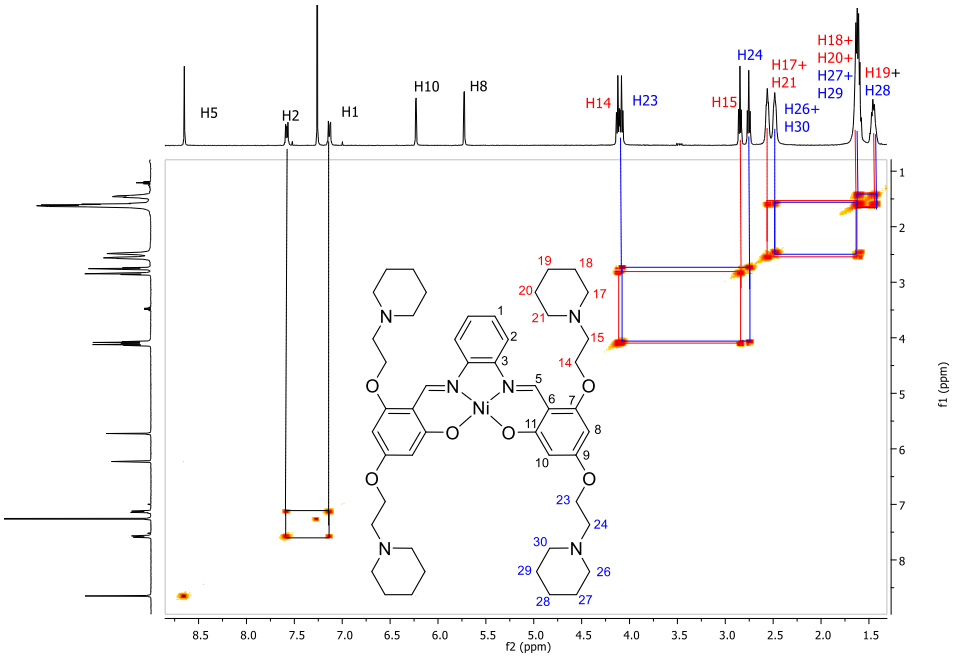

Figure S3.1: gCOSY NMR spectrum of (**53**), with H-H correlations highlighted.

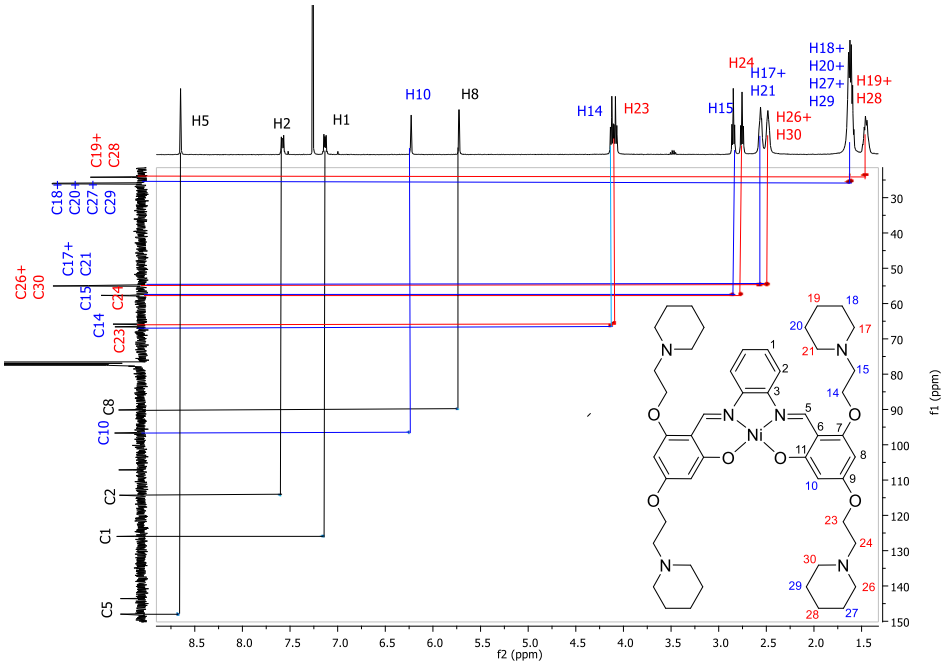

Figure S3.2: HSQC NMR spectrum of (**53**), with selected C-H correlations highlighted.

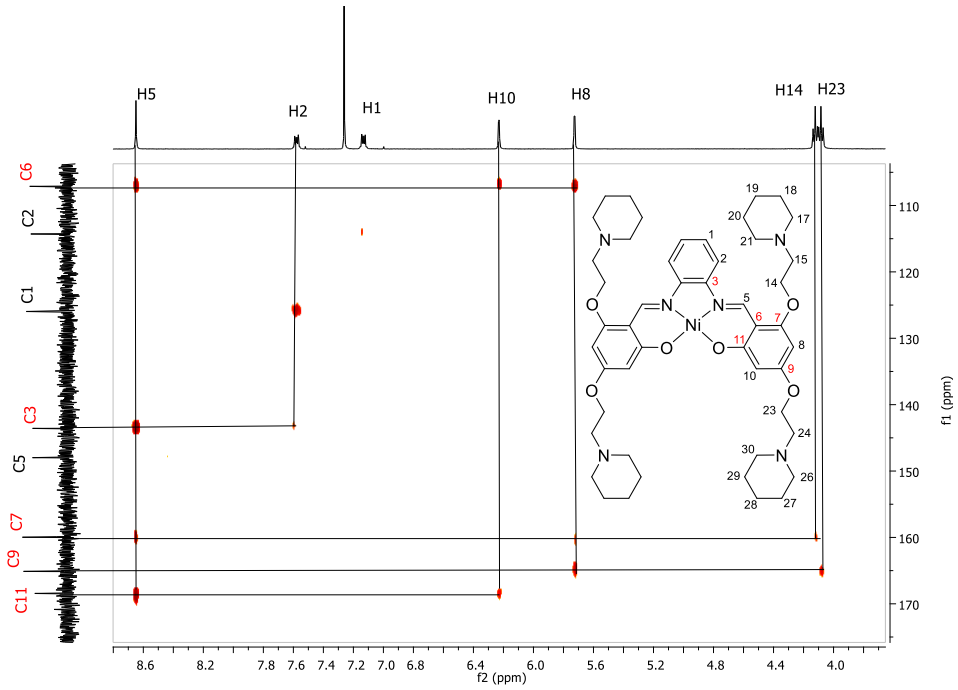

Figure S3.3: HMBC NMR spectrum of (**53**), with selected C-H correlations highlighted.

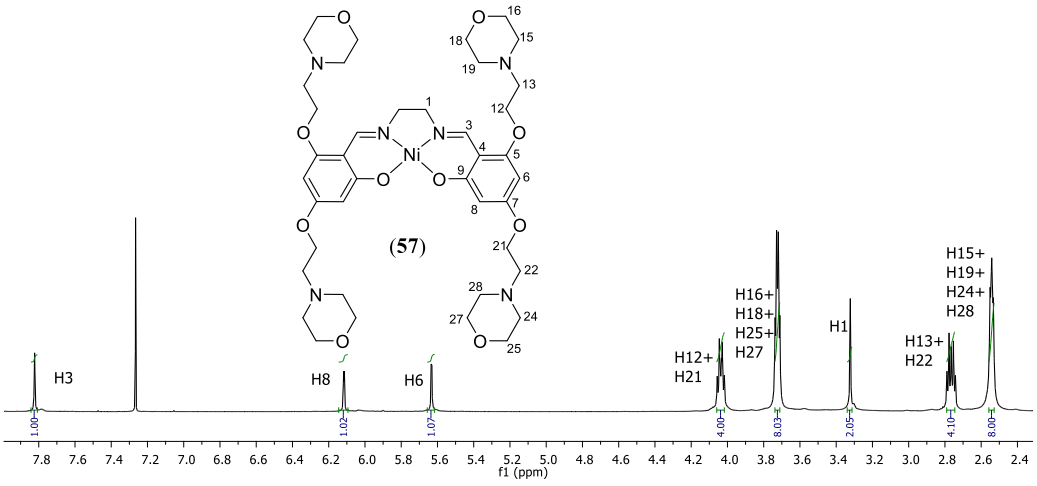

Figure S3.4: ^{1}H NMR spectrum of (**57**).

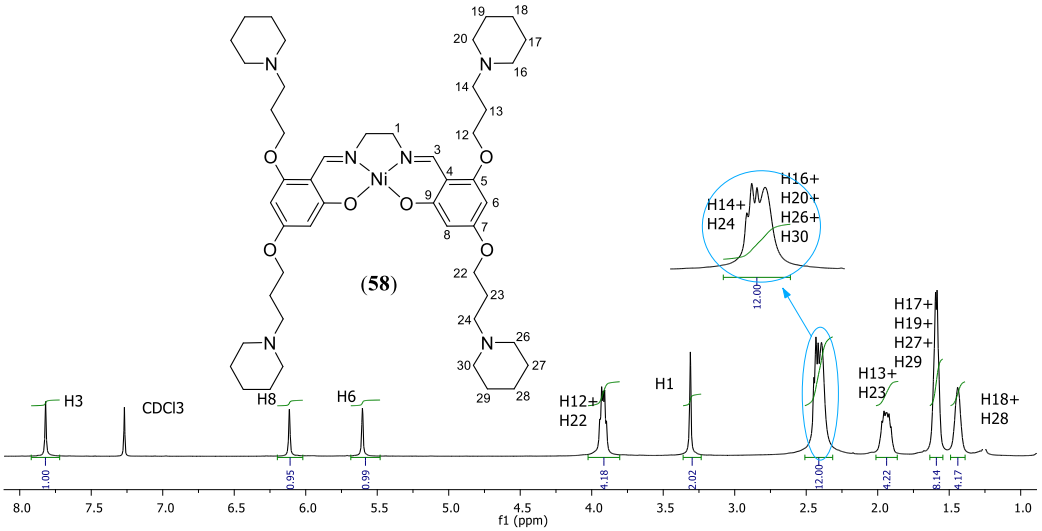

Figure S3.5:: ^{1}H NMR spectrum of (**58**), with an expansion of some signals, for clarity.

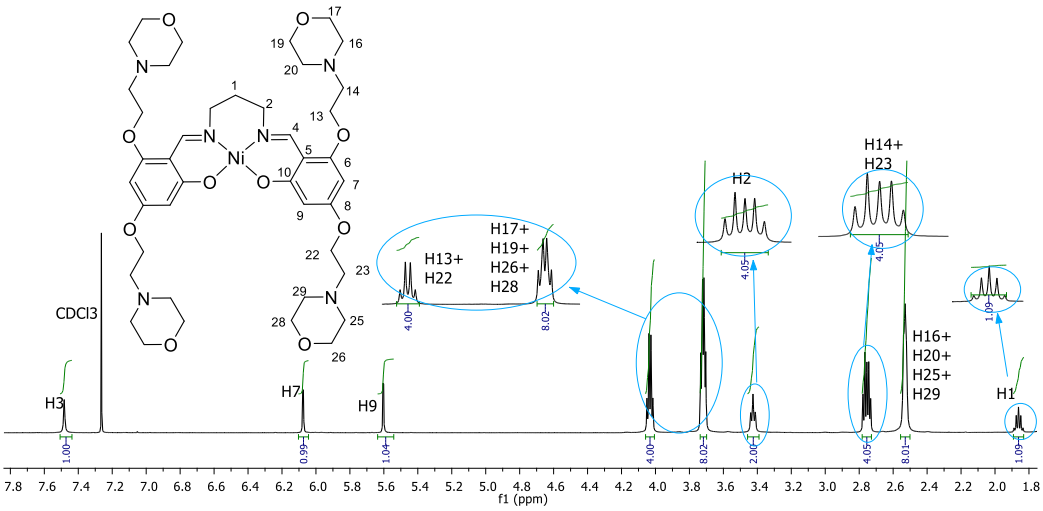

Figure S3.6: ^{1}H NMR spectrum of (**60**), with an expansion of some signals, for clarity.

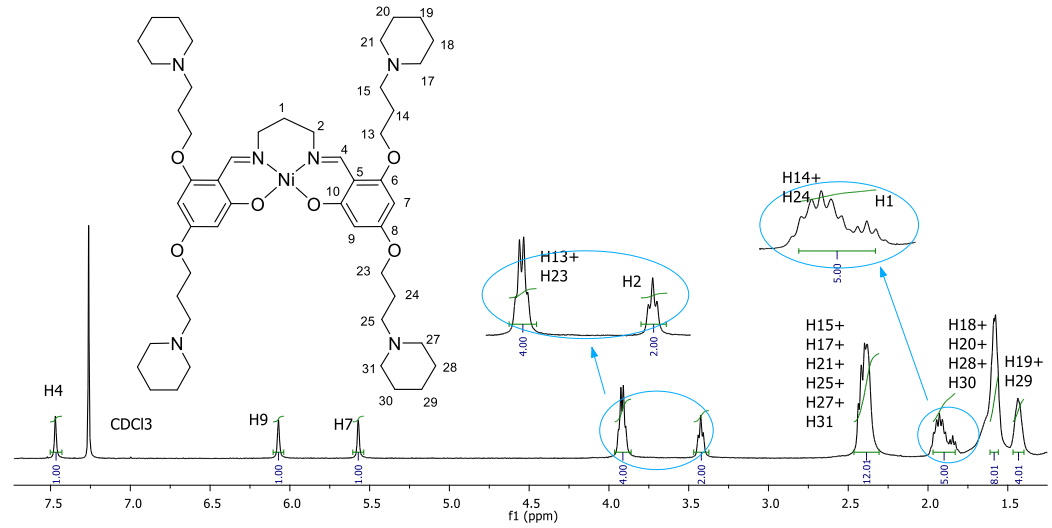

Figure S3.7: ^{1}H NMR spectrum of (**61**), with an expansion of some signals, for clarity.

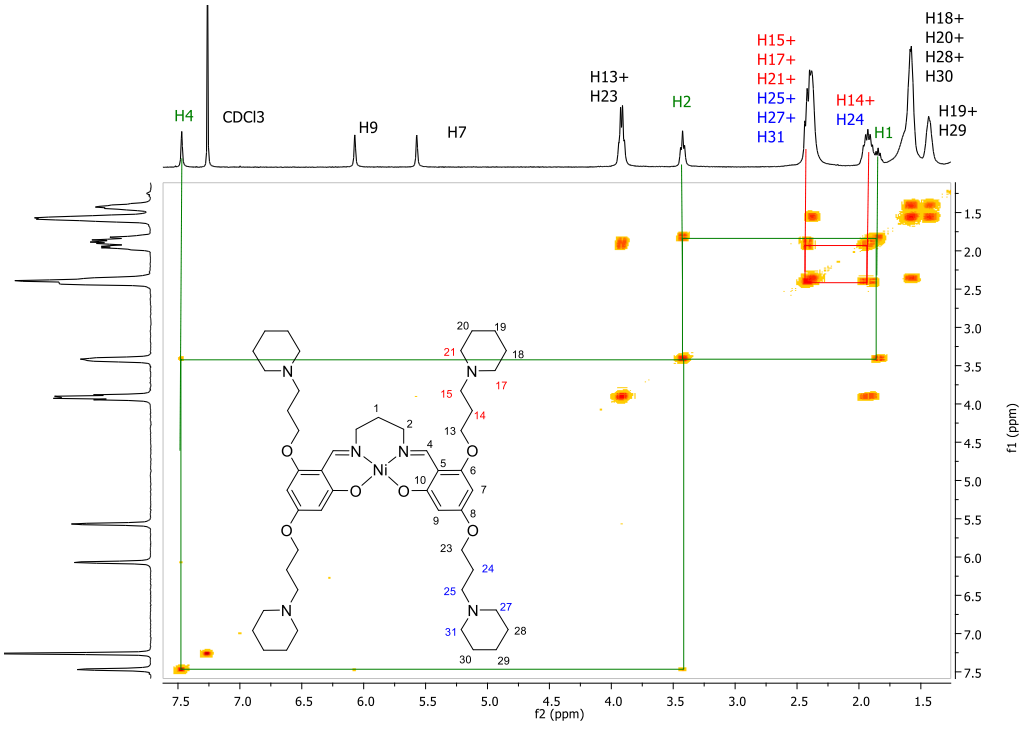

Figure S3.8: gCOSY NMR spectrum of (**61**), with selected H-H correlations highlighted.

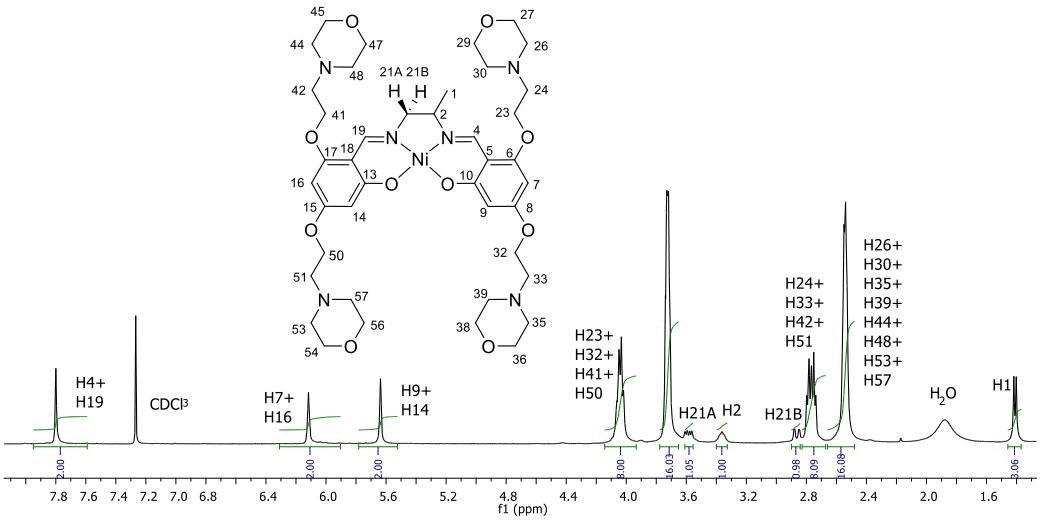

Figure S3.9: ^{1}H NMR spectrum of (**63**).

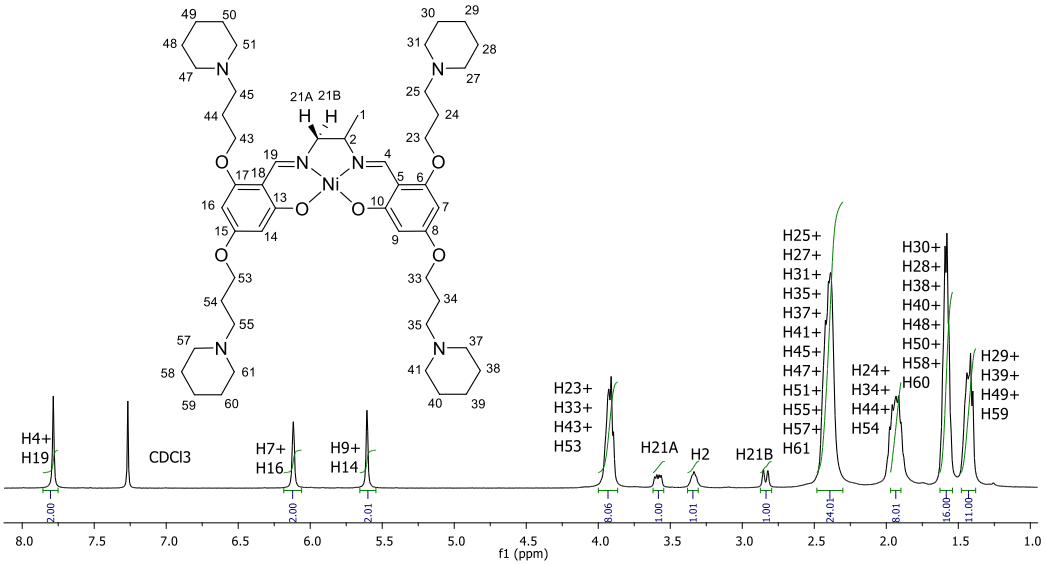

Figure S3.10: ^{1}H NMR spectrum of (**64**).

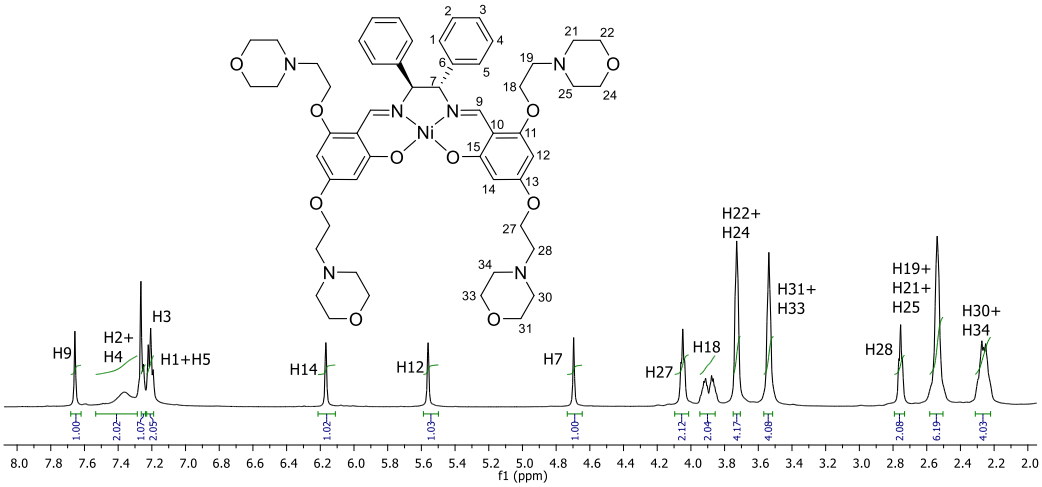

Figure S3.11: ^{1}H NMR spectrum of (**66**).

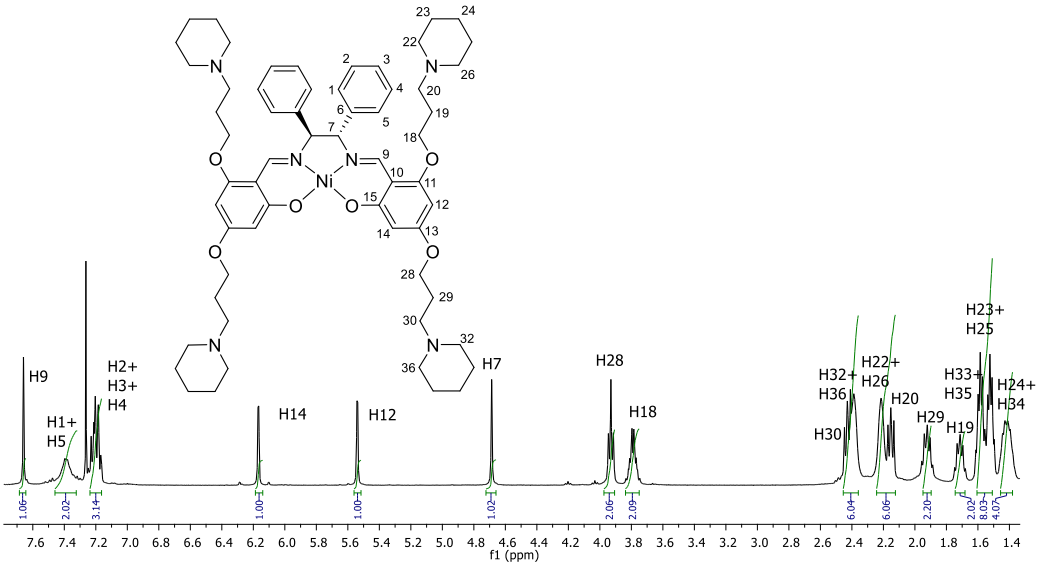

Figure S3.12: ^{1}H NMR spectrum of (**67**).

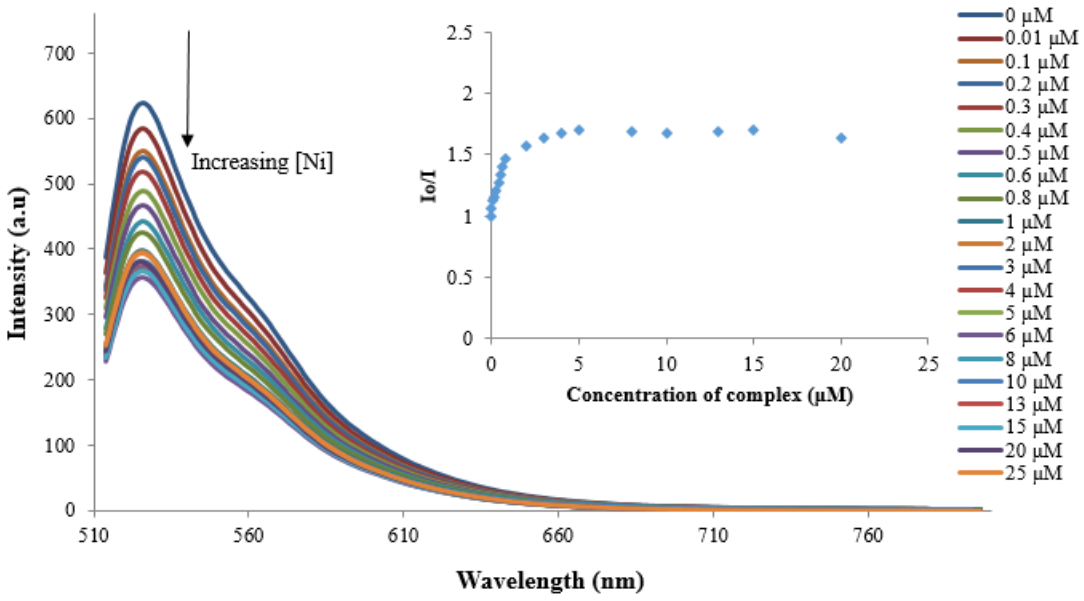

Figure S5.1: Results obtained from an FID assay involving addition of increasing amounts of (**60**) to a solution containing thiazole orange and D2. The inset shows a Stern-Volmer plot derived from the data, which was then used to determine the value of DC_{50} for (**60**) with this DNA sequence.

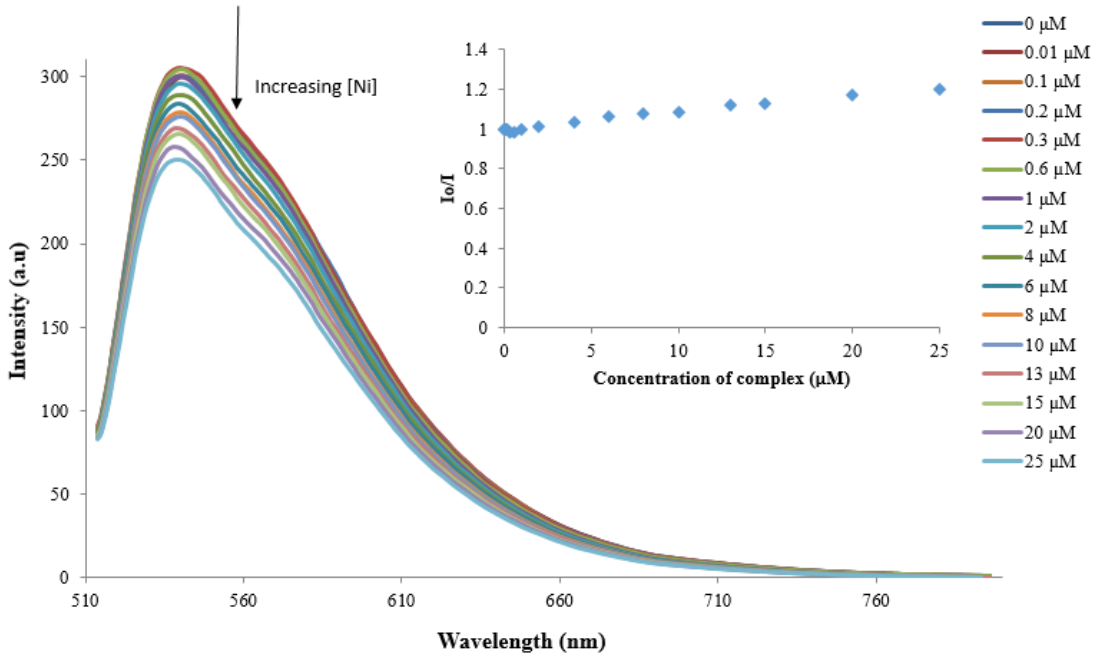

Figure S5.2: Results obtained from an FID assay involving addition of increasing amounts of (**60**) to a solution containing thiazole orange and parallel Q1. The inset shows a Stern-Volmer plot derived from the data, which was then used to determine the value of DC_{50} for (**60**) with this DNA sequence.

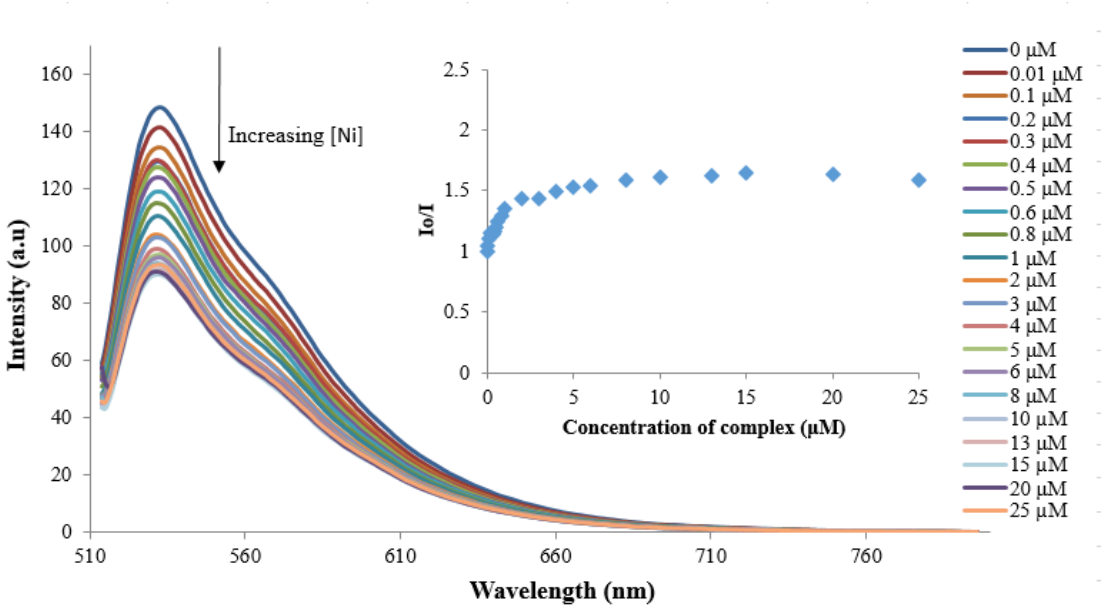

Figure S5.3: Results obtained from an FID assay involving addition of increasing amounts of (**60**) to a solution containing thiazole orange and parallel Q4. The inset shows a Stern-Volmer plot derived from the data, which was then used to determine the value of DC_{50} for (**60**) with this DNA sequence.

References

(1) Gonzalez-Ruiz, V.; Olives, A. I.; Martin, M. A.; Ribelles, P.; Ramos, M. T.; Menendez, J. C. *Biomed. Eng., Trends, Res. Technol.* **2011**, 65-90.

(2) Watson, J. D.; Crick, F. H. *Nature* **1953**, *171*, 737-738.

(3) Belmont, P.; Constant, J.-F.; Demeunynck, M. *Chem. Soc. Rev.* **2001**, *30*, 70-81.

(4) Bang, I. *Biochem. Z.* **1910**, *26*, 293-311.

(5) Martin, G.; Marie, N. L.; David, R. D. *Proc. Natl. Acad. Sci. U. S. A.* **1962**, *48*, 2013-2018.

(6) Sen, D.; Gilbert, W. *Nature (London)* **1988**, *334*, 364-366.

(7) Bhattacharyya, D.; Mirihana Arachchilage, G.; Basu, S. *Front. Chem.* **2016**, *4*, 38.

(8) Burge, S.; Parkinson, G. N.; Hazel, P.; Todd, A. K.; Neidle, S. *Nucleic Acids Res.* **2006**, *34*, 5402-5415.

(9) Hänsel-Hertsch, R.; Di Antonio, M.; Balasubramanian, S. *Nat. Rev. Mol. Cell Biol.* **2017**, *18*, 279-284.

(10) Tateishi-Karimata, H.; Sugimoto, N. *Nucleic Acids Res.* **2014**, *42*, 8831-8844.

(11) Nieuwland, C.; Zaccaria, F.; Fonseca Guerra, C. *PCCP* **2020**, *22*, 21108-21118.

(12) Bugaut, A.; Balasubramanian, S. *Biochemistry.* **2008**, *47*, 689-697.

(13) Fujii, T.; Podbevšek, P.; Plavec, J.; Sugimoto, N. *J. Inorg. Biochem.* **2017**, *166*, 190-198.

(14) Wang, Y.; Patel, D. J. *Structure* **1993**, *1*, 263-282.

(15) Parkinson, G. N.; Lee, M. P.; Neidle, S. *Nature* **2002**, *417*, 876-880.

(16) Lim, K. W.; Amrane, S.; Bouaziz, S.; Xu, W.; Mu, Y.; Patel, D. J.; Luu, K. N.; Phan, A. T. n. *J. Am. Chem. Soc.* **2009**, *131*, 4301-4309.

(17) Phan, A. T. *The FEBS Journal* **2010**, *277*, 1107-1117.

(18) Bochman, M. L.; Paeschke, K.; Zakian, V. A. *Nat. Rev. Genet.* **2012**, *13*, 770-780.

(19) Han, H.; Hurley, L. H. *Trends Pharmacol. Sci* **2000**, *21*, 136-142.

(20) Arola, A.; Vilar, R. *Curr. Top. Med. Chem.* **2008**, *8*, 1405-1415.

(21) Wang, W.; Hu, S.; Gu, Y.; Yan, Y.; Stovall, D. B.; Li, D.; Sui, G. *Biochim. Biophys. Acta* **2020**, *1874*, 188410.

(22) Rhodes, D.; Lipps, H. J. *Nucleic Acids Res.* **2015**, *43*, 8627-8637.

(23) Biffi, G.; Tannahill, D.; McCafferty, J.; Balasubramanian, S. *Nat. Chem.* **2013**, *5*, 182-186.

(24) Henderson, A.; Wu, Y.; Huang, Y. C.; Chavez, E. A.; Platt, J.; Johnson, F. B.; Brosh, R. M.; Sen, D.; Lansdorp, P. M. *Nucleic Acids Res.* **2014**, *42*, 860-869.

(25) Liu, H.-Y.; Zhao, Q.; Zhang, T.-P.; Wu, Y.; Xiong, Y.-X.; Wang, S.-K.; Ge, Y.-L.; He, J.-H.; Lv, P.; Ou, T.-M.; Tan, J.-H.; Li, D.; Gu, L.-Q.; Ren, J.; Zhao, Y.; Huang, Z.-S. *Cell Chem. Biol* **2016**, *23*, 1261-1270.

(26) Chambers, V. S.; Marsico, G.; Boutell, J. M.; Di Antonio, M.; Smith, G. P.; Balasubramanian, S. *Nat. Biotechnol.* **2015**, *33*, 877-881.

(27) Neidle, S.; Parkinson, G. N. *Curr. Opin. Struct. Biol.* **2003**, *13*, 275-283.

(28) Siddiqui-Jain, A.; Grand, C. L.; Bearss, D. J.; Hurley, L. H. *Proc. Natl. Acad. Sci.* **2002**, *99*, 11593-11598.

(29) Dexheimer, T. S.; Sun, D.; Hurley, L. H. *J. Am. Chem. Soc.* **2006**, *128*, 5404-5415.

(30) Cogoi, S.; Xodo, L. E. *Nucleic Acids Res.* **2006**, *34*, 2536-2549.

(31) Cogoi, S.; Paramasivam, M.; Spolaore, B.; Xodo, L. E. *Nucleic Acids Res.* **2008**, *36*, 3765-3780.

(32) Rankin, S.; Reszka, A. P.; Huppert, J.; Zloh, M.; Parkinson, G. N.; Todd, A. K.; Ladame, S.; Balasubramanian, S.; Neidle, S. *J. Am. Chem. Soc.* **2005**, *127*, 10584-10589.

(33) Todd, A. K.; Haider, S. M.; Parkinson, G. N.; Neidle, S. *Nucleic Acids Res.* **2007**, *35*, 5799-5808.

(34) Huppert, J. L.; Balasubramanian, S. *Nucleic Acids Res.* **2006**, *35*, 406-413.

(35) Todd, A. K.; Johnston, M.; Neidle, S. *Nucleic Acids Res.* **2005**, *33*, 2901-2907.

(36) Patel, D. J.; Phan, A. T.; Kuryavyi, V. *Nucleic Acids Res.* **2007**, *35*, 7429-7455.

(37) Qin, Y.; Hurley, L. H. *Biochimie* **2008**, *90*, 1149-1171.

(38) Rigo, R.; Palumbo, M.; Sissi, C. *Biochim Biophys Acta Gen Subj.* **2017**, *1861*, 1399-1413.

(39) Bryan, T. M. *Molecules* **2019**, *24*, 3439.

(40) Nayun, K. *Curr. Med. Chem.* **2019**, *26*, 2898-2917.

(41) De, S.; Michor, F. *Nat. Struct. Mol. Biol.* **2011**, *18*, 950-955.

(42) Maizels, N. *EMBO reports* **2015**, *16*, 910-922.

(43) Neidle, S. *Nat. Rev. Chem.* **2017**, *1*, 1-10.

(44) Henderson, E.; Hardin, C. C.; Walk, S. K.; Tinoco, I., Jr.; Blackburn, E. H. *Cell* **1987**, *51*, 899-908.

(45) Lipps, H. J.; Rhodes, D. *Trends Cell Biol.* **2009**, *19*, 414-422.

(46) Brosh, J. R. M. *Nat. Rev. Cancer.* **2013**, *13*, 542-558.

(47) Wickramasinghe, C. M.; Arzouk, H.; Frey, A.; Maiter, A.; Sale, J. E. *DNA Repair* **2015**, *29*, 83-90.

(48) McKenzie, K. E.; Umbricht, C. B.; Sukumar, S. *Mol. Med. Today* **1999**, *5*, 114-122.

(49) Balakrishnan, L.; Bambara, R. A. *Cold Spring Harb. Perspect. Biol.* **2013**, *5*, a010173.

(50) Okazaki, R.; Okazaki, T.; Sakabe, K.; Sugimoto, K.; Sugino, A. *Proc. Natl. Acad. Sci. U. S. A.* **1968**, *59*, 598-605.

(51) Ohki, R.; Tsurimoto, T.; Ishikawa, F. *Mol. Cell. Biol.* **2001**, *21*, 5753-5766.

(52) McEachern, M. J.; Krauskopf, A.; Blackburn, E. H. *Annu. Rev. Genet.* **2000**, *34*, 331-358.

(53) Martínez, P.; Blasco, M. A. *Aging cell.* **2010**, *9*, 653-666.

(54) Griffith, J. D.; Comeau, L.; Rosenfield, S.; Stansel, R. M.; Bianchi, A.; Moss, H.; de Lange, T. *Cell (Cambridge)* **1999**, *97*, 503-514.

(55) de Lange, T. *Genes Dev.* **2005**, *19*, 2100-2110.

(56) Zhong, Z.; Shiue, L.; Kaplan, S.; De Lange, T. *Mol. Cell. Biol.* **1992**, *12*, 4834-4843.

(57) Lee, C. Y.; McNerney, C.; Myong, S. *Methods Mol. Biol.* **2019**, *2035*, 309-322.

(58) Kim, N. W.; Piatyszek, M. A.; Prowse, K. R.; Harley, C. B.; West, M. D.; Ho, P. L. C.; Coviello, G. M.; Wright, W. E.; Weinrich, S. L.; Shay, J. W. *Science* **1994**, *266*, 2011-2015.

(59) Shay, J. W.; Bacchetti, S. *Eur. J. Cancer* **1997**, *33*, 787-791.

(60) Smolikov, S.; Mazor, Y.; Krauskopf, A. *Proc. Natl. Acad. Sci.* **2004**, *101*, 1656-1661.

(61) Wheelhouse, R. T.; Sun, D.; Han, H.; Han, F. X.; Hurley, L. H. *J. Am. Chem. Soc* **1998**, *120*, 3261-3262.

(62) Sun, D.; Thompson, B.; Cathers, B. E.; Salazar, M.; Kerwin, S. M.; Trent, J. O.; Jenkins, T. C.; Neidle, S.; Hurley, L. H. *J. Med. Chem* **1997**, *40*, 2113-2116.

(63) Fedoroff, O. Y.; Salazar, M.; Han, H.; Chemeris, V. V.; Kerwin, S. M.; Hurley, L. H. *Biochemistry.* **1998**, *37*, 12367-12374.

(64) Neidle, S. *J. Med. Chem* **2016**, *59*, 5987-6011.

(65) Ali, A.; Bhattacharya, S. *Bioorg. Med. Chem* **2014**, *22*, 4506-4521.

(66) Williamson, J. R. *Annu. Rev. Biophys. Biomol. Struct* **1994**, *23*, 703-730.

(67) Neidle, S.; Parkinson, G. *Nat. Rev. Drug Discov.* **2002**, *1*, 383-393.

(68) Li, J.; Correia, J. J.; Wang, L.; Trent, J. O.; Chaires, J. B. *Nucleic Acids Res.* **2005**, *33*, 4649-4659.

(69) Sanchez-Martin, V.; Soriano, M.; Garcia-Salcedo, J. A. *Cancers (Basel)* **2021**, *13*, 3156.

(70) Neidle, S. *FEBS J.* **2010**, *277*, 1118-1125.

(71) Ou, T.-m.; Lu, Y.-j.; Tan, J.-h.; Huang, Z.-s.; Wong, K.-Y.; Gu, L.-q. *ChemMedChem* **2008**, *3*, 690-713.

(72) Miglietta, G.; Russo, M.; Capranico, G. *Nucleic Acids Res.* **2020**, *48*, 11942-11957.

(73) Li, Q.; Xiang, J.-F.; Yang, Q.-F.; Sun, H.-X.; Guan, A.-J.; Tang, Y.-L. *Nucleic Acids Res.* **2013**, *41*, D1115-D1123.

(74) Sanchez-Martin, V.; Lopez-Pujante, C.; Soriano-Rodriguez, M.; Garcia-Salcedo, J. A. *Int. J. Mol. Sci.* **2020**, *21*, 8900.

(75) Kosiol, N.; Juranek, S.; Brossart, P.; Heine, A.; Paeschke, K. *Mol. Cancer* **2021**, *20*, 40.

(76) Awadasseid, A.; Ma, X.; Wu, Y.; Zhang, W. *Biomed. Pharmacother.* **2021**, *139*, 111550.

(77) Savva, L.; Georgiades, S. N. *Molecules* **2021**, *26*, 841.

(78) Campbell, N. H.; Parkinson, G. N.; Reszka, A. P.; Neidle, S. *J. Am. Chem. Soc* **2008**, *130*, 6722-6724.

(79) Drewe, W. C.; Nanjunda, R.; Gunaratnam, M.; Beltran, M.; Parkinson, G. N.; Reszka, A. P.; Wilson, W. D.; Neidle, S. *J. Med. Chem.* **2008**, *51*, 7751-7767.

(80) White, E. W.; Tanious, F.; Ismail, M. A.; Reszka, A. P.; Neidle, S.; Boykin, D. W.; Wilson, W. D. *Biophys. Chem.* **2007**, *126*, 140-153.

(81) Gunaratnam, M.; Greciano, O.; Martins, C.; Reszka, A. P.; Schultes, C. M.; Morjani, H.; Riou, J.-F.; Neidle, S. *Biochem. Pharmacol.* **2007**, *74*, 679-689.

(82) Incles, C. M.; Schultes, C. M.; Kempski, H.; Koehler, H.; Kelland, L. R.; Neidle, S. *Mol. Cancer Ther.* **2004**, *3*, 1201-1206.

(83) Burger, A. M.; Dai, F.; Schultes, C. M.; Reszka, A. P.; Moore, M. J.; Double, J. A.; Neidle, S. *Cancer Res.* **2005**, *65*, 1489-1496.

(84) Zhou, G.; Liu, X.; Li, Y.; Xu, S.; Ma, C.; Wu, X.; Cheng, Y.; Yu, Z.; Zhao, G.; Chen, Y. *Oncotarget* **2016**, *7*, 14925-14939.

(85) Taetz, S.; Baldes, C.; Klotz, U.; Lehr, C. M.; MÜRdter, T. E.; Kleideiter, E.; Piotrowska, K.; Bock, U.; Haltner-Ukomadu, E.; Mueller, J.; Huwer, H.; Schaefer, U. F. *Pharm. Res.* **2006**, *23*, 1031-1037.

(86) Pérez-Arnaiz, C.; Busto, N.; Santolaya, J.; Leal, J. M.; Barone, G.; García, B. *Biochim Biophys Acta Gen Subj.* **2018**, *1862*, 522-531.

(87) Ji, N.; Shi, H.-Q.; Fang, X.-Y.; Wu, Z.-Y. *Anal. Chim. Acta* **2020**, *1106*, 126-132.

(88) Izbicka, E.; Wheelhouse, R. T.; Raymond, E.; Davidson, K. K.; Lawrence, R. A.; Sun, D.; Windle, B. E.; Hurley, L. H.; Von Hoff, D. D. *Cancer research (Chicago, Ill.)* **1999**, *59*, 639-644.

(89) Grand, C. L.; Han, H.; Muñoz, R. M.; Weitman, S.; Von Hoff, D. D.; Hurley, L. H.; Bearss, D. J. *Mol. Cancer Ther.* **2002**, *1*, 565-573.

(90) Mikami-Terao, Y.; Akiyama, M.; Yuza, Y.; Yanagisawa, T.; Yamada, O.; Yamada, H. *Cancer Lett.* **2007**, *261*, 226-234.

(91) Mikami-Terao, Y.; Akiyama, M.; Yuza, Y.; Yanagisawa, T.; Yamada, O.; Kawano, T.; Agawa, M.; Ida, H.; Yamada, H. *Exp. Eye Res.* **2009**, *89*, 200-208.

(92) Rapozzi, V.; Zorzet, S.; Zacchigna, M.; Della Pietra, E.; Cogoi, S.; Xodo, L. E. *Mol. Cancer* **2014**, *13*, 75.

(93) Gaw, H. Y.; Phan, A. T.; Patel, D. J.; Kuryavyi, V. *Nat. Chem. Biol.* **2005**, *1*, 167-173.

(94) Parkinson, G. N.; Ghosh, R.; Neidle, S. *Biochemistry (Easton)* **2007**, *46*, 2390-2397.

(95) Martino, L.; Pagano, B.; Fotticchia, I.; Neidle, S.; Giancola, C. *J. Phys. Chem. B.* **2009**, *113*, 14779-14786.

(96) Ruan, T. L.; Davis, S. J.; Powell, B. M.; Harbeck, C. P.; Habdas, J.; Habdas, P.; Yatsunyk, L. A. *Biochimie* **2017**, *132*, 121-130.

(97) Rha, S. Y.; Izbicka, E.; Lawrence, R.; Davidson, K.; Sun, D.; Moyer, M. P.; Roodman, G. D.; Hurley, L.; Von Hoff, D. *Clin. Cancer. Res.* **2000**, *6*, 987-993.

(98) Guliaev, A. B.; Leontis, N. B. *Biochemistry (Easton)* **1999**, *38*, 15425-15437.

(99) Shin-ya, K.; Wierzba, K.; Matsuo, K.-i.; Ohtani, T.; Yamada, Y.; Furihata, K.; Hayakawa, Y.; Seto, H. *J. Am. Chem. Soc* **2001**, *123*, 1262-1263.

(100) Kim, M.-Y.; Vankayalapati, H.; Shin-ya, K.; Wierzba, K.; Hurley, L. H. *J. Am. Chem. Soc* **2002**, *124*, 2098-2099.

(101) Rezler, E. M.; Seenisamy, J.; Bashyam, S.; Kim, M.-Y.; White, E.; Wilson, W. D.; Hurley, L. H. *J. Am. Chem. Soc.* **2005**, *127*, 9439-9447.

(102) Gomez, D.; Paterski, R.; Lemarteleur, T.; Shin-Ya, K.; Mergny, J.-L.; Riou, J.-F. *J. Biol. Chem.* **2004**, *279*, 41487-41494.

(103) Tahara, H.; Shin-Ya, K.; Seimiya, H.; Yamada, H.; Tsuruo, T.; Ide, T. *Oncogene* **2006**, *25*, 1955-1966.

(104) Gomez, D.; Wenner, T.; Brassart, B.; Douarre, C.; O'Donohue, M.-F.; El Khoury, V.; Shin-ya, K.; Morjani, H.; Trentesaux, C.; Riou, J.-F. *J. Biol. Chem.* **2006**, *281*, 38721-38729.

(105) Temime-Smaali, N.; Guittat, L.; Sidibe, A.; Shin-ya, K.; Trentesaux, C.; Riou, J.-F. *PLoS One* **2009**, *4*, e6919-e6919.

(106) Tauchi, T.; Shin-Ya, K.; Sashida, G.; Sumi, M.; Okabe, S.; Ohyashiki, J. H.; Ohyashiki, K. *Oncogene* **2006**, *25*, 5719-5725.

(107) Sumi, M.; Tauchi, T.; Sashida, G.; Nakajima, A.; Gotoh, A.; Shin-Ya, K.; Ohyashiki, J. H.; Ohyashiki, K. *Int. J. Oncol.* **2004**, *24*, 1481-1487.

(108) Seenisamy, J.; Bashyam, S.; Gokhale, V.; Vankayalapati, H.; Sun, D.; Siddiqui-Jain, A.; Streiner, N.; Shinya, K.; White, E.; Wilson, W. D.; Hurley, L. H. *J. Am. Chem. Soc.* **2005**, *127*, 2944-2959.

(109) Sun, D.; Liu, W.-J.; Guo, K.; Rusche, J. J.; Ebbinghaus, S.; Gokhale, V.; Hurley, L. H. *Mol. Cancer Ther.* **2008**, *7*, 880-889.

(110) Micco, M.; Collie, G. W.; Dale, A. G.; Ohnmacht, S. A.; Pazitna, I.; Gunaratnam, M.; Reszka, A. P.; Neidle, S. *J. Med. Chem.* **2013**, *56*, 2959-2974.

(111) Ohnmacht, S. A.; Marchetti, C.; Gunaratnam, M.; Besser, R. J.; Haider, S. M.; Di Vita, G.; Lowe, H. L.; Mellinas-Gomez, M.; Diocou, S.; Robson, M.; Šponer, J.; Islam, B.; Barbara Pedley, R.; Hartley, J. A.; Neidle, S. *Sci. Rep.* **2015**, *5*, 11385.

(112) Reed, J. E.; Neidle, S.; Vilar, R. *Chem. Commun.* **2007**, 4366-4368.

(113) Georgiades, S. N.; Abd Karim, N. H.; Suntharalingam, K.; Vilar, R. *Angew. Chem., Int. Ed* **2010**, *49*, 4020-4034.

(114) Ralph, S. F. *Curr. Top. Med. Chem.* **2011**, *11*, 572-590.

(115) Zhang, J.; Zhang, F.; Li, H.; Liu, C.; Xia, J.; Ma, L.; Chu, W.; Zhang, Z.; Chen, C.; Li, S.; Wang, S. *Curr. Med. Chem.* **2012**, *19*, 2957-2975.

(116) Cao, Q.; Li, Y.; Freisinger, E.; Qin, P. Z.; Sigel, R. K. O.; Mao, Z.-W. *Inorganic Chemistry Frontiers* **2017**, *4*, 10-32.

(117) Palma, E.; Carvalho, J.; Cruz, C.; Paulo, A. *Pharmaceuticals* **2021**, *14*, 605.

(118) Dixon, I. M.; Lopez, F.; Esteve, J.-P.; Tejera, A. M.; Blasco, M. A.; Pratviel, G.; Meunier, B. *ChemBioChem* **2005**, *6*, 123-132.

(119) Dixon, I. M.; Lopez, F.; Tejera, A. M.; Esteve, J.-P.; Blasco, M. A.; Pratviel, G.; Meunier, B. *J. Am. Chem. Soc* **2007**, *129*, 1502-1503.

(120) Monchaud, D.; Teulade-Fichou, M.-P. *Org. Biomol. Chem.* **2008**, *6*, 627-636.

(121) Bertrand, H.; Monchaud, D.; De Cian, A.; Guillot, R.; Mergny, J.-L.; Teulade-Fichou, M.-P. *Org. Biomol. Chem* **2007**, *5*, 2555-2559.

(122) Largy, E.; Hamon, F.; Rosu, F.; Gabelica, V.; De Pauw, E.; Guédin, A.; Mergny, J.-L.; Teulade-Fichou, M.-P. *Chem. Eur. J.* **2011**, *17*, 13274-13283.

(123) Czerwinska, I.; Sato, S.; Takenaka, S. *Biorg. Med. Chem.* **2012**, *20*, 6416-6422.

(124) Reed, J. E.; Arnal, A. A.; Neidle, S.; Vilar, R. *J. Am. Chem. Soc* **2006**, *128*, 5992-5993.

(125) Arola-Arnal, A.; Benet-Buchholz, J.; Neidle, S.; Vilar, R. *Inorg. Chem* **2008**, *47*, 11910-11919.

(126) Ansari, K. I.; Grant, J. D.; Kasiri, S.; Woldemariam, G.; Shrestha, B.; Mandal, S. S. *J. Inorg. Biochem* **2009**, *103*, 818-826.

(127) Ansari, K. I.; Kasiri, S.; Grant, J. D.; Mandal, S. S. *J. Biomol. Screening.* **2011**, *16*, 26-35.

(128) Terenzi, A.; Bonsignore, R.; Spinello, A.; Gentile, C.; Martorana, A.; Ducani, C.; Högberg, B.; Almerico, A. M.; Lauria, A.; Barone, G. *RSC Advances* **2014**, *4*, 33245-33256.

(129) Terenzi, A.; Lötsch, D.; van Schoonhoven, S.; Roller, A.; Kowol, C. R.; Berger, W.; Keppler, B. K.; Barone, G. *Dalton Trans* **2016**, *45*, 7758-7767.

(130) Campbell, N. H.; Karim, N. H. A.; Parkinson, G. N.; Gunaratnam, M.; Petrucci, V.; Todd, A. K.; Vilar, R.; Neidle, S. *J. Med. Chem* **2012**, *55*, 209-222.

(131) Bonsignore, R.; Terenzi, A.; Spinello, A.; Martorana, A.; Lauria, A.; Almerico, A. M.; Keppler, B. K.; Barone, G. *J. Inorg. Biochem.* **2016**, *161*, 115-121.

(132) Abd Karim, N. H.; Mendoza, O.; Shivalingam, A.; Thompson, A. J.; Ghosh, S.; Kuimova, M. K.; Vilar, R. *RSC Adv* **2014**, *4*, 3355-3363.

(133) Lecarme, L.; Prado, E.; Rache, A. D.; Nicolau-Travers, M.-L.; Bonnet, R.; Heyden, A. v. D.; Philouze, C.; Gomez, D.; Mergny, J.-L.; Jamet, H.; Defrancq, E.; Jarjayes, O.; Thomas, F. *Inorg. Chem* **2014**, *53*, 12519-12531.

(134) Lecarme, L.; Prado, E.; De Rache, A.; Nicolau-Travers, M.-L.; Gellon, G.; Dejeu, J.; Lavergne, T.; Jamet, H.; Gomez, D.; Mergny, J.-L.; Defrancq, E.; Jarjayes, O.; Thomas, F. *ChemMedChem* **2016**, *11*, 1133-1136.

(135) Davis, K. J.; Richardson, C.; Beck, J. L.; Knowles, B. M.; Guedin, A.; Mergny, J.-L.; Willis, A. C.; Ralph, S. F. *Dalton Trans* **2015**, *44*, 3136-3150.

(136) Davis, K. J.; Assadawi, N. M. O.; Pham, S. Q. T.; Birrento, M. L.; Richardson, C.; Beck, J. L.; Willis, A. C.; Ralph, S. F. *Dalton Trans* **2018**, *47*, 13573-13591.

(137) Pham, S. Q. T.; Assadawi, N.; Wells, J.; Sophocleous, R. A.; Davis, K. J.; Yu, H.; Sluyter, R.; Dillon, C. T.; Kelso, C.; Beck, J. L.; Richardson, C.; Ralph, S. F.; Willis, A. C. *Dalton Trans* **2020**, *49*, 4843-4860.

(138) Cozzi, P. G. *Chem. Soc. Rev.* **2004**, *33*, 410-421.

(139) Silvestri, A.; Barone, G.; Ruisi, G.; Anselmo, D.; Riela, S.; Liveri, V. T. *J. Inorg. Biochem.* **2007**, *101*, 841-848.

(140) Schmeyers, J.; Toda, F.; Boy, J.; Kaupp, G. *J. Chem. Soc., Perkin Trans. 2.* **1998**, 989-994.

(141) Guzen, K. P.; Guarezemini, A. S.; Órfão, A. T. G.; Cella, R.; Pereira, C. M. P.; Stefani, H. A. *Tetrahedron Lett.* **2007**, *48*, 1845-1848.

(142) Arafa, W. *Arkivoc.* **2016**, *2016*, 187-201.

(143) Ferguson, M.; Giri, N.; Huang, X.; Apperley, D.; James, S. L. *Green Chem.* **2014**, *16*, 1374-1382.

(144) Fernández-Bertran, J. F. *Pure Appl. Chem.* **1999**, *71*, 581-586.

(145) James, S. L.; Adams, C. J.; Bolm, C.; Braga, D.; Collier, P.; Friščić, T.; Grepioni, F.; Harris, K. D. M.; Hyett, G.; Jones, W.; Krebs, A.; Mack, J.; Maini, L.; Orpen, A. G.; Parkin, I. P.; Shearouse, W. C.; Steed, J. W.; Waddell, D. C. *Chem. Soc. Rev.* **2012**, *41*, 413-447.

(146) Do, J.-L.; Friščić, T. *ACS Central Science* **2017**, *3*, 13-19.

(147) Howard, Joseph L.; Cao, Q.; Browne, D. L. *Chemical Science* **2018**, *9*, 3080-3094.

(148) Tan, D.; Friščić, T. *Eur. J. Org. Chem.* **2018**, *2018*, 18-33.

(149) Tan, D.; García, F. *Chem. Soc. Rev.* **2019**, *48 8*, 2274-2292.

(150) Kaupp, G.; Schmeyers, J.; Naimi-Jamal, M. R.; Zoz, H.; Ren, H. *Chem. Eng. Sci.* **2002**, *57*, 763-765.

(151) Kaupp, G.; Reza Naimi-Jamal, M.; Schmeyers, J. *Tetrahedron* **2003**, *59*, 3753-3760.

(152) Colacino, E.; Nun, P.; Colacino, F. M.; Martinez, J.; Lamaty, F. *Tetrahedron* **2008**, *64*, 5569-5576.

(153) Achar, T. K.; Bose, A.; Mal, P. *Beilstein J. Org. Chem.* **2017**, *13*, 1907-1931.

(154) Leoni, L.; Carletta, A.; Fusaro, L.; Dubois, J.; Tumanov, N. A.; Aprile, C.; Wouters, J.; Dalla Cort, A. *Molecules* **2019**, *24*, 2314.

(155) Leonardi, M.; Villacampa, M.; Menéndez, J. C. *Chem. Sci.* **2018**, *9*, 2042-2064.

(156) Domel. https://www.domel.com/products/laboratory-equipment/homogenizers (accessed 15/07/2021.

(157) Dolomanov, O. V.; Bourhis, L. J.; Gildea, R. J.; Howard, J. A. K.; Puschmann, H. *J. Appl. Cryst.* **2009**, *42*, 339-341.

(158) Sheldrick, G. M. *Acta Cryst. A.* **2015**, *71*, 3-8.

(159) Sheldrick, G. M. *Acta Cryst. C.* **2015**, *71*, 3-8.

(160) Urathamakul, T. PhD Thesis, University of Wollongong, 2006.

(161) Talib, J. PhD Thesis, University of Wollongong, 2008.

(162) Davis, K. J. PhD Thesis, University of Wollongong, 2015.

(163) Kibbe, W. A. *Nucleic Acids Res.* **2007**, *35*, W43-W46.

(164) Carvalho, J.; Nottelet, P.; Mergny, J.-L.; Queiroz, J. A.; Salgado, G. F.; Cruz, C. *Biochimie* **2017**, *135*, 186-195.

(165) Munira Haidad Ali, S.; Yan, Y.-K.; Lee, P. P. F.; Khong, K. Z. X.; Alam Sk, M.; Lim, K. H.; Klejevskaja, B.; Vilar, R. *Dalton Trans* **2014**, *43*, 1449-1459.

(166) Li, Y.; Yang, Z.-Y. *Inorg. Chim. Acta* **2009**, *362*, 4823-4831.

(167) Tuc, N. V. PhD Thesis, University of Wollongong, 2015.

(168) Nguyen, P. T. V.; Yu, H.; Keller, P. A. *J. Mol. Graph. Model.* **2015**, *57*, 1-8.

(169) Pham, S. Q. T. PhD thesis, University of Wollongong, 2019.

(170) Sanner, M. F. *J. Mol. Graph. Model.* **1999**, *17*, 57-61.

(171) Tisné, C.; Hantz, E.; Hartmann, B.; Delepierre, M. *J. Mol. Biol.* **1998**, *279*, 127-142.

(172) O'Boyle, N. M.; Banck, M.; James, C. A.; Morley, C.; Vandermeersch, T.; Hutchison, G. R. *J. Cheminform.* **2011**, *3*, 1-14.

(173) Hanwell, M. D.; Curtis, D. E.; Lonie, D. C.; Vandermeerschd, T.; Zurek, E.; Hutchison, G. R. *J. Cheminform.* **2012**, *4*, 17-17.

(174) Frisch, M. J.; Trucks, G. W.; Schlegel, H. B.; Scuseria, G. E.; Robb, M. A.; Cheeseman, J. R.; Scalmani, G.; Barone, V.; Mennucci, B.; Petersson, G. A.; Nakatsuji, H.; Caricato, M.; Li, X.; Hratchian, H. P.; Izmaylov, A. F.; Bloino, J.; Zheng, G.; Sonnenberg, J. L.; Hada, M.; Ehara, M.; Toyota, K.; Fukuda, R.; Hasegawa, J.; Ishida, M.; Nakajima, T.; Honda, Y.; Kitao, O.; Nakai, H.; Vreven, T.; Montgomery Jr., J. A.; Peralta, J. E.; Ogliaro, F.; Bearpark, M. J.; Heyd, J. J.; Brothers, E. N.; Kudin, K. N.; Staroverov, V. N.; Keith, T. A.; Kobayashi, R.; Normand, J.; Raghavachari, K.; Rendell, A. P.; Burant, J. C.; Iyengar, S. S.; Tomasi, J.; Cossi, M.; Millam, J. M.; Klene, M.; Knox, J. E.; Cross, J. B.; Bakken, V.; Adamo, C.; Jaramillo, J.; Gomperts, R.; Stratmann, R. E.; Yazyev, O.; Austin, A. J.; Cammi, R.; Pomelli, C.; Ochterski, J. W.; Martin, R. L.; Morokuma, K.; Zakrzewski, V. G.; Voth, A.; Salvador, P.; Dannenberg, J. J.; Dapprich, S.; Daniels, A. D.; Farkas, O.; Foresman, J. B.; Ortiz, J. V.; Cioslowski, J.; Fox, D. J.: Gaussian 09 Rev. E.01. Gaussian, Inc.: Wallingford, CT, 2013.

(175) Trott, O.; Olson, A. J. *J. Comput. Chem.* **2010**, *31*, 455-461.

(176) Schrodinger, LLC: The PyMOL Molecular Graphics System, Version 1.3.

(177) Tada, H.; Shiho, O.; Kuroshima, K.; Koyama, M.; Tsukamoto, K. *J. Immunol. Methods* **1986**, *93*, 157-165.

(178) Mosmann, T. *J. Immunol. Methods* **1983**, *65*, 55-63.

(179) Hayon, T.; Dvilansky, A.; Shpilberg, O.; Nathan, I. *Leuk. Lymphoma* **2003**, *44*, 1957-1962.

(180) Rosu, F.; De Pauw, E.; Gabelica, V. *Biochimie* **2008**, *90*, 1074-1087.

(181) Beck, J. L.; Colgrave, M. L.; Ralph, S. F.; Sheil, M. M. *Mass Spectrom. Rev.* **2001**, *20*, 61-87.

(182) Gupta, R.; Beck, J. L.; Ralph, S. F.; Sheil, M. M.; Aldrich-Wright, J. R. *J. Am. Soc. Mass Spectrom* **2004**, *15*, 1382-1391.

(183) Paramasivan, S.; Rujan, I.; Bolton, P. H. *Methods* **2007**, *43*, 324-331.

(184) Chang, Y. M.; Chen, C. K.; Hou, M. H. *Int. J. Mol. Sci.* **2012**, *13*, 3394-3413.

(185) Kypr, J.; Kejnovska, I.; Renciuk, D.; Vorlickova, M. *Nucleic Acids Res.* **2009**, *37*, 1713-1725.

(186) Vorlíčková, M.; Kejnovská, I.; Bednářová, K.; Renčiuk, D.; Kypr, J. *Chirality* **2012**, *24*, 691-698.

(187) Karsisiotis, A. I.; Hessari, N. M. a.; Novellino, E.; Spada, G. P.; Randazzo, A.; Webba da Silva, M. *Angewandte Chemie (International ed.)* **2011**, *50*, 10645-10648.

(188) Vorlickova, M.; Kejnovska, I.; Sagi, J.; Renciuk, D.; Bednarova, K.; Motlova, J.; Kypr, J. *Methods* **2012**, *57*, 64-75.

(189) Pham, S. Q. T.; Richardson, C.; Kelso, C.; Willis, A. C.; Ralph, S. F. *Dalton Trans* **2020**, *49*, 10360-10379.

(190) Carvalho, J.; Queiroz, J. A.; Cruz, C. *J. Chem. Educ.* **2017**, *94*, 1547-1551.

(191) Hou, M.-H.; Lu, W.-J.; Lin, H.-Y.; Yuann, J.-M. P. *Biochemistry* **2008**, *47*, 5493-5502.

(192) Le, D. D.; Di Antonio, M.; Chan, L. K. M.; Balasubramanian, S. *Chem. Commun.* **2015**, *51*, 8048-8050.

(193) Gregory-Bryson, E.; Bartlett, E.; Kiupel, M.; Hayes, S.; Yuzbasiyan-Gurkan, V. *BMC Cancer* **2010**, *10*, 559.

(194) Metcalfe, D. D. *Blood* **2008**, *112*, 946-956.

(195) Wang, W. L.; Healy, M. E.; Sattler, M.; Verma, S.; Lin, J.; Maulik, G.; Stiles, C. D.; Griffin, J. D.; Johnson, B. E.; Salgia, R. *Oncogene* **2000**, *19*, 3521-3528.

(196) Bejugam, M.; Gunaratnam, M.; Müller, S.; Sanders, D. A.; Sewitz, S.; Fletcher, J. A.; Neidle, S.; Balasubramanian, S. *ACS Med. Chem. Lett.* **2010**, *1*, 306-310.

(197) Balasubramanian, S.; Hurley, L. H.; Neidle, S. *Nat. Rev. Drug Discov.* **2011**, *10*, 261-275.

(198) Ducani, C.; Bernardinelli, G.; Högberg, B. r.; Keppler, B. K.; Terenzi, A. *J. Am. Chem. Soc.* **2019**, *141*, 10205-10213.

(199) Bejugam, M.; Sewitz, S.; Shirude, P. S.; Rodriguez, R.; Shahid, R.; Balasubramanian, S. *J. Am. Chem. Soc.* **2007**, *129*, 12926-12927.

(200) Gunaratnam, M.; Swank, S.; Haider, S. M.; Galesa, K.; Reszka, A. P.; Beltran, M.; Cuenca, F.; Fletcher, J. A.; Neidle, S. *J. Med. Chem.* **2009**, *52*, 3774-3783.

(201) Nielsen, M. C.; Larsen, A. F.; Abdikadir, F. H.; Ulven, T. *Eur. J. Med. Chem.* **2014**, *72*, 119-126.

(202) Chen, Z. F.; Qin, Q. P.; Qin, J. L.; Liu, Y. C.; Huang, K. B.; Li, Y. L.; Meng, T.; Zhang, G. H.; Peng, Y.; Luo, X. J.; Liang, H. *J. Med. Chem.* **2015**, *58*, 2159-2179.

(203) Diveshkumar, K. V.; Sakrikar, S.; Harikrishna, S.; Dhamodharan, V.; Pradeepkumar, P. I. *ChemMedChem* **2014**, *9*, 2754-2765.

(204) Diveshkumar, K. V.; Sakrikar, S.; Rosu, F. d. r.; Harikrishna, S.; Gabelica, V. r.; Pradeepkumar, P. I. *Biochemistry (Easton)* **2016**, *55*, 3571-3585.

(205) Dhamodharan, V.; Harikrishna, S.; Bhasikuttan, A. C.; Pradeepkumar, P. I. *ACS Chem. Biol.* **2015**, *10*, 821-833.

(206) Zorzan, E.; Da Ros, S.; Musetti, C.; Shahidian, L. Z.; Coelho, N. F. R.; Bonsembiante, F.; Létard, S.; Gelain, M. E.; Palumbo, M.; Dubreuil, P.; Giantin, M.; Sissi, C.; Dacasto, M. *Oncotarget* **2016**, *7*, 21658-21675.

(207) Marchetti, C.; Minarini, A.; Tumiatti, V.; Moraca, F.; Parrotta, L.; Alcaro, S.; Rigo, R.; Sissi, C.; Gunaratnam, M.; Ohnmacht, S. A.; Neidle, S.; Milelli, A. *Biorg. Med. Chem.* **2015**, *23*, 3819-3830.

(208) De Cian, A.; Guittat, L.; Kaiser, M.; Sacca, B.; Amrane, S.; Bourdoncle, A.; Alberti, P.; Teulade-Fichou, M.-P.; Lacroix, L.; Mergny, J.-L. *Methods* **2007**, *42*, 183-195.

(209) Renciuk, D.; Zhou, J.; Beaurepaire, L.; Guedin, A.; Bourdoncle, A.; Mergny, J.-L. *Methods* **2012**, *57*, 122-128.

(210) Nygren, J.; Svanvik, N.; Kubista, M. *Biopolymers.* **1998**, *46*, 39-51.

(211) Boger, D. L.; Tse, W. C. *Biorg. Med. Chem.* **2001**, *9*, 2511-2518.

(212) Tse, W. C.; Boger, D. L. *Acc. Chem. Res.* **2004**, *37*, 61-69.

(213) Monchaud, D.; Allain, C.; Teulade-Fichou, M. P. *Nucleosides Nucleotides Nucleic Acids.* **2007**, *26*, 1585-1588.

(214) Monchaud, D.; Allain, C.; Teulade-Fichou, M.-P. *Bioorg. Med. Chem. Lett.* **2006**, *16*, 4842-4845.

(215) Xing, Y.-P.; Liu, C.; Zhou, X.-H.; Shi, H.-C. *Sci. Rep.* **2015**, *5*, 8125-8125.

(216) Lubitz, I.; Zikich, D.; Kotlyar, A. *Biochemistry* **2010**, *49*, 3567-3574.

(217) Lee, L. G.; Chen, C. H.; Chiu, L. A. *Cytometry* **1986**, *7*, 508-517.

(218) Bal-Demirci, T.; Congur, G.; Erdem, A.; Erdem-Kuruca, S.; Özdemir, N.; Akgün-Dar, K.; Varol, B.; Ülküseven, B. *New J. Chem.* **2015**, *39*, 5643-5653.

(219) Haribabu, J.; Jeyalakshmi, K.; Arun, Y.; Bhuvanesh, N. S. P.; Perumal, P. T.; Karvembu, R. *RSC Advances* **2015**, *5*, 46031-46049.

(220) Raj Kumar, R.; Ramesh, R. *RSC advances* **2015**, *5*, 101932-101948.

(221) Li, Y.; Yang, Z.; Zhou, M.; Li, Y. *RSC Advances* **2017**, *7*, 49404-49422.

(222) Huang, K.-B.; Chen, Z.-F.; Liu, Y.-C.; Wang, M.; Wei, J.-H.; Xie, X.-L.; Zhang, J.-L.; Hu, K.; Liang, H. *Eur. J. Med. Chem.* **2013**, *70*, 640-648.

(223) Senthil Raja, D.; Ramachandran, E.; Bhuvanesh, N. S. P.; Natarajan, K. *Eur. J. Med. Chem.* **2013**, *64*, 148-159.

(224) Talib, J.; Harman, D. G.; Dillon, C. T.; Aldrich-Wright, J.; Beck, J. L.; Ralph, S. F. *Dalton Trans.* **2009**, 504-513.